

292

# SECONDARY BATTERIES USING ELECTRONICALLY CONDUCTIVE POLYMER CATHODES

## A FINAL REPORT

for

NASA GRANT NAG 9-173

for the period January 1, 1989 to June 30, 1991

Submitted to

Scientific & Technical Information Facility

P. O. Box 8757

Baltimore/Washington International Airport

Maryland 21240

prepared by

Charles R. Martin

Department of Chemistry

Colorado State University

Ft. Collins, Colorado 80523

and

Ralph E. White

Department of Chemical Engineering

Texas A&M University

College Station, Texas 77843-3122

May 1991

NASA-CR-91-004 SECONDARY BATTERIES USING ELECTRONICALLY CONDUCTIVE POLYMER CATHODES Final Report, 1 Jan. 1989 - 30 Jun. 1991 (Colorado State Univ.) 312 p. OSCL OVC	95/32 0020554
--	------------------

NEW SECONDARY BATTERIES USING ELECTRONICALLY  
CONDUCTIVE POLYMER CATHODES

A FINAL REPORT

for

NASA GRANT NAG 9-173

For the period January 1, 1989 to June 30, 1991

Submitted to  
NASA Scientific & Technical Information Facility  
P. O. Box 8757  
Baltimore/Washington International Airport  
Maryland 21240

prepared by

Charles R. Martin  
Department of Chemistry  
Colorado State University  
Ft. Collins, Colorado 80523

and

Ralph E. White  
Department of Chemical Engineering  
Texas A&M University  
College Station, Texas 77843-3122

May 1991

## INTRODUCTION

In this project, a Li/Polypyrrole secondary battery was designed and built, and the effect of controlling the morphology of the polymer on enhancement of counterion diffusion in the polymer phase was explored. This project was a joint project under the direction of Dr. Charles R. Martin (Department of Chemistry, Colorado State University) and Dr. Ralph E. White (Department of Chemical Engineering, Texas A&M University). Experimental work was undertaken by Dr. Martin's research group and mathematical modeling of the battery was undertaken by Dr. White's research group.

This final report consists of two manuscripts. One is a master's thesis by one of Dr. Martin's students, Marjorie A. Nicholson, entitled "Effect of Polymer Electrode Morphology on Performance of a Lithium/Polypyrrole Battery" and is presented in Appendix A. The other is a doctoral dissertation by one of Dr. White's students, Taewhan Yeu, entitled "New Secondary Batteries Utilizing Electronically Conductive Polypyrrole Cathode" and is presented in Appendix B.

Four publications have resulted from this project. They are listed as follows:

1. Taewhan Yeu, Trung Nguyen, and R. E. White, "A Mathematical Model for Predicting Cyclic Voltammograms of Electronically Conductive Polypyrrole," *Journal of the Electrochemical Society*, **135** (1988), 1971-1976.

2. Taewhan Yeu and R. E. White, "Mathematical Model of a Lithium/Polypyrrole Cell," *Journal of the Electrochemical Society*, **137** (1990), 1327-1336.

3. Taewhan Yeu, Ken-Ming Yin, José Carbajal and R. E. White, "Electrochemical Characterization of Electronically Conductive Polypyrrole on Cyclic Voltammograms," accepted by *Journal of the Electrochemical Society*, May 1991.

4. M. A. Nicholson, L. S. Van Dyke, and C. R. Martin, "Effect of Polymer Electrode Morphology on Performance of a Lithium/Polypyrrole Battery," submitted to *Journal of the Electrochemical Society*, July 1991.



## APPENDIX A

NAG 9-173

EFFECT OF POLYMER ELECTRODE MORPHOLOGY ON  
PERFORMANCE OF A LITHIUM/POLYPYRROLE BATTERY

A Thesis

by

MARJORIE ANNE NICHOLSON

Submitted to the Office of Graduate Studies of  
Texas A&M University

in partial fulfillment of the requirements for the degree of

MASTER OF SCIENCE

May 1991

Major Subject: Chemistry

9

5-12-91  
126P

7-33

N91-25323-55  
7-129

EFFECT OF POLYMER ELECTRODE MORPHOLOGY ON  
PERFORMANCE OF A LITHIUM/POLYPYRROLE BATTERY

A Thesis

by

MARJORIE ANNE NICHOLSON

Submitted to the Office of Graduate Studies of  
Texas A&M University  
in partial fulfillment of the requirements for the degree of

MASTER OF SCIENCE

May 1991

Major Subject: Chemistry

EFFECT OF POLYMER ELECTRODE MORPHOLOGY ON  
PERFORMANCE OF A LITHIUM/POLYPYRROLE BATTERY

A Thesis

by

MARJORIE ANNE NICHOLSON

Approved as to style and content by



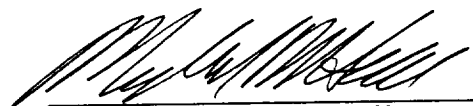
Charles R. Martin  
(Chair of Committee)



A. John Appleby  
(Member)



Manuel P. Soriaga  
(Member)



Michael B. Hall  
(Head of Department)

May 1991

## ABSTRACT

Effect of Polymer Electrode Morphology on Performance of a  
Lithium/Polypyrrole Battery. (May 1991)

Marjorie A. Nicholson, B.A., Texas A&M University

Chair of Advisory Committee: Dr. Charles R. Martin

A variety of conducting polymer batteries have been described in the recent literature. In this work, a Li/Polypyrrole secondary battery is described. The effect of controlling the morphology of the polymer on enhancement of counterion diffusion in the polymer phase is explored. A method of preparing conducting polymers has been developed which yields high surface area per unit volume of electrode material. A porous membrane is used as a template in which to electrochemically polymerize pyrrole, then the membrane is dissolved, leaving the polymer in a fibrillar form. Conventionally, the polymer is electrochemically polymerized as a dense polymer film on a smooth Pt disk electrode. Previous work has shown that when the polymer is electrochemically polymerized in fibrillar form, charge transport rates are faster and charge capacities are greater than for dense, conventionally grown films containing the same amount of polymer.

The purpose of this work is to expand previous work by further investigating the possibilities of the optimization of transport rates in polypyrrole films by controlling the morphology of the films. The utility of fibrillar polypyrrole as a cathode material in a lithium/polymer secondary battery is then assessed. The performance of the fibrillar battery is compared to the performance of an analogous battery which

employed a conventionally grown polypyrrole film. The study includes a comparison of cyclic voltammetry, shape of charge/discharge curves, discharge time and voltage, cycle life, coulombic efficiencies, charge capacities, energy densities, and energy efficiencies.

## DEDICATION

This thesis is dedicated to God  
and my children, who I also dedicate to Him,



## ACKNOWLEDGMENTS

I would like to take this opportunity to acknowledge my highly effective research director, Dr. Charles R. Martin. A brilliant scientist and a paragon of brevity and clarity in his spoken and written communication, he demands excellence not only from those under his responsibility but also from himself. Without him and a grant from NASA Johnson Space Center, this work would not have been possible. I would like to thank Bob Bragg and Eric Darcy at NASA Johnson Space Center for their interest in this work.

I would also like to acknowledge others who contributed to this thesis. I thank Reginald Penner for familiarizing me with the laboratory equipment. I thank Charles Brumlik, Mark Espenscheid, and James Long and Randy Scott for their help with the electron microscopy. I thank Del and Norma Lawson and Dr. Manuel Soriaga for sharing their computer expertise with me, as well as Susan Michelhaugh and Michael Bothwell. I thank Dr. John Appleby for sharing his knowledge about working with lithium. I thank Leon Van Dyke, with whom I worked on this project, for the countless hours he spent consulting with me on designing the experiments, carrying them out, analyzing the data and working on its presentation. I also thank Dr. Trung Nguyen for helpful discussions on data analysis. I thank my research group members and colleagues Lisa Whitely, Robert and Mary Lou Moore, Jorge and Marta Colon, David Liu, Edward Cai, J-T Lei, Arvind and Jayanthi Parthasarathy, Bhaskar and Sandra Dave, Joseph



and Nira Gruberger, Wen-Jang Chen, Tom Gregg, Michael Tierney, William Curtis, Wenbin Liang, and Frank Cheng for their support.

I would like to acknowledge Warren and Juanita Dowling and Brazos Christian School to whom I entrusted my children while I pursued this endeavor, as well as my brother Ted, my parents, and other friends and family members. I thank my friends at Parkway Baptist Church for nurturing my children and for their prayers of encouragement the past few years. My deepest appreciation goes to my husband Ralph, for his financial and moral support and the care he has shown for our children.

Finally, I would like to thank the Lord for His love, mercy and strength, and for giving me the ability to do this work.

## TABLE OF CONTENTS

	Page
ABSTRACT.....	iii
DEDICATION.....	v
ACKNOWLEDGMENTS.....	vi
TABLE OF CONTENTS.....	viii
LIST OF TABLES.....	ix
LIST OF FIGURES.....	x
LIST OF SYMBOLS.....	xiii
CHAPTER	
I    INTRODUCTION .....	1
II   EXPERIMENTAL.....	13
Materials.....	13
Equipment.....	13
Electrochemical Cell Design and Electrode Preparation..	14
Procedure for Preparing Electron Microscopy Stages.....	26
Battery Charge/Discharge Experiment .....	26
III  THEORETICAL.....	29
Mechanism of Polypyrrole Film Growth.....	29
Energy Density.....	30
IV  RESULTS AND DISCUSSION.....	47
Capacitance Studies and Electron Microscopy.....	47
Cyclic Voltammetry.....	59
Discussion of Battery Charge/Discharge Curves .....	63
V    CONCLUSIONS .....	103
REFERENCES.....	105
APPENDICES	
A    EXPERIMENTAL CHECKLIST.....	108
B    DEFINITIONS OF TERMS.....	110
VITA.....	112

## LIST OF TABLES

TABLE	Page
I Capacitive studies of Au/membrane electrodes .....	54
II Nuclepore® membrane data.....	57
III Energy densities.....	95
IV Energy efficiencies.....	97
V Coulombic efficiencies.....	99

## LIST OF FIGURES

FIGURE	Page
1 Structure of polypyrrole.....	1
2 Mechanism for the electrochemical polymerization of pyrrole...	2
3 Electron micrograph of a conventional polypyrrole film .....	3
4 A hypothetical Li/polypyrrole battery.....	5
5 Schematic cross-sectional diagram of the procedure for preparing fibrillar polypyrrole films.....	7
6 Electron micrograph of a fibrillar polypyrrole film.....	8
7 Schematic diagram of counterion diffusion in a conventional film vs. counterion diffusion in a fibrillar film.....	10
8 Schematic diagram of electrode employed for preparation of fibrillar polypyrrole films (38). a. 7 mm glass tube, b. Cu wire, c. Kel-f® electrode body, d. Ag epoxy contact, e. convex platinum disk, f. rubber collar, g. porous template membrane..	11
9 Schematic for Li/polypyrrole conventional film cathode.....	15
10 Schematic of preparation of fibrillar polypyrrole electrode.....	17
11 Electron micrograph of 0.2 $\mu\text{m}$ diameter polypyrrole fibrils prepared using Anopore® $\text{Al}_2\text{O}_3$ membrane as the template material.....	19
12 Schematic of fibrillar polypyrrole battery cathode .....	21
13 Schematic of polypyrrole battery reservoir.....	22
14 Schematic of Li/polypyrrole battery anode.....	24
15 Schematic of completely assembled Li/polypyrrole battery.....	25
16 Charge/discharge curve for Li/polypyrrole battery.....	34
17 Circuit diagrams for battery discharge. a. constant current discharge, b. constant load discharge, c. constant power discharge, d. constant potential discharge.....	36
18 Cross-section of fibrillar polypyrrole electrode .....	48
19 Nuclepore® polycarbonate membrane with 0.03 $\mu\text{m}$ pore	

## LIST OF FIGURES (Continued)

FIGURE	Page
diameter and sputtered with 0.01 $\mu\text{m}$ of Au at 3000 X magnification.....	50
20 Nuclepore <sup>®</sup> polycarbonate membrane with 0.03 $\mu\text{m}$ pore diameter and sputtered with 0.06 $\mu\text{m}$ of Au at 3,000 X magnification.....	51
21 Nuclepore <sup>®</sup> polycarbonate membrane with 0.03 $\mu\text{m}$ pore diameter and sputtered with 0.09 $\mu\text{m}$ of Au at 3,000 X magnification.....	52
22 Cross-section of fibrillar polypyrrole on gold surface with template membrane dissolved. 1.0 cm = 1.0 $\mu\text{m}$ .....	56
23 Electron micrograph of high density (@ $10^{10}$ pores/cm <sup>2</sup> ) Poretics <sup>®</sup> membrane. 1cm = 0.25 $\mu\text{m}$ .....	58
24 Scanning electron micrograph of the surface of an Anopore <sup>®</sup> filtration membrane with 0.2 $\mu\text{m}$ diameter pores.....	60
25 Cyclic voltammogram of Li/PPy battery with 2 $\mu\text{m}$ conventional PPy film. Scan rate = 1mV/sec. ....	62
26 $I_p$ vs. scan rate for 0.032 $\mu\text{m}$ conventional PPy film.....	64
27 $I_p$ vs. scan rate for 0.064 $\mu\text{m}$ conventional PPy film.....	65
28 $I_p$ vs. scan rate for 0.128 $\mu\text{m}$ conventional PPy film.....	66
29 $I_p$ vs. scan rate for 0.89 $\mu\text{m}$ conventional PPy film.....	67
30 Cyclic voltammogram of Li/PPy battery with 2 $\mu\text{m}$ fibrillar equivalent PPy film. Scan rate = 10 mV/sec.....	68
31 Cyclic voltammogram of PPy with amount of 1Q charge and irreversible oxidation region illustrated.....	70
32 Protocol for battery experiment.....	72
33 Charge/discharge curves of Li/PPy conventional film battery using 1Q CV charge. First three cycles. ....	73
34 Charge/discharge curves of Li/PPy conventional film battery using 2Q CV charge.....	74
35 Charge/discharge curves of Li/PPy conventional film battery using 3Q CV charge.....	75

## LIST OF FIGURES (Continued)

FIGURE	Page
36 Charge/discharge curve of Li/PPy conventional film battery using 4Q CV charge.....	76
37 Charge/discharge curves of Li/PPy fibrillar film battery using 1Q CV charge. First three cycles.....	77
38 Charge/discharge curves of Li/PPy fibrillar film battery using 2Q CV charge.....	78
39 Charge/discharge curves of Li/PPy fibrillar film battery using 3Q CV charge.....	78
40 Charge/discharge curves of Li/PPy fibrillar film battery using 4Q CV charge.....	80
41 Charge/discharge curve of Li/PPy fibrillar film battery using 5Q CV charge.....	81
42 Charge/discharge curves of Li/PPy conventional film battery using 1Q CV charge between 3 cycles each of 1Q, 2Q, 3Q, & 4Q CV charge.....	82
43 Charge/discharge curves of Li/PPy fibrillar film battery using 1Q CV charge between 3 cycles each of 1Q, 2Q, 3Q, & 4Q CV charge.....	83
44 Charge/discharge curves of Li/PPy conventional film battery and fibrillar film battery using 1Q CV charge.....	84
45 Charge/discharge curves of Li/PPy conventional film battery and fibrillar film battery using 2Q CV charge.....	85
46 Charge/discharge curves of Li/PPy conventional film battery and fibrillar film battery using 3Q CV charge.....	86
47 Charge/discharge curves of Li/PPy conventional film battery and fibrillar film battery using 4Q CV charge.....	87
48 Charge/discharge curves of Li/PPy conventional film battery using 1Q, 2Q, 3Q, & 4Q CV charge.....	89
49 Charge/discharge curves of Li/PPy fibrillar film battery using 1Q, 2Q, 3Q, 4Q & 5Q CV charge.....	90

## LIST OF SYMBOLS

SYMBOL	Meaning	Units
A	electrode area	cm <sup>2</sup>
A <sub>c</sub>	calculated electrode area	cm <sup>2</sup>
A <sub>g</sub>	geometric electrode area	cm <sup>2</sup>
A <sub>f</sub>	fractional electrode area	cm <sup>2</sup>
C	capacitance	microfarads
C <sub>o</sub> *	bulk concentration of oxidized species	moles/l
C <sub>p</sub>	practical capacity	microfarads
C <sub>t</sub>	theoretical capacity	microfarads
D <sub>o</sub>	diffusion coefficient	m <sup>2</sup> /sec
e. d.	energy density	watthours/kg
E	potential	volts
E <sup>o</sup>	standard electrode potential	volts
E <sub>ave</sub>	average discharge potential	volts
E <sub>cell</sub>	overall cell potential	volts
E	energy	watthours
F	Faraday's constant	96,487 coulombs/mole
g	gravitational constant	9.8 m/sec <sup>2</sup>
ΔG <sup>o</sup>	Gibbs free energy	joules
i	current density	milliamps/cm <sup>2</sup>
I	current	milliamps
I <sub>ave</sub>	average discharge current	milliamps
I <sub>c</sub>	capacitive current	microamps
I <sub>p</sub>	peak current	current
m	mass	kg
M	molecular weight	g/mole
n	number of moles of electrons	moles
Q	charge	coulombs
Q <sub>f</sub>	electropolymerization charge	coulombs
Q <sub>in</sub>	amount of charge injected	coulombs
Q <sub>out</sub>	amount of charge withdrawn	coulombs
t	time	seconds
t'	time of discharge	seconds
W	weight	lbf
v	scan rate	mV/sec
hν	photon energy	ergs

## CHAPTER I

### INTRODUCTION

Electronically conducting polymers are organic compounds which conduct electricity. They have extended  $\pi$ -conjugated backbones of alternating single and double bonds along the polymer chain (1). Many contain a ring structure which may include nitrogen, sulfur, or phosphorous in the ring. An example of such a polymer is polypyrrole (1,2) (Fig. 1).

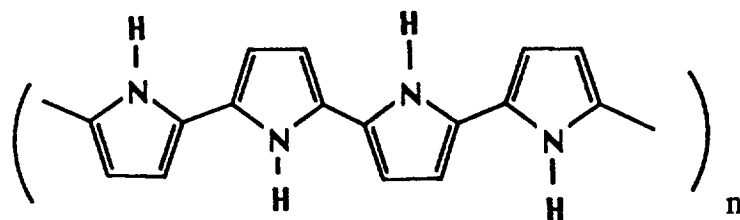


Figure 1. Structure of Polypyrrole

Polypyrrole can be electrochemically synthesized by the oxidation of pyrrole monomer at an electrode surface. A film of polypyrrole is formed (3) which adheres to the electrode surface (Fig. 2). An electron micrograph of the surface of a polypyrrole film is shown in Fig. (3). Anions are incorporated into the film during polymerization and the film is said to be "doped" with anions. Polypyrrole is positively charged when doped, so it is referred to as a "p-doped" electronically conducting

---

The format of this thesis follows that of the Journal of the Electrochemical Society.



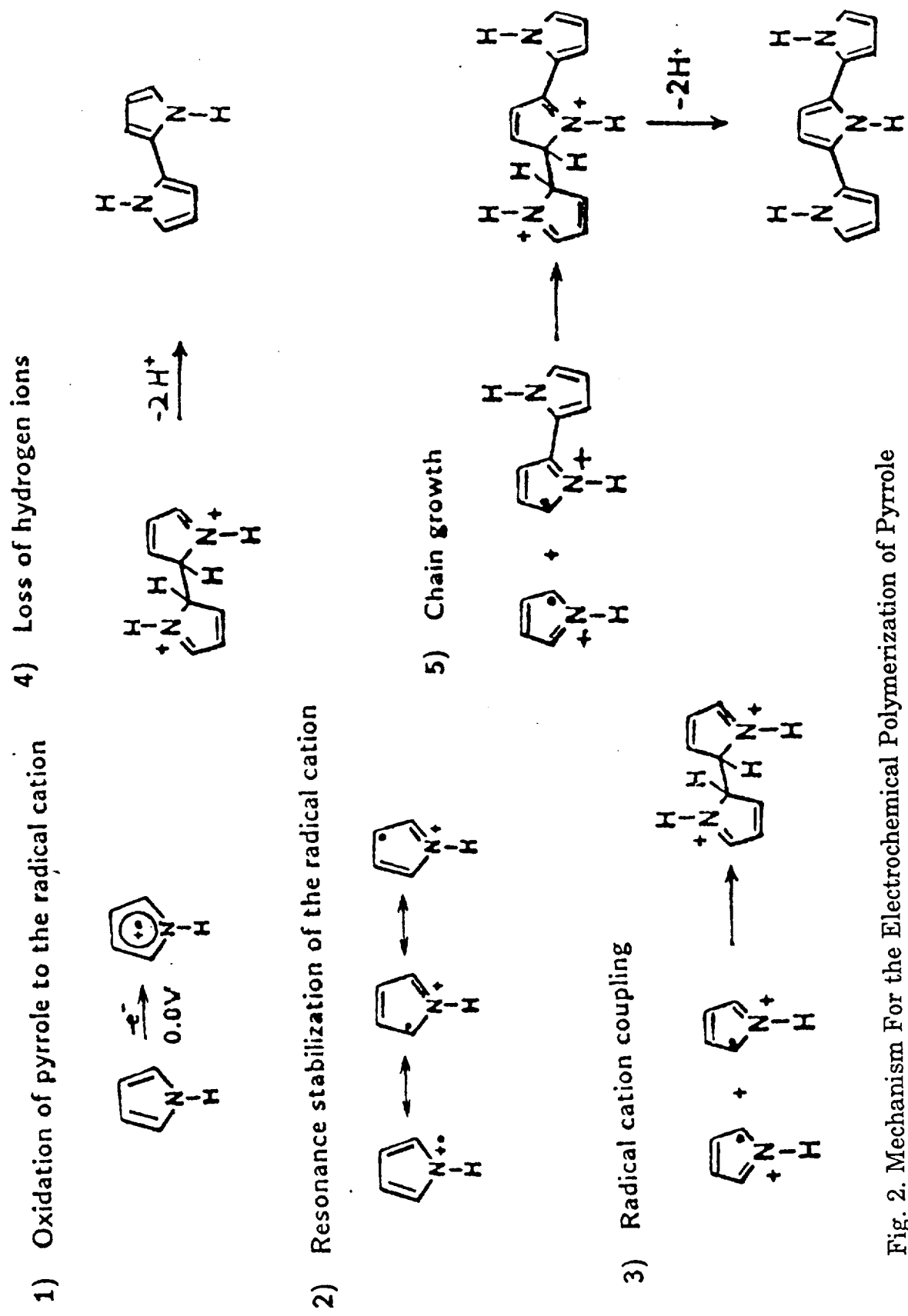


Fig. 2. Mechanism For the Electrochemical Polymerization of Pyrrole

ORIGINAL PAGE  
BLACK AND WHITE PHOTOGRAPH

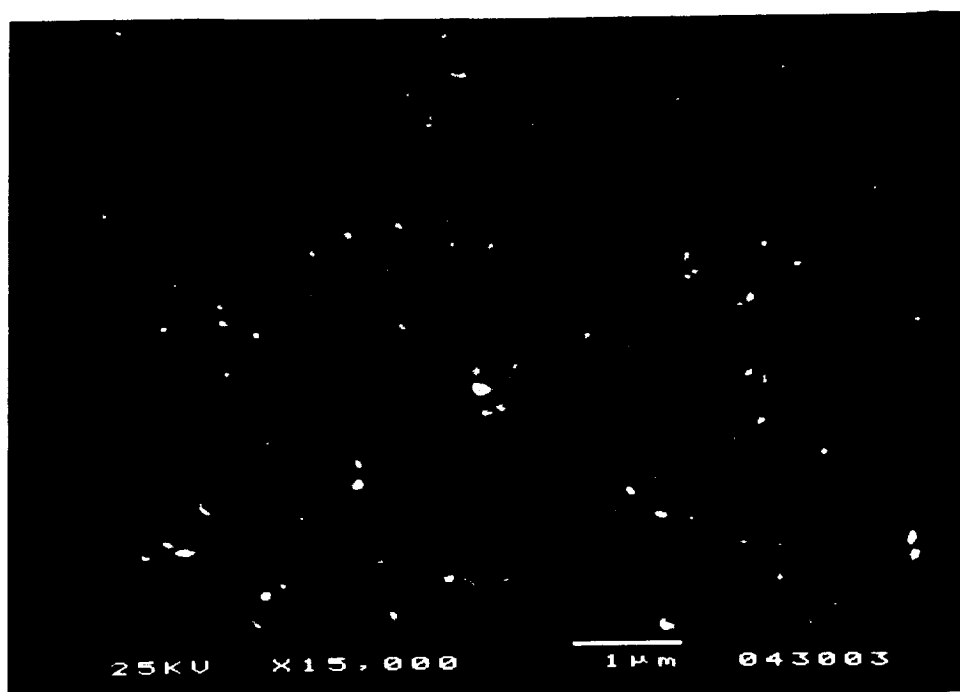
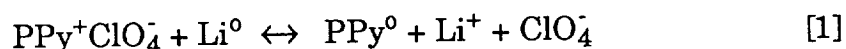


Fig. 3. Electron Micrograph of a Conventional Polypyrrole Film.

ORIGINAL PAGE IS  
OF POOR QUALITY

polymer. The positive charge is delocalized by the  $\pi$ -conjugated system of the polymer (Fig. 1). When the film is fully doped, polypyrrole has one positive charge, and likewise one anion, for every 3-4 pyrrole monomer units (4).

While polypyrrole (PPy) is synthesized in its oxidized (p-doped) form, it can be reduced to a neutral form. For example, polypyrrole can be reduced by metallic Li; the counterion is expelled from the polymer during reduction.



This oxidation/reduction process is reversible. Oxidation can be viewed as charge storage, and reduction can be viewed as release of stored charge. For this reason, and because conducting polymers are lightweight materials, conducting polymers have been explored as cathode materials in secondary lithium batteries (5-28).

A schematic of a hypothetical Li/PPy battery is shown in Fig. 4. Of particular interest in battery applications is the relatively high doping level of the polypyrrole and the possibility of switching it quickly and reversibly from the oxidized form to the reduced form (Eq. [1]). Since the switching is reversible, a battery made with polypyrrole would be rechargeable.

A fast switching reaction rate means that a battery utilizing such an electrode could be discharged at a high rate, or amperage, which in turn means that it could handle a greater load. When oxidizing or reducing polypyrrole, the rate determining step is counterion diffusion in the polymer phase (29-32). When the film is oxidized, counterions are incorporated into the film to maintain charge neutrality in the film. During reduction, anions have to diffuse out of the polymer phase into

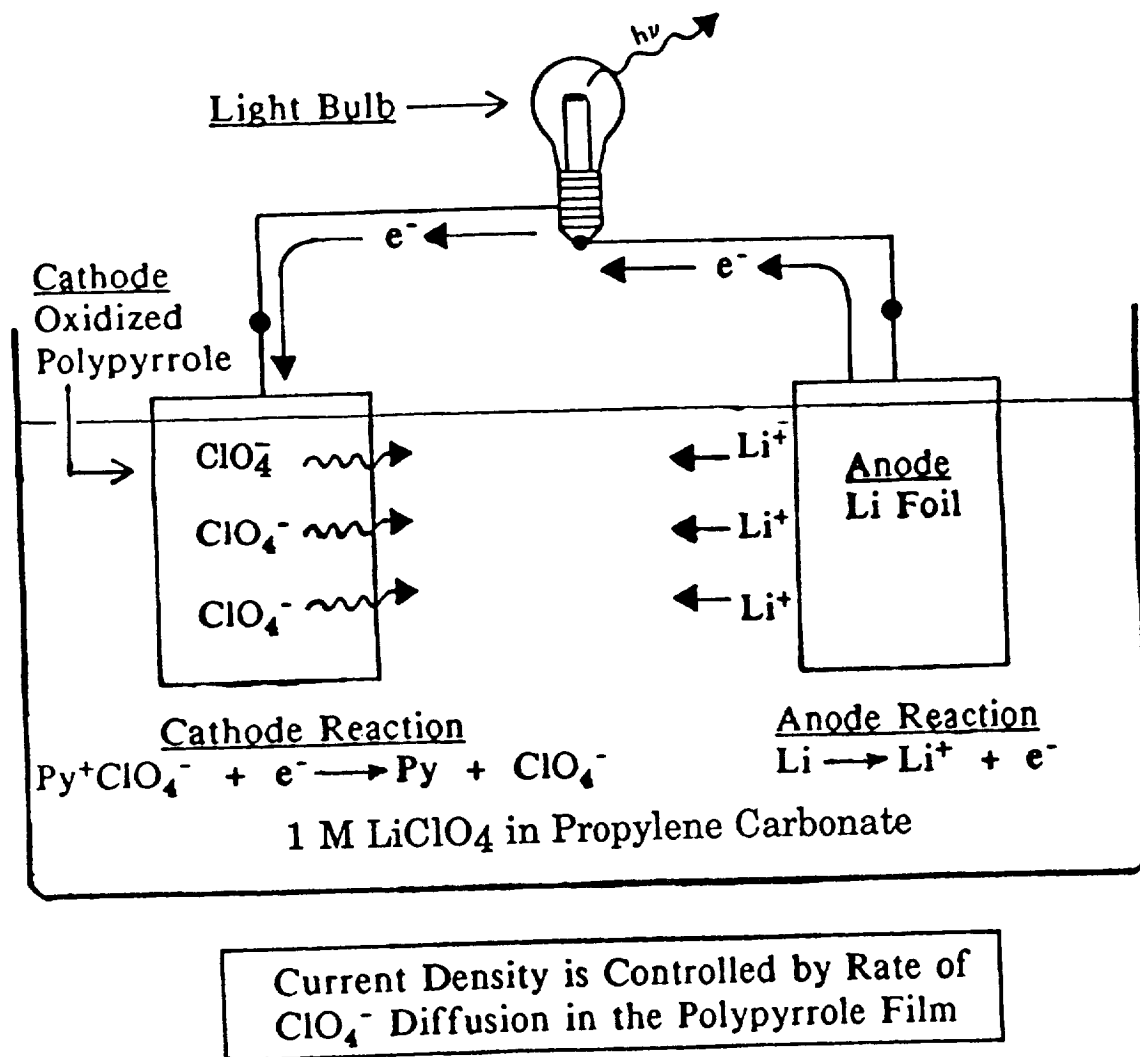


Fig. 4. A Hypothetical Li/Polypyrrole Battery.

the solution phase to maintain the film's charge balance. If the rate of ion transport in the polymer phase could be increased, better battery performance would be obtained. Unfortunately, ion transport in a thick film of conventionally grown polypyrrole is slower than in a thin film (15, 18, 29, 33-35). Therefore, growing a thicker film of polypyrrole does not enhance battery performance (13, 17). Also, charge trapping occurs as oxidized pyrrole sites are isolated by proximate polymer chains in a conventionally grown film. As a result, the polymer cannot become fully doped. However, if the morphology of the film can be changed so that ion transport is facilitated, a higher doping level would result and a battery made with the polymer could be discharged at a higher rate.

Previous research in this laboratory (36) investigated the effect of controlling the morphology of the polymer on enhancement of counterion diffusion in the polymer phase. A method of preparing conducting polymers was developed which yields a much higher surface area per unit volume of polymer than conventionally grown polypyrrole films. A film with a higher surface area results in a greater number of electroactive sites being accessible to counterions. The film is grown in a fibrillar form by using a porous membrane as a template. The membrane is attached to the electrode surface, then the electrode is introduced into a solution containing pyrrole monomer. The pyrrole is polymerized potentiostatically in the pores of the membrane, then the membrane is dissolved away, leaving behind the polypyrrole fibrils standing upright on the electrode surface (Fig. 5). An electron micrograph of 2000 Å diameter fibrils is shown in Fig. 6.

Counterions can diffuse much faster in the solution phase than in the polymer phase (31). Theoretically, the longest distance a counterion

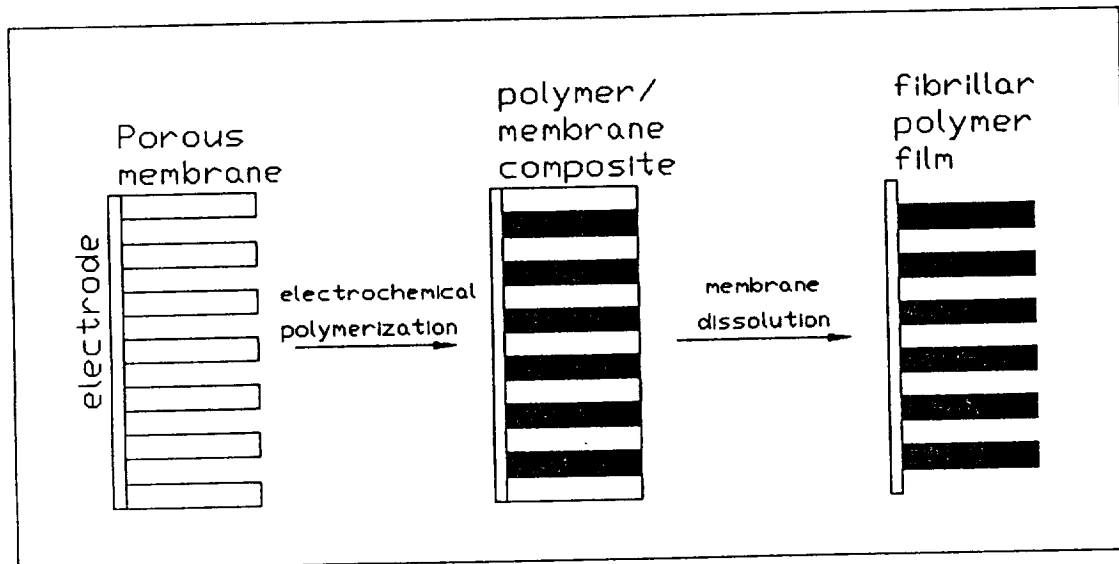


Fig. 5. Schematic Cross-Sectional Diagram of the Procedure for Preparing Fibrillar Conducting Polymer Films.

ORIGINAL PAGE  
BLACK AND WHITE PHOTOGRAPH

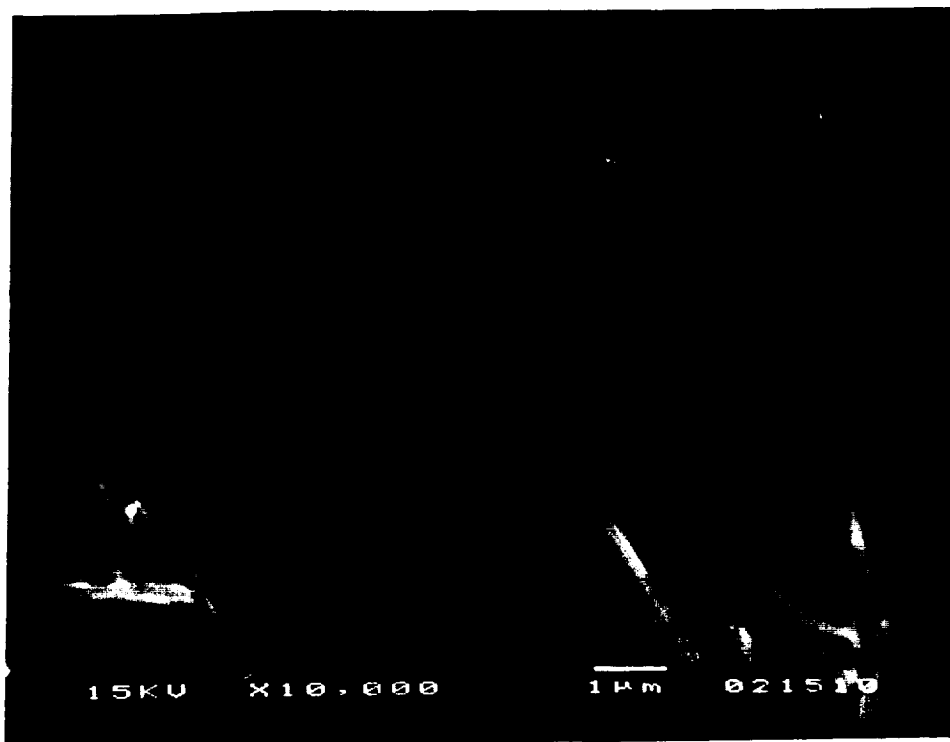


Fig. 6. Electron Micrograph of a Fibrillar Polypyrrole Film.

ORIGINAL PAGE IS  
OF POOR QUALITY

would have to diffuse in the fibrillar film before reaching the solution phase would be half the diameter of one of the fibrils, as illustrated in Fig. 7. Therefore, a fibrillar film should show a faster switching rate than a conventionally grown dense polymer film with the same electrode area and a comparable amount of polymer. Previous work (37, 38) has shown that when the polymer is electrochemically polymerized in fibrillar form, the fibrils produce a faster charge transfer rate, greater charge capacities, and higher doping level than a conventionally grown film.

Following this work, attempts have been made to improve the performance of these electrodes by making the diameter of the fibrils smaller. A smaller fibril diameter would provide the counterion an even shorter diffusion path from polymer phase to solution phase, and ion transport should be facilitated. Investigation showed that although the performance of the smaller diameter fibrils was better, the current density and charge capacity did not increase proportionately with decreasing fibril diameter, as expected (36). This could be due to the growth of a base layer of polypyrrole between the porous template membrane and the platinum substrate of the electrode. For 0.2 micron fibrils, this base layer was as thick as 0.3-0.5 microns (36). A detailed schematic of an electrode used to make fibrillar films is shown in Fig. 8. The template membrane was stretched across a platinum electrode ('e' of Fig. 8) and held in place by a rubber sheath ('f' of Fig. 8). When the electrode was immersed in solution containing pyrrole monomer, some of the solution leaked into the space between the platinum substrate and the template membrane ('g' of Fig. 8). Upon application of potential, the pyrrole present in the solution between the platinum and the membrane



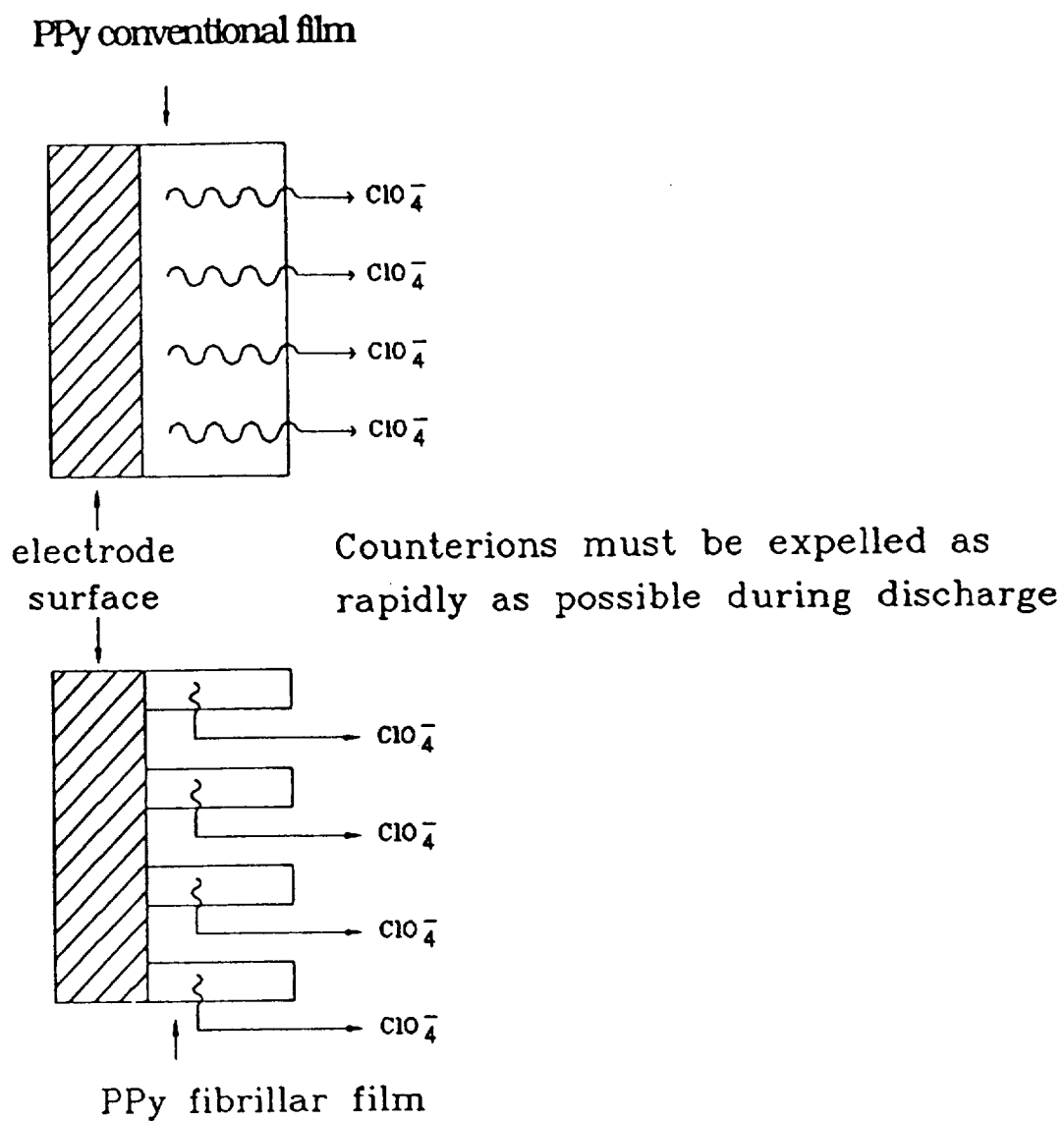


Fig. 7. Schematic Diagram of Counterion Diffusion in a Conventional Film vs. Counterion Diffusion in a Fibrillar Film. Counterions Can Be Expelled More Rapidly in a Fibrillar Film.

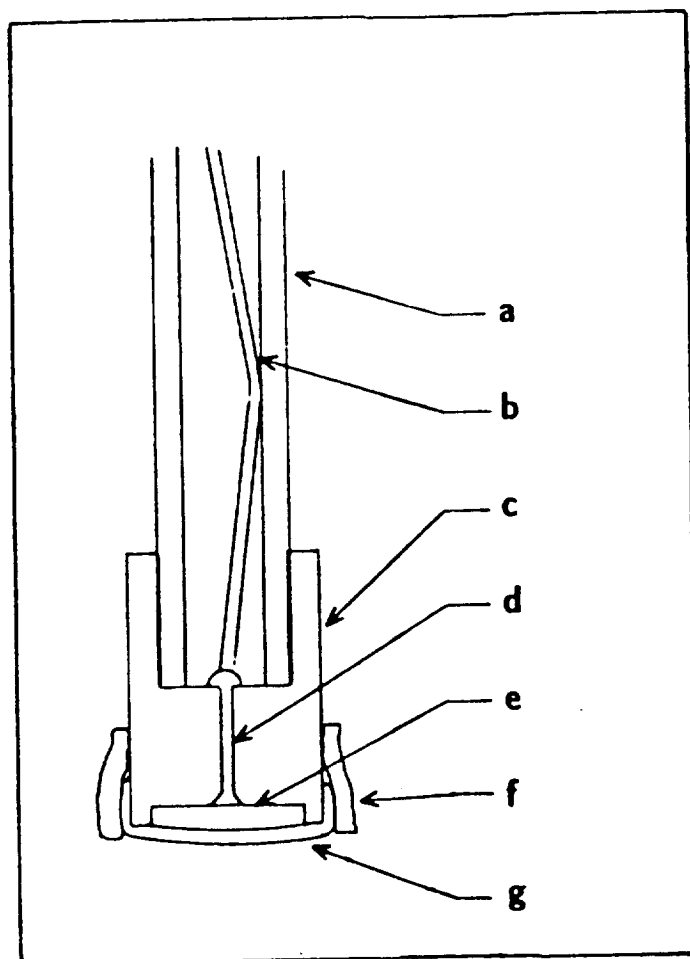


Fig.8. Schematic Diagram of Electrode Employed for Preparation of Fibrillar Polypyrrole Films (38). a. 7mm Glass Tube, b. Cu Wire, c. Kel-f<sup>®</sup> Electrode Body, d. Ag Epoxy Contact, e. Convex Platinum Disk, f. Rubber Collar, g. Porous Template Membrane.

was polymerized to form a base layer of polypyrrole.

It is logical to assume that a base layer of polypyrrole which is thicker than the fibril diameter itself would serve to negate the advantages of fibrillar morphology described above. Since the base layer of polypyrrole would have to be oxidized and reduced as well as the fibrils, the switching reaction rate of the entire film would be slowed. Eliminating this base layer would allow determination of whether using smaller fibril diameters would provide faster ion transport and greater charge capacity. One of the objectives of this work was to develop a procedure for synthesizing fibrillar polypyrrole that does not have a base layer of conventional polypyrrole.

In this work, a Li/Polypyrrole secondary battery is described. The purpose of this work is to expand previous work by further investigating the possibilities of the optimization of transport rates in polypyrrole films by controlling the morphology of the films and eliminating the formation of a polypyrrole base layer. The utility of fibrillar polypyrrole as a cathode material in a lithium/polymer secondary battery is then assessed. The performance of the fibrillar battery is compared to the performance of an analogous battery which employed a conventionally grown polypyrrole film. The study includes a comparison of cyclic voltammetry, shape of charge/discharge curves, discharge times and voltages, cycle life, coulombic efficiencies, charge capacities, energy densities, and energy efficiencies.

## CHAPTER II

### EXPERIMENTAL

Materials. The electrolyte used for some of the cyclic voltammetry studies was 0.2 M  $\text{Et}_4\text{BF}_4$  (Aldrich) in acetonitrile (UV grade, Burdick and Jackson). The tetraethyl ammonium salt ( $\text{Et}_4\text{BF}_4$ ) was recrystallized twice from methanol and dried in a vacuum oven 24 hours at  $100^\circ\text{C}$  before use. Acetonitrile was used as received and was stored over 4A molecular sieves or  $\text{CaH}_2$ . Orotemp 24 Au(I)CN gold plating solution was used for fabrication of fibrillar electrodes. Nuclepore<sup>®</sup> and Poretics<sup>®</sup> polycarbonate membranes as well as Anopore<sup>®</sup>  $\text{Al}_2\text{O}_3$  membranes were used as template materials for the synthesis of the fibrillar polypyrrole.

The electrolyte used for the battery work was 1 M  $\text{LiClO}_4$  in propylene carbonate (4-methyl-1,3-dioxolan-2-one). Propylene carbonate (Burdick and Jackson) was fractionally distilled under vacuum before use and the second of three fractions was retained for use. The  $\text{LiClO}_4$  (Fluka) was heated at  $100^\circ\text{C}$  in a vacuum oven for 24 hours to eliminate any absorbed water. Pyrrole (99%, Aldrich), used for electropolymerization of the polypyrrole, was distilled under nitrogen prior to use. Platinum foil (Alfa, 0.25 mm thick) imbedded in inert Kel-f<sup>®</sup> (3/8" diameter, Afton Plastics) was used as a current collector for conventionally grown polypyrrole film electrodes. Lithium foil (Alfa) and Ni gauze (20x20 mesh, 0.014" wire diameter, 99.75 %, Newark Wire Cloth) were used to make the lithium electrode.

Equipment. All work involving lithium batteries was done in a glove box to prevent oxidation of the lithium electrode by atmospheric oxygen.

Polypyrrole is also subject to permanent oxidation by atmospheric oxygen, but is stable at higher levels of O<sub>2</sub> than lithium. Therefore, cyclic voltammetry studies involving a polypyrrole working electrode and a platinum counter electrode were done in a glove bag rather than a glove box. The glove box used for the lithium battery studies was made by Vacuum Atmospheres Corporation and was equipped with a Dri-Train<sup>®</sup> atmosphere regenerator and a Photohelic<sup>®</sup> pressure sensor and controller. Glove bags for cyclic voltammetry studies not involving lithium were obtained from Instruments for Industry and Research (I<sup>2</sup>R). An EG&G PAR Model 273 Potentiostat/Galvanostat was used for cyclic voltammetry, potential step experiments, and battery charge/discharge studies. A Soltec VP-6424S X-Y recorder was used to record cyclic voltammograms and a Linear strip-chart recorder was used for recording battery charges and discharges. A 3.5 digit Metex M-3650 digital voltmeter was used to check electrode resistances and circuit voltages and currents. Data analysis was conducted using a Macintosh IICI computer with Cricketgraph<sup>®</sup> and Kaleidagraph<sup>®</sup> software. Schematics were drawn using an IBM Model 50 PS/2 with Autocad<sup>®</sup> software and a Macintosh IICI computer with Superpaint<sup>®</sup>.

Electrochemical cell design and electrode preparation. Figure 9 shows a schematic of the polypyrrole film electrode, which is the cathode during battery discharge. The polypyrrole electrode will henceforth be referred to as the cathode and the lithium electrode will be referred to as the anode, since the lithium electrode acts as the anode during battery discharge. Two types of polypyrrole films were used in performing these studies. One was a dense mat film electropolymerized on a Pt disk

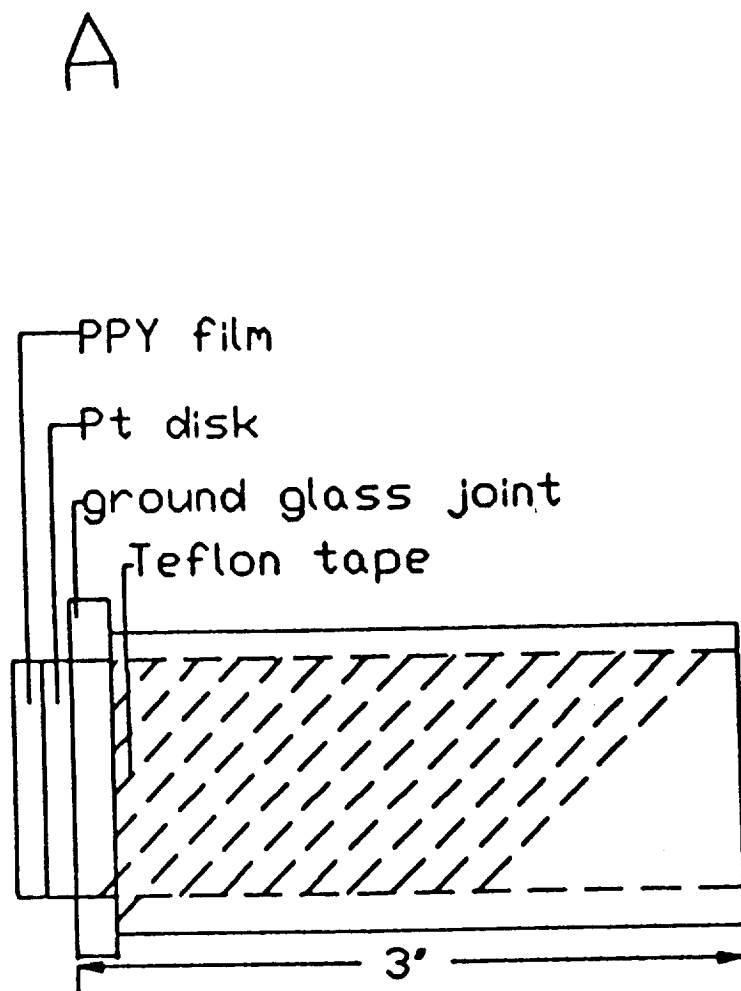


Fig. 9. Schematic for Li/Polypyrrole Conventional Film Cathode.

electrode; such films have been the subject of much investigation (5, 6, 9, 10, 13, 14, 16-18). This type of film will be referred to, henceforth, as a "conventional polypyrrole film."

Conventional polypyrrole films were made by constant-current polymerization of pyrrole at a platinum disk electrode at  $1 \text{ mA/cm}^2$ . A charge of 376 mC was passed, which resulted in a film that was  $2 \mu\text{m}$  thick (36). Figure 9 shows the battery cathode with a conventional polypyrrole film. An electron micrograph of a conventional polypyrrole film is shown in Fig. 3. The film was grown on a platinum disk, which was heat-sealed onto a piece of Kel-f<sup>®</sup> rod with a hole drilled in the center. Electrical contact was made by silver epoxy and a copper wire through the hole in the Kel-f<sup>®</sup>. The electrode was held in place by an electrode holder made of teflon rod and housed in glass tubing.

The surface of the electrode was renewed between experiments by polishing with 0.5 micron alumina, rinsing it with Millipore<sup>®</sup> deionized water, and drying it with a heat gun to reseal it. Teflon tape was used to seal the teflon electrode holder into its glass housing if needed. One end of the glass tubing was flared and had a ground glass joint. This type of joint was chosen because it seals well and allows for facile assembly and disassembly of the cell, which was particularly important when working in the glove box.

The other type of polypyrrole film studied in this work was electropolymerized using a template membrane; this polypyrrole has a fibrillar morphology and will be referred to as a "fibrillar polypyrrole film." Figure 10 is a detailed schematic that illustrates how fibrillar polypyrrole films were made (39). Fibrillar films were prepared by first sputter depositing a thin layer of gold on an  $\text{Al}_2\text{O}_3$  template membrane

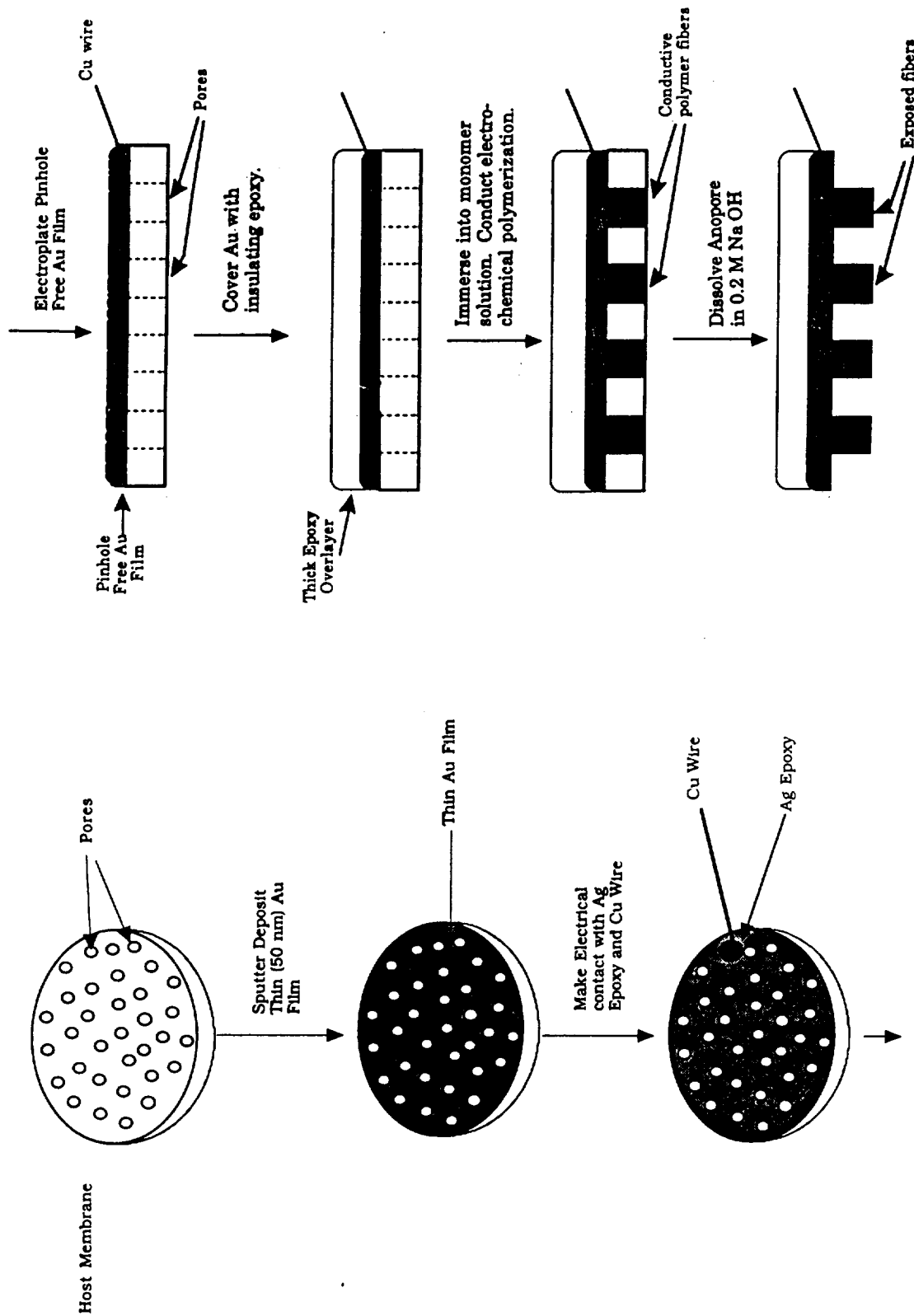


Fig. 10. Schematic of Preparation of Fibrillar Polypyrrole Electrode.



to make it conductive. Electrical contact was then made with silver epoxy and a copper wire. The electrode was immersed in gold plating solution and electroplated until a pinhole-free Au film was obtained on one side of the electrode. The electrode was then coated with Torr-Seal<sup>®</sup>, an inert epoxy, except for the portion which is to be exposed to solution.

Next, the electrode was immersed into a solution of 1 M LiClO<sub>4</sub> and 0.5 M pyrrole in propylene carbonate. Pyrrole is polymerized in the pores of the template membrane at a constant current of 1 mA/cm<sup>2</sup> until 376 mC are passed, which is the same amount of charge passed when growing a 2 μm thick conventional film.

The template membrane was then dissolved, leaving behind the polypyrrole fibrils standing upright (Fig 11). The medium used for dissolution depended on the chemical identity of the membrane. Methylene chloride was used for polycarbonate membranes and 1 M NaOH was used for Al<sub>2</sub>O<sub>3</sub> Anopore<sup>®</sup> membranes. Anopore<sup>®</sup> membranes have a pore diameter of 2000 Å, while the polycarbonate membranes used had pore diameters ranging from 300 Å to 10,000 Å. The fibril diameter is the same as the pore diameter of the template membrane used to make it. After dissolution of the membrane, the fibrillar film is treated with acid to reprotonate the polypyrrole. For some of the cyclic voltammetry studies, where NH<sub>4</sub>BF<sub>4</sub> was used as the electrolyte, HBF<sub>4</sub> was used to reprotonate. For the battery studies, HClO<sub>4</sub> was used as the acid because the electrolyte employed was LiClO<sub>4</sub>. Therefore, it is ensured that there is only one anion present in each system. After rinsing with fresh electrolyte solution, the fibrillar film is ready to be used for cyclic voltammetry and battery charge/discharge experiments.

ORIGINAL PAGE  
BLACK AND WHITE PHOTOGRAPH

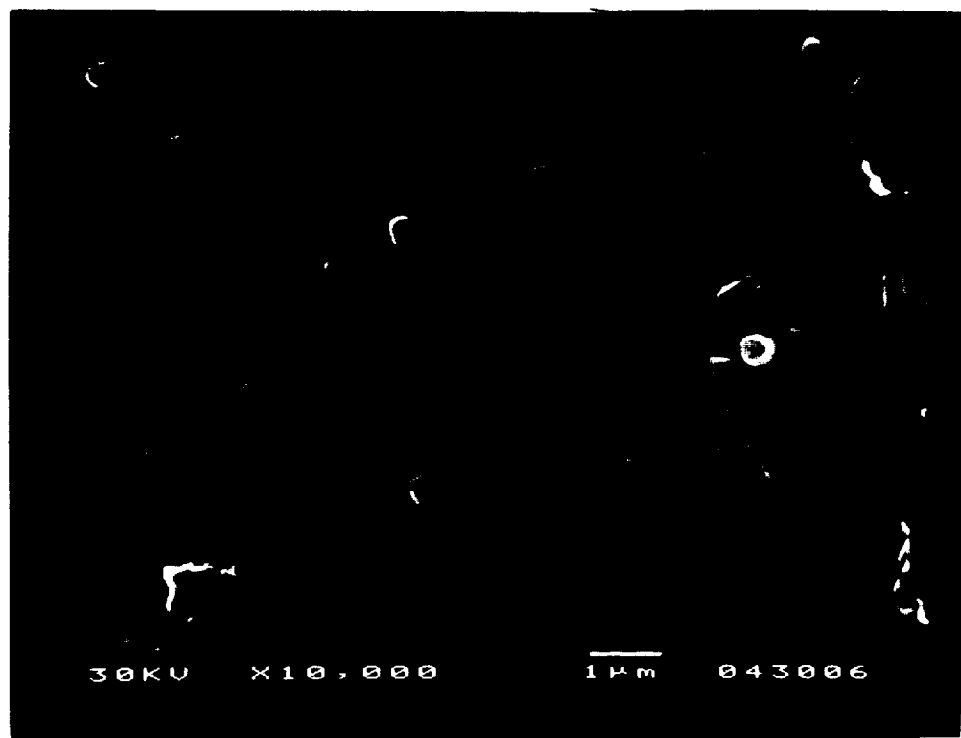


Fig. 11. Electron Micrograph of 0.2  $\mu\text{m}$  Diameter Polypyrrole Fibrils Prepared Using Anopore<sup>®</sup>  $\text{Al}_2\text{O}_3$  Membrane as the Template Material.

ORIGINAL PAGE IS  
OF POOR QUALITY

Figure 12 is a schematic of a battery cathode used to make a fibrillar polypyrrole film. A gold-coated Anopore<sup>®</sup> electrode is attached to one side of a Kel-f<sup>®</sup> plug with silver epoxy before inserting it into the teflon electrode holder. Electrical contact is made from the other side of the Kel-f plug with silver epoxy and a copper wire. The wire runs out of the cell through a hole drilled in the teflon rod. Since Anopore<sup>®</sup> membranes are very brittle, they were sometimes attached to a thin ring of glass tubing with five minute epoxy to give them mechanical stability during electrode assembly. The glass tubing and surrounding epoxy were removed before the electrode was used.

Figure 13 is a schematic of the battery cell reservoir. It is made of glass and has a ground glass joint at each end. A glass reservoir is used so that the electrodes and solution can be observed visually. The polypyrrole film could become separated from its current collector or the lithium anode could become passivated during the course of the experiment. Also, degradation of the solvent could occur, evidenced by discoloration of the solution. Being able to monitor visually the experiment in progress prevents erroneous data from being collected and saves valuable time. There is an opening in the top of the solution reservoir to allow the solution to be introduced into the cell. It also serves as a receptacle for the reference electrode. The reference electrode used for battery studies was a Ag/AgNO<sub>3</sub> reference electrode. The Ag/AgNO<sub>3</sub> reference was chosen because both the SCE and AgCl references proved unsuitable. The SCE contains an aqueous solution, which, if it leaked into the cell, could passivate the lithium anode. The AgCl reference was ruled out because AgCl is too soluble in propylene carbonate. For some cyclic voltammetric studies carried out in acetonitrile, however, a SCE

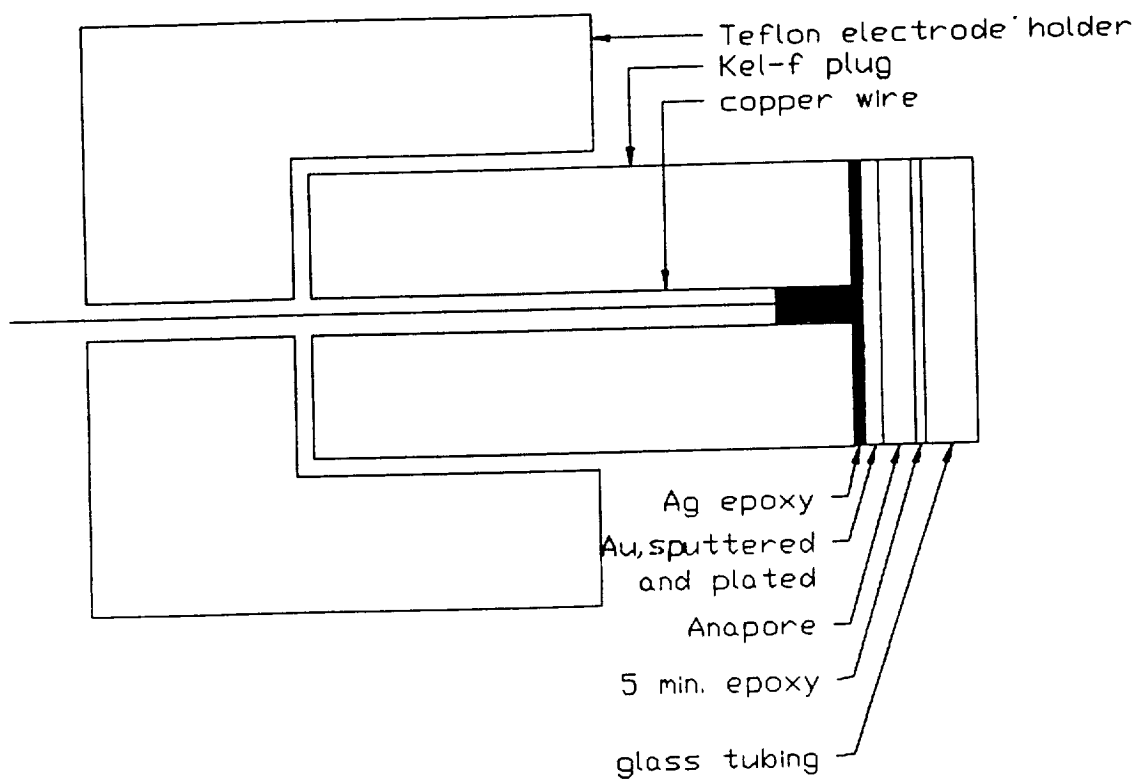


Fig. 12. Schematic of Fibrillar Polypyrrole Battery Cathode.

B

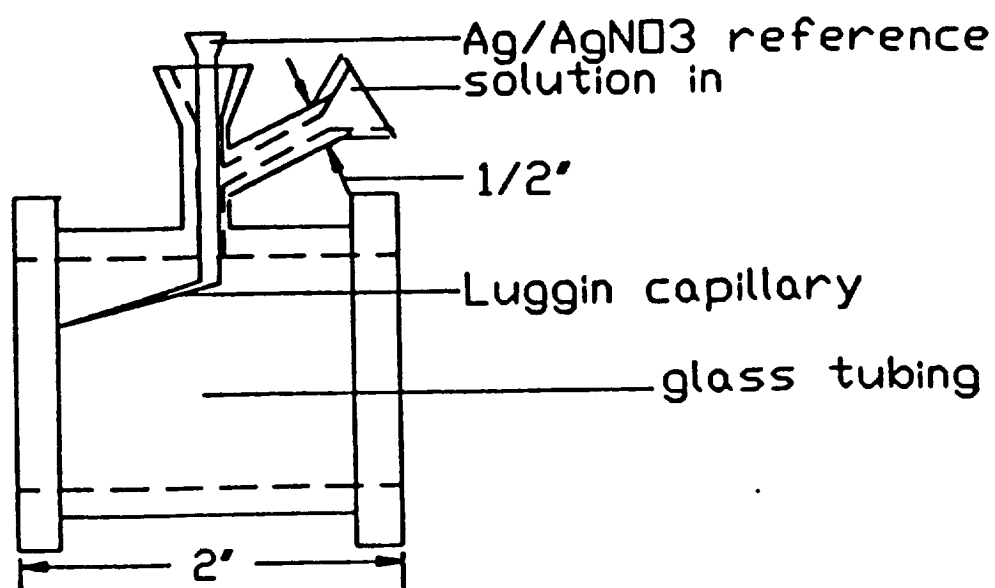


Fig. 13. Schematic of Polypyrrole Battery Reservoir.

reference electrode was used.

Figure 14 is a schematic of the lithium anode. It was constructed by first spot welding a 3/8 inch diameter disc of Ni gauze to a Ni wire. The gauze served as the current collector and the Ni wire served as the electrical contact. The gauze was then imbedded in a Kel-f<sup>®</sup> plug with the Ni gauze on one side and the Ni wire running out the other side. Lithium foil was pressed onto the Ni gauze and was allowed to cold-weld. The lithium electrode was then placed in a teflon electrode holder equipped with a screw mechanism. This mechanism was used to control the position of the electrode in the electrochemical cell. Before each experiment, the surface of the lithium electrode was renewed by scraping the passivated portion with a scalpel. The screw mechanism was then employed to return the electrode to its original position in the cell. The completely assembled cell is shown in Fig. 15. It is held together with two large metal clamps. An O-ring is used in the joint between the cell reservoir and the anode since the electrode holder for the anode is made out of teflon rather than glass.

As mentioned earlier, cyclic voltammetry studies involving a polypyrrole film-coated working electrode and a platinum counter electrode were done in a glove bag using a 5 dram vial as a cell reservoir. The platinum counter electrode consisted of a 3/8 inch Pt disk spot welded to a Pt wire, which was heat sealed in glass tubing. It was cleaned by soaking it in chromic acid 5-10 minutes on low heat. All solutions were degassed for 20-30 minutes before use in the glove bag or glove box. Also, for the cyclic voltammetric studies using the glove bag, 1% water (0.15 cc in 15 ml) was used in the pyrrole polymerization solution as in previous work done in this laboratory and by Diaz (3, 37). Water was not used for

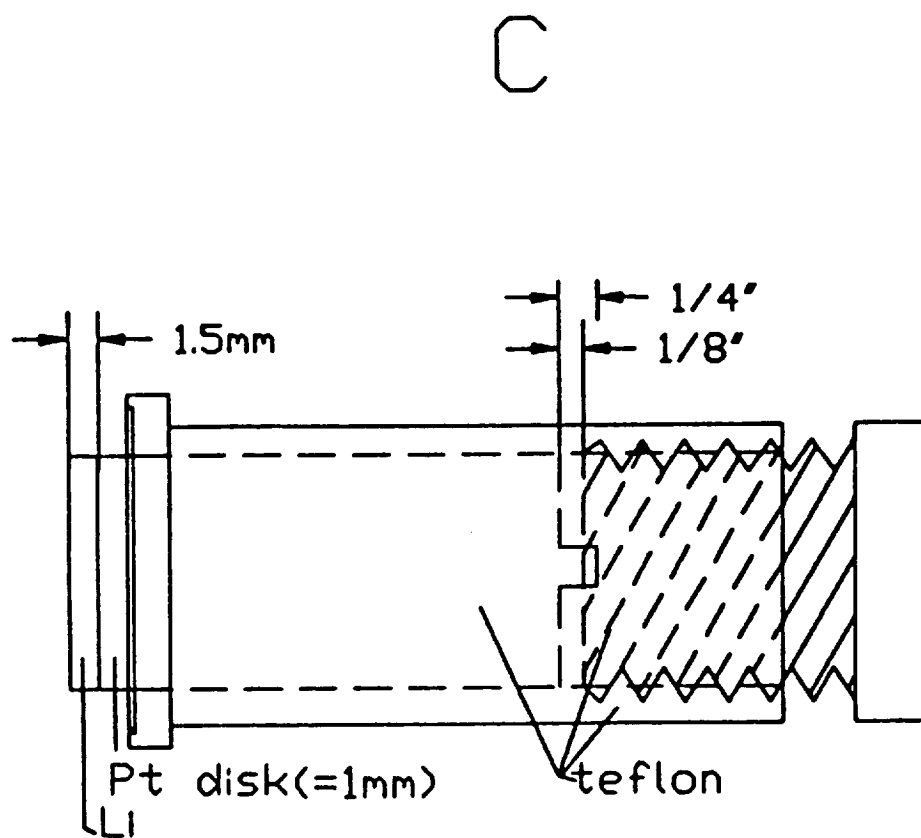


Fig. 14. Schematic of Li/Polypyrrole Battery Anode.

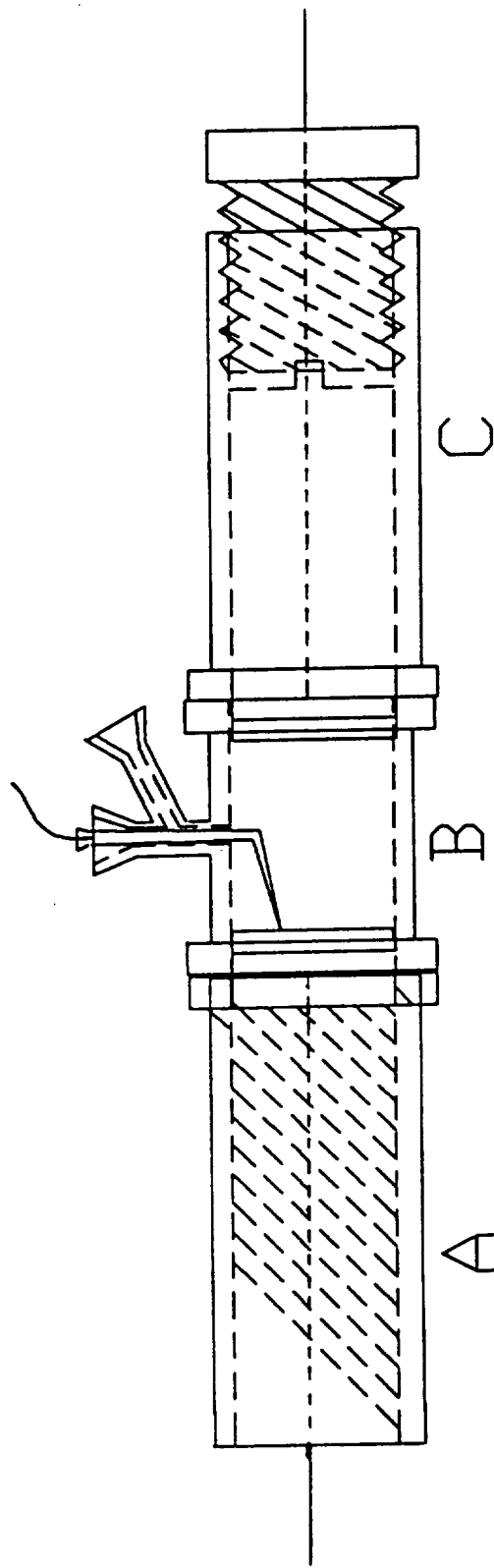


Fig. 15. Schematic of Completely Assembled Li/Polypyrrole Battery.



polymerization in any studies involving lithium.

Procedure for preparing electron microscopy stages. Stages for electron microscopy were made from 3/8 inch long sections of stainless steel rod (3/8 inch diameter). One end was polished with 1  $\mu\text{m}$  alumina so that it could serve as a level base for mounting samples. Samples were mounted using either carbon paint or silver epoxy and sputter deposited with approximately 100  $\text{\AA}$  of gold. The samples were allowed to air dry 24 hours before electron microscopy was conducted. This method of preparing samples ensures that the samples are sufficiently conductive and are completely dry so that no outgassing occurs in the vacuum chamber of the electron microscope. The surface of some of the electron microscopy stages were ground at a 45° or 90° angle so that the edge of the sample could be viewed and photographed.

Battery charge/discharge experiment. Solutions used in the battery charge/discharge experiment and a materials checklist are presented in Appendix A. The battery charge/discharge experiment was conducted as follows. First, the atmosphere in the glove box was checked. If the oxygen or moisture content was too high, it was purged until the  $\text{O}_2$  content was under 10 ppm and the  $\text{H}_2\text{O}$  concentration is less than 20 ppm. This was determined by keeping a vial of  $\text{TiCl}_4$  and a vial of  $\text{Et}_2\text{Zn}$  in the glove box.  $\text{TiCl}_4$  will vaporize at 10 ppm of  $\text{H}_2\text{O}$  and  $\text{Et}_2\text{Zn}$  will vaporize at 20 ppm  $\text{O}_2$ . After the cell was assembled and checked for leaks, the solution in the  $\text{Ag}/\text{AgNO}_3$  reference electrode was checked for clarity. If it was black, there was metallic silver present and the frit could have been clogged. To ascertain whether the electrode was still serviceable, the resistance was checked with a multimeter and a silver

wire in an electrolyte solution to see if the electrode was still conductive. Also, if there was another Ag/AgNO<sub>3</sub> reference electrode available, the potential difference between them was checked with the multimeter. If there was a difference of only a few millivolts, the electrode was still considered serviceable. If the electrode was not conductive or had a potential more than a few millivolts different from another Ag/AgNO<sub>3</sub> reference, it was replaced.

A background cyclic voltammogram from +0.4 V to -1.25 V vs. Ag/AgNO<sub>3</sub> was conducted before growing the polypyrrole film. The cell was then returned to open circuit while the pyrrole monomer solution was added and mixed. After programming the PAR 273 in the galvanostatic mode and resetting the coulometer, the polypyrrole film was grown ( -0.32 mA , 567 sec for conventional films; -0.3 mA, 604 sec for fibrillar films). The potential during polymerization was about 0.6 V vs. Ag/AgNO<sub>3</sub>. The cell was again returned to open circuit and if the film was fibrillar, the template membrane was dissolved. This was accomplished by continuous stirring in 0.2 M NaOH solution for approximately 30 minutes. The film was then gently rinsed with dry propylene carbonate and exposed to 1% HClO<sub>4</sub> for approximately five minutes while being stirred continuously. The film was returned to the cell, which contained fresh electrolyte solution. The film was potentiostatically reduced at -1.25 V vs Ag/AgNO<sub>3</sub>, a cyclic voltammogram was conducted, then the film was reduced again. The galvanostat was then programmed to conduct a constant current charge/discharge experiment. The battery was charged at -0.032 mA for 600 sec for a conventional film and at -0.03 mA for a fibrillar film. Though the currents used for the two types of films were slightly different, the

current densities were the same. Cycling was continued using more increments of charge until the battery failed. After the completion of the battery charge/discharge experiment, another cyclic voltammetry was conducted to ascertain that the polypyrrole film was irreversibly damaged.

## CHAPTER III

### THEORETICAL

Mechanism of polypyrrole film growth. In order to understand the calculation of the amount of polymer deposited on the electrode when a certain amount of charge is passed, the subjects of polymerization, chain propagation and electronic conduction along a chain must be addressed. A repeating unit of polymer with a known number of counterions involved in the doping reaction is needed in order to calculate amount of polymer deposited on the electrode. In addition, the doping level is needed to calculate the energy density of the battery. Polymerization of polypyrrole can be accomplished either chemically (27) or electrochemically (3). For the entire body of this work, electrochemical polymerization was employed.

First, pyrrole monomer is oxidized at the electrode surface by removal of an electron from the monomer. The radical cation formed undergoes resonance stabilization (Fig. 2). Chain formation begins when two radical cations couple and two hydrogen ions are given off, leaving two neutral pyrrole monomers joined. Chain growth continues as free radical cations attack sites on the end of existing polypyrrole chains. As is evident from Fig. 2, two electrons are removed during polymerization to form a dimer, and two more are removed to form a trimer. Likewise, two more must be removed to form a tetramer. In order for the tetramer to be part of a repeating unit on a polymer chain, another two electrons must be removed.

Previous work by Diaz (3) suggests a 25% doping level for polypyrrole. One counterion is assumed present for each repeating unit of four

pyrrole monomers. Therefore, there is an additional electron taken away for every four monomer units when the polymer is in its oxidized form, as it is at the time of polymerization. This means that 2.25 electrons are required from each monomer unit for polymerization. Calculation of the amount of polymer deposited on the electrode from amount of charge passed during polymerization is discussed in detail in the following section on energy density. Energy density calculations for the Li/polymer battery are also included.

Energy density. The energy density of a battery, or specific energy as it is sometimes called, is defined (40) as the ratio of the energy obtainable from a cell or battery to its volume (in watt-hours/liter or Joules/liter) or mass (watt-hours/kg or J/kg). Definitions of related terms are given in Appendix B. Energy densities are often used as a measure of battery performance and are used to compare different types of batteries. This section discusses the terms used in battery comparisons, and includes an explanation of how energy density is theoretically and experimentally determined. Other work done in this area is discussed and examples of calculations are given.

The theoretical energy density of a battery is based only on the active materials that participate in the electrochemical reaction and the potential of the cell. Water, electrolyte, and any other material not involved in the electrochemical reaction are not included. Free energy values are used to calculate the theoretical energy density from the relationship

$$-\Delta G^{\circ} = nFE^{\circ} \quad [2]$$

where  $n$  = the number of electrons involved in each of the half-cell reactions that sum to the overall reaction,  $F$  = Faraday's constant (96,487 coulombs or 26.8 amp-hours per mole of electrons involved in the half-cell reactions), and  $E^0$  = standard cell potential in volts. Thus, one gram-equivalent weight of material theoretically releases one Faraday of coulombs.

One way to calculate the theoretical energy density of a battery is to assume that one gram of active mass consists of a material whose molecular weight is the sum of the molecular weights of the active mass components. This one gram of mass can be divided by the collective molecular weight,  $M$ :

$$\frac{1 \text{ gram of active material}}{M} = \# \text{ moles total reactant}$$

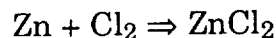
$$(\# \text{ moles total reactant})(n) = \text{moles of electrons}$$

$$(\text{moles of electrons})(F) = \# \text{ of coulombs (or amp-hours)} = \text{capacity}$$

$$(\text{capacity})(E^0) = \# \text{ of watt-hours} = \text{energy}$$

$$\frac{\text{energy}}{1 \text{ g of active material}} = \text{energy density}$$

For example, for a Zn/Cl<sub>2</sub> system, assume 1 g of active material. The overall reaction is:



for this system,

$$M = 65.4 (\text{Zn}) + 70.9 (\text{Cl}_2) = 136.3 \text{ g/mole}$$

$$n = 2$$

$$F = 26.8 \text{ Ahr/mole of electrons}$$

$$\text{and } E^0 = 2.12 \text{ V} = 2.12 \text{ J/C}$$

Using 1 kilogram as a basis,

$$\frac{1 \text{ kg}}{0.136 \text{ kg/mole}} = 7.34 \text{ mole of active material}$$

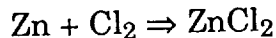
$$(7.34 \text{ mole}) \left( 2 \frac{\text{moles of electrons}}{\text{mole active material}} \right) = 14.68 \text{ moles of electrons}$$

$$(14.68 \text{ moles of electrons}) \left( 26.8 \frac{\text{Ahr}}{\text{mole of electrons}} \right) = 394 \text{ Ahr}$$

$$(394 \text{ Ahr})(2.12 \text{ V}) = 835 \text{ Whr}$$

and, finally, divide by the number of grams of material used as a basis, 1 kg in this case, to get the energy density. Therefore, the theoretical energy density of the Zn/Cl<sub>2</sub> battery = 835 Whr/kg.

The units of energy density often cause confusion. One might ask, per kilogram of what? Recall the reaction:



The  $\Delta G^0$  value given is per 1 mole of Zn, per one mole of Cl<sub>2</sub>, or per one mole of ZnCl<sub>2</sub>. It is therefore 1,738 Whr per gram of Zn, 1600 Whr per gram of Cl<sub>2</sub>, or 835 Wh/kg of “active material,” or for both the mass of the Zn and Cl<sub>2</sub> added together, which is the value obtained in the example above. The experimental energy density is lower than the theoretical energy density because in practice one gram-equivalent weight of reactant will not totally react to release a full 26.8 Ahr, and because the entire mass of the battery must be included in calculating the experimental energy density. In fundamental studies of new battery systems, the experimental energy density is often defined using only the active ingredients (14) rather than the entire mass of the battery in order

to simplify calculations and free the experimentalist from engineering restraints. After the basic premise of the battery has been proven, refinement of the system to streamline it using different materials and design can be undertaken. Experimental energy densities in this work are calculated using the formula

$$e. d. = \frac{iEtA}{m} \quad [3]$$

where e.d = energy density,  $i$  = current density during discharge,  $E$  = potential during discharge,  $t$  = time of discharge,  $A$  = electrode surface area, and  $m$  = mass of active components. Since the potential varies during battery discharge, the value  $Et$  was obtained from the area under the potential/time curve.

These values are calculated from data recorded during constant current charge/discharge experiments. When discharged at constant current, the potential/time transient looks like the one in Fig. 16. While the theoretical capacity of the battery would be calculated using the following equation:

$$\text{Theoretical capacity} = C_t = \frac{mnF}{M} \quad [4]$$

the practical capacity can now be calculated from experimental data using the equation:

$$\text{Practical capacity} = C_p = \frac{it'A}{m} \quad [5]$$



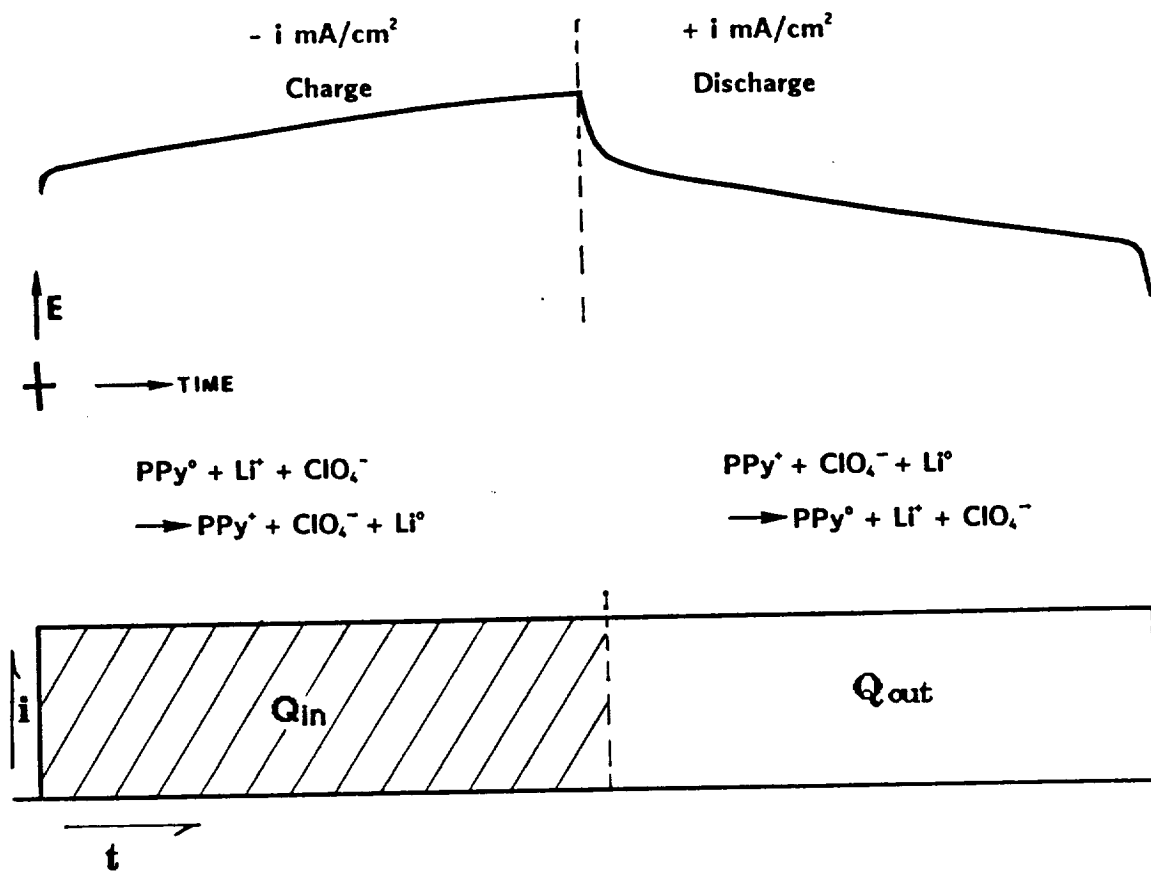


Fig. 16. Charge/Discharge Curve for Li/Polypyrrole Battery.

The time  $t'$  is the discharge time after which the battery can no longer maintain its rated voltage when a constant current is drawn. Getting a average value of potential,  $E_{ave}$ , from the plateau of the discharge curve allows calculation of the energy density, as explained below.

For a constant current discharge, the circuit is as shown in Fig. 17.

a. Ohm's law for an electronic circuit states that  $E = IR$ , where  $E$  = potential,  $I$  = current (not current density), and  $R$  = resistance. In this experiment,  $I$ , the current, is constant and  $E$  and  $R$  change. The galvanostat includes a variable resistor and draws a constant current. The potential/time transient is recorded and the practical energy density is calculated from the values of  $E$ ,  $t'$ ,  $I$  and battery mass in Eq. [3] above.

Another way to determine the energy density experimentally is with a fixed load (resistor). This experimental setup is shown in Fig 17. b. Both the potential/time transient and the current/time transient are recorded, and the areas under both curves are used to determine the total amount of energy,  $E$ , obtained from the battery from the relationship

$$E = \int_{t=0}^{t=\infty} EI dt \quad [6]$$

This problem can be solved using a simple numerical method such as the trapezoid rule, making a table of  $IE$  vs. time to use as input. If the data can be stored in digital form on a computer, a software package such as Kaleidagraph® can be used to determine the area under each curve and then obtain the total energy.

A constant power device can also be used to determine the energy available from a battery. A light bulb or small motor will provide a constant draw of power from the battery. Power =  $IE$ ; so if the

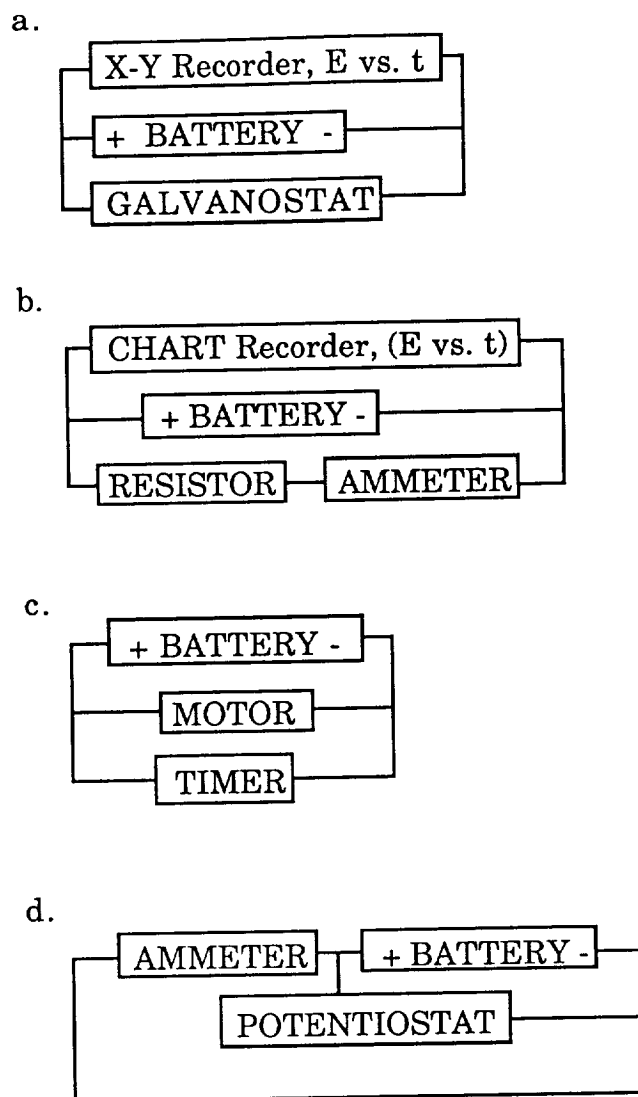


Fig. 17. Circuit Diagrams for Battery Discharge. a. Constant Current Discharge, b. Constant Load Discharge, c. Constant Power Discharge, d. Constant Potential Discharge.

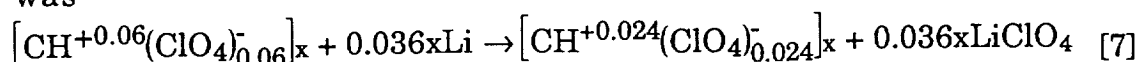
power/time transient is recorded, the area under the power/time curve divided by the total mass of the battery would give the practical energy density of the battery. The circuit diagram for a constant power discharge is shown in Fig. 17. c.

A constant potential discharge is yet another method that can be used to get the energy density of a battery. A potentiostat, which has a variable resistor, draws a constant potential from the battery. The circuit diagram for the constant potential discharge of the battery is shown in Fig. 17. d. The current/time transient resulting from the battery discharge provides information needed in order to calculate the energy density of the battery. An average value of the current,  $I_{ave}$ , can be used with the discharge time and value of constant potential to calculate energy, which is equal to  $IEt$ . Alternatively, the area under the current/time curve can be used as in Eq. [6] to calculate the energy,  $E$ .

A review of recent literature (5-28) reveals that the most common method of determining the energy density of a Li/polymer battery is by constant-current charge and discharge of the battery. In most cases, an average potential,  $E_{ave}$ , was multiplied by  $t'$  as in Eq. [3] rather than determining the area under the curve. In some papers by MacDiarmid et al. (19-26) an  $E$  vs.  $Q$  (charge) curve was constructed by multiplying the time axis of the  $E/t$  transient by the constant current used in the experiment. The charge was also correlated to the percent doping of the polymer film.

Methods of determining the denominator of Eq. [3] were varied, as were experimental results. Some work involving a Li/Polyacetylene battery by MacDiarmid et al. (19-26) was reviewed to gain a better understanding of doping level calculations. The discharge equation used

was



This equation deals with the percent doping of the polymer film being 0.06 before discharge and 0.024 after discharge. Energy densities are calculated by using the mass of film employed and the amount of lithium consumed. In one paper (26) the mass of the polymer used in the cell was considered in the calculation of the energy density. The theoretical energy density for a lithium/ polyacetylene cell was given as 307 Wh/kg and the experimental energy density reported as 176 Whr/kg. An energy density estimate for a packaged battery including the mass of the solvent, electrolyte, and casing was given as either 25 Wh/kg (24, 26), a reduction factor of 7, or 30 Wh/kg, a reduction factor of 6. Attempts to calculate these energy densities from the data given in the papers was unsuccessful. A better definition of the values for  $E_{\text{ave}}$ ,  $t'$ , and the mass of materials to be considered in the calculations is needed.

Petiot et al. (27) report data in Ahr/kg and call it the "massic capacity." The equation used is:

$$\text{massic capacity} = \frac{It'}{W} \quad [8]$$

where  $W$  = weight of active components. Chemically synthesized 30 mg pellets of polypyrrole were used. The anode during discharge was a Li/Al alloy or Al foil. Data were obtained by constant current discharge and the massic capacity or capacity reported for the cell was 120-140 Ah/kg.

Shacklette et al. (10) also report capacity rather than energy density and call it gravimetric capacity, in Ah/g. A constant current discharge was employed to collect the data, and the anodes were a Li/Al alloy, a

Li/WO<sub>2</sub> alloy, and Li. PPy film was used for the anode. Capacities were based on polymer weights only, including the weight of the BF<sub>4</sub><sup>-</sup> anions.

Energy density in the work of Munstedt et al. (5) was calculated using the mass of the polypyrrole plus the dopant anion, BF<sub>4</sub><sup>-</sup>. Lithium was used as the negative electrode and a value of 297 Wh/kg was reported. The mass of the entire packaged battery was considered for each of three battery types, sandwich #1, sandwich #2, and a spirally-wound cylindrical battery. Sandwich #1 had an energy density of 20 Whr/kg, sandwich #2 had an energy density of 20 Whr/kg, and the cylindrical battery had an energy density of 15 Wh/kg. The battery was cycled using a potential step and a charge/time transient was recorded. The "charge density" in Ah/kg was multiplied by the open circuit potential (vs. Li) to calculate energy density. A reduction factor is the quotient of the experimental energy density calculated using only the mass of active ingredients and the experimental energy density calculated using the weight of the entire packaged battery. The reduction factor for (297 Wh/kg)/(20 Whr/kg) is 14.9, much larger than the empirical reduction factor estimated by MacDiarmid.

In a paper by B. Scrosati et al. (7), a constant current density (33  $\mu\text{A}/\text{cm}^2$ ) discharge was carried out to determine  $E_{\text{ave}}$  (3.3 V), which was multiplied by the "specific capacity" in Ahr/g to get an energy density of 100 Wh/kg. The reference electrode and anode were lithium metal. The energy density is quoted for the "Li/polythiophene(ClO<sub>4</sub><sup>-</sup>) couple only," so only the mass of the active material involved was considered. The authors state that the specific conductivity corresponds to a 10% doping level. The thickness of the film was given, that is, the total charge used to make the film.

In a general paper by Passiniemi and Osterholm (9) entitled "Critical aspects of Organic Polymer Batteries," values for specific charge were given for polyaniline, poly-(p-phenylene), polypyrrole, and polythiophene (PT) were calculated from an assumed polymer density of  $0.7 \text{ g/cm}^3$  and a  $100 \text{ }\mu\text{m}$  thick film. These are not consistent with values found elsewhere which give a density of  $1.1\text{-}1.6 \text{ g/cm}^3$  for polythiophene and  $1.45\text{-}1.51 \text{ g/cm}^3$  (depending on the dopant anion used) for PPy. The capacity density is given as  $103 \text{ mAh/g}$ . This value is multiplied by the open circuit potential and some conversion factors to get the energy density. Apparently the mass used in calculations was based on the assumed polymer densities only.

A paper by Yamamoto et al. (28) gives the surface area of the electrode as well as the mass of the polymer (PPy and PT) on the electrode, a rarity in the papers reviewed. A constant current discharge was done and a potential/time transient was measured. The average discharge potential,  $E_{\text{ave}}$ , was  $1.22 \text{ V}$  for the PT cell. The anode used was  $\text{Zn/ZnI}_2/\text{I}_2$ . Although no energy density was given, an energy density of  $195 \text{ Wh/kg}$  could be calculated considering only polymer mass, which compares very favorably with other reported values for polymer batteries.

Trinidad et al. (18) performed a constant current discharge on a PPy/Li battery, and from the potential/time transient, numbers for  $E_{\text{ave}}$  and  $t'$  could be obtained. Using a value of  $1.51 \text{ g/cm}^3$  for density of polypyrrole, an energy density of  $127 \text{ Wh/kg}$  could be calculated. Using the open circuit potential, instead of  $E_{\text{ave}}$  as some authors do, would result in a value of  $174 \text{ Whr/kg}$  for the energy density.

Also reviewed were recent papers by Osaka, et al. (11-17). Equation [3] was used;

$$e. d. = \frac{iEtA}{m}$$

where e.d = energy density, i = current density during discharge, E = average discharge potential, t = time of discharge, A = electrode surface area and m = mass of active components. However, the surface area of the electrode was not given. The mass of the polypyrrole film only was considered, and it was actually weighed, not estimated from the amount of charge applied during polymerization and doping level. Unfortunately, the mass was not given, so attempts at reproducing the calculation of energy density, given as 85.6 Wh/kg, were unsuccessful. In one of the papers (15), a value for energy density can be estimated from the total charge during polymerization, using the density of polypyrrole and considering the mass of the polymer only. This estimated value is 75 Wh/kg.

In many papers, the mass of materials used to calculate the energy density is reported in kg, g, or mg, but is referred to as weight. The units of weight are Newtons, dynes, or pounds force (lbf), and the units of mass are kilograms, grams, or pounds mass (lb<sub>m</sub>) (41). The equation that relates weight to mass is

$$W = \frac{(m)(g)}{g_c} \quad [9]$$

where W = the weight of an object,

g = the acceleration of gravity,

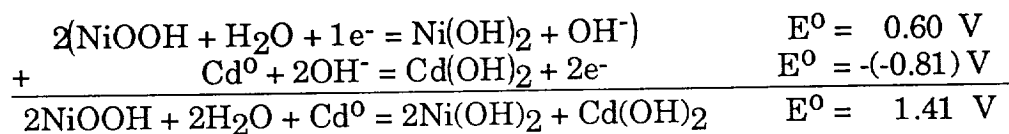
and g<sub>c</sub> = a conversion factor:

$$g_c = 1 \frac{\text{kg m}}{\text{N}} = 1 \frac{\text{g cm}}{\text{dyne}} = 32.174 \frac{\text{lb}_m \text{ ft}}{\text{lb}_f} \quad [10]$$



From Eq [9] and Eq. [10], one can see that mass and weight are numerically the same unless they are reported in  $lb_m$  and  $lb_f$ , respectively. Even using  $lb_m$  and  $lb_f$  interchangeably could be a mistake, because while  $g_c$  is constant,  $g$  varies with position. Therefore mass, unlike weight, is constant. An object at sea level would weigh slightly more than it would in Denver, and in Denver it would weigh considerably more than it would in space. Lithium batteries are particularly applicable for space applications because they have lower mass than most batteries, so mass and weight should not be confused with each other in the literature.

This project includes the determination of the theoretical and experimental energy densities of the Li/PPy battery. The experimental energy densities are determined from data collected using the constant-current method of charging and discharging a battery. This method was chosen because it is commonly used in the literature and for purposes of comparison of data it seems the most useful. The experiments were first performed on a commercial Ni/Cd secondary battery. The theoretical energy density of a Ni/Cd Battery can be calculated using the method described earlier and illustrated by the Zn/Cl<sub>2</sub> example. The half reactions and overall reactions are as follows (42):



As can be seen in the overall cell reaction above, two moles of NiOOH are needed for every one mole of Cd. Water is not considered in the calculation of the energy density since it is the solvent.

As stated above, to calculate the theoretical energy density of a battery, it is necessary to start with a known amount of active material, called a

basis. Starting with a basis of 1 kg of active material and knowing that the molecular weight of Cd = 112.41 and the molecular weight of NiOOH is 91.7, then it can be calculated that 1 kg of active material = 3.39 moles of active material:

$$2 \left( 91.7 \frac{\text{g}}{\text{mole of Cd}} \right) + 112.41 \frac{\text{g}}{\text{mole of NiOOH}} = 295 \frac{\text{g}}{\text{mole of active material}}$$

$$295 \frac{\text{g}}{\text{mole of active material}} \left( \frac{1 \text{ kg}}{1000 \text{ g}} \right) = 0.295 \frac{\text{kg}}{\text{mole of active material}}$$

$$\frac{\text{Basis of 1 kg}}{0.295 \frac{\text{kg}}{\text{mole of active material}}} = 3.39 \text{ moles of active material}$$

Now that the number of moles of active material has been calculated, recall Eq. [2]:

$$-\Delta G^{\circ} = nFE^{\circ}$$

where, in this example,

$$n = 3.39 \text{ moles of active material} \left( 2 \frac{\text{moles of e}^{-}}{\text{moles of active material}} \right) = 6.78 \text{ moles of e}^{-}$$

$$F = 26.8 \frac{\text{Ah}}{\text{mole of electrons}}$$

$$\text{and } E^{\circ} = 1.41 \text{ V.}$$

The theoretical energy of a Ni/Cd battery is then

$$E = (6.78 \text{ moles of electrons}) \left( 26.8 \frac{\text{Ah}}{\text{mole of electrons}} \right) (1.41 \text{ V}) = 256.2 \text{ Wh}$$

for 1 kg of active material, therefore the theoretical energy density is 256.2 Wh/kg. When experimental techniques were mastered using the Ni/Cd

battery, a lithium/polypyrrole battery was designed and built, using as guidelines diagrams from references (5) and (28). Both conventional film batteries and fibrillar film batteries were constructed and tested and comparisons were made.

The theoretical energy density of the Li/PPy battery can be calculated as in the previous Zn/Cl<sub>2</sub> and Ni/Cd examples. First, the cell potential can be obtained from summing the standard half reactions as before:



The molecular weight of active materials is calculated using the doping level of the polypyrrole. If an optimistic 33% doping level is assumed, then the molecular weight of three units of polypyrrole is used and the molecular weight of one counterion is used. In this work, a conservative 25% doping level was assumed. The molecular weight of one pyrrole monomer is 67 g/mole, but since two hydrogen ions per pyrrole monomer are removed during polymerization, 65 g/mole is used as the molecular weight of a pyrrole unit on a polymer chain. The molecular weight of four pyrrole units on a chain is  $4(65 \text{ g/mole}) = 260 \text{ g/mole}$ . The molecular weight of one ClO<sub>4</sub><sup>-</sup> ion = 99 g/mole, and the atomic weight of Li = 7 g/mole. Therefore, the molecular weight of active materials =  $260 \text{ g/mole} + 99 \text{ g/mole} + 7 \text{ g/mole} = 366 \text{ g/mole}$ .

If a basis of 1kg, or 1000 g, is used, then

$$\frac{1000\text{g}}{366 \frac{\text{g}}{\text{mole of active materials}}} = 2.73 \text{ moles of active materials}$$

and the energy is

$$E = nFE^{\circ} = (2.73 \text{ moles of electrons}) \left( \frac{27 \text{ Ah}}{\text{mole of electrons}} \right) (3.2 \text{ V}) = 236 \text{ Wh}$$

for a basis of 1 kg.

Therefore, e.d. = 236 Wh/kg for a Li/LiClO<sub>4</sub>/PPy battery. However, the use of a counterion other than ClO<sub>4</sub><sup>-</sup> or an assumption of a different doping level would change the calculations and result in a different value.

When calculating the energy density for a battery, the mass of the materials must be measured or calculated. For the theoretical energy density, a basis of, for instance, 1 kilogram or 1 gram of active material is used. For determination of the experimental energy, the mass of only the active ingredients are used, and for the practical energy density, the mass of all the materials used to make the battery are included in the calculation, even the packaging. In this work, as in most of the similar work reviewed, only the amount of active ingredient was used in the calculations. The procedure used to determine the amount of active ingredient is as follows. As discussed in the previous section on pyrrole polymerization, there are 2e<sup>-</sup> taken from each monomer unit during polymerization. Assuming a 25% doping level (one counterion for every 4 pyrrole monomer units), there is an additional electron taken away for every 4 monomer units, therefore 2.25 electrons are required from each monomer unit for polymerization.

$$\frac{Q_f \text{ (polymerization charge)}}{F \left( 2.25 \frac{\text{moles of e}^-}{\text{moles of Py monomer}} \right)} = \# \text{ of moles of Py monomer polymerized}$$

For example, if  $Q_f = 184 \text{ mC}$ ,

$$\frac{0.184 \text{ C}}{\left(96487 \frac{\text{C}}{\text{moles of e}^-}\right) 2.25 \frac{\text{moles e}^-}{\text{moles Py}}} = 0.847 \text{ } \mu\text{moles}$$

If there are 0.847  $\mu\text{moles}$  of pyrrole, then there are 0.847  $\mu\text{moles}$  of  $\text{LiClO}_4$ . The total amount of active material is:

$$0.847 \text{ } \mu\text{moles Py} \left( 65.1 \frac{\text{g Py}}{10^6 \text{ } \mu\text{mole of Py}} \right) = 5.51 \times 10^{-5} \text{ g} = 5.51 \times 10^{-8} \text{ kg}$$

$$0.847 \text{ } \mu\text{moles LiClO}_4 \left( \frac{106.5 \text{ g LiClO}_4}{10^6 \text{ } \mu\text{mole LiClO}_4} \right) = 9.03 \times 10^{-5} \text{ g} = 9.03 \times 10^{-8} \text{ kg}$$

---


$$\text{Total} = 14.54 \times 10^{-8} \text{ kg}$$

Therefore, for a battery with a capacity of  $1.93 \times 10^{-5} \text{ Wh}$ ,

$$\text{e. d.} = \frac{1.93 \times 10^{-5} \text{ Wh}}{14.54 \times 10^{-8} \text{ kg}} = 130.6 \frac{\text{Wh}}{\text{kg}} .$$

## CHAPTER IV

### RESULTS AND DISCUSSION

Capacitance studies and electron microscopy As mentioned in the introduction, early versions of fibrillar electrodes made in this laboratory showed a base layer of polypyrrole between the template membrane and the current collector. Recall the electrode schematic in Fig. 8, in which the template membrane was attached to the current collector by pressure. In order to eliminate the leakage of polymerization solution between the membrane and the current collector, electrode/membrane adhesion had to be improved. This was accomplished by sputtering or vapor depositing Au directly onto one side of the template membrane. The electrode was then assembled as described in more detail below. Figure 18 is a schematic of a cross section of the electrode used for this work. The membrane is attached to a section of glass tubing to hold it flat and give it mechanical stability, then sputtered with gold. More gold is vapor deposited or electroplated on top. Contact is made with silver epoxy and a copper wire, then Torr Seal<sup>®</sup>, an inert epoxy, is used to seal the electrode and make it more mechanically stable. Polypyrrole (PPy) was then grown galvanostatically through the pores in the template membrane, and the membrane was dissolved.

In order to ensure that there would be no leakage of solution through the Au layer, experiments were conducted to determine how much Au was needed to deposit a pinhole-free Au film. To determine whether the pores in the template membrane were completely covered, electron micrographs (EMs) were taken of membranes with

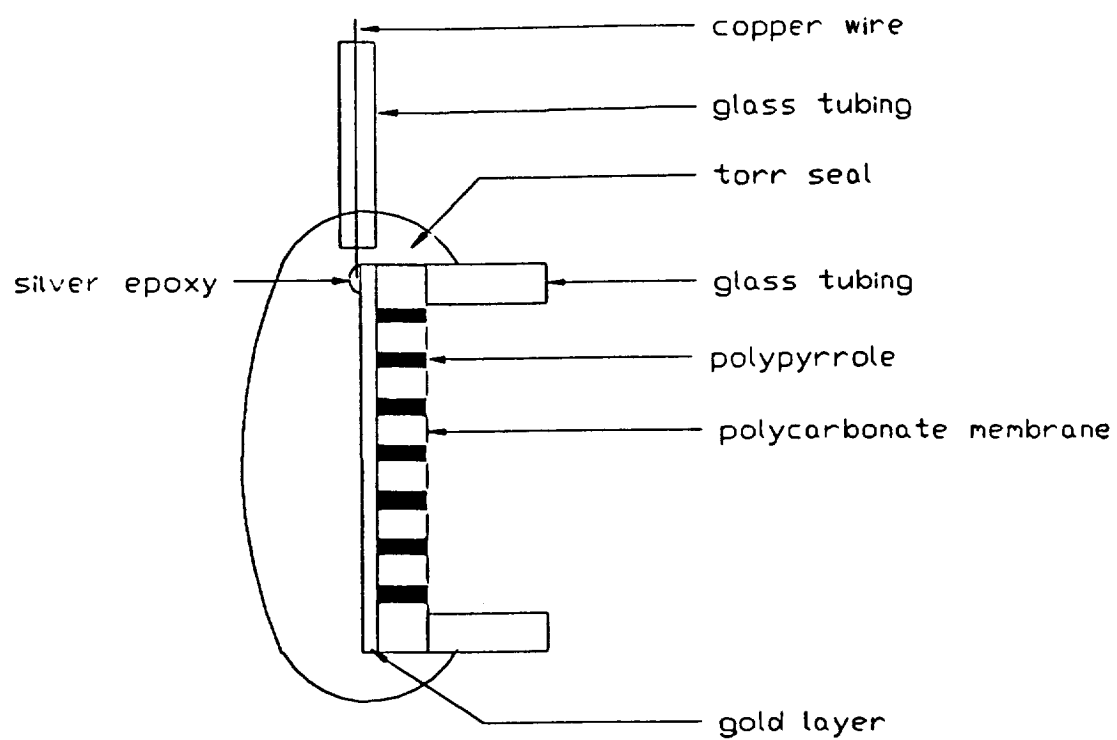


Fig. 18. Cross-section of Fibrillar Polypyrrole Electrode.

varying thicknesses of gold deposited on them. Figures 19-21 show a series of electron micrographs of 300 Å pore diameter polycarbonate membranes with 100 Å, 600 Å, and 900 Å of gold sputtered on them, respectively. Pores are no longer visible in Fig. 21. Also, a spot test with a highly colored (orange) ion,  $\text{Ru}(\text{bpy})_3^{2+}$ , was performed. In this test, a drop of  $\text{Ru}(\text{bpy})_3^{2+}$  in KCl solution was placed on the Au side of a membrane which had been placed on a piece of white filter paper. The ion did not leak through the membrane shown in Fig. 21. Membranes with pores of 1000 Å diameter and 7000 Å of gold vapor deposited on them also passed the EM and spot tests. When electroplating was used as a method of Au deposition, 30 C/cm<sup>2</sup> were required for membranes with 2000 Å diameter pores to pass the EM and spot tests. The amount of gold necessary to achieve a pinhole-free film on the membrane had been determined for each pore diameter.

Capacitive studies were conducted using various methods of deposition of gold on Poretics® and Nuclepore® membranes. These studies were done to find the method of Au deposition that resulted in the best adhesion between membrane and Au layer. Cyclic voltammetry of an electrolyte solution with no redox couple was conducted so that the electroactive area could be calculated from the capacitive current of the cyclic voltammogram. The equation:

$$I_c = C\nu A_c \quad [11]$$

where  $I_c$  is the capacitive current measured from the cyclic voltammogram,  $C$  is the standard capacitance of a gold electrode, and  $\nu$  is the scan rate, gives a value for the electroactive area that will be



ORIGINAL PAGE  
BLACK AND WHITE PHOTOGRAPH



Fig. 19. Nuclepore® Polycarbonate Membrane with 0.03  $\mu\text{m}$  Pore Diameter and Sputtered with 0.01  $\mu\text{m}$  of Au at 3000 X Magnification.

ORIGINAL PAGE IS  
OF POOR QUALITY

ORIGINAL PAGE  
BLACK AND WHITE PHOTOGRAPH

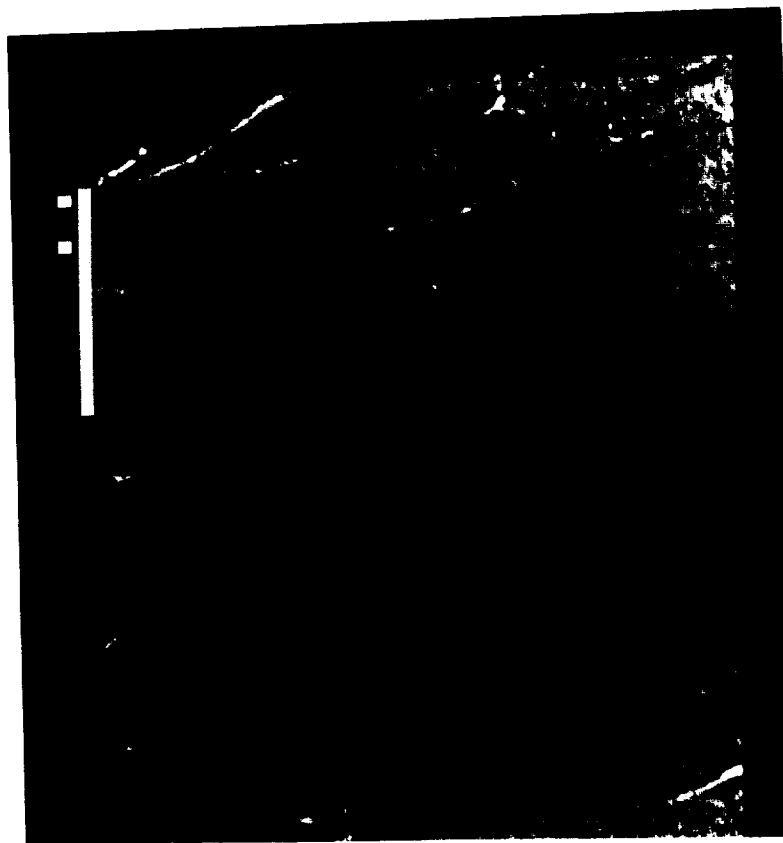


Fig. 20. Nuclepore® Polycarbonate Membrane with 0.03  $\mu\text{m}$  Pore Diameter and Sputtered with 0.06  $\mu\text{m}$  of Au at 3,000 X Magnification.

ORIGINAL PAGE IS  
OF SUPERIOR QUALITY

ORIGINAL PAGE  
BLACK AND WHITE PHOTOGRAPH

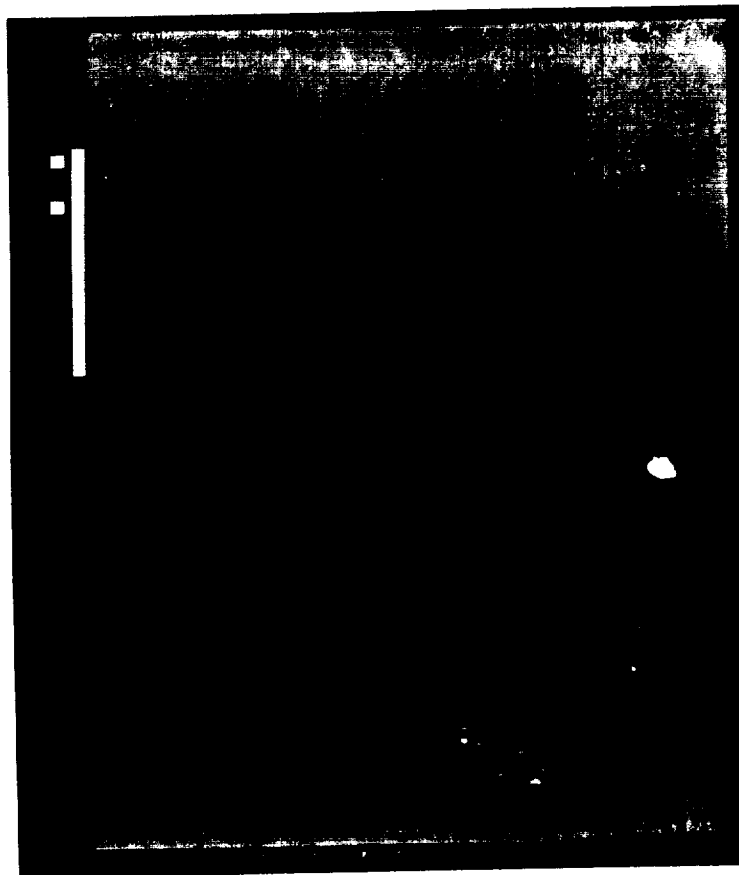


Fig. 21. Nuclepore® Polycarbonate Membrane with  $0.03 \mu\text{m}$  Pore Diameter and Sputtered with  $0.09 \mu\text{m}$  of Au at 3,000 X Magnification.

referred to as  $A_c$ . The total electrode area including the part covered by the nonporous portion of the template membrane will be referred to as  $A_g$  (geometric area).  $A_f$  (fractional area) is that part of the geometric area not covered by the nonporous portion of the template membrane. The fractional area can also be defined as the area of the surface of the template membrane which is porous. It should be equal to  $A_c$ , the area calculated from the capacitive current of the cyclic voltammogram, if there is no leakage of solution between the Au layer and the template membrane. If a good seal has been made, only the area in the pores of the membrane should contribute to the electroactive area.

The two types of polycarbonate membranes investigated were a 0.1  $\mu\text{m}$  pore diameter membrane made by the Poretics<sup>®</sup> Corporation and a 0.176  $\mu\text{m}$  pore diameter membrane made by the Nuclepore<sup>®</sup> Corporation. The two methods employed for depositing gold were sputtering and vapor deposition. Both involve the use of a vacuum chamber and sputtering uses an Argon plasma as the medium in which to carry out the deposition. Sputter deposition is achieved by the bombardment of an Au target with Argon atoms. The gold removed from the target by this bombardment is deposited on the sample. In vapor deposition, gold shavings are heated until they vaporize and gold deposits on the sample as it cools. More gold can be deposited in less time with vapor deposition. Electrodes were made using each of the two methods separately, then some were made with a layer of sputtered gold and a layer of vapor deposited gold on top of the sputtered layer.

Results are tabulated in Table I. In order to determine which of the methods was superior, the data were analyzed in the following manner. If a good seal has been made, then the fractional area and the area

Table I. Capacitive Studies of Au/Membrane Electrodes.

		$A_c$ (cm <sup>2</sup> )	$A_c/A_f$	$A_c/A_g$
Nuclepore® (0.1 μm pore diameter)	Sputtered only, with 0.1 μm of Au	$0.22 \pm 0.19$	9.94	0.23
	Vapor deposited only, with 0.7 μm Au	$0.33 \pm 0.19$	14.7	0.343
	Sputtered and vapor deposited, with 0.7 μm Au	$0.38 \pm 0.09$	16.9	0.395
Poretics® membrane (0.176 μm pore diameter)	Vapor Deposited only	$0.53 \pm 0.34$	1153	0.56
	Sputtered and vapor deposited	0.9	1956	0.95

calculated from the cyclic voltammograms should be the same, and the ratio  $A_c/A_f$  should be equal to 1. On the other hand, if a very poor seal has been made, the calculated area should be closer to the geometric area, and the ratio  $A_c/A_g$  should be closer to one. As can be seen in Table I, the latter is the case. None of the electrodes have an  $A_c/A_f$  ratio of one, and the Poretics® membranes were particularly poorly sealed. It was concluded that the polycarbonate membranes were not sealing well enough, and perhaps an inorganic membrane would make a better metal/membrane seal than an organic membrane. Other work done in the laboratory supported this conclusion. An aluminum oxide membrane made by the Anopore® Corporation was introduced. When the aluminum oxide Anopore® was used, there was no leakage of solution between polypyrrole and no evidence of base layer growth, as shown in Fig. 22. The polypyrrole fibrils are directly attached to gold posts, with no base layer of conventional polypyrrole.

Another issue that must be addressed is pore density. A higher pore density leads to higher fibril density since the fibrils are synthesized within the pores. A higher fibril density would result in increased charge capacity for the same electrode area. One drawback of using Nuclepore® as a template membrane is that the pore density does not increase proportionately with decreasing pore diameter. As can be seen in Table II, the electroactive area of an electrode made with a Nuclepore® membrane with a pore diameter of 0.01  $\mu\text{m}$  would have an electroactive area of only 0.02% of the geometric area. Another company, the Poretics® corporation, can make membranes of much higher pore densities. Figure 23 is an electron micrograph of a Poretics® membrane with a pore density of  $10^{10}$  pores/cm<sup>2</sup>, which is two orders of magnitude

ORIGINAL PAGE  
BLACK AND WHITE PHOTOGRAPH

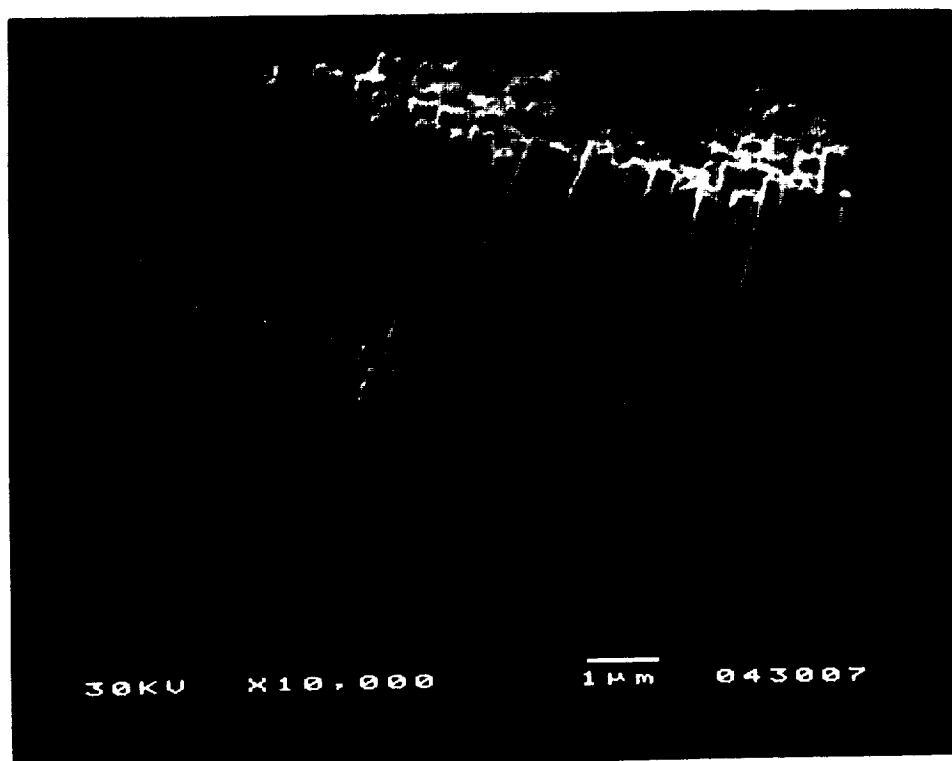


Fig. 22. Cross-section of Fibrillar Polypyrrole on Gold Surface with  
Template Membrane Extracted. 1.0 cm = 1.0  $\mu$ m.

ORIGINAL PAGE IS  
OF POOR QUALITY

Table II. Nuclepore® Membrane Data.

Pore Diameter ( $\mu\text{m}$ )	Pore Density (per $\text{cm}^2$ )	Porous Area (%)
12	$1.0 \times 10^5$	11.3
10	$1.0 \times 10^5$	7.8
8	$1.0 \times 10^5$	5.0
5	$4.0 \times 10^5$	7.9
3	$2.0 \times 10^6$	14.1
2	$2.0 \times 10^6$	6.3
1	$2.0 \times 10^7$	15.7
0.8	$3.0 \times 10^7$	15.1
0.6	$3.0 \times 10^7$	8.5
0.4	$1.0 \times 10^8$	12.6
0.2	$3.0 \times 10^8$	9.4
0.1	$3.0 \times 10^8$	2.4
0.08	$3.0 \times 10^8$	1.5
0.05	$3.0 \times 10^8$	0.6
0.03	$3.0 \times 10^8$	0.2
0.015	$3.0 \times 10^8$	0.05
0.01	$3.0 \times 10^8$	0.02



ORIGINAL PAGE  
BLACK AND WHITE PHOTOGRAPH

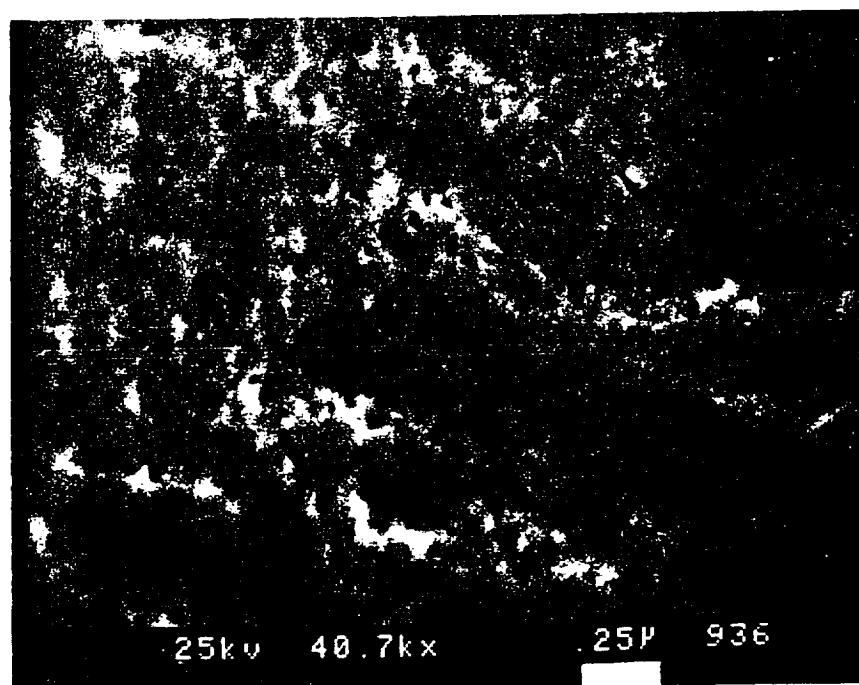


Fig. 23. Electron Micrograph of High Density ( $\text{@}10^{10}$  pores/ $\text{cm}^2$ )  
Poretics<sup>®</sup> Membrane. 1cm = 0.25  $\mu\text{m}$ .

ORIGINAL PAGE IS  
OF POOR QUALITY

higher than the highest pore density that the Nuclepore<sup>®</sup> corporation offers. However, the aluminum oxide membrane made by the Anopore<sup>®</sup> Corporation has the highest porosity (Fig. 24). Since the template membrane is about 60%-70% porous, the resulting fibrils cover about 60% of the electrode surface. We are limited to a fibril diameter of 2000 Å with the Anopore<sup>®</sup> membranes because Anopore<sup>®</sup> is commercially available only in the 2000 Å size.

Electron micrographs were taken of both conventionally grown films and fibrillar films. Figure 3 shows a representative conventional polypyrrole film and Fig. 11 shows a representative fibrillar film. It was found that for electrodes with the same geometric area, fibril length was approximately 1.6-2.0 times the thickness of a conventionally grown film.

Cyclic voltammetry A cyclic voltammogram is a plot of potential vs. current, with potential as the independent variable. The potential is varied at a fixed rate, beginning at a certain starting potential, continuing to a certain terminal potential, then scanning back to the starting potential without pause. For the cyclic voltammetry in this work, the potential was held at a value at which the film should exist in its neutral, or reduced, state. This potential is around -1.0 V vs Ag/Ag<sup>+</sup> for polypyrrole. When the film was completely reduced, the potential scan was begun. As the potential is scanned positively, a current peak arises corresponding to the oxidation of the polypyrrole film. After the current has reached its maximum, it will decay to a constant value which is greater than the starting potential and remain there until the direction of the potential scan is reversed or another reaction begins to occur. This region is where the polymer is oxidized and conductive, as

ORIGINAL PAGE  
BLACK AND WHITE PHOTOGRAPH

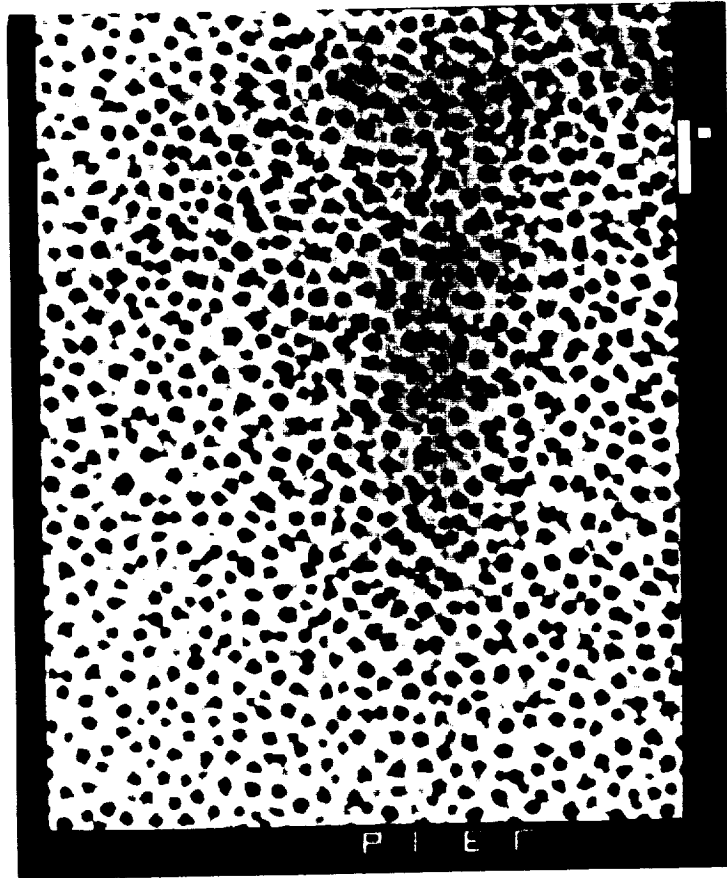


Fig. 24. Scanning Electron Micrograph of the Surface of an Anopore® Filtration Membrane with 0.2  $\mu\text{m}$  Diameter Pores.

ORIGINAL PAGE IS  
OF POOR QUALITY

evidenced by the capacitive current present. When the potential scan is reversed, a reduction current peak arises, then the current decays to its original value as it was before the scan was begun. In this region there is negligible current and the polymer is in its insulating, or reduced, form again.

Cyclic voltammetry was conducted after the growth of every film to determine whether oxidation and reduction peaks characteristic of polypyrrole were present and to determine the potential at which each of these peaks occur. A representative cyclic voltammogram of a 2  $\mu\text{m}$  thick conventionally grown film in 1 M  $\text{LiClO}_4$  in propylene carbonate is shown in Fig. 25.

In order to determine rate of ion transport in thick films vs. thin films, a study was made of  $I_p$  (anodic peak current) vs. scan rate for various film thicknesses. If diffusion of ions is facile in a thin film, the peak current for oxidation of polypyrrole in the cyclic voltammogram should be directly proportional to scan rate. In a thick film, ion transport is less facile and should be a diffusion-controlled process. One way to determine this is to conduct cyclic voltammetry at different scan rates for different film thicknesses. The peak current ( $I_p$ ) for the anodic peak for each cyclic voltammogram (CV) is measured and plotted as a function of scan rate. For a thin film, the plot should be linear. As film thickness increases and ion transport becomes diffusion-controlled, the plot should begin to fall away from linearity and level off. Instead of being linear with respect to scan rate, the plot should be linear with respect to the square root of scan rate, in accordance with the Sevcik relationship (43):

$$I_p = (2.69 \times 10^5) n^{3/2} A D_0^{1/2} v^{1/2} C_0^* \quad [12]$$

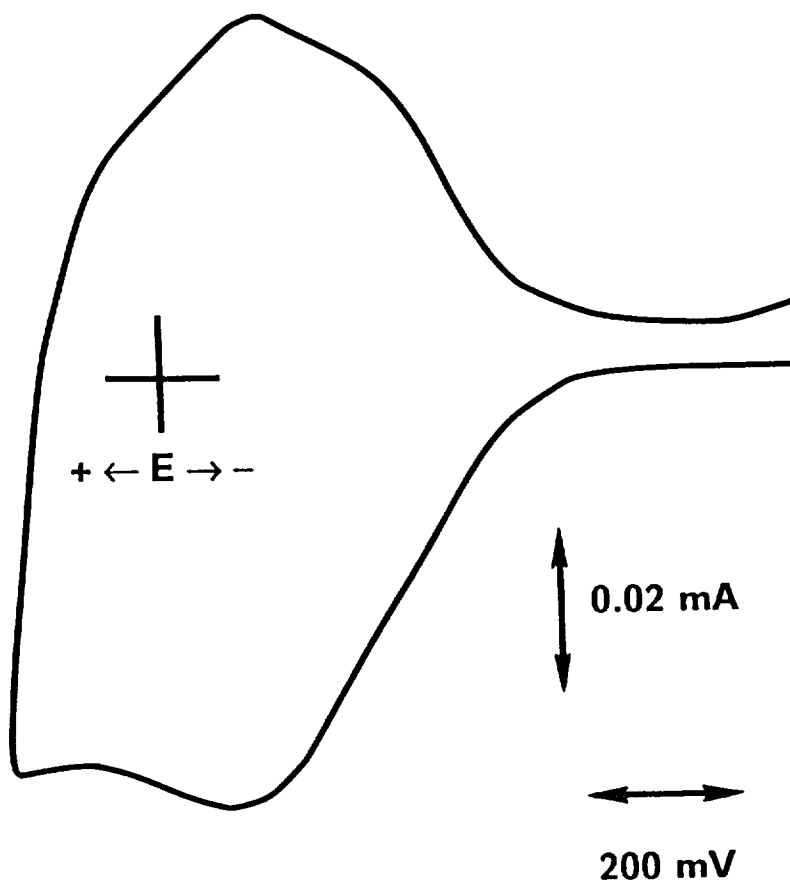


Fig. 25. Cyclic Voltammogram of Li/PPy Battery with 2  $\mu\text{m}$  Conventional PPy Film. Scan Rate = 1mV/sec.

In fact, this is what was observed when cyclic voltammetry was conducted on films of thicknesses of 0.032  $\mu\text{m}$ , 0.064  $\mu\text{m}$ , 0.128  $\mu\text{m}$  and 0.89  $\mu\text{m}$ . The plots of  $I_p$  vs. scan rate were linear for the thinner films, but the plots fell off from linearity as film thickness increased (see Figs. 26-29). Scan rates used were 20 mV/sec, 50 mV/sec, 100 mV/sec, 200 mV/sec, 500 mV/sec, and 1000 mV/sec.

The fibrillar films must be treated with base to dissolve the template membrane. Treating the polypyrrole with strong base (NaOH) has been shown to have a dramatic effect on the cyclic voltammetry of the polymer (44). That is, oxidation and reduction peaks can be shifted negatively as much as one volt. We have found that subsequent treatment of the polymer with strong acid such as 1 %  $\text{HClO}_4$  restores most of the electrochemical properties, but the oxidation and reduction peaks of the polypyrrole are both shifted about 350-500 mV negatively of their original positions. Note the shift in  $E_p$  (peak potential) between a conventional PPy film (Fig. 25) and a fibrillar PPy film (Fig. 30). Using the acid  $\text{HClO}_4$  ensures that there is only one counterion present in the system, since the electrolyte for battery studies is  $\text{LiClO}_4$ .

Discussion of battery charge/discharge curves. Experiments were conducted with both fibrillar and conventional films to determine the maximum amount of charge that each type of battery could store and discharge. Experiments were designed so that the coulombic efficiencies, energy efficiencies, and energy densities could also be determined. The data analysis was conducted in such a way as to facilitate comparison between the shapes of the charging and discharging curves of both conventional film batteries and fibrillar batteries. Results from these studies are discussed in this section.

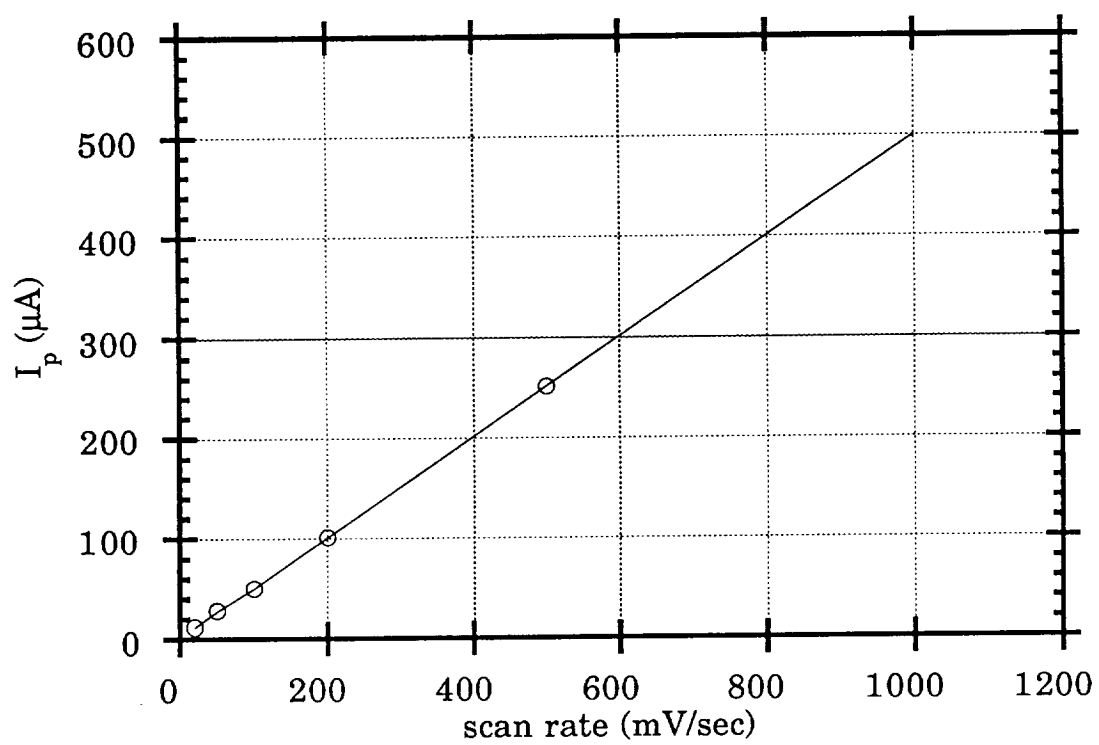


Fig. 26.  $I_p$  vs. Scan Rate for  $0.032 \mu\text{m}$  Conventional PPy Film.

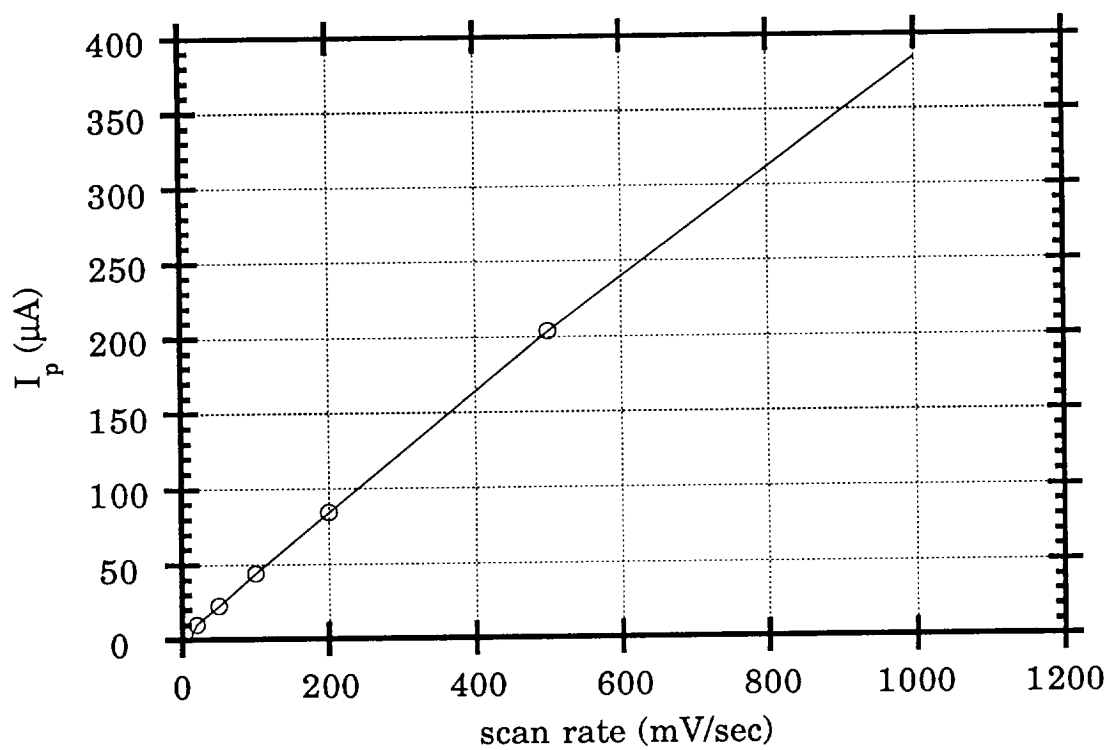


Fig. 27.  $I_p$  vs. Scan Rate for 0.064  $\mu\text{m}$  Conventional PPy Film.



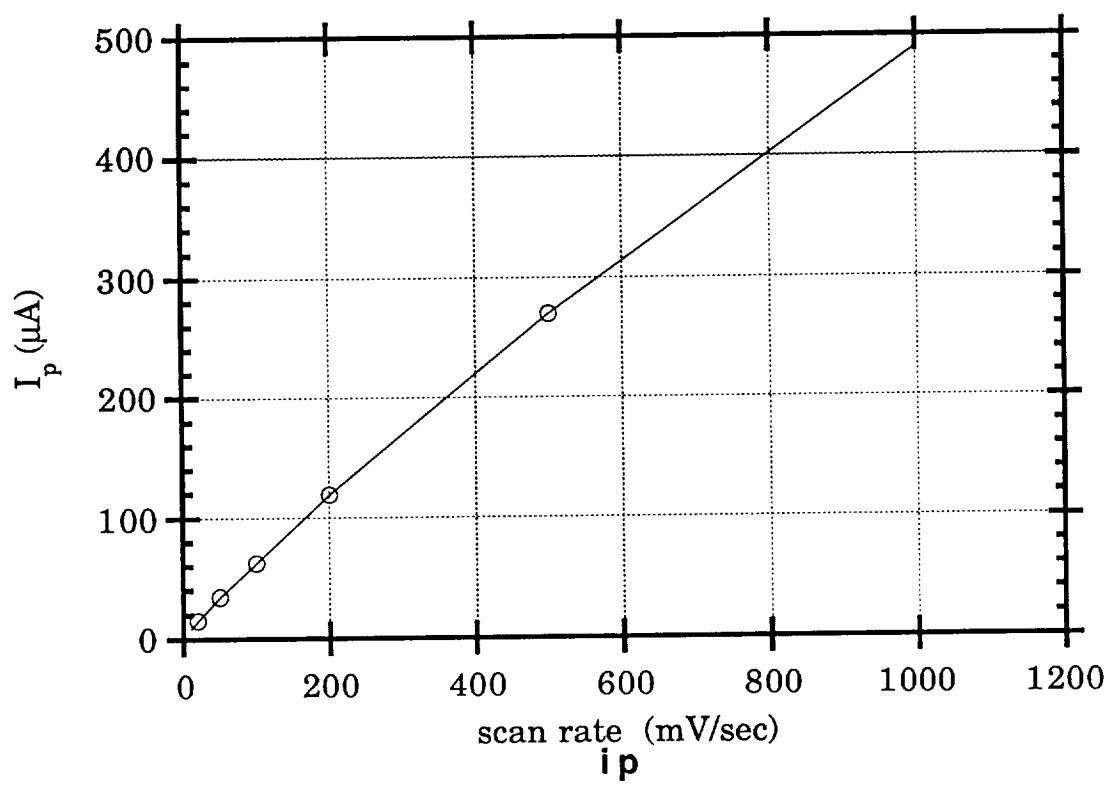


Fig. 28.  $I_p$  vs. Scan Rate for 0.128  $\mu\text{m}$  Conventional PPy Film.

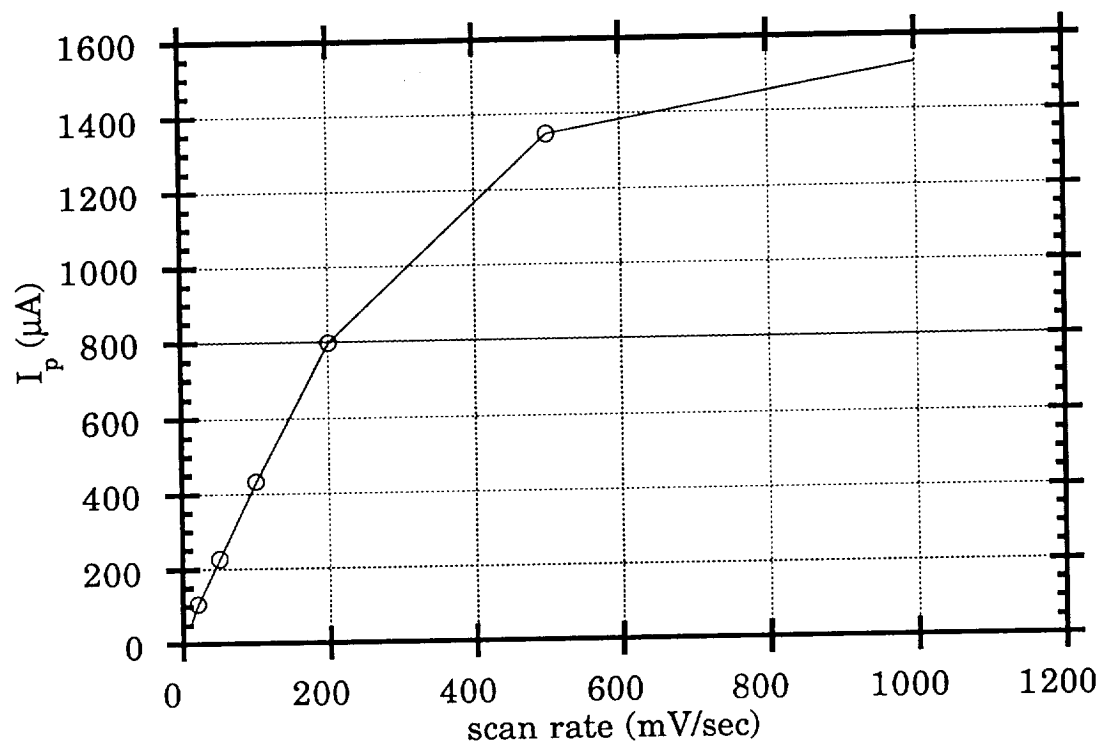


Fig. 29.  $I_p$  vs. Scan Rate for 0.89  $\mu\text{m}$  Conventional PPy Film.

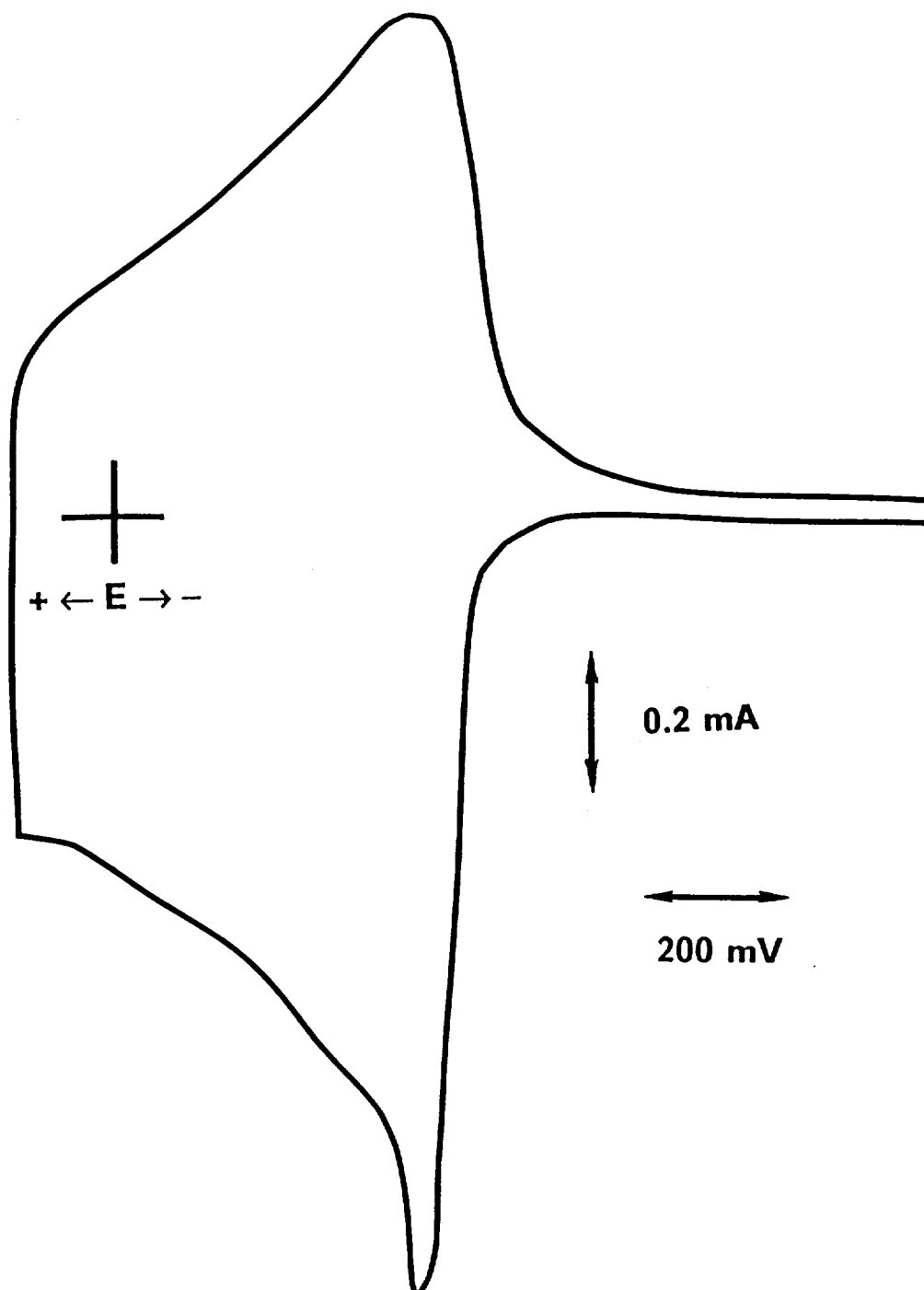


Fig. 30. Cyclic Voltammogram of Li/PPy Battery with 2  $\mu\text{m}$  Fibrillar Equivalent PPy Film. Scan Rate = 10 mV/sec.

A cyclic voltammogram was recorded after the growth of each film, then the film was potentiostatically reduced until no measurable current flowed. The amount of charge under the oxidation portion of the cyclic voltammetry curve was used as a basis from which to start charging the battery. Since that amount of charge, which will hereafter be referred to as  $1Q$ , was passed during oxidation of the polymer film, it was assumed that the battery could store at least that amount of charge.

If the potential on the cyclic voltammogram is scanned more positively after the polymer is oxidized, a potential region is reached at which an irreversible oxidative process occurs. Figure 31 shows a CV which illustrates this region and also the region designated as  $1Q$ . The area under the wave corresponding to the irreversible oxidation process could contain both a reversible contribution and an irreversible contribution. This is evidenced by data presented later in this section that show that more charge than that found under the oxidation wave of the CV can be extracted from the film during battery discharge.

The battery was then charged at a constant current of  $0.5 \text{ mA/cm}^2$  until the same amount of charge that was measured under the oxidation portion of the CV had been put back into the film. The battery was then discharged at a constant current of  $0.5 \text{ mA/cm}^2$  and the cell potential was measured as a function of time. When the potential dropped to a value of  $2.5 \text{ V}$ , the discharge of the battery was terminated because the discharge curve dropped off rapidly at this point. The battery was then held at a constant potential until there was negligible current flow. The potential was held in the region in which the polypyrrole film was completely reduced. This potential was determined from the cyclic voltammogram taken at the beginning of the experiment, which showed

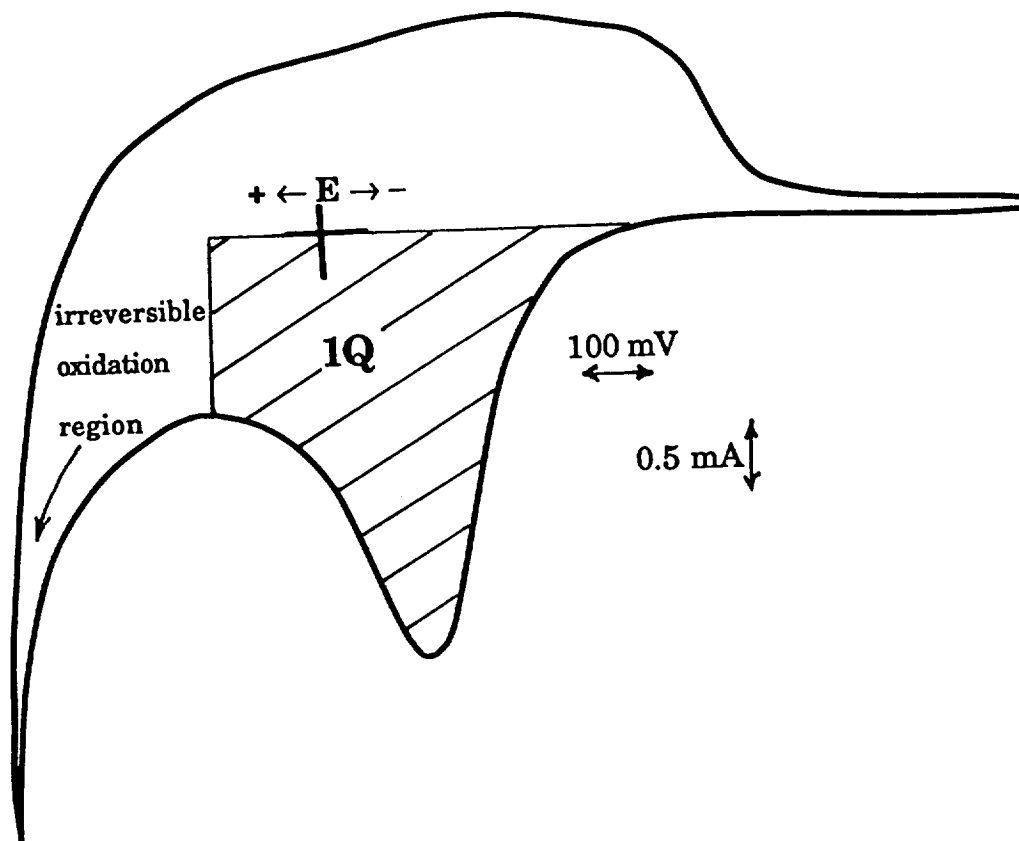


Fig. 31. Cyclic Voltammogram of PPy with Amount of 1Q Charge and Irreversible Oxidation Region Illustrated.

the potentials at which the polypyrrole film was completely oxidized or reduced. When the film was fully reduced, the battery was again charged and discharged using the charge under the oxidation portion of the CV as a basis, and again reduced completely at a constant potential.

Figure 32 is a flow chart that describes the protocol for the experiment. After three cycles using the CV charge, the battery was cycled three times using twice the charge under the CV. Again, between every charge/discharge cycle, the film was potentiostatically reduced. After reduction, the battery was then cycled once again using once the charge under the original CV. The PPy film was reduced again and the battery was cycled three more times using three times the charge under the CV as a basis. This pattern of three cycles, reduction, one cycle using once the charge under the CV, reduction, and three more cycles using a higher increment of charge under the CV was used until the battery failed. Battery failure was defined by a discharge curve that was almost vertical and lasted a considerably shorter time than the first cycle, for which only one times the CV charge was used. These experiments were designed to determine the effect of amount of charge on battery cycle life and to determine the maximum charge each battery could store.

Several series of plots have been made in order to interpret these data. The first series, Figures 33-41, represent each set of three cycles taken with 1Q (one times the charge under the CV), 2Q (twice the charge under the CV), 3Q, and so forth, for both a conventional film and a fibrillar film. The second series of curves, Figures 42 and 43, show the charge/discharge curves of a conventional film and a fibrillar film, respectively, comparing the 1Q the CV charge curves taken between the three cycles each of 2Q, 3Q, & 4Q the CV charge. Figures 44-47 compare

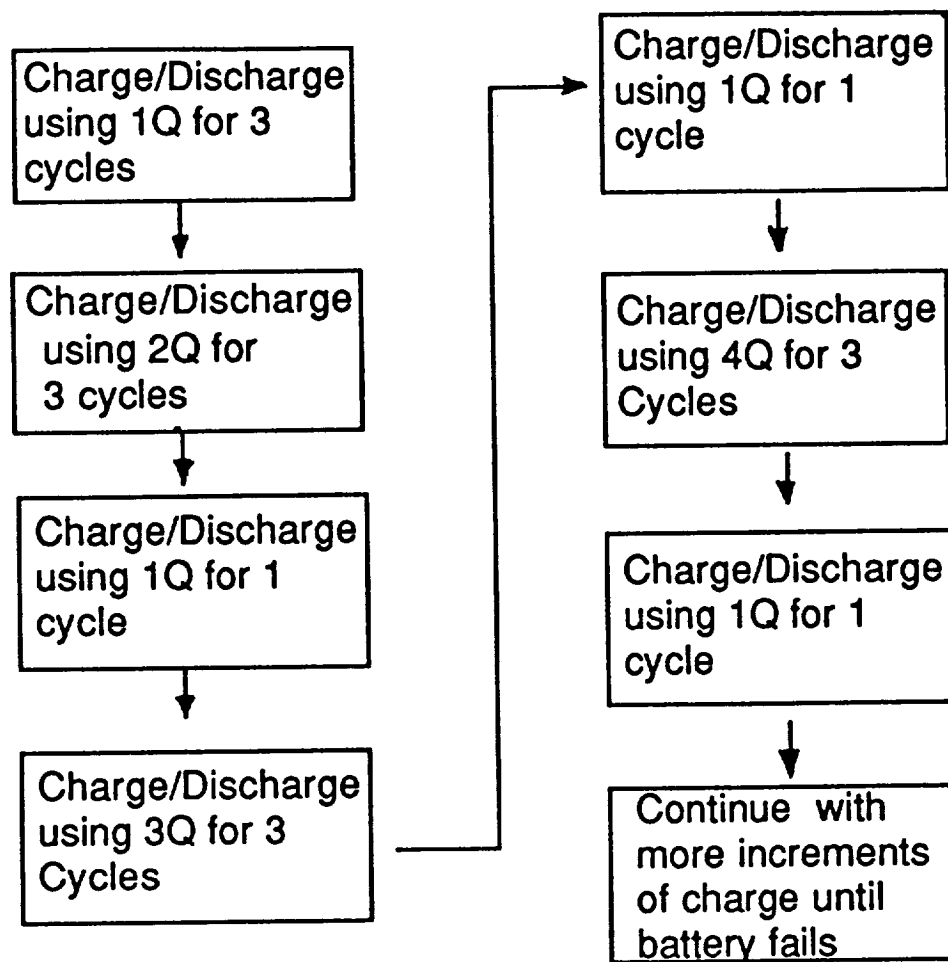


Fig. 32. Protocol for Battery Experiment.

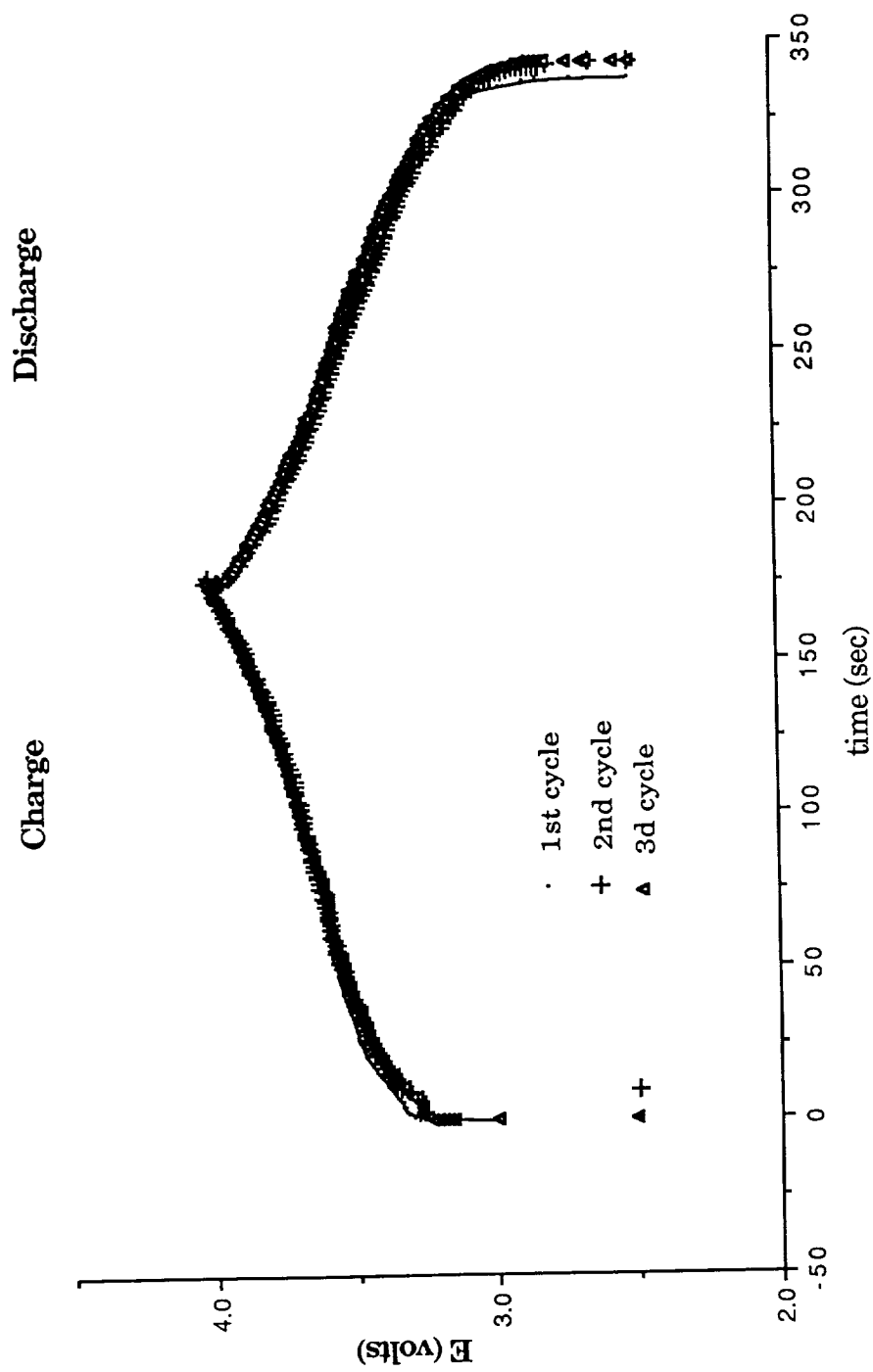


Fig. 33. Charge/Discharge Curves of Li/PPy Conventional Film Battery Using 1Q CV Charge. First Three Cycles.



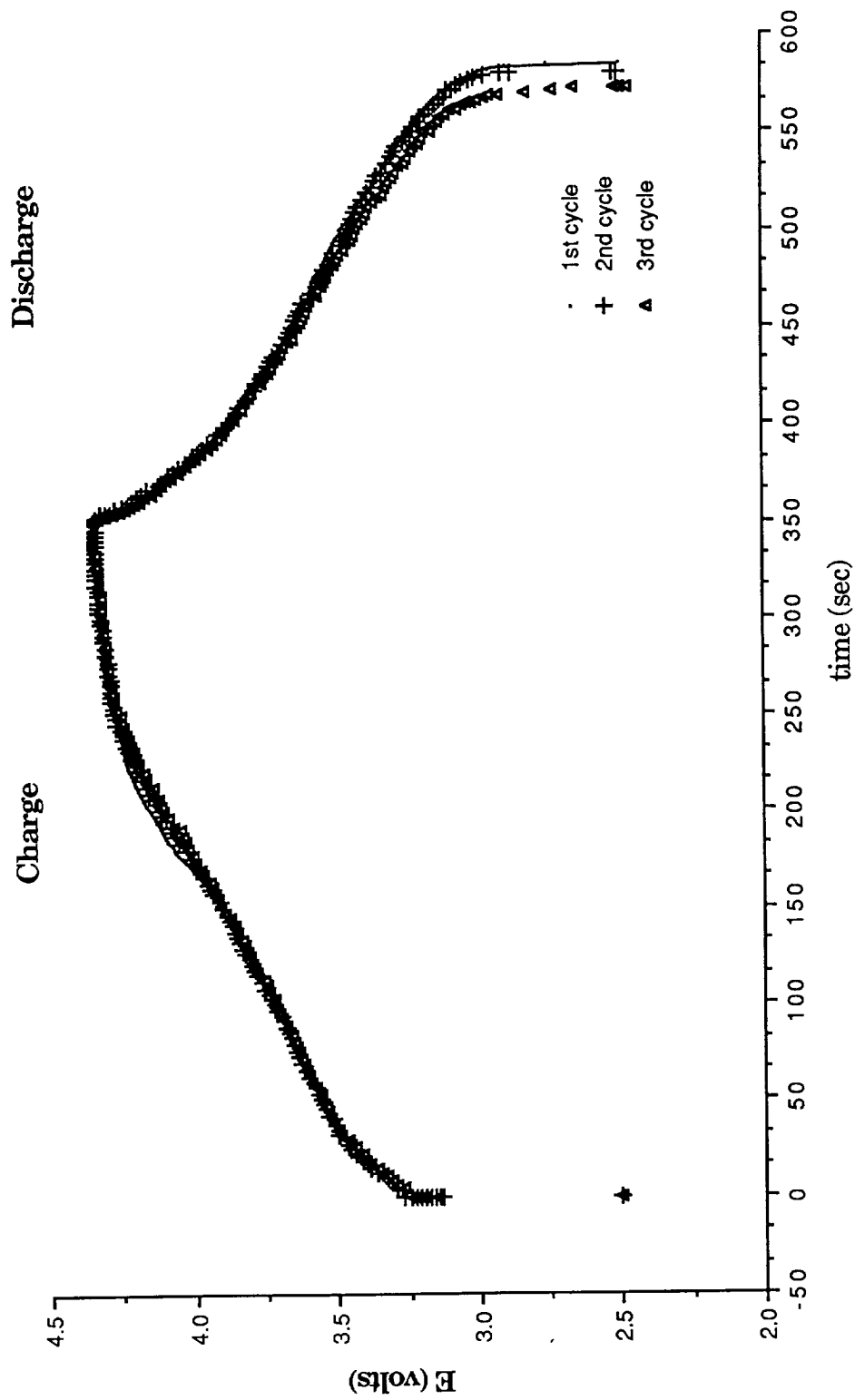


Fig. 34. Charge/Discharge Curves of Li/PPy Conventional Film Battery Using 2Q CV Charge.

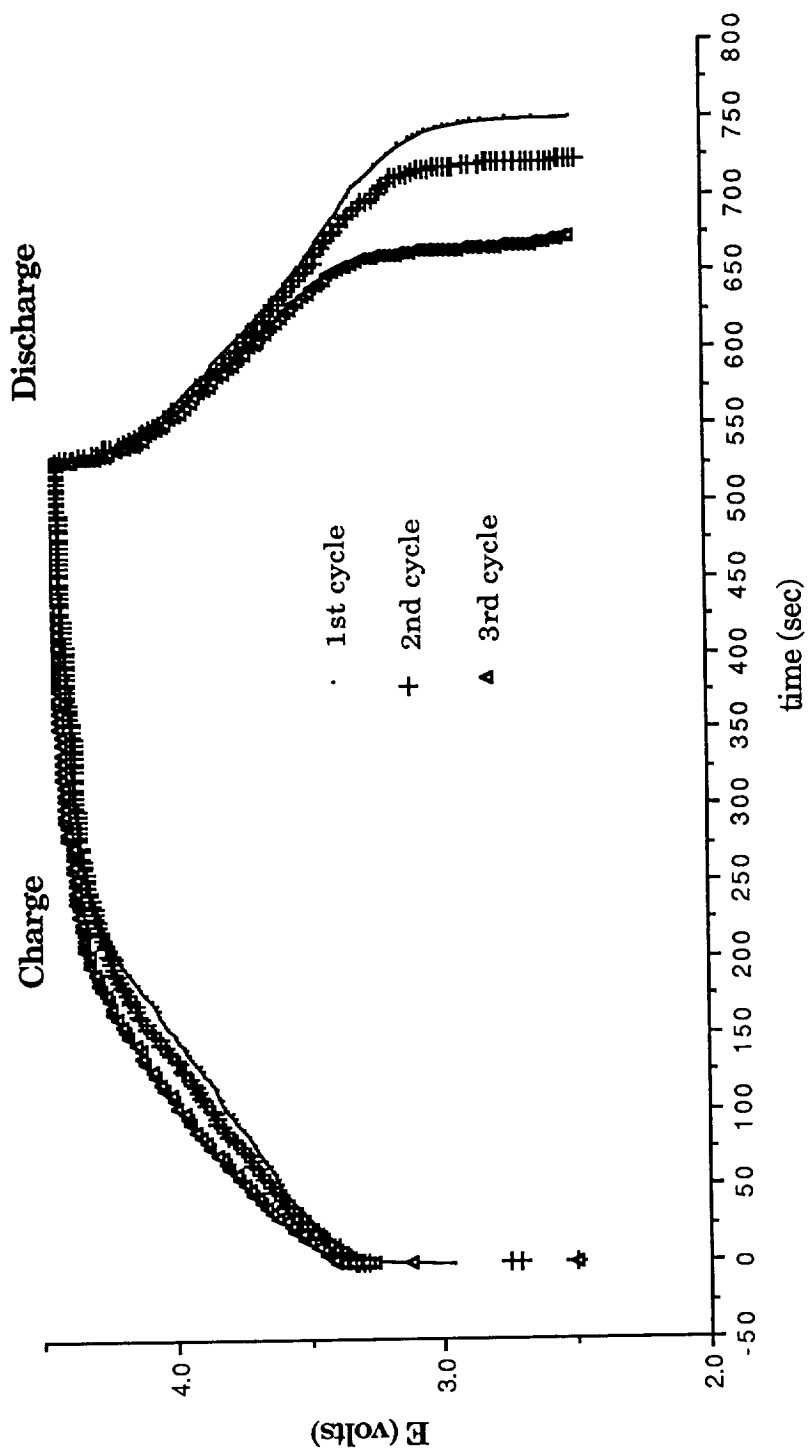


Fig. 35. Charge/Discharge Curves of Li/PPy Conventional Film Battery Using 3Q CV Charge.

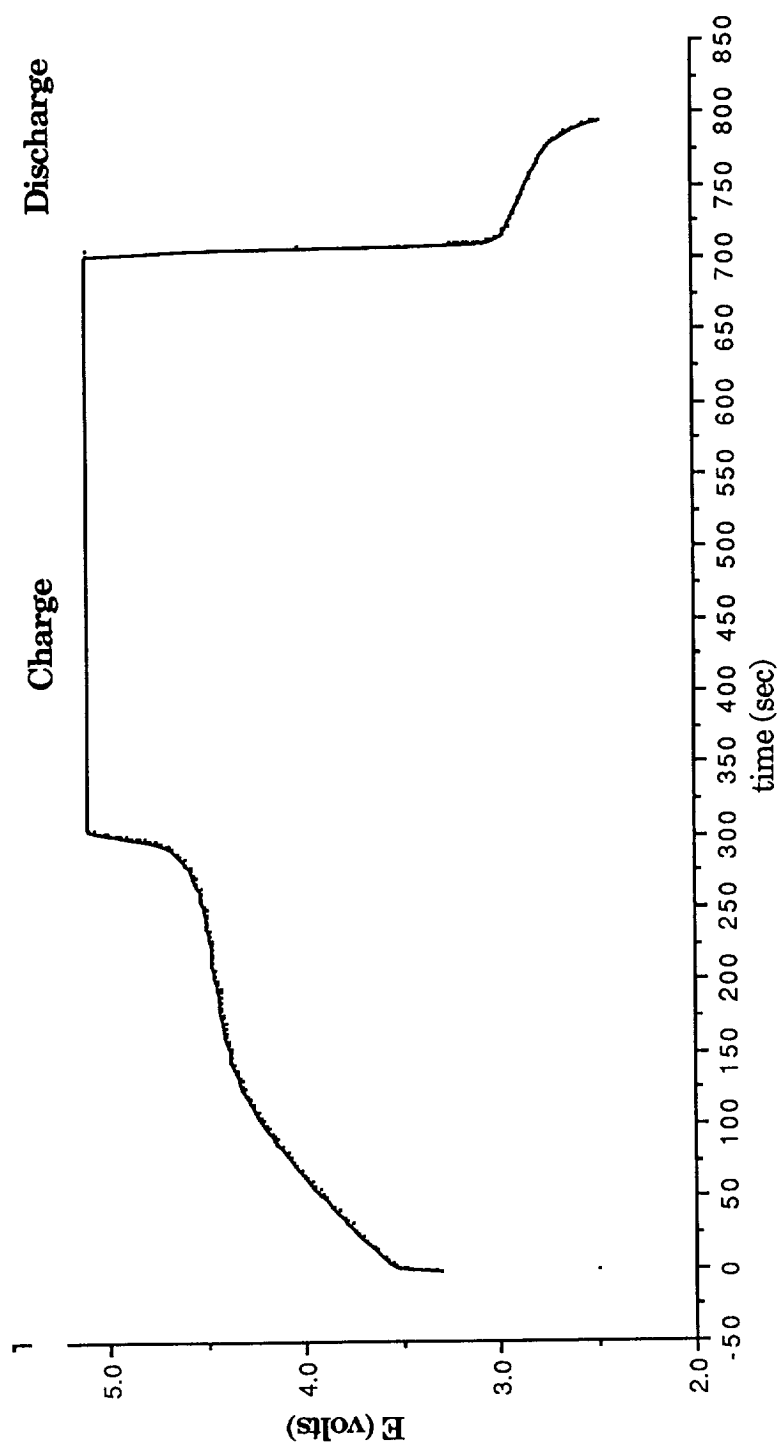


Fig. 36. Charge/Discharge Curve Of Li/PPy Conventional Film Battery Using 4Q CV Charge.

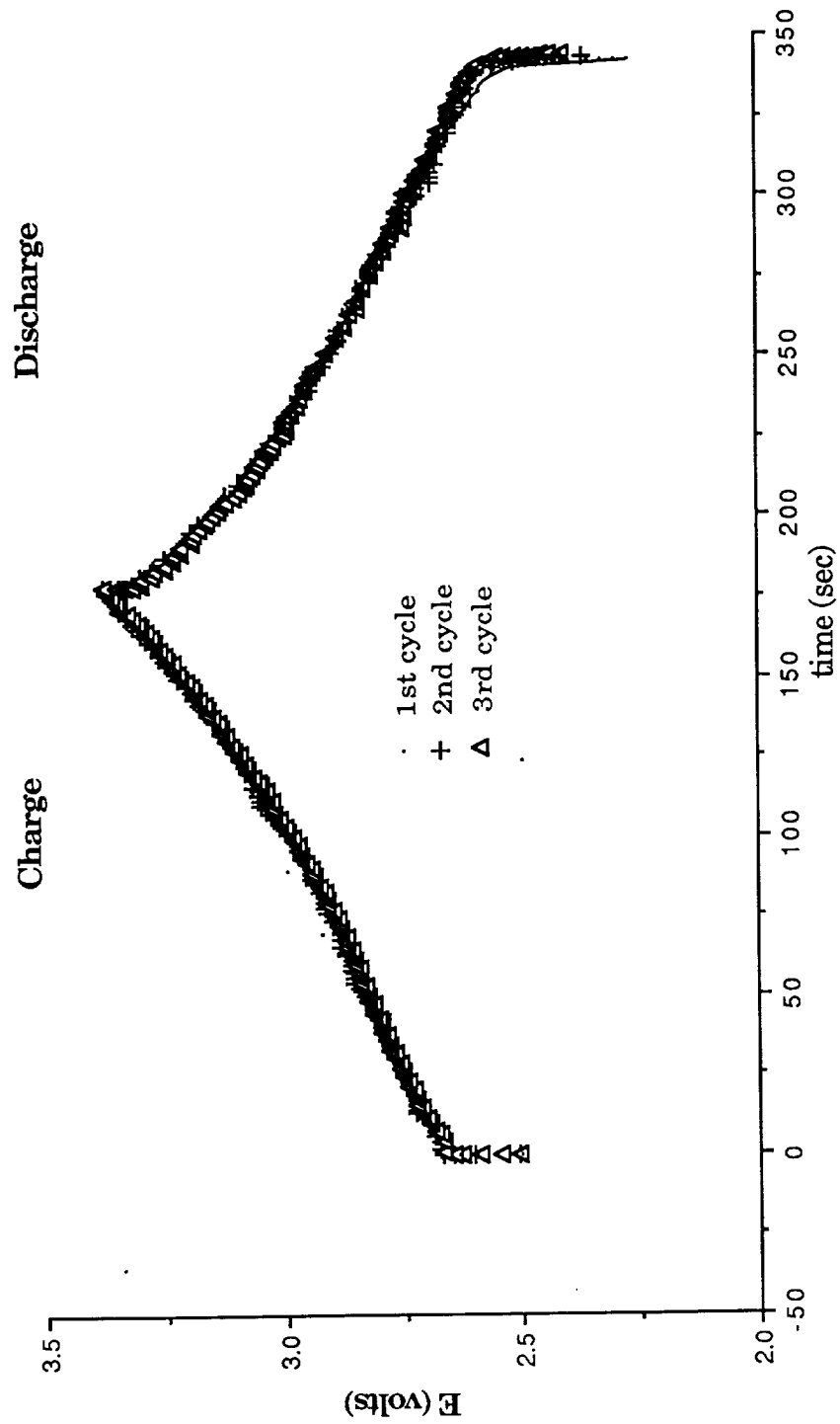


Fig. 37. Charge/Discharge Curves of Li/PPy Fibrillar Film Battery Using 1Q CV Charge. First Three Cycles.

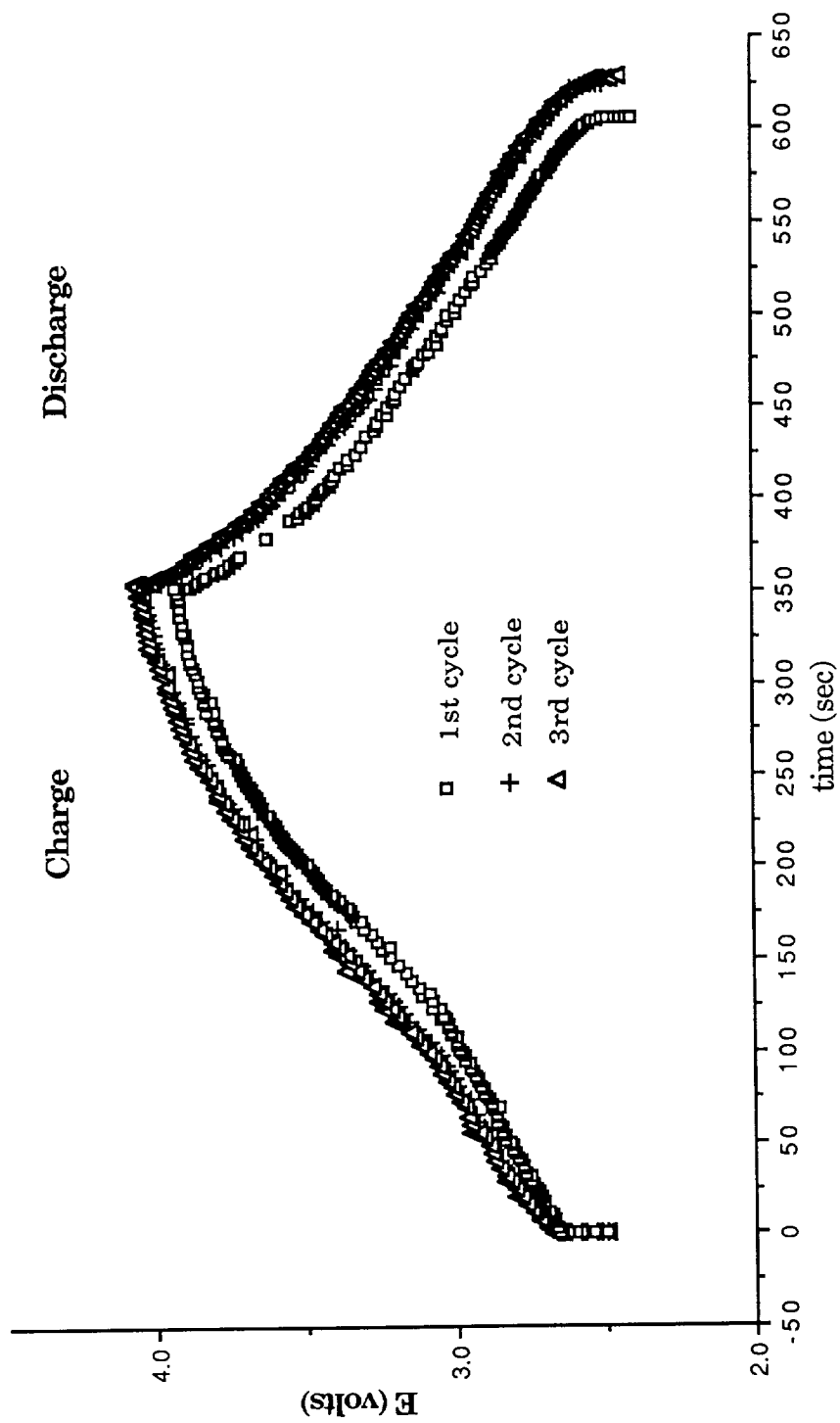


Fig. 38. Charge/Discharge Curves of Li/PPy Fibrillar Film Battery Using 2Q CV Charge.

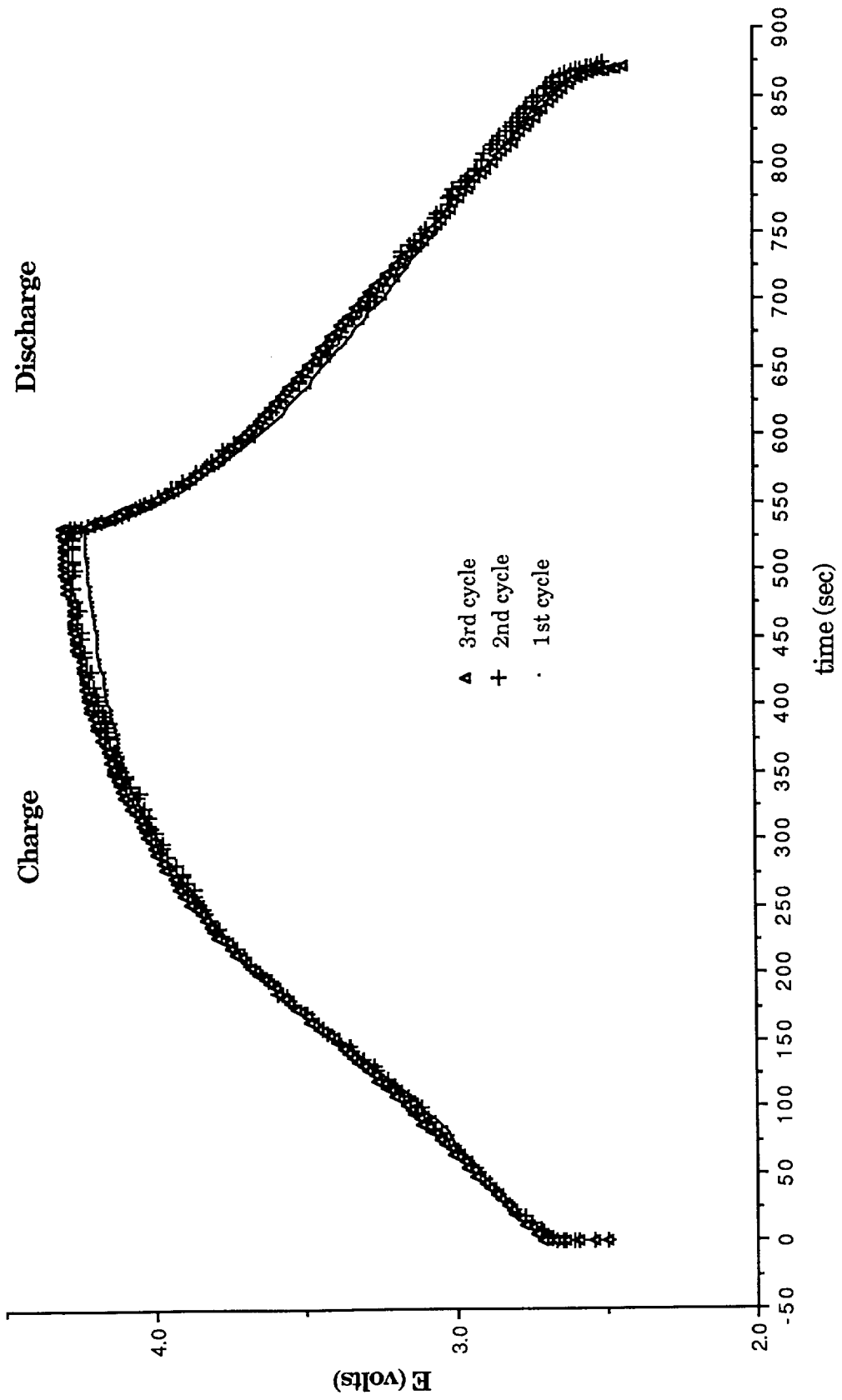


Fig. 39. Charge/Discharge Curves of Li/PPy Fibrillar Film Battery Using 3Q CV Charge.

C-2

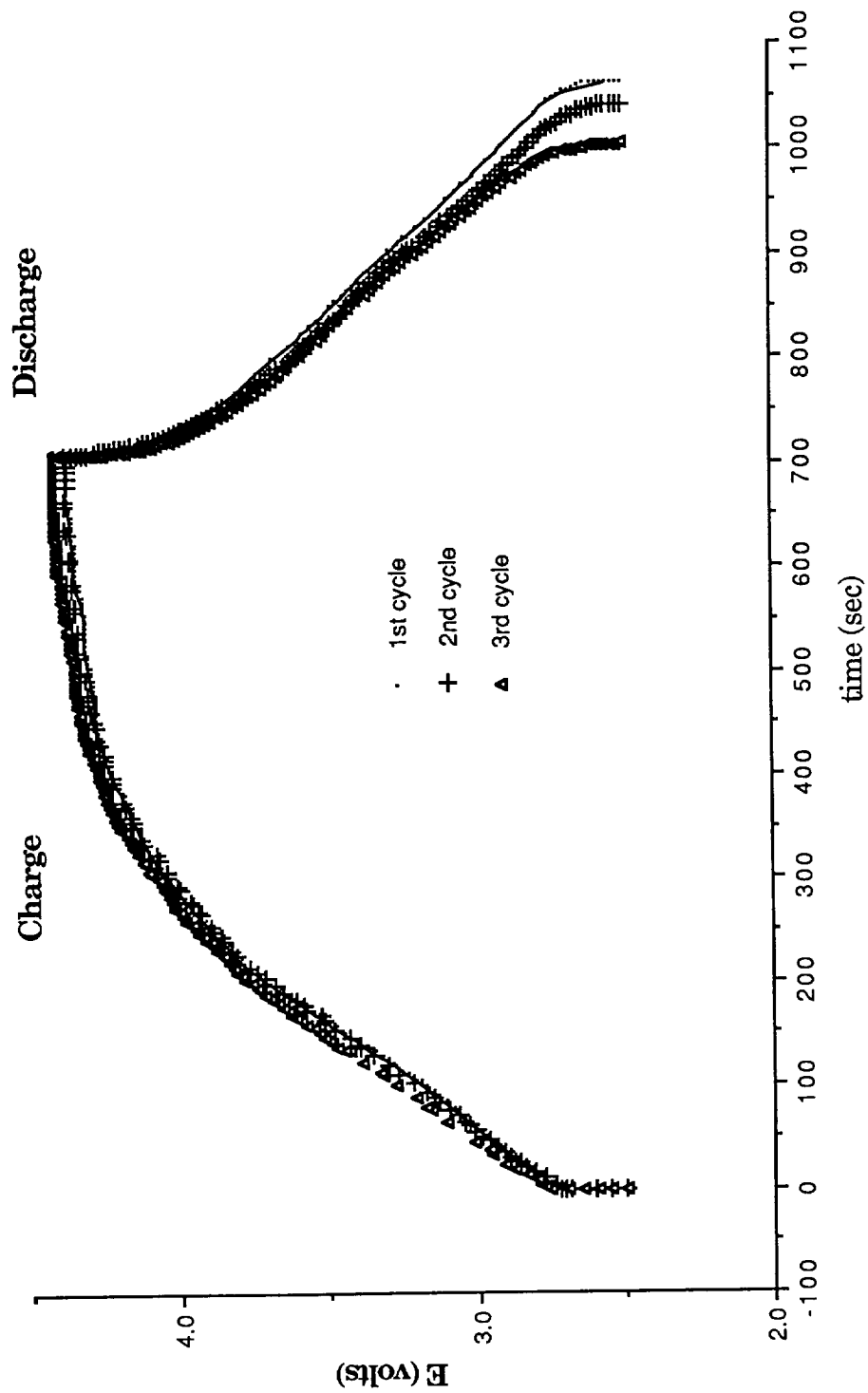


Fig. 40. Charge/Discharge Curves of Li/PPy Fibrillar Film Battery Using 4Q CV Charge.

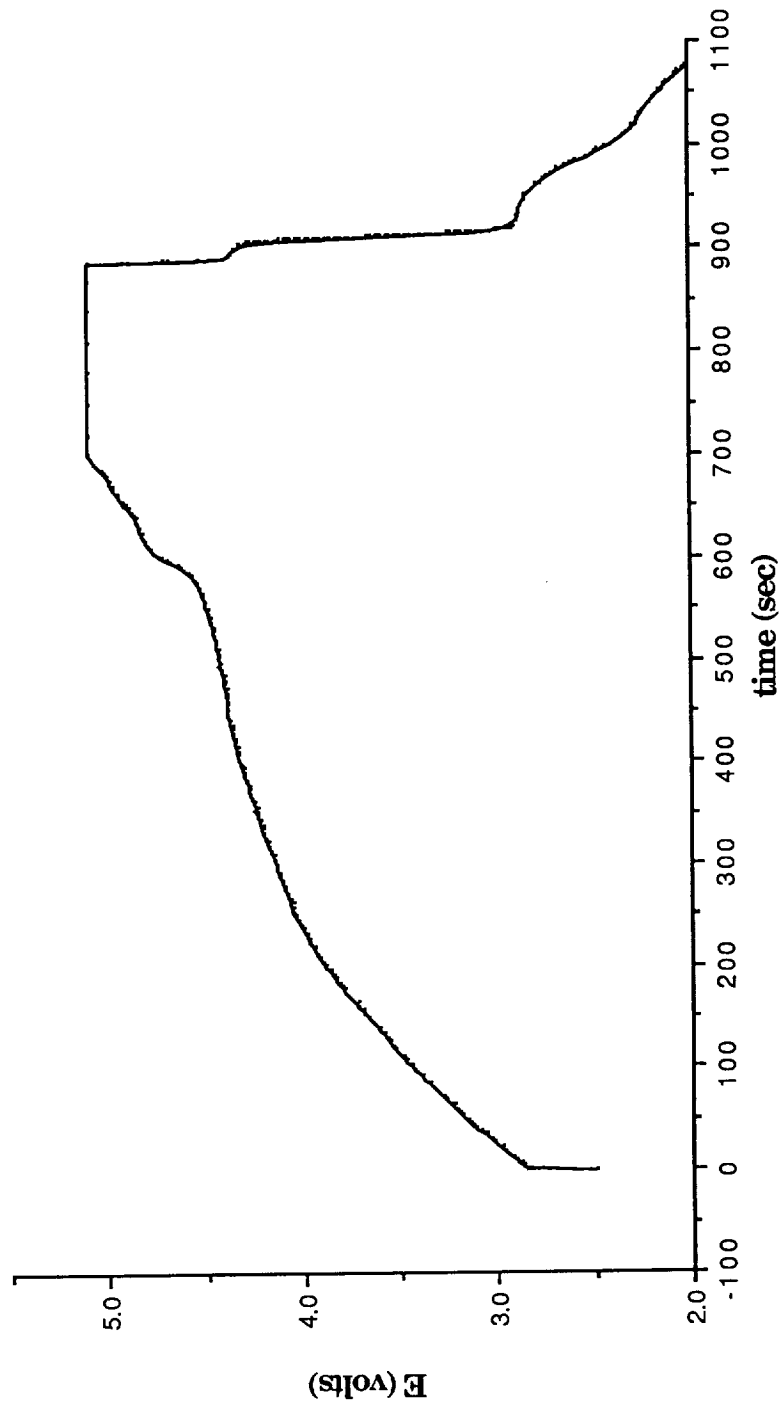


Fig. 41. Charge/Discharge Curve of Li/PPy Fibrillar Film Battery Using 5Q CV Charge.



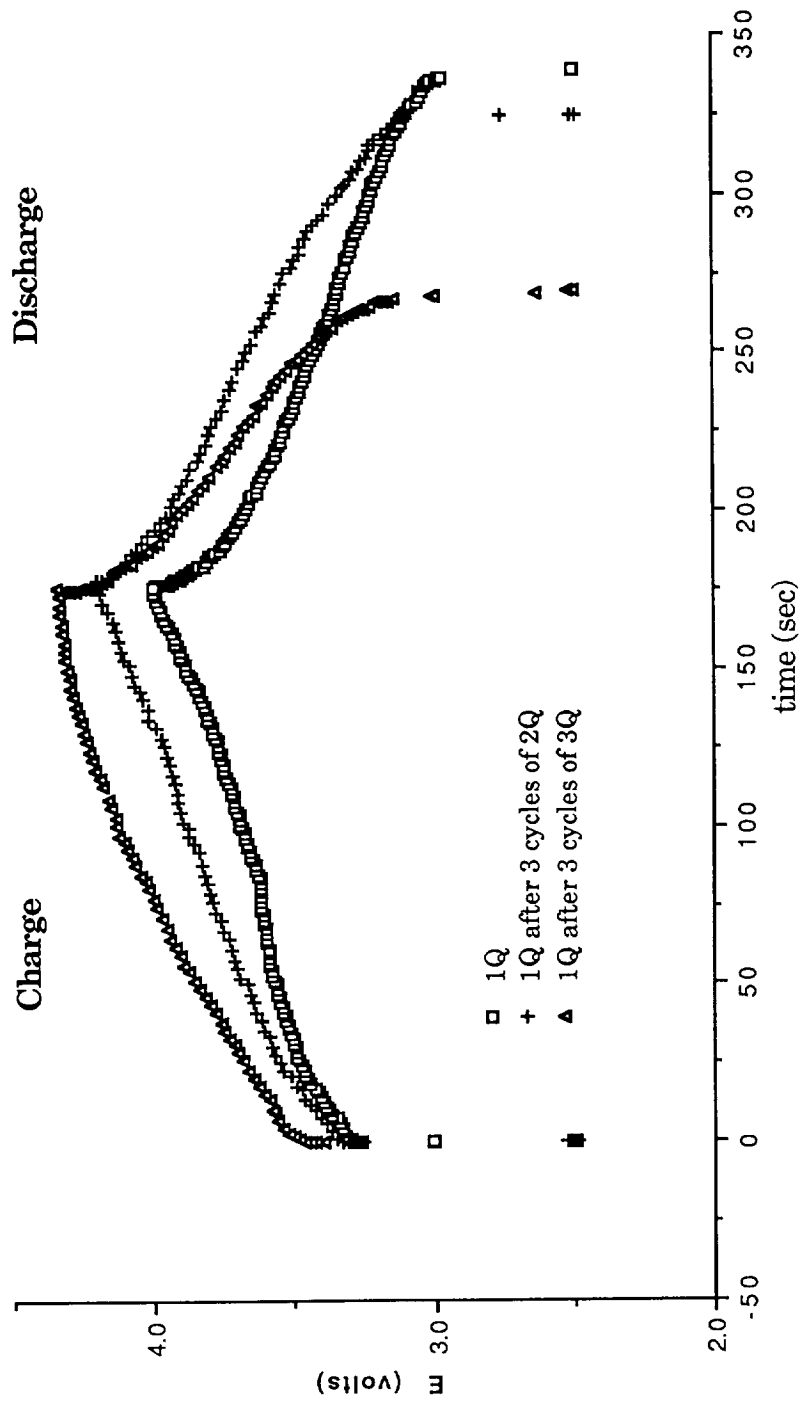


Fig. 42. Charge/Discharge Curves of Li/PPy Conventional Film Battery Using 1Q CV Charge Between 3 Cycles Each of 1Q, 2Q, 3Q, and 4Q CV Charge.

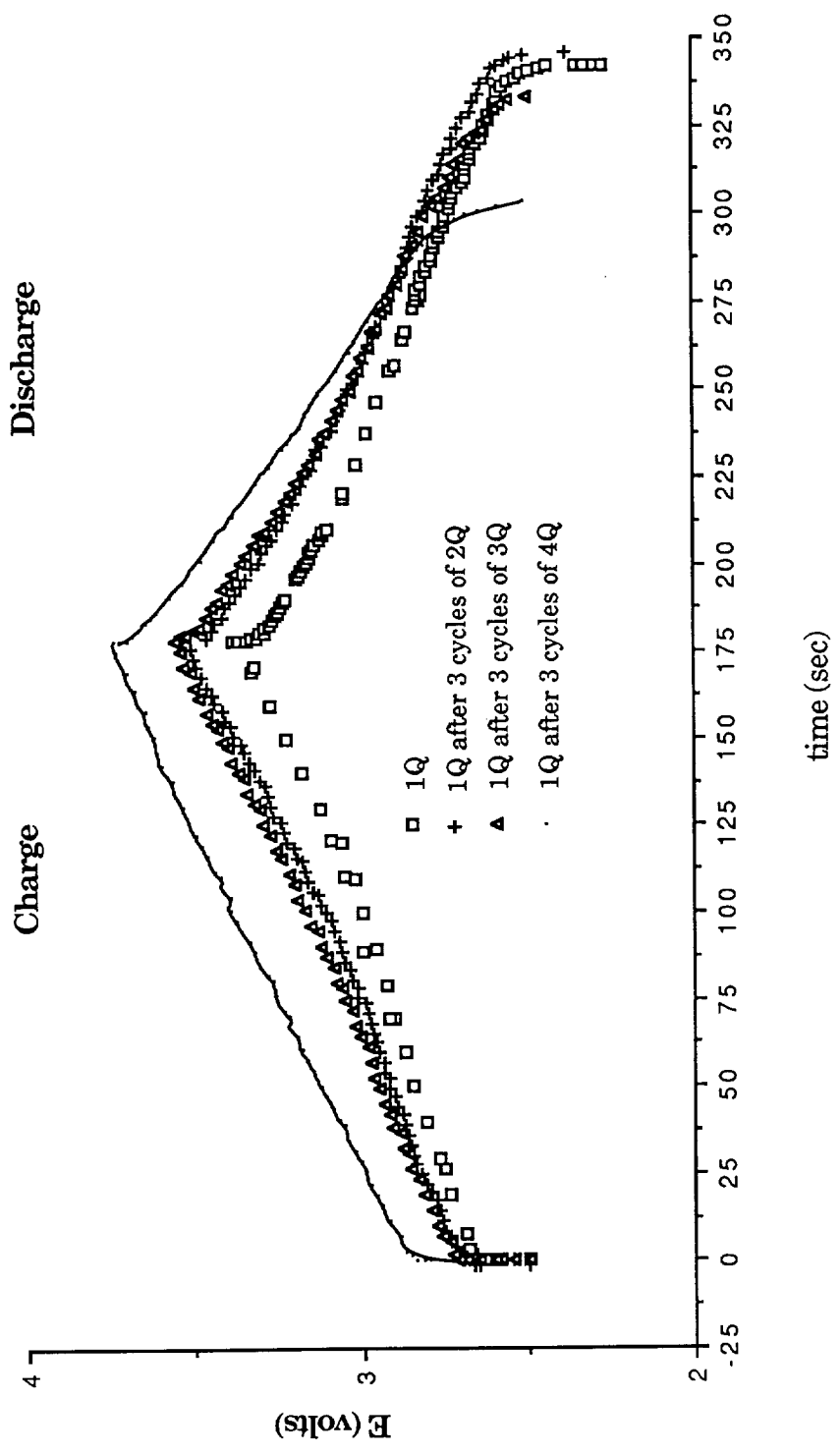


Fig. 43. Charge/Discharge Curves of Li/PPy Fibrillar Film Battery Using 1Q CV Charge Between 3 Cycles Each of 1Q, 2Q, 3Q, and 4Q CV Charge.

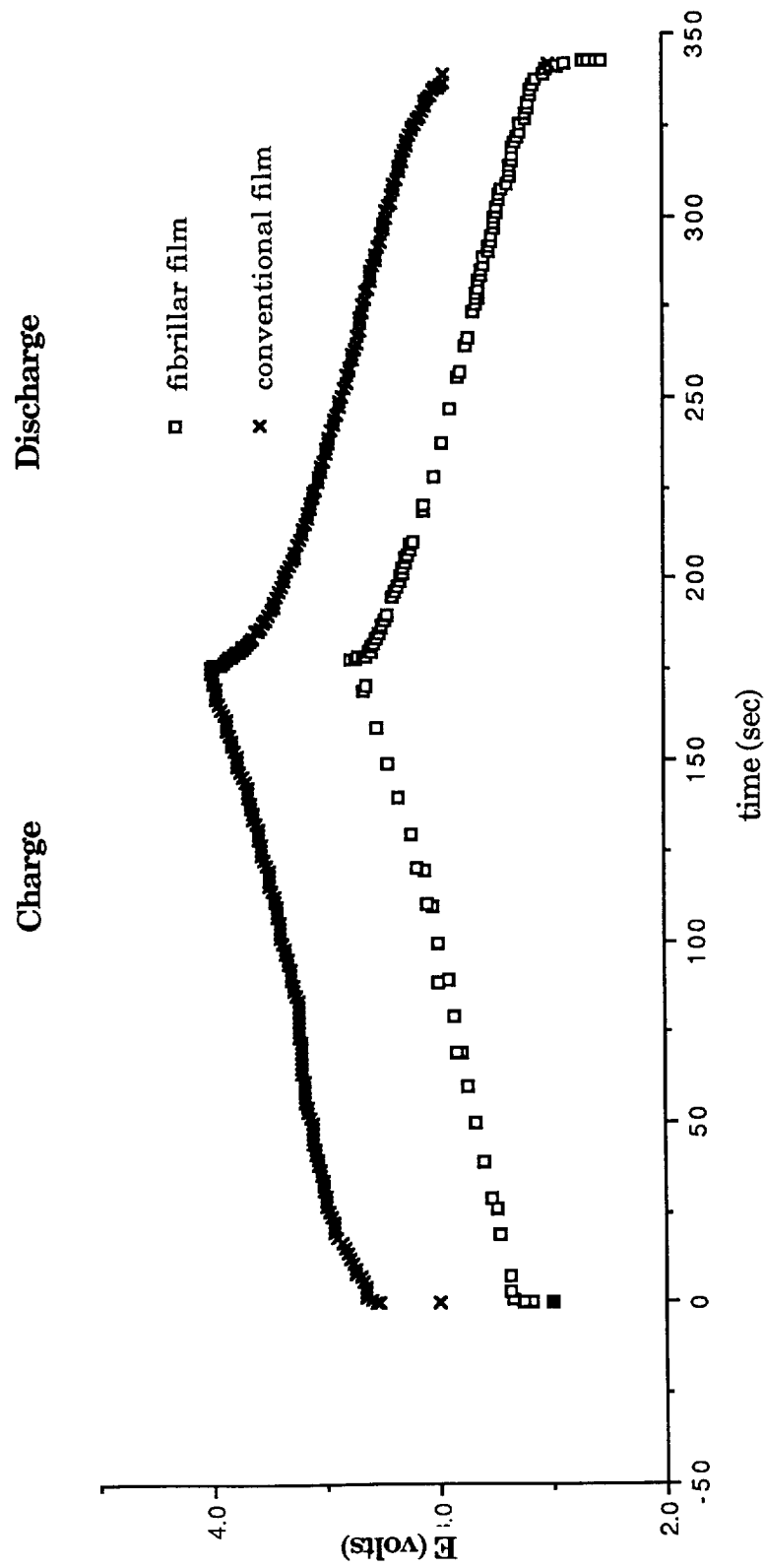


Fig. 44. Charge/Discharge Curves of Li/PPy Conventional Film Battery and Fibrillar Film Battery Using 1Q CV Charge.

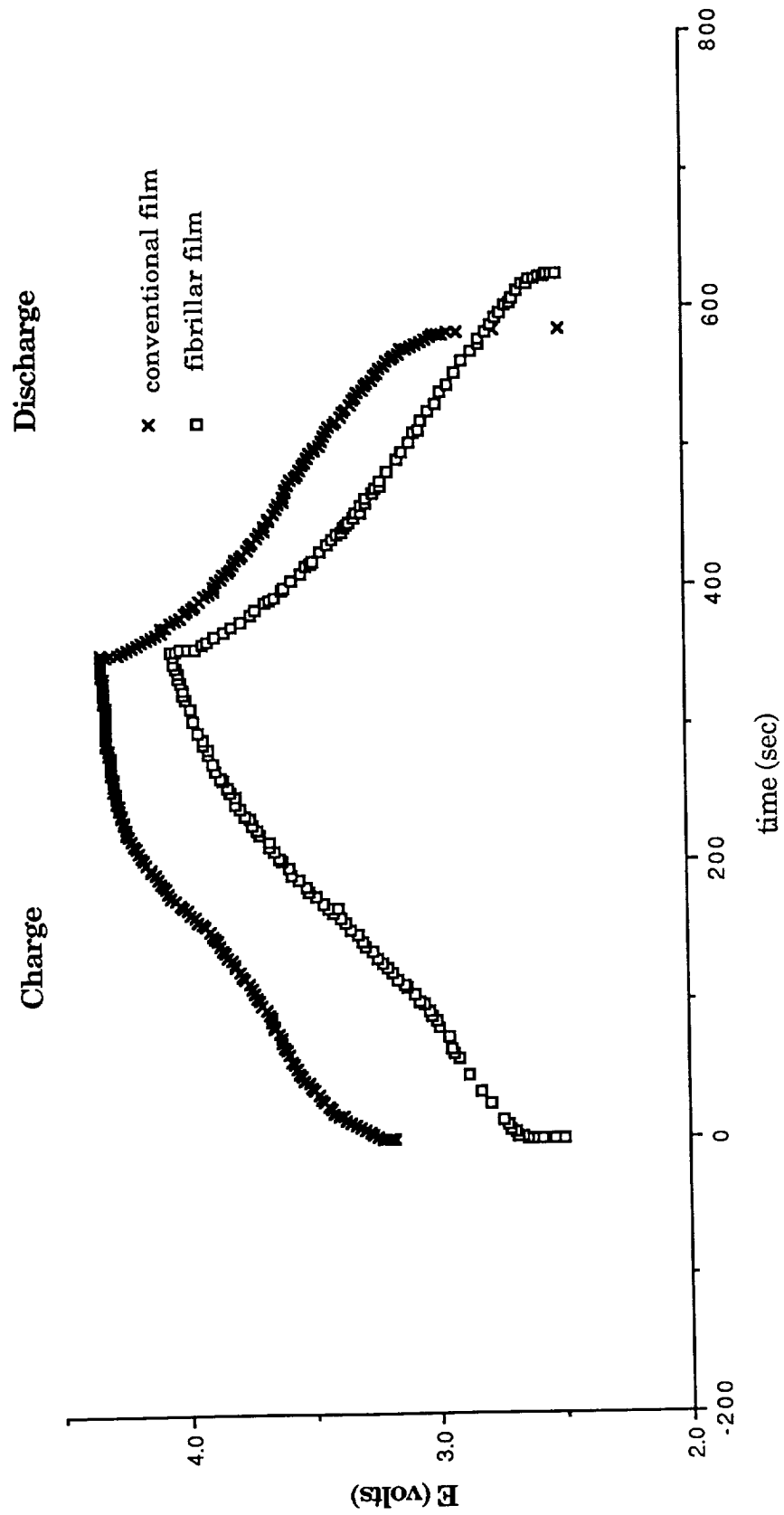


Fig. 45. Charge/Discharge Curves of Li/PPy Conventional Film Battery and Fibrillar Film Battery Using 2Q CV Charge.

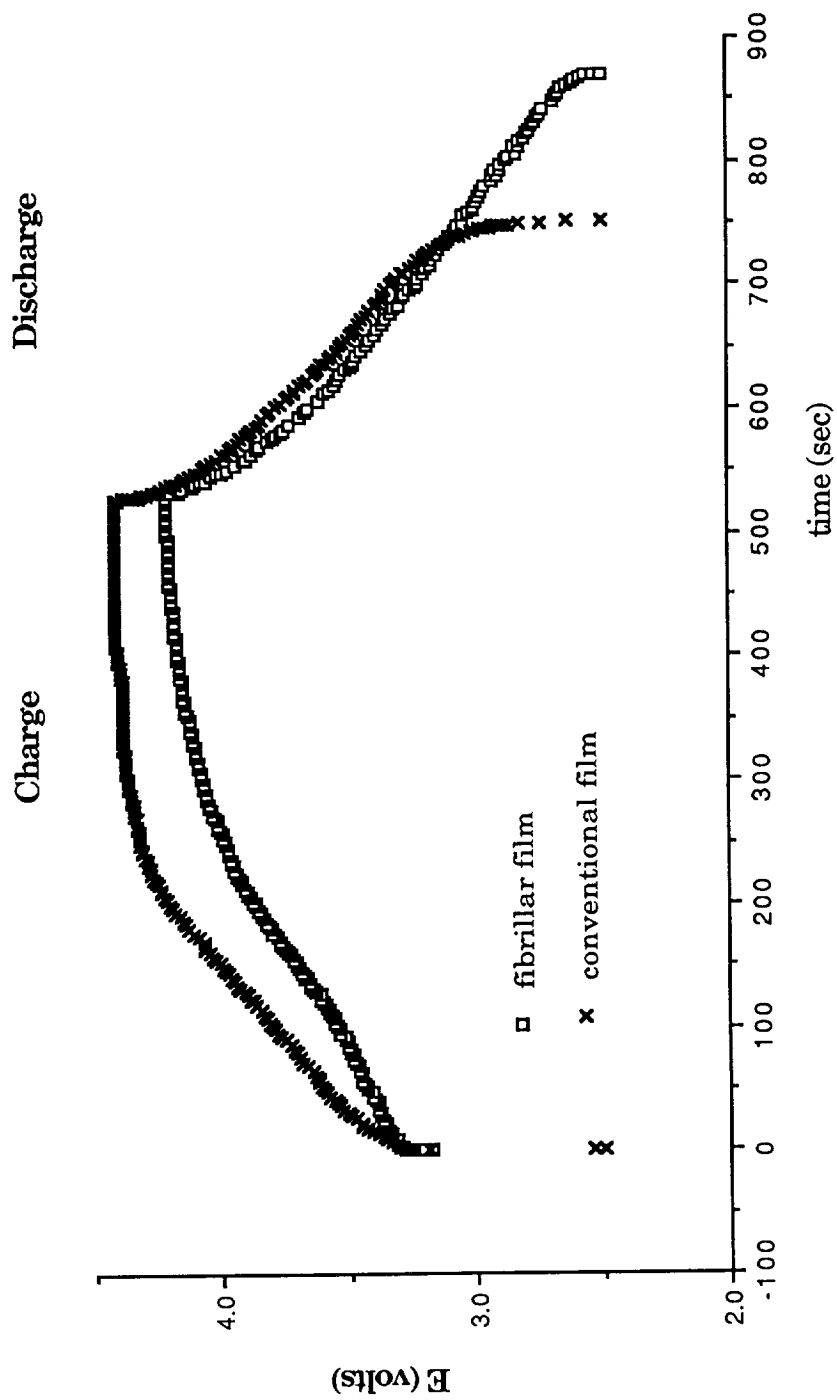


Fig. 46. Charge/Discharge Curves of Li/PPy Conventional Film Battery and Fibrillar Film Battery Using 3Q CV Charge.

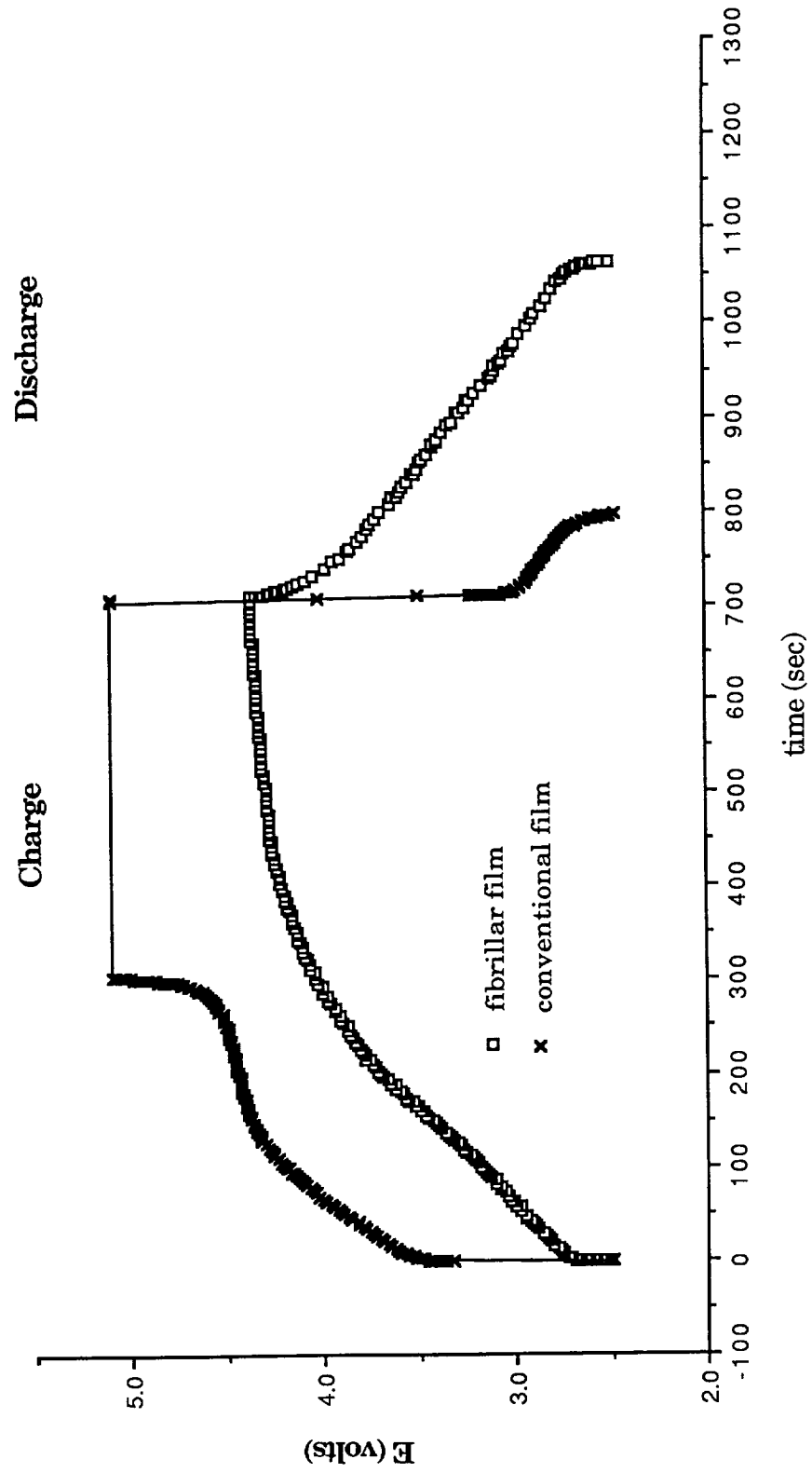


Fig. 47. Charge/Discharge Curves of Li/PPy Conventional Film Battery and Fibrillar Film Battery Using 4Q CV Charge.

various conventional and fibrillar charge/discharge curves into which the same amount of charge was injected. Figures 48 and 49 show charge/discharge curves using 1Q, 2Q, 3Q, 4Q, and 5Q for both a conventional film and a fibrillar film, respectively.

Figure 33 shows the charge/discharge curves from the first three cycles of the conventional film battery using once the charge under the cyclic voltammogram. The curves are very similar in shape and peak current, as well as length of time of discharge. The last two of the three cycles lasted a few seconds longer than the first. This could be because the film may not have been completely reduced after the first charge/discharge cycle, so that the film was still partially charged when the second cycle began.

The next figure, Figure 34, represents three cycles of the same film with twice the amount of CV charge injected. There is a plateau in the charging curve at about the time that 1.5Q CV charge has been injected into the film. This could mean that the battery has reached a maximum charging potential above which it cannot rise until the polymer is completely oxidized. The polymer is considered to be the limiting factor in this experiment because of the amount of lithium used versus the amount of polypyrrole used. There is more lithium metal than polypyrrole present, so the the polypyrrole would become completely oxidized before the lithium electrode would become completely oxidized. The peak potentials rise slightly from first to third cycles, but they are still very similar. The slight rise could be attributed to electrode resistance caused by the film beginning to pull away from the current collector or the beginning of damage to the polymer caused by side reactions not associated with charging. Another sign that polymer

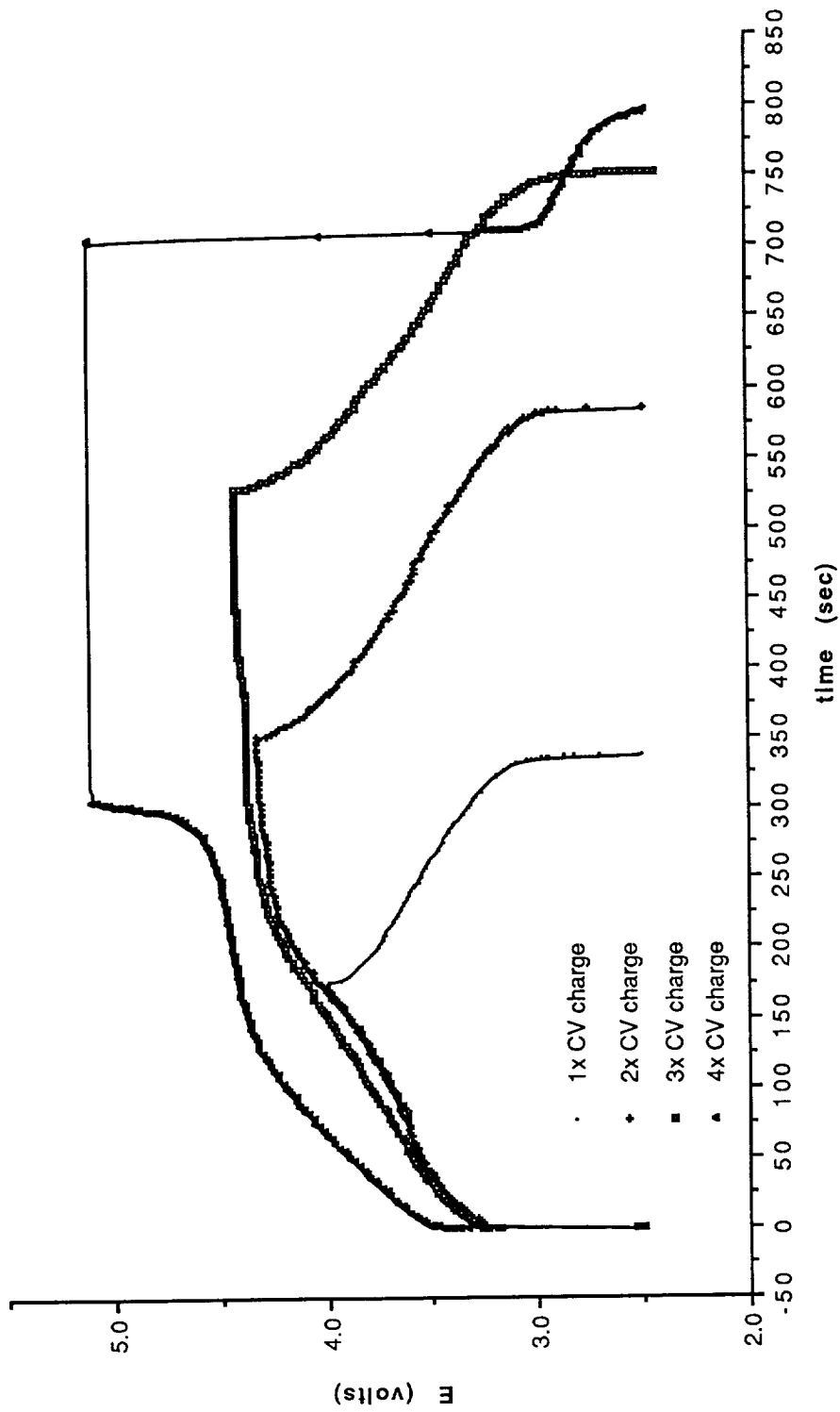


Fig. 48. Charge/Discharge Curves of Li/PPy Conventional Film Battery Using 1Q, 2Q, 3Q, and 4Q CV Charge.



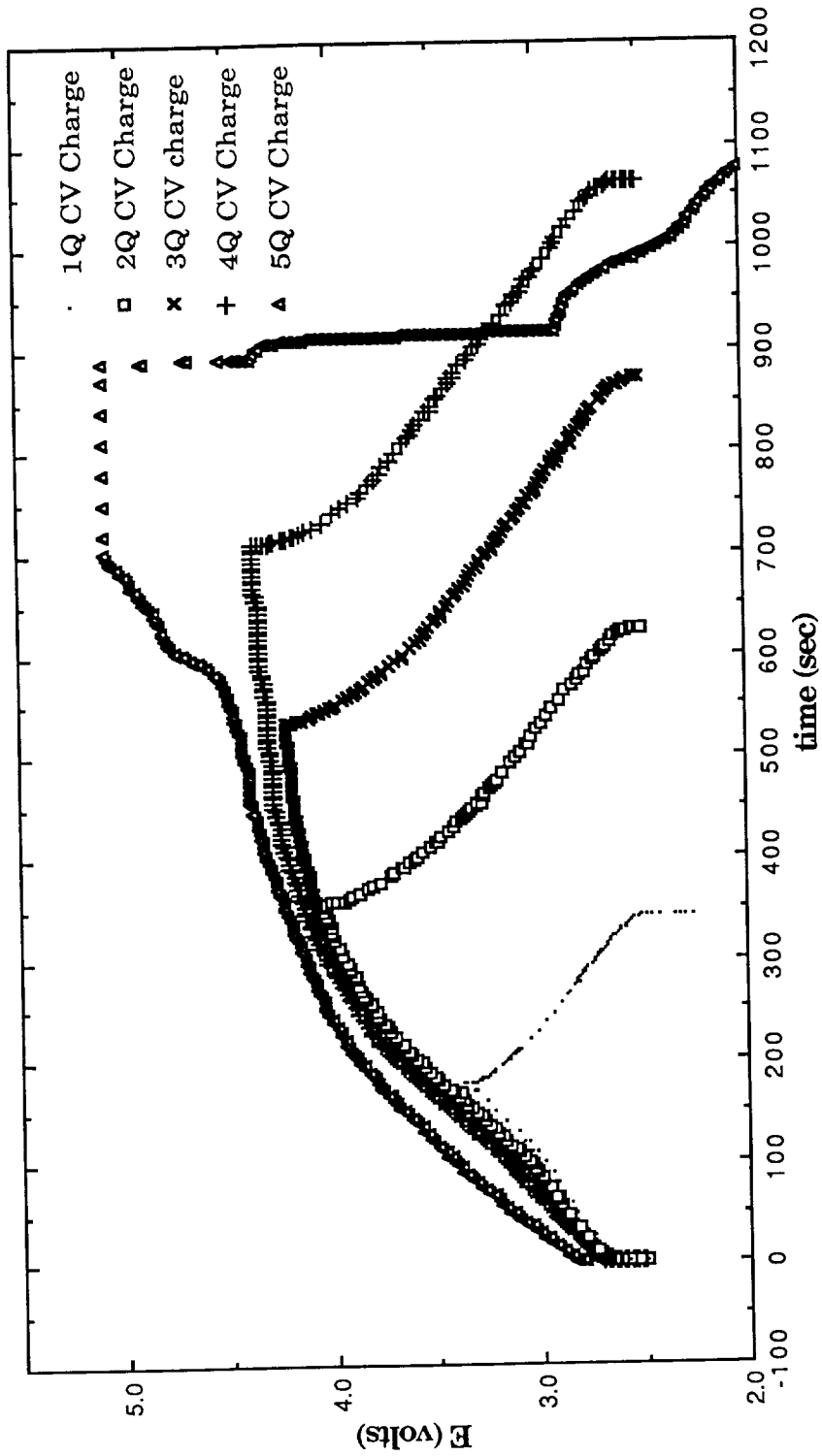


Fig. 49. Charge/Discharge Curves of Li/PPy Fibrillar Film Battery Using 1Q, 2Q, 3Q, 4Q, & 5Q CV Charge.

damage is beginning to occur is the slight decrease in discharge time for the third cycle.

After cycling the battery once using 1Q CV charge, the battery was charged using 3Q CV charge. Figure 35 shows these three charge/discharge curves. Again the charging curve reaches a plateau when approximately 1.5 Q CV charge has been put into the film. The curve rises more sharply and the peak potential rises with subsequent cycles. The discharge time decreased with subsequent cycles, indicating that the battery was beginning to fail.

The battery was cycled using 4Q CV charge after cycling once at 1Q CV charge (Fig. 36). The charging curve rises slightly more sharply and the potential begins to plateau sooner than in the previous figure, where 3Q CV charge was used. The potential begins to rise again when about 1.5 Q CV charge has been injected into the film, and becomes almost vertical before going off scale at 5.1 volts, beyond which the chart recorder being used could not measure the potential. At the start of discharge, the potential dropped immediately to about 3 volts, which was the potential where the discharge curve in the previous figure began to drop off sharply.

The time of discharge in Fig. 36 was less than 100 seconds, which was less than the discharge time of the third cycle of the series of cycles using 3Q CV charge. Therefore, although more charge was put into the battery, 4Q CV charge rather than 3Q CV charge, less charge has been drawn from the battery at this point than was drawn when 3Q CV charge was used. This fact and the fact that the potential went off scale during charging were used as criteria for battery failure. The polymer has undoubtedly suffered irreversible damage, and delamination from the

substrate has occurred. One explanation for these data could be gas evolution at the polypyrrole electrode during overcharging.

The next series of graphs, Figs. 37-41, is similar to Figs. 33-36 in that they represent the same series of experiments that were conducted with a conventional film battery, but a fibrillar battery was used. A cyclic voltammogram was taken after growing the film and before conducting battery charge/discharge experiments. When the first three curves representing cycling the battery three times using the charge found under the the oxidation portion of the cyclic voltammogram (Fig. 37) are superimposed on each other, they look almost identical, showing that the experiment is highly reproducible.

In Fig. 38, the first cycle has a lower peak voltage and a shorter discharge time than the subsequent two cycles. This could be a reflection of a change in IR drop caused by a slight movement of the reference electrode during the changing of the experiment from the galvanostatic to the potentiostatic mode. This is unlikely, however, because the reference electrode was fixed in position by a rubber stopper inserted into an orifice in the top of the cell. Another possibility is that since the chart speed of the chart recorder was changed between the first and second cycles of this series, the shape of the curve could not be accurately reproduced by the digitization method used to transfer the data from chart paper to computer diskette. The shorter discharge time for the first cycle, as found for Fig. 33 for the conventional film, could be caused by the film not being fully discharged after the first cycle with twice the CV charge injected. If residual charge remained in the film after the battery was discharged, it would follow that the next discharge curve would last longer if the same current density were used, which it was. As for the

peak potential for the first cycle being lower than the second and third cycles, this result is similar to those for the conventional film battery in Figs. 33-34. Increased resistance associated with battery age (cycle life) could be the cause of this phenomena. The shape of the curve for the first cycle is nearly identical to the second and third cycle, however, and the data for the first curve is aberrant when compared to the entire body of data. Therefore, the height of the first curve and its length of discharge should not be weighted heavily when considering the data as a whole.

Figure 39 shows data that are more in line with the rest of the work. Charge/discharge curves are shown for a fibrillar film with 3Q CV charge injected into the battery. The shape of the charging and discharging curves are almost identical, with the peak potential rising slightly for each successive cycle. No substantial polymer damage can be seen, as was apparent by this point in the experiment for the cycling of the conventional film battery. However, in the next figure, Fig. 40, some polymer damage is evident, as time of discharge decreases with cycle number. Also, the charging curve for the third cycle occurred at a slightly higher potential than the charging curves of the first two cycles of the battery, where 4Q CV charge was used to charge the battery. Upon using 5Q CV charge to cycle the battery (Fig. 41), after about 575 seconds or 3.3Q CV charge has been put into the battery, the potential begins to rise sharply. At about 690 seconds, or at about 4Q CV charge, the potential rises off scale at approximately 5.2 V. The discharge curve indicates a two step process, and since the polypyrrole reduction reaction is a one step process, the data indicate that another reaction took place in addition to the oxidation and reduction of polypyrrole, one that did irreparable damage to the polymer film. The discharge time of 100 sec

was only a third of the shortest discharge time for the cycles using only 4Q CV charge. In comparison, the conventional film battery failed after only one cycle using 4Q CV charge.

The next two figures, Figures 42 and 43, compare charge/discharge curves of conventional and fibrillar film batteries using 1Q CV charge between 3 cycles each of 1Q, 2Q, 3Q, etc. the CV charge. This was done in order to get an indicator of resiliency of the battery. Would the battery yield a reproducible cycle using 1Q CV charge between increasing increments of charge? As the figures show, the cycles were not very reproducible, but are representative of the battery life and agree well with the other data shown in Figures 33-41. For both the conventional and fibrillar films, the peak potential rises with cycles that were performed later in the experiment, and the discharge time decreases when the battery nears the point of failure.

The peak potentials, and consequently the average discharge potentials, are higher for the conventional film batteries with less than 3Q of charge injected. This makes calculated energy densities (Wh/kg) higher for the conventional film batteries with less than 3Q of charge injected. Table III compares conventional and fibrillar battery energy densities for each of the curves in the experiment. At the point in the experiment that 3Q CV charge is injected into the battery and thereafter, fibrillar film batteries have higher energy efficiencies. Also, the maximum energy density for a fibrillar film is higher than that for a conventional film.

The discharge times for the fibrillar film batteries are longer than the corresponding discharge times for the conventional film batteries, so calculated capacity densities (Ah/kg) are higher for the fibrillar film

Table III. Energy Densities (Wh/kg).

<u>Cycle</u>	<u>Fibrillar</u>	<u>Conventional</u>
1Q #1	94.5	130.7
1Q #2	94.6	133.1
1Q #3	95.2	134.7
2Q #1	156.6	191.4
2Q #2	170.3	188.7
2Q #3	174.6	181.2
1Q	101.3	124.6
3xQ #1	218.5	184.6
3Q #2	223.2	161.6
3Q #3	221.2	122.5
1Q	93.5	79.2
4Q #1	235.4	61.8
4Q #2	219.5	
4Q #3	197.6	
1Q	79.4	
5Q	64.0	

batteries. Capacity densities are calculated from the charge, in amp-hours, released during battery discharge.  $\text{Charge} = It$ , so since this is a constant current experiment, a longer discharge time results in a larger capacity density. Also, the shapes of the charge and discharge curves indicate that the energy efficiencies for the fibrillar film batteries should be higher than the energy efficiencies for the conventional film batteries. The energy efficiency is calculated from the ratio of the area under the discharge curve versus the area under the charging curve, so the less symmetrical the charge and discharge curves are, the lower the energy efficiency will be. Energy efficiencies for conventional and fibrillar film batteries are given in Table IV.

Energy efficiencies for the first three cycles are very similar, but thereafter the energy efficiencies are higher for the fibrillar film batteries. The charge and discharge curves in Fig. 42, representing the conventional film battery, begin to plateau near the peak potentials and drop off sharply before beginning a steady decline. The voltage plateau near the end of the charging curve raises the energy put into the battery, and the drop off at the beginning of the discharge curve decreases the area under that curve relative to that of the charging curve, lowering the energy efficiency measured in that cycle. In contrast, the charge/discharge curves for the fibrillar battery shown in Fig. 43 are more symmetrical, with the exception of the curve recorded after 3 cycles of 4Q CV charge had been performed, and the discharge time was much shorter than the charging time. The symmetry of these curves suggests higher energy efficiencies for the fibrillar films.

Coulombic efficiencies for the fibrillar films are higher also. Coulombic efficiency is defined as charge drawn out of the battery divided

Table IV. Energy Efficiencies (%) -  $Q_{out}/Q_{in}$ .

<u>Cycle</u>	<u>Fibrillar</u>	<u>Flat</u>
1Q #1	89.9	88.7
1Q #2	90.2	90.3
1Q #3	90.9	91.4
2Q #1	67.0	59.9
2Q #2	70.4	59.0
2Q #3	71.7	56.8
1Q	94.3	81.0
3Q #1	55.9	36.8
3Q #2	56.8	32.0
3Q #3	55.9	23.9
1Q	84.8	48.9
4Q #1	42.8	8.1
4Q #2	39.7	
4Q #3	35.4	
1Q	67.9	
5Q	8.4	



by charge put into the battery. If all the charge which has been put into the battery could be extracted from the battery, the coulombic efficiency would be 100%. Coulombic efficiencies are tabulated in Table V. As with the energy efficiencies, the coulombic efficiencies are similar for the first three cycles but the fibrillar batteries show superior performance thereafter. The discharge times for the fibrillar curves are longer than those for the corresponding conventional film batteries for the cycles recorded later in the battery life (i.e., 2Q, 3Q, and 4Q CV charge). So, although the conventional films have higher energy densities than the fibrillar films because of their higher average discharge voltages, the fibrillar films have higher energy efficiencies because of their symmetry, and higher coulombic efficiencies because of their longer discharge times.

Figures 44-47 illustrate the differences between the charge/discharge curves of the conventional film battery and the fibrillar film battery with the same injected charge. For 1Q CV charge injected, represented in Fig.44, there is no marked difference in time of discharge and curve shape between the conventional and fibrillar batteries. The peak potential and average discharge voltage for the fibrillar film battery are 0.6 V lower than the conventional film battery, making its energy density lower than the conventional film battery. In Fig. 45, charge/discharge curves for 2Q CV charge injected for the conventional and fibrillar films are shown. The peak potential is still higher for the conventional film battery, but this battery fails sooner. The voltage begins to reach a plateau sooner for the charging curve of the conventional film battery. This indicates that it can be saturated with a lesser amount of charge, although it has the same amount of polymer as the fibrillar polypyrrole battery.

Table V. Coulombic Efficiencies (%).

<u>Cycle</u>	<u>Fibrillar</u>	<u>Conventional</u>
1Q #1	90.8	90.6
1Q #2	88.4	91.6
1Q #3	90.4	91.7
2Q #1	69.6	63.9
2Q #2	74.2	64.5
2x #3	76.4	61.9
1Q	92.8	85.6
3Q #1	62.2	44.9
3Q #2	63.0	39.3
3Q #3	63.1	27.0
1Q	86.5	49.9
4Q #1	49.1	12.7
4Q #2	45.7	
4Q #3	40.5	
1Q	67.4	
5Q	16.0	

The steeper drop-off in the discharge curve for the conventional film battery means that IR drop makes a greater percentage contribution to the peak potential of that battery than it does to the peak potential of the fibrillar battery.

Again, since the fibrillar charge and discharge curves are more symmetrical, its energy efficiency will be higher. When 3Q CV charge is injected into each type of battery (Fig. 46), similar effects can be seen. The conventional film battery charging curve reaches a plateau at the same time it did previously, when approximately 1.5 Q CV charge has been used as a basis. The fibrillar film charging curve plateaus when 2Q CV charge has been used, indicating that although it stores more charge before becoming saturated, its full capacity at this current density has been reached. The potential at its peak is still higher for the conventional film battery here, but drops within a few seconds to near the value of the fibrillar battery, and fails over 125 seconds sooner.

In Fig. 47, which shows the conventional film and fibrillar film charge and discharge curves using 4Q CV charge, differences between the two types of batteries are even more pronounced. The potential for the conventional film battery rises immediately upon beginning the charging cycle to 3.6 V, about 0.5 V higher than previously when 3Q CV charge was injected, indicating increased resistance in the battery. As mentioned before, it rises off scale at 1.5Q CV charge and fails in less than 100 seconds upon discharge. The voltage during charging of the fibrillar film battery does not rise off scale when 4Q amount of charge is put into the battery but does begin to plateau at about 2Q CV charge. The discharge time is 362 seconds, more than three times as long as the conventional film battery. However, upon twice more cycling at 4Q CV

charge and once at 1Q CV charge, the fibrillar battery fails during the cycle when 5Q CV charge is used. The potential begins to rise at about 575 seconds into the charging curve and goes off scale at about 4Q CV charge. The discharge curve was recorded for a longer time than the others to illustrate the multi-step process that occurs when the battery is overcharged. The potential rises to several plateaus in the charging curve and drops to several plateaus during discharge. This series of figures (Figs. 44-47) has illustrated that the conventional film batteries charge and discharge at a higher potential than the fibrillar ones, but have shorter discharge times when more than 1Q CV charge is injected and have a shorter cycle life for the experiment conducted.

Figures 48 and 49 compare the charge and discharge curves for the first cycle of every charge increment put into each type of batteries. Figure 48 shows cycles of 1Q, 2Q, 3Q, and 4Q CV charge for the conventional film battery and Fig. 49 pictures cycles of 1Q, 2Q, 3Q, 4Q, and 5Q CV charge for the fibrillar film battery. The charging curve for 4Q CV charge in Fig. 48, for the conventional film, departs from the rest of the charging curves at the beginning of the cycle, indicating that the resistance in the battery has increased. Also, it can be seen that although 1.5 times the amount of charge has been put into the film, the discharge time for 3Q CV charge curve is slightly less (223.8 sec) than the discharge time for the 2Q CV charge (229.5 sec). When 4Q amount of CV charge is put into the film, the discharge time (92 sec) is considerably less than even the discharge time when 1Q amount of charge under the CV is used (162.5 sec).

In Fig. 49, which shows data for the fibrillar film, the potential of the charging curve for 5Q CV charge used remains similar to the

previously recorded curves in the experiment until the potential rises off the plateau, which shows lesser internal resistance in the battery and little polymer electrode damage up to that point. More evidence that the polymer remains undamaged until that point can be found when comparing discharge times. Each time the battery is cycled using a greater increment of charge, more charge is obtained from the battery, until battery failure occurred. The discharge times are 158.5 seconds for the 1Q cycle, 252 seconds for the 2Q cycle, 338 seconds for the 3Q cycle, 354 seconds for the 4Q cycle, and 105 seconds for the 5Q cycle. The data in Fig. 49, when compared with the conventional film data in Fig. 48, show that the conventional film battery has increased internal resistance at an earlier point in the experiment, at the beginning of the first 4Q cycle rather than near the end of the first 5Q cycle. Also, the lesser relative discharge times for the conventional films are well illustrated in these two figures.

## CHAPTER V

### CONCLUSIONS

Li/polypyrrole batteries have been made and studied using electron microscopy, cyclic voltammetry, and constant current charge and discharge. Electron microscopy showed that one side of a porous  $\text{Al}_2\text{O}_3$  membrane can be covered with a pinhole-free Au film and the base layer of PPy present in previous work can be eliminated. Cyclic voltammetry showed that as conventional film thickness increases, charge transport in the film becomes diffusion-controlled. The peak current,  $I_p$ , is directly proportional to scan rate for thin films, but as film thickness increases,  $I_p$  becomes directly proportional to the square root of scan rate as is expected for diffusion-controlled processes.

Battery charge/discharge studies showed that a battery made with fibrillar polypyrrole film can store more charge than one made with a conventionally grown polypyrrole film. For greater increments of charge injected into the battery, fibrillar film batteries exhibit higher charge capacities, energy densities and coulombic efficiencies. However, for lesser increments of charge, battery performance was very similar for the two types of batteries. A higher degree of charge /discharge curve symmetry resulted in higher energy efficiencies for the fibrillar film batteries.

Future work in this area should include investigation into improving treatment of the fibrillar polypyrrole films so that the negative shift in  $E_p$  seen in the cyclic voltammetry (Figs. 25 and 30) can be eliminated. Elimination of this negative shift would result in a rise in the cell potential during discharge. This would in turn result in higher

energy densities for the fibrillar film batteries. Alternatively, a polymer with a higher oxidation potential (e.g., polythiophene) could be used. A study of fibrillar film batteries with different amounts of polymer discharged at different current densities would also be useful in order to find the optimum value of energy density for the battery. Also, a constant load or constant potential discharge of the battery rather than a constant current discharge might give a better overall view of the battery's utility.

## REFERENCES

1. M. Kanatzidis, *C&E News*, 36, December (1990).
2. J. R. Reynolds, *CHEMTECH*, 440, July (1988).
3. A. Diaz, *Chemica Scripta*, 17, 145 (1981).
4. G. B. Street, R. H. Geiss, S. E. Lindsay, A. Nazzal, and P. Pfluger, in *Proceedings of the Conference on Electronic Excitation, and Interaction Processes in Organic Molecular Aggregates*, P. Reineker, H. Haken, and H. C. Wolf, eds., Springer, New York, 242 (1983).
5. H. Munstedt, G. Kohler, H. Mohwald, D. Naegle, R. Bitthin, G. Ely, and E. Meissner, *Synthetic Metals*, 18, 259 (1987).
6. S. Panero, P. Prospero, and B. Scrosati, *Electrochimica Acta*, 32, 1465 (1987).
7. S. Panero, P. Prospero, B. Klapptse, and B. Scrosati, *Electrochimica Acta*, 31, 1597 (1986).
8. P. Buttol, M. Mastragostino, S. Panero, and B. Scrosati, *Electrochimica Acta*, 31, 783 (1986).
9. P. Passiniemi and J.-E. Osterholm, *Synthetic Metals*, 18, 637 (1987).
10. L. W. Shacklette, M. Maxfield, S. Gould, J. S. Wolf, T. R. Jow, and R. H. Baughman, *Synthetic Metals*, 18, 611 (1987).
11. T. Osaka, K. Naoi, M. Maeda, and S. Nakamura, *J. Electrochem. Soc.*, 136, 1385 (1989).
12. K. Naoi and T. Osaka, *J. Electrochem. Soc.*, 134, 2479 (1987).
13. T. Osaka, K. Naoi, and S. Ogano, *J. Electrochem. Soc.*, 134, 2096 (1987).
14. T. Osaka, K. Naoi, H. Sakai, and S. Ogano, *J. Electrochem. Soc.*, 134, 285 (1987).



15. K. Naoi, A. Ishijima, and T. Osaka, *J. Electroanalytical Chem.*, **217**, 203 (1987).
16. K. Naoi, T. Hirabayashi, I. Tsubota, and T. Osaka, *Bull. Chem. Soc. Jpn.*, **60**, 1213 (1987).
17. T. Osaka, K. Naoi, S. Ogano, and S. Nakamura, *Chemistry Letters*, 1687 (1986).
18. F. Trinidad, J. Alonso-Lopez, and M. Nebot, *J. App. Electrochem.*, **17**, 215 (1987).
19. A. G. MacDiarmid, L. S. Kang, W. S. Huang, and B. D. Humphrey, *Synthetic Metals*, **18**, 393 (1987).
20. R. B. Kaner and A. G. MacDiarmid, *Synthetic Metals*, **14**, 3 (1986).
21. M. Maxfield, S. L. Mu, and A. G. MacDiarmid, *J. Electrochem. Soc.*, **134**, 838 (1985).
22. W. Wanqun, R. J. Mammone, and A. G. MacDiarmid, *Synthetic Metals*, **10**, 235 (1985).
23. J. Caja, R. B. Kaner, A. G. MacDiarmid, *J. Electrochem Soc.*, **131**, 2744 (1984).
24. K. Kaneto, M. Maxfield, D. P. Nairns, A. G. MacDiarmid, and A. J. Heeger, *J. Am. Chem. Soc., Faraday Trans. 1*, **78**, 3417 (1982).
25. P. J. Nigrey, A. G. MacDiarmid, and A. J. Heeger, *Mol. Cryst. Liq. Cryst*, **83**, 309 (1982).
26. P. J. Nigrey, David MacInnes, Jr., D. P. Nairns, A. G. MacDiarmid, and A. J. Heeger, *J. Electrochem. Soc.*, **128**, 1652 (1981).
27. N. Mermilliod, J. Tanguy, and F. Petiot, *J. Electrochem. Soc.*, **133**, 1073 (1986).
28. T. Yamamoto, M. Zama, and A. Yamamoto, *Chemistry Letters (Chemical Soc. Japan)*, 563 (1985).

29. A. F. Diaz, J. I. Castillo, J. A. Logan, and W. Lee, *J. Electroanal. Chem.*, **129**, 115 (1981).
30. B. J. Feldman, R. Burgmayer, and R. W. Murray, *J Am. Chem. Soc.*, **107**, 872 (1985).
31. M. Gazzard, in "Handbook of Conducting Polymers", vol. 1 , T. A. Skotheim, ed., New York: Marcel Dekker, 673 (1986).
32. J. W. Thackeray, H. S. White, and M. S. Wrighton, *J. Phys. Chem.*, **89**, 5133 (1985).
33. A. F. Diaz and J. I. Castillo, *J. C. S. Chem Comm*, 397 (1980).
34. G. B. Street, in "Handbook of Conducting Polymers," vol. 1 , T. A. Skotheim, ed., New York: Marcel Dekker, 265 (1986).
35. D. A. Buttry, Invited Lecture, , 193rd ACS National Meeting, Denver, CO, April 5 (1987).
36. R. M. Penner, Ph. D. Dissertation, Texas A&M University (1987).
37. R. M. Penner, L. Van Dyke and C. Martin, *J. Phys. Chem.*, **92**, 5274 (1988).
38. L. Van Dyke and C. Martin, *Langmuir*, **6**, 1118 (1990).
39. L. Van Dyke and C. Martin, *Synthetic Metals*, **36**, 275 (1990).
40. "Handbook of Batteries and Fuel Cells," ed. by D. Linden, McGraw-Hill, Inc., New York, A3-A10 (1984).
41. R. M. Felder and R. W. Rousseau, in "Elementary Principles of Chemical Processes," Wiley & Sons, New York, 385 (1978).
42. Derek Pletcher, "Industrial Electrochemistry," Chapman and Hall, New York, 242 (1982).
43. A. J. Bard, and L. R. Faulkner, in "Electrochemical Methods, Fundamentals and Applications," Wiley & Sons, New York, 218 (1980).
44. W. Wernet and G. Wegner, *Makromol. Chem.*, **188**, 1465 (1987).

APPENDIX A  
EXPERIMENTAL CHECKLIST

The solutions used for the battery experiments include 1 M LiClO<sub>4</sub> in PC (propylene carbonate) in the reaction chamber and 0.2 M AgNO<sub>3</sub> in 1M LiClO<sub>4</sub> (PC) for the Ag/Ag<sup>+</sup> reference electrode. The solution used for all other experiments was 0.2 M Et<sub>4</sub>NBF<sub>4</sub> in acetonitrile. Necessary calculations for preparing these solutions are included in this appendix.

Molecular weight :

LiClO<sub>4</sub> 106.46 g/mole

AgNO<sub>3</sub> 169.89 g/mole

Et<sub>4</sub>NBF<sub>4</sub> 217.06 g/mole = 8(12.011) + 20(1) + 14.007 + 10.81 + 4(18.999)

(element)	C	H	N	B	F
-----------	---	---	---	---	---

LiClO<sub>4</sub> 1.0 M in 250 ml: (106.46 g/mole)(1.0 mole/l)(0.25 l) = 26.6 grams

AgNO<sub>3</sub> 0.2 M in 100 ml: (169.89 g/mole)(0.2 mole/l)(0.10 l) = 3.4 grams

Et<sub>4</sub>NBF<sub>4</sub> 0.2 M in 250 ml: (217.06 g/mole)(0.2 mole/l)(0.25 l) = 10.85 grams

Et<sub>4</sub>NBF<sub>4</sub> 0.2 M in 100 ml: (217.06 g/mole)(0.2 mole/l)(0.10 l) = 4.34 grams

Before beginning any experiment, it is important to gather all essential materials so that the experiment will not be delayed at a crucial point. Below is a checklist of materials needed for the Li/PPy battery charge/discharge experiment.

Beaker for waste

Disposable pipettes and bulb

25 ml or 10 ml graduated cylinder

Electrodes: working - platinum disk for conventionally grown

polypyrrole film

- Au-plated Anopore<sup>®</sup> for fibrillar films
- counter - Li foil with imbedded Ni gauze for battery charge/discharge, platinum disk for growing film
- reference - Ag/AgNO<sub>3</sub> (0.2 M) in 1 M LiClO<sub>4</sub>/PC

Battery cell reservoir

Pyrrole in vial

Syringe for pyrrole

Dry PC or MeCN (acetonitrile) for rinsing

Par 273 or 173/175 with leads

X-Y recorder and strip chart recorder

Magnetic stirrer and stirring magnet

Degassed electrolyte solution and extraction solutions (NaOH and HBF<sub>4</sub> or HClO<sub>4</sub>, depending on the work done)

Vials in which to conduct membrane dissolution

APPENDIX B  
DEFINITIONS OF TERMS

Ampere - hour Capacity - the quantity of electricity measured in ampere-hours (Ah) which may be delivered by a cell or battery under specified conditions (also coulombic efficiency).

Available Capacity - the total capacity, in Ah, that will be obtained from a cell or battery, at a defined discharge rate or other specified discharge or operating conditions.

Capacity - the total number of ampere-hours or coulombs that can be drawn from a fully charged cell or battery under specified conditions of discharge.

Capacity Density - capacity per unit volume or mass, reported in units of Ah/cm, Ah/l, or Ah/kg.

Cutoff Voltage - The cell or battery potential at which the discharge (or charge) is terminated, generally a function of discharge rate. Also referred to as the end voltage.

Discharge Rate - usually for a constant current discharge, the rate in amperes at which current is drawn from the cell. For a constant potential discharge, it is an average value.

Energy Density - the ratio of the energy available from a battery or cell to its volume (in Wh/l or  $J/m^3 = 1 \text{ kg/msec}^2$ ) or mass (in Wh/kg or J/kg).  
One kilowatt hour =  $3.6 \times 10^6$  joules. One joule = one watt-second =  $1 \text{ kgm}^2/\text{sec}^2$ .

Power - current multiplied by potential, or  $IE$ , measured in watts. A watt =  $(1A)(1V) = (1 \text{ C/second})(1 \text{ joule/C}) = 1 \text{ joule/second}$ .

Power Density - the ratio of the power available from a battery to its mass ( $W/kg$ ) or volume ( $W/l$ ).

Rated Capacity - the number of Ampere - hours a cell or battery can deliver under specific conditions (rate of discharge, cutoff voltage, temperature); usually the manufacturer's rating.

## VITA

Marjorie Anne Nicholson was born at [REDACTED]  
[REDACTED], on [REDACTED], the fifth of seven children born to Samuel  
and Priscilla Kresge Nicholson. She graduated from Killeen High  
School, Killeen, Texas, in May of 1976, and was a National Merit  
Scholarship Finalist. She continued her education at Texas A&M  
University, where she was a member of the Corps of Cadets. While a  
cadet in ROTC, she completed Army Airborne School and Missile  
Launch Officer's Training School. Upon graduating in December 1980  
with a Bachelor's degree in Chemistry, she worked at Dow Chemical  
Company, Freeport, Texas, first as a chemist at Chlor-alkali Research  
where she worked on methods of on-line analysis and then at Chlorine  
Plant #6. There she managed the analysis laboratory and installed  
multi-sample equipment to monitor the anolyte and catholyte of twelve  
series of chlorine/caustic cells. She returned to College Station in 1982 to  
obtain a teaching certificate in secondary science and math, and then to  
pursue a Master of Science degree in Chemistry. She is married to Dr.  
Ralph E. White and has four children: [REDACTED]  
[REDACTED]

Permanent Mailing Address for Ms. Nicholson is 2912 Arroyo Court  
South, College Station, Texas 77845.

---

## APPENDIX B



NAG 9-173

BATTERIES UTILIZING ELECTRONICALLY  
CONDUCTIVE POLYPYRROLE CATHODE

A Dissertation  
by  
TAEWHAN YEU

submitted to the Graduate College of  
Texas A&M University  
in fulfillment of the requirement for the degree of  
DOCTOR OF PHILOSOPHY

December 1990

Major Subject: Chemical Engineering

3.23  
20356

N91-25<sup>P159</sup>324

NEW SECONDARY BATTERIES UTILIZING ELECTRONICALLY  
CONDUCTIVE POLYPYRROLE CATHODE

A Dissertation

by

TAEWHAN YEU

Submitted to the Graduate College of  
Texas A&M University  
in partial fulfillment of the requirement for the degree of  
DOCTOR OF PHILOSOPHY

December 1990

Major Subject: Chemical Engineering

NEW SECONDARY BATTERIES UTILIZING ELECTRONICALLY  
CONDUCTIVE POLYPYRROLE CATHODE

A Dissertation

by

TAEWHAN YEU

Approved as to style and content by:

---

Ralph E. White  
(Chairman of Committee)

---

Rayford G. Anthony  
(Member)

---

James C. Holste  
(Member)

---

Richard B. Griffin  
(Member)

---

Raymond W. Flumerfelt  
(Head of Department)

December 1990

## ABSTRACT

New Secondary Batteries Utilizing Electronically  
Conductive Polypyrrole Cathode. (December 1990)

Taewhan Yeu, B.S., Chung-Ang University

M.S., University of Detroit

Chairman of Advisory Committee: Dr. Ralph E. White

To gain a better understanding of the dynamic behavior in electronically conducting polypyrroles and to provide guidance toward designs of new secondary batteries based on these polymers, two mathematical models are developed; one for the potentiostatically controlled switching behavior of polypyrrole film, and one for the galvanostatically controlled charge/discharge behavior of lithium/polypyrrole secondary battery cell.

The first model is used to predict the profiles of electrolyte concentrations, charge states, and electrochemical potentials within the thin polypyrrole film during switching process as functions of applied potential and position. Thus, the detailed mechanisms of charge transport and electrochemical reaction can be understood. Sensitivity analysis is performed for independent parameters, describing the physical and electrochemical characteristic of polypyrrole film, to verify their influences on the model performance. The values of independent parameters are estimated by comparing model predictions with experimental data obtained from identical conditions.

The second model is used to predict the profiles of electrolyte concentrations, charge state, and electrochemical potentials within the battery system during

charge and discharge processes as functions of time and position. Energy and power densities are estimated from model predictions and compared with existing battery systems. The independent design criteria on the charge and discharge performance of the cell are provided by studying the effects of design parameters.

To My Parents, Dalyoung and Hwoaja

## ACKNOWLEDGMENTS

The author would like to give special thanks to his parents who gave unfailing encouragement and instilled in him a belief that hard work and dedication can overcome obstacles even in the most trying of circumstances. This work is in no small part due to their guidance and willingness to express their belief in his abilities. The author also would like to give thanks to his wife, Kyung Mi, and his son, Christopher Edward, for their love, patience, humor, advice, and constant support.

The author wishes to express his sincere gratitude to Professor Ralph E. White for his guidance and support throughout the period of this work. Special thanks also go to Professor James C. Holste and Rayford G. Anthony of the Chemical Engineering Department and Professor Richard B. Griffin of the Mechanical Engineering Department for serving as advisory Committee members, and Dr. Mary K. Wicksten from the Department of Biology for serving as a representative of the Graduate Council to the Advisory Committee.

In addition, the author thanks to Professor Charles R. Martin and his research group of the Chemistry Department for their valuable contribution to this work. The author also wishes to express deep appreciation to all members, past and present, of the Electrochemical Engineering Center for upholding and advocating his ability to reach his goal. The author gratefully acknowledges all of unselfish contributions made toward this work.

## TABLE OF CONTENTS

	Page
I. INTRODUCTION . . . . .	1
II. LITERATURE SURVEY . . . . .	5
A. Historical Background . . . . .	5
B. Polymerization . . . . .	7
1. Chemical Synthesis . . . . .	8
2. Electrochemical Synthesis . . . . .	9
C. Structure and Polymerization Mechanisms . . . . .	10
1. Structure . . . . .	10
2. Polymerization Mechanisms . . . . .	13
D. Electrochemical Properties . . . . .	15
E. Transport Properties . . . . .	21
1. Electronic Transport . . . . .	21
2. Mass Transport . . . . .	27
F. Dependency of Properties on Polymerization Conditions . . . . .	30
1. Electrodes . . . . .	30
2. Solvents . . . . .	31
3. Electrolytes . . . . .	33
4. Driving Forces . . . . .	38
5. Others . . . . .	39
G. Modifications of Properties . . . . .	40
H. Applications . . . . .	42
1. Energy Storage Devices . . . . .	43
2. Solar Energy Devices . . . . .	44
3. Electrochromic Display Devices . . . . .	44
4. Others . . . . .	45
III. MATHEMATICAL TREATMENT OF MATERIALS . . . . .	47
A. Electrochemistry . . . . .	47
B. Properties of 1M LiClO <sub>4</sub> -PC Electrolyte . . . . .	48



## TABLE OF CONTENTS (Continued)

	Page
C. Properties of Polypyrrole . . . . .	50
D. Electrochemical Reaction Rate of Polypyrrole . . . . .	52
E. Electrochemical Reaction Rate of Lithium . . . . .	55
IV. CYCLIC VOLTAMMETRY . . . . .	57
A. Experimental Descriptions . . . . .	58
B. Model Descriptions . . . . .	60
1. Governing Equations – Polypyrrole Electrode Region . . . . .	60
2. Governing Equations – Solution Diffusion Layer . . . . .	67
3. Boundary and Interface Conditions . . . . .	68
4. Initial Conditions . . . . .	71
5. Solution Method . . . . .	71
C. Results and Discussion . . . . .	73
1. Experimental Results . . . . .	74
2. Simulated Results . . . . .	77
3. Sensitivity Analysis . . . . .	87
4. Effects of Parameters . . . . .	90
D. Conclusions and Recommendations . . . . .	96
V. SECONDARY BATTERY . . . . .	99
A. System Descriptions . . . . .	100
B. Model Descriptions . . . . .	102
1. Governing Equations – Polypyrrole Positive Electrode . . . . .	104
2. Governing Equations – Reservoir . . . . .	106
3. Governing Equations – Separator . . . . .	107
4. Boundary and Interface Conditions . . . . .	108
5. Initial Conditions . . . . .	112
6. Solution Method . . . . .	112
C. Results and Discussion . . . . .	114
1. Charge and Discharge Behavior . . . . .	115
2. Dependent Variables profiles . . . . .	119

## TABLE OF CONTENTS (Continued)

	Page
3. Effects of Operating Conditions . . . . .	123
4. Effects of Design Parameters . . . . .	124
D. Conclusions and Recommendations . . . . .	128
LIST OF SYMBOLS . . . . .	132
REFERENCES . . . . .	136
APPENDIX A . . . . .	146
VITA . . . . .	147

## LIST OF TABLES

Table	Page
I. Electronically conducting polyheterocycles. . . . .	2
II. Solvent effects on the quality of the polypyrrole films. . . . .	32
III. Anion effects on the properties of the polypyrrole films. . . . .	35
IV. Properties of 1M LiClO <sub>4</sub> -PC electrolyte at 25°C. . . . .	50
V. Properties of polypyrrole film doped with perchlorate. . . . .	51
VI. Properties of polypyrrole film as a function of its oxidation state. . . . .	53
VII. Kinetic parameter values used for polypyrrole. . . . .	54
VIII. Kinetic parameter values used for lithium. . . . .	56
IX. System of equations for cyclic voltammetry of polypyrrole. . . . .	72
X. Operating conditions used for cyclic voltammograms of polypyrrole. . . . .	74
XI. Electrochemical Characteristics of the 1 μm polypyrrole film in the 1M LiClO <sub>4</sub> -PC electrolyte. . . . .	76
XII. Fixed parameter values used for polypyrrole. . . . .	79
XIII. Sensitivity analysis on various physical parameters. . . . .	88
XIV. Sensitivity analysis on various electrochemical parameters. . . . .	89
XV. Sensitivity analysis on various operating conditions. . . . .	90
XVI. System of equations for charge/discharge behavior of lithium/polypyrrole secondary battery cell. . . . .	113
XVII. Operating conditions used for charge/discharge behavior of lithium/polypyrrole secondary battery cell. . . . .	114
XVIII. Electrochemical characteristic of one square centimeter lithium/polypyrrole secondary battery cell during discharge. . . . .	117

## LIST OF FIGURES

Figure	Page
1. Proposed stoichiometry of oxidized and neutral polypyrrole films . . . . .	12
2. Generally accepted mechanism for electrochemical polymerization of polypyrrole film. . . . .	14
3. Experimental cyclic voltammograms for a 20 nm polypyrrole film in 0.1M Et <sub>4</sub> NBF <sub>4</sub> -CH <sub>3</sub> CN electrolyte. . . . .	17
4. Scanning electron micrographs of polypyrrole film surface with different anions. . . . .	37
5. A schematic diagram of a single-compartment electrochemical cell with a rotating disk electrode. . . . .	59
6. A schematic diagram of modeling regions closed to the rotating disk electrode in the single-compartment electrochemical cell. . . . .	61
7. Experimental cyclic voltammograms for a 1 μm polypyrrole film in 1M LiClO <sub>4</sub> -PC electrolyte at scan rates of 10 and 20 mV/sec. . . . .	75
8. Simulated cyclic voltammograms for a 1 μm polypyrrole film in 1M LiClO <sub>4</sub> -PC electrolyte at scan rates of 10 and 20 mV/sec. . . . .	78
9. Decomposition of a cyclic voltammogram into its two components, the faradaic and capacitive current densities, at a scan rate of 20 mV/sec. . . . .	80
10. Dimensionless concentration profiles of the anion (ClO <sub>4</sub> <sup>-</sup> ) within the polypyrrole electrode region at a scan rate of 20 mV/sec. . . . .	82
11. Dimensionless faradaic charge profiles within the polypyrrole electrode region at a scan rate of 20 mV/sec. . . . .	84
12. Potential difference between solid and solution phases within the polypyrrole electrode region at a scan rate of 20 mV/sec. . . . .	86
13. The effects of maximal faradaic charge ( $Q_{f,oxd}$ ) on the cyclic voltammograms at a scan rate of 20 mV/sec. . . . .	91
14. The effects of double layer constant ( $a^*$ ) on the cyclic voltammograms at a scan rate of 20 mV/sec. . . . .	93

## LIST OF FIGURES (Continued)

Figure	Page
15. The effects of anodic transfer coefficient ( $\alpha_{a1}$ ) on the cyclic voltammograms at a scan rate of 20 mV/sec. . . . .	94
16. The effects of exchange current per unit volume ( $ai_{o1,ref}$ ) on the cyclic voltammograms at a scan rate of 20 mV/sec. . . . .	95
17. A schematic diagram of a typical monopolar Li/LiClO <sub>4</sub> -PC/PPy secondary battery cell. . . . .	101
18. A schematic diagram of modeling regions in Li/LiClO <sub>4</sub> -PC/PPy secondary battery cell. . . . .	103
19. Simulated charge and discharge behaviors of a typical Li/LiClO <sub>4</sub> -PC/PPy secondary battery cell at $i_{cell} = 0.2$ mA/cm <sup>2</sup> . . . . .	116
20. Faradaic and capacitive current components within the polypyrrole positive electrode during charge at $i_{cell} = 0.2$ mA/cm <sup>2</sup> . . . . .	118
21. Dimensionless concentration profiles of the anion (ClO <sub>4</sub> <sup>-</sup> ) across a typical cell during charge and discharge at $i_{cell} = 0.2$ mA/cm <sup>2</sup> . . . . .	120
22. Dimensionless faradaic charge profiles across a typical cell during charge and discharge at $i_{cell} = 0.2$ mA/cm <sup>2</sup> . . . . .	122
23. Solution potential profiles across a typical cell during charge and discharge at $i_{cell} = 0.2$ mA/cm <sup>2</sup> . . . . .	124
24. The effect of the discharge rate on the cell discharge performance. . . . .	125
25. The effect of the thickness of the polypyrrole positive electrode on the cell discharge performance at $i_{cell} = 0.2$ mA/cm <sup>2</sup> . . . . .	126
26. The effect of the thickness of the reservoir on the cell discharge performance at $i_{cell} = 0.2$ mA/cm <sup>2</sup> . . . . .	127
27. The effect of the thickness of the separator on the cell discharge performance at $i_{cell} = 0.2$ mA/cm <sup>2</sup> . . . . .	129

## I. INTRODUCTION


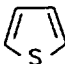
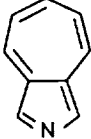
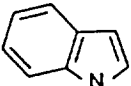
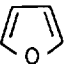
Electronically conducting polyheterocyclics are an interesting class of materials that have gained popularity in the last decade. Although most of the studies have been devoted to polypyrrole, extensive work on other polyheterocyclics such as polythiophene, polyfuran, polyazulene, polyindole, polycarbazole, and their derivatives, has been carried out by a number of investigators (1,2). Table I lists the structural and electrochemical analysis data for various conducting polyheterocyclics (1-3). The polyheterocycles derived from heterocyclic monomers are p-type conductors and are relatively stable in the air over extended periods of time. They possess high electronic conductivities as well as they can be employed as their own current collectors.

Electronically conducting polyheterocyclics have a number of potential technological applications because of their ability to switch between the conducting and nonconducting states. They can be used as energy storage devices, solar energy devices, electrochromic display devices, and electronic devices. One of the most promising applications is the development of new high-energy-density secondary batteries because of prospect for a long-term supply of inexpensive, lightweight, and noncorrodible electrode materials. In the design of high-energy-density batteries, conducting polymers fulfill the most important characteristic: a large amount of energy stored per unit weight. Another novel feature is that they can be fabricated into any desired shape, thereby providing unusual design flexibility.

---

This document follows the style of the *Journal of the Electrochemical Society*.

Table I. Electronically conducting polyheterocycles.

Electronically Conductive Polyheterocycles	Structure of Monomer	Maximum Doping Level	Anion Content (% by wt)	Electronic Conductivity ( $/\Omega\text{-cm}$ )
Polypyrrole		0.25 - 0.33	25 - 30	0.01 - 200
Polythiophene		0.06 - 0.30	7 - 25	10 - 20
Polyazulene		0.25	15 - 28	0.01 - 1
Polyindole		0.20 - 0.30	15 - 20	0.001 - 0.01
Polycarbazole	-	0.45	21	0.001 - 0.1
Polyfuran		-	26	-
Polypyrene	-	0.45	-	0.1 - 1

Among the recently available electronically conducting polyheterocyclics, polypyrrole has been received the most attention as a secondary battery electrode material because the electrochemical features of polypyrrole epitomize the polyheterocyclics in many important respects. Electrochemically synthesized polypyrrole can be produced from commercially available chemicals by a simple one-step electrochemical oxidation process. Polypyrrole has high conductivity and specific charge capacity, and exhibits a stable and reversible electrochemical redox behavior. There is no doubt that polypyrrole remains an interesting electrode material. However, the knowledge of electrochemical behavior and the application of polypyrrole published to date is still in the experimental stage and remains far from completion.

The main objectives of this study are to gain a better understanding of the dynamic behavior in electronically conducting polypyrrole films, and to provide guidance toward designs of new secondary batteries based on this polymer as a cathode material. To accomplish these objectives, two mathematical models are developed; one for simulating the cyclic voltammetric behavior of polypyrrole in a single-compartment cell, and one for simulating charge/discharge behavior of a lithium/polypyrrole (Li/PPy) secondary battery cell. Mathematical modeling is an integral part of the design and development of polymer batteries because it enables us to learn the cause and effect relationships, reveals phenomena in fine details, and suggests directions for improvements.

Simulation of cyclic voltammograms of polypyrrole film makes it possible to clarify the electrochemical reaction mechanism and charge transport phenomena. The model is used to study the effect of electrochemical parameters to characterize the electrochemical properties of polypyrrole. Thus, it is possible to obtain



values for the electrochemical parameters that would yield the best agreement between model predictions and experimental data. Based on the model of cyclic voltammogram and its estimated results, a mathematical model to simulate the charge/discharge behavior of lithium/polypyrrole secondary battery is then developed. This model is used to understand charge/discharge behavior and provide design criteria of new secondary batteries that utilize electronically conducting polypyrrole.

The treatment presented here is general and can be extended easily to account for other complex electroanalytical experiments (such as, chronoamperometry, chronopotentiometry, AC impedance, etc.) and other conducting polymers (such as, polyacetylene, polythiophene, polyparaphenylene, etc.) with the appropriate modifications in operating conditions and physical properties.

## II. LITERATURE SURVEY

The worldwide interest in electronically conductive polypyrrole films is readily gauged by the large number of publications in this field. This chapter reviews the historical background (4-24), the polymerization and structure (25-40), the physical and chemical properties (41-104), and potential technological applications (105-117).

### A. Historical Background

Polypyrrole was first chemically prepared as a powder by Angeli *et al.* (4,5) in 1916.  $H_2O_2$  was used as the oxidizing agent and gave a material which is commonly known as 'pyrrole black'. Pyrrole black is an amorphous powder and it is insoluble in organic solvents. Because of its undesirable properties, no further interest was shown in this material.

The electrochemical oxidation of pyrrole in aqueous sulfuric acid to produce a powdery, insoluble precipitate on a platinum electrode was first reported by Dall'Olio *et al.* (6) in 1968. Elemental analysis showed that the resulting polypyrrole consisted of 76% polypyrrole, the remainder being sulfate ions making this polymer cationic. Although this procedure represented the first electrochemical synthesis of a conducting polypyrrole, the undesirable physical properties and the relatively low room temperature conductivity ( $8 \Omega^{-1}cm^{-1}$ ) limited the interest generated by this synthetic route.

A new chapter in the evolution of electronically conducting polymers began with the discovery of the chemically synthesized pristine polysulfurnitride by Walatka *et al.* (7) in 1973. The resulting inorganic polymer itself behaves like

a metal over the entire temperature range from 4.2 to 300 K. The experimental information indicated that polysulfurnitride has a crystalline form and a quasi-one-dimensional structure. The conductivity of polysulfurnitride was reported as  $1000 \Omega^{-1}\text{cm}^{-1}$  and was attributed to impurity or defect scattering (8). This is also the first polymeric system known to exhibit superconductivity at a transition temperature below 0.3 K (8).

Attempts to find a covalent organic polymer, with high conductivity, lead to the discovery of polyacetylene in 1977 (9-11). The discovery of this semiconducting and metallic organic polyacetylene introduced new concepts in the field of the organic conducting polymers and intensified research in the synthesis and characterization of this class of compounds. Polyacetylene is one of the simplest linear conjugated polymers with a single-chain structure. It was found that exposure of films of either *cis*- or *trans*-polyacetylene to iodine, bromine, or arsenic pentafluoride vapor led to an oxidized form (p-type) while treatment with a solution of sodium naphthalide led to a reduced form (n-type). In 1979, it was discovered that p- or n-type polyacetylene could be accomplished electrochemically and that these processes were electrochemically reversible (12). Moreover, the oxidation or reduction of the film was accompanied by an increase in conductivity from  $10^{-8} \Omega^{-1}\text{cm}^{-1}$  for the neutral film to a value of up to  $10^3 \Omega^{-1}\text{cm}^{-1}$  for the oxidized film. These led naturally to the conclusion that polyacetylene and its various oxidized or reduced forms might act as promising charge storing materials for use in secondary batteries. Polyacetylene had been extensively investigated as an electrode material in secondary battery technologies (13,14). However, the main problem with using polyacetylene as an electrode material is its poor stability in the presence of oxygen and water (15).

The discovery of polyacetylene touched off a flurry of research directed towards the study and discovery of new conducting polymeric systems such as polypyrrole (16,17) and poly(paraphenylene) (18). In 1979, Diaz *et al.* (16,17) reported that the electronically conductive polypyrrole films could be produced by the anodic oxidation of pyrrole in acetonitrile with the presence of tetraethylammonium tetrafluoroborate. Resulting films could be cycled between the doped (oxidized) and undoped (neutral) states without loss of electroactivity. The doped films become good electronic conductors ( $100 \Omega^{-1}\text{cm}^{-1}$ ) whereas the undoped films are only moderate conductors ( $10^{-10} \Omega^{-1}\text{cm}^{-1}$ ). The film was continuous and could be peeled off the platinum substrate electrodes to yield free-standing, easily manageable films that were stable in air and had much higher electrical conductivities than achieved before (Dall'Olio *et al.*). The attractiveness of the polypyrrole system stems from several factors. The most important were undoubtedly the chemical and thermal stability of these polymers and their ease of preparation relative to polysulfurnitride and polyacetylene.

The successful synthesis of polypyrrole led to synthesis of similar electronically conducting polyheterocyclics. The most important are polypyrrole derivatives (19), polythiophene (20-23), and polythiophene derivatives (22-24). The discovery of these polymers was particularly significant since they are extremely stable in oxygen and moisture environments, even in their neutral state.

## B. Polymerization

Polypyrrole can be produced by either chemical or electrochemical synthesis. The chemical route generally leads to a conducting powder, whereas the electrochemical route yields a continuous film which is also conducting. Although the

chemical preparation of polypyrrole remains a desirable goal, presently, the electrochemical synthesis provides the only satisfactory route for producing these films.

### 1. Chemical Synthesis

Polypyrrole can be prepared by the chemical oxidation of the monomer with exposure to a wide variety of oxidizing conditions because of pyrrole's extremely high reactivities. For instance, polypyrrole has been prepared by oxidative pyrrolysis of tetraiododpyrrole (25). In this case, varying degrees of oxidation are attained by varying the temperature of pyrrolysis. The oxidized changes in the polymer are compensated by  $I_3^-$  formed from pyrrolytically cleaved iodide. Oxidatively polymerized polypyrrole has also been synthesized by exposure of the monomer to mild oxidizing reagents such as potassium persulfate ( $K_2S_2O_8$ ) (25), and iron(III) (26). Salmon *et al.* (27) demonstrated chemically synthesized polypyrrole by a simple one step chemical oxidation of the monomer by a strong oxidant, such as  $Fe_3(ClO_4)_3$ , in various solvents. This chemically synthesized polypyrrole is a black and conducting powder which exhibits electronic and electrochemical properties similar to those of the electrochemically synthesized polypyrrole. Pyrrole also forms polymers under acidic conditions (28). In this case, however, the polymers contain alternating pyrrole and pyrrolidine units and therefore do not have an extended  $\pi$ -system.

In general, conducting polypyrrole by the chemical synthesis has two major limitations. First, the resulting polymer yields a finely divided precipitate which is completely insoluble in any solvent (26). Thus, the characterization of this polymer is very difficult because of those insolubility. Second, the presence of catalysts in many of the chemical synthesis allows for the introduction of

impurities into the polymer during synthesis. The electronic conductivities observed from these polymer are likely to be compromised by the presence of these impurities. For all these reasons, the discovery of an electrochemical synthesis route for the preparation of coherent polypyrrole films by Diaz *et al.* (16,17) in 1979 was regarded as an important break-through in the field of electronically conductive polymers.

## 2. Electrochemical Synthesis

Electrochemical synthesis is now the most commonly used synthetic approach for preparing electronically conductive polypyrrole films. The polymerization is carried out in a single-compartment electrochemical cell with the classic three-electrode configuration (2,29):

- a) working electrode; Pt, Au, or glass carbon,
- b) reference electrode; saturated calomel electrode (SCE),
- c) and auxiliary electrode; Pt, Li.

The electrolytic medium typically consists of an organic solvent (e.g., acetonitrile, propylene carbonate, etc.), a supporting electrolyte MX ( $M^+ = Et_4N^+$ ,  $Bu_4N^+$ ,  $Li^+$ ;  $X^- = ClO_4^-$ ,  $BF_4^-$ ,  $PF_6^-$ ,  $AsF_6^-$ ), and a pyrrole monomer (0.1M to 1M). The solvent, the monomer, and the supporting salt are generally purified by distillation or recrystallization just prior to electrolysis. The solutions are deoxygenated prior to electrolysis by nitrogen bubbling.

The electrochemical synthesis of polypyrrole is accomplished by anodic oxidation of pyrrole monomer from the electrolyte (17). Pyrrole is dissolved into the electrolyte solvent, along with a desired salt. Application of a constant potential (positive of +0.2 V versus SCE) to the electrode results in oxidation of the pyrrole monomer. As long as pyrrole monomer is being oxidized at the

electrode via the applied potential, the polymer grows continuously. In addition, the polymer can also be prepared by application of a constant current, usually on the order of  $0.2 \text{ mA/cm}^2$  (16,30,31). This method allows control over the total charge passed, and thereby, the film thickness. Third method involves cycling the potential over a range which polymerizes pyrrole at the anodic scan and reduces the polypyrrole products at the cathodic scan (32). This method exhibits an increase in current due to concomitant oxidation of the growing polymer at the electrode surface.

In general, electrochemical polymerization of pyrrole produces a strongly adhered, durable film with metal-like conductivity. The thickness of the resulting film can be controlled by the total charge passed through the cell. The resulting film is an oxidized conducting state because the aromatic dimer and higher molecular weight oligomers have lower oxidation potentials than the monomer. The conducting polycationic polymer consists of a densely packed insoluble material and is subsequently reduced chemically or electrochemically to the neutral polymer. The properties of polypyrrole film very much depend on the electrochemical environment. These effects will be discussed in a later section.

### C. Structure and Polymerization Mechanisms

#### 1. Structure

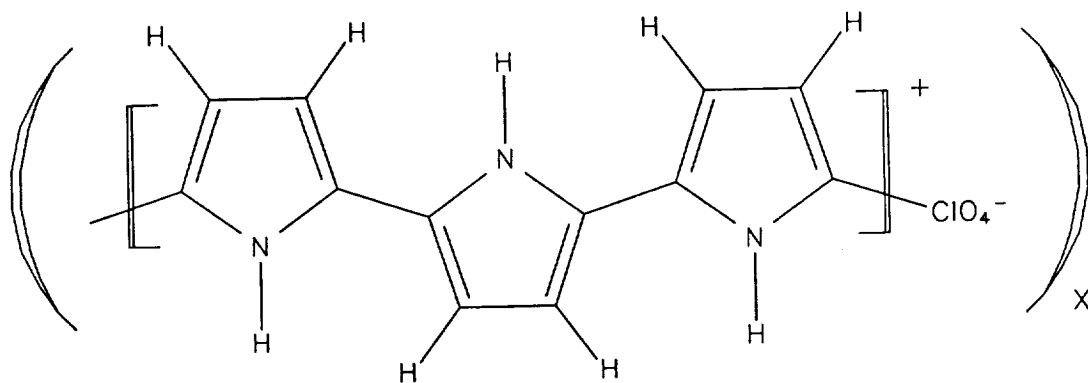
All forms of polypyrrole reported so far are poorly crystalline and completely insoluble which means that much of our knowledge of the structure of these systems is obtained from a variety of indirect measurements.

Generally accepted structure of oxidized and neutral polypyrrole films are shown in Fig. 1 (2,29). Polypyrrole films are primarily bonded *via*  $\alpha$ - $\alpha'$  linkages.

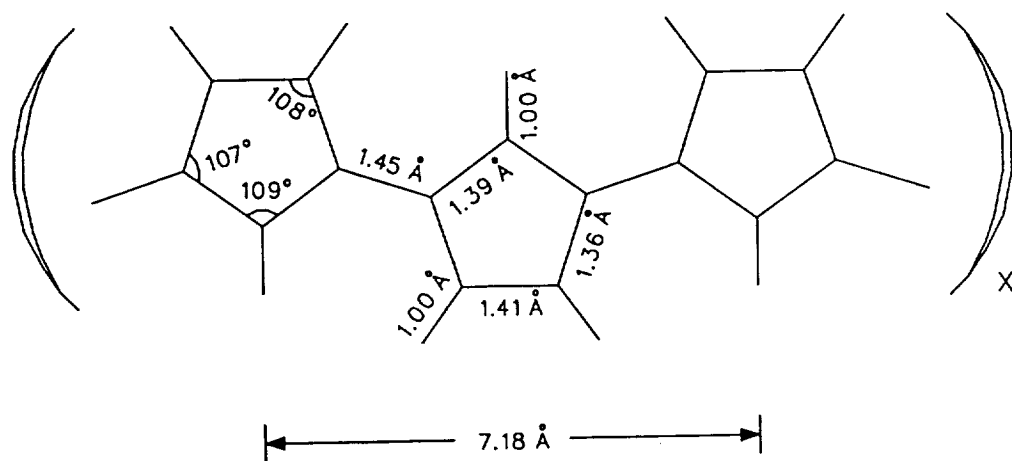
This is based largely on the demonstration that blocking  $\alpha$  and  $\alpha'$  positions seems to prevent the electrochemical polymerization of pyrroles (33). Also, the dominance of the  $\alpha$ - $\alpha'$  linkage in polypyrrole has been confirmed by  $^{13}\text{C}$  nuclear magnetic resonance spectrum analysis (29). However, analysis shows that the polymer is far from ideal, with less than two-thirds of the repeat units in this form (34). There is some involvement of the  $\beta$ -carbons in the chain bonding which could cause some crosslinking of the polymer (29).

Electrochemical synthesis of polypyrrole generates the film in the oxidized state, but the thin films can then be electrochemically cycled between the oxidized and neutral states by sweeping of the potential. The oxidized film (Fig. 1-A) has an extensively conjugated  $\pi$ -system, doped by oxidation so as to have unpaired electrons. Thus, the oxidized film contains anions, which are often referred to as dopants and act as counterions to balance the positive charge on the polymer and maintain electroneutrality. Determination of the amount of counterion in fully oxidized polypyrrole indicates the doping level and the amount of charge stored in the polymer. Diaz *et al.* (16) suggested approximately four pyrrole rings per tetrafluoroborate anion ( $\text{BF}_4^-$ ), while Street *et al.* (29) found three pyrrole rings per perchlorate anion ( $\text{ClO}_4^-$ ). The analysis of the inner structure of these polymers performed by scanning and transmission electron microscopy reveals that the doping process is inhomogeneous and the doping level must be considered as statistical (29). Electrochemical reduction of polypyrrole reduces the number of charged sites in the  $\pi$  structure of the polymer (Fig. 1-B). This results in the counterion leaving the film to maintain electroneutrality. There are no reports of doping with cations by the reduction of the neutral film.





A. Oxidized Polypyrrole Film



B. Neutral Polypyrrole Film

Fig. 1. Proposed stoichiometry of oxidized and neutral polypyrrole films.

## 2. Polymerization Mechanisms

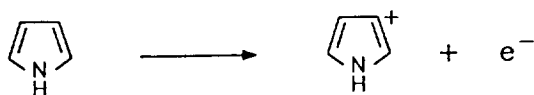
Although the mechanism of the electrochemical polymerization has been discussed by several group (2,29,35-37), a detailed mechanism has as yet to be unambiguously established. The generally accepted mechanism for the electrochemical polymerization of the polypyrrole film is radical coupling mechanisms as shown in Fig. 2 (36,37).

The first step in the electrochemical polymerization of pyrrole to polypyrrole is removal of one electron from the pyrrole monomer to form a positively charged radical cation by anodic oxidation (step 1). Since the radical cation species is unstable and highly reactive, it reacts immediately with a second radical cation of the monomer to give a dication (step 2). This dication then forms a neutral dimer by the elimination of two protons, which is more easily oxidized (step 3). Again, one electron is removed from dimer to form a positively charged radical dimer by anodic oxidation. The resulting cationic dimer couples either with another cationic dimer or radical cation to form a higher oligomer. Since dimers or higher oligomers are more easily oxidized than monomers, these could react further to build up the polymer chain (step 4).

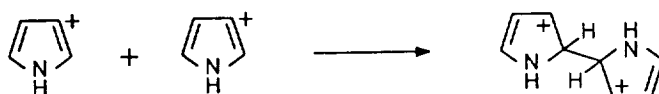
The chain growth is terminated either when the radical cation of the growing chain becomes unreactive or, more likely, when the reactive end of the chain becomes sterically blocked (37). The final polymer chain bears a charge of unity for every three to four pyrrole rings, and this positive charge is counterbalanced by the anion which originates from the electrolyte salt. The deposition of polypyrrole on the surface of the electrode is described as a nucleation and growth mechanism very similar to the electrodeposition of metals (30,36)

Asavapiriyant *et al.* (30) concluded that the rate of polymerization is

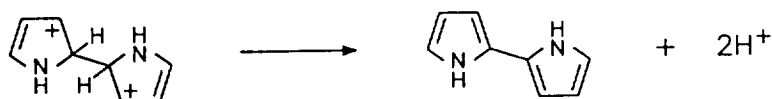
Step 1:



Step 2:



Step 3:



Step 4:

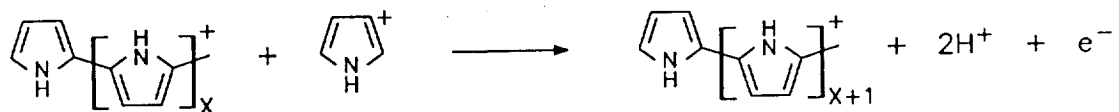


Fig. 2. Generally accepted mechanism for electrochemical polymerization of polypyrrole film.

controlled by the rate of electron transfer from the cyclic voltammetry and step potential experiments. However, Genies *et al.* (36) observed the coupling of the pyrrole radical cations to be the rate determining step. The role and positioning of the anion in the film remains one of the key questions in the electrochemical polymerization of conducting polypyrrole.

The radical coupling mechanism shown in Fig. 2 accounts for the following experimental observations regarding the polymerization reaction (35): a) electrochemical polymerization is a surface localized phenomenon. No evidence for polymerization in the bulk of the feed solution has been observed as expected from a polymerization mechanism where radical cations react with a neutral monomer, b) the polymerization of polypyrrole dimers (23) and trimers (38) has been demonstrated, c) the spectroelectrochemical experiments of Genies *et al.* (36) reveal that polypyrrole film deposition proceeds linearly with time. This observation is consistent with radical cation coupling as the rate limiting step of the polymerization reaction rather than diffusion, d) the elimination of the  $\alpha$  protons indicated by this mechanism is consistent with a decrease in the pH of the electrolyte solution during electrochemical polymerizations (29, 39). The loss of protons is commensurate with coupling of the radical cations as predicted, e) the number of electrons consumed in the polymerization of pyrrole, which has been estimated to be between 2.25 and 2.33 per pyrrole monomer, is consistent with the above mechanism. These numbers also agree with the number of anions found in the polymer films (40).

#### D. Electrochemical Properties

Electrochemically prepared polypyrrole films are electroactive and can be

switched between the neutral nonconducting state to the oxidized conducting state with a change of oxidation level. This change in oxidation level is accompanied by strong changes in both conductivity and spectral properties. The redox reaction is chemically reversible and can be driven repeatedly without loss of electroactivity. The conductivity of polypyrrole can change several orders of magnitude between the neutral and oxidized states. Because of the low oxidation potential of this polymer, it is very sensitive to oxygen in the atmosphere. Therefore, switching experiments must be performed in the absence of oxygen. Electrochemical switching between conducting and insulating states can be well presented by a cyclic voltammetry because thin films of the polymer exhibit well defined oxidation and reduction curves.

Typical cyclic voltammograms for a 20 nm polypyrrole film in 0.1M  $\text{Et}_4\text{NBF}_4\text{-CH}_3\text{CN}$  at scan rates of 10, 20, 40, 50, 60, 80, and 100 mV/sec are shown in Fig. 3 (40). At potentials negative of  $-0.3$  V versus SCE, the polypyrrole film is in its fully neutral nonconducting state. Anodic sweep of potential yields conversion of neutral polypyrrole to an oxidized, conducting state with increases in the capacitive background at potentials positive of  $-0.3$  V. At a potential  $+0.2$  V versus SCE, the oxidation reaction is completed and polypyrrole is in its fully oxidized conducting state. At potentials positive  $+0.2$  V versus SCE, polypyrrole film behaves like a capacitor and may be further charged. The large background capacitive currents in this region can be explained by that oxidized polypyrrole is porous to electrolyte with a high surface-to-volume ratio (41). If the potential is taken too positive, an irreversible loss of activity occurs. The loss of activity appears to occur gradually with increasing potential and has been attributed to a decrease in the conductivity of the film due to oxidation reactions

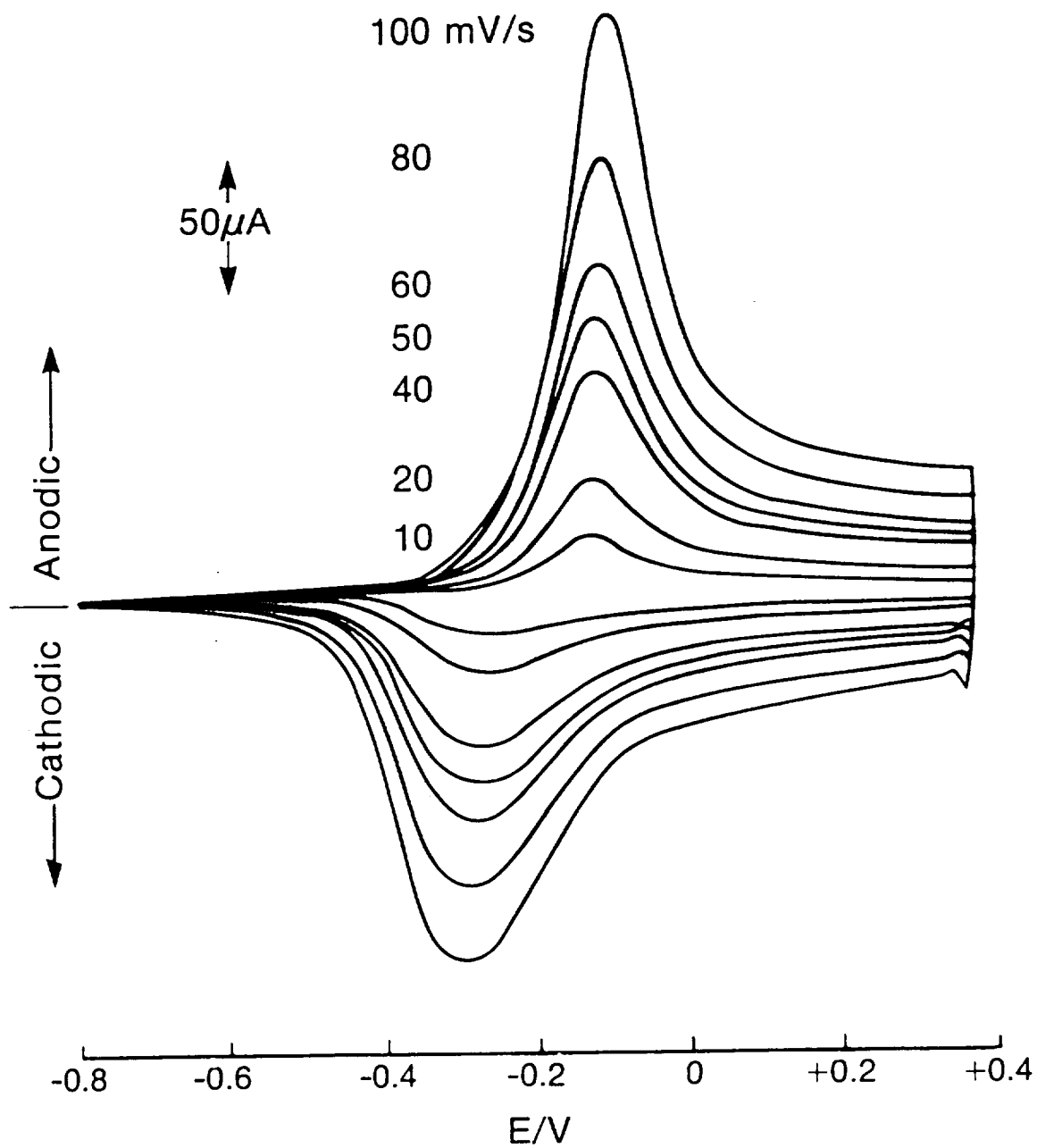


Fig. 3. Experimental cyclic voltammograms for a 20 nm polypyrrole film in 0.1M  $\text{Et}_4\text{NBF}_4\text{-CH}_3\text{CN}$  electrolyte.

which lead to loss of conjugation (30).

Cathodic sweep of potential yields conversion of oxidized polypyrrole to neutral, nonconducting state with decreases in the capacitive background current at potentials negative of +0.2 V. At a potential  $-0.5$  V versus SCE, polypyrrole is again in its fully neutral state. Extending potentials to negative direction had little effect on the properties of polypyrrole films. This process can be done repeatedly with no evidence of decomposition of the polymer in the absence of oxygen.

The cyclic voltammograms of electronically conducting polypyrrole are not symmetrical. The shape of the anodic and cathodic current responses and the difference between anodic and cathodic peak potentials suggest that the electrochemical reaction of polypyrrole is quasi-reversible and that the reduction and oxidation kinetics may be limited by a slow ion diffusion in the film or by a slow electron transfer process. It has been observed that the cathodic peak is significantly broader than the anodic peak, and that the oxidation capacitive current is higher than the corresponding reduction current. The broadening of the observed cathodic peak is currently not well understood, but it could reflect the electrochemical nonequivalence of redox sites in the polypyrrole film. These effects can be explained on the basis of a large uncompensated resistance caused by the neutral polymer film (42). In the neutral state, polypyrrole has a high ionic resistance because of the presence of an ion gate. Both anodic and cathodic voltammograms are broader than expected for a Nernstian redox couple.

A distinctive color change accompanies the redox reaction involving polypyrrole polymer (30,40). The colors observed reflect the solid state electronic properties of the polymer in each of its redox states. Oxidized conducting polypyrrole

is brown-black due to the existence of interband electronic transitions. In contrast, neutral, nonconducting polypyrrole is light yellow due to the existence of a substantial band-gap. In the neutral state, yellow polypyrrole has a strong absorption band in the ultraviolet-blue range and the absorption in the visible range increases when the film is oxidized, giving the coating a brown color (43). The yellow color of polypyrrole during electrochemical cycling of the polymer between neutral and oxidized redox states indicates that the polymer is quantitatively reduced.

AC impedance measurements also have been used to characterize electrochemical properties of polypyrrole films, especially the nature and the origin of a large capacitance taking place in the oxidized polymer. Most of the experimental data obtained from these studies are analyzed in terms of an "equivalent circuit", an electrical circuit which is considered to model correctly the electrical behavior of the electrode interface when its calculated impedance, as a function of frequency, agrees with the experimentally determined impedance behavior.

AC impedance studies of polypyrrole by Burgmayer *et al.* (44,45) and Tanguy *et al.* (46,47) have employed relatively thick ( $\geq 5$  mm) films. Such films cannot be quantitatively addressed electrochemically, i.e., the as-synthesized oxidized polymer cannot be quantitatively reduced (3,36). Consequently, the extraction of mass transport and kinetic information from these data is not straight forward.

Bull *et al.* (41) examined the AC impedance behavior of thin polypyrrole films over a broad frequency band. They discussed results only in the potential region around +0.1 V versus SCE, where negligible faradaic processes occur, and did not consider mass transport in the analysis of these data. In this region, the



admittance can primarily be attributed to double layer charging. Penner *et al.* (48) demonstrated that both mass transport and structural information can be gleaned from AC impedance analysis. They interpreted the AC impedance data in the context of the limiting behavior of thin polypyrrole film for neutral and fully oxidized states.

Because of complexities in the switching process of polypyrrole film, these studies have employed only limiting cases of polypyrrole films, either at low doping level (where only faradaic reaction occurs) or at high doping level (where only double layer charging occurs). At intermediate states, significant concentrations of both oxidized and neutral polypyrrole are present in the film, which makes it a good electronic conductor. The electrochemical properties (such as, conductivity, diffusivity, differential capacitance, etc.,) are varied with oxidation state of polypyrrole film. Under these circumstances, the conventional equivalent circuits model is not adequate to describe the AC impedance responses of the polypyrrole film. Recently, Hauser *et al.* (49) presented a more realistic approach to the analysis of AC impedance data. Their approach, which is based on a mechanistic modeling approach as opposed to a circuit analog modeling approach for analysis of AC impedance data, shows the possibility to be adequate for conducting polymers.

The majority of conductivity ( $\sigma$ ) measurements have been carried out by Diaz *et al.* (33,50). These workers measured the room temperature conductivity, using a four-probe technique, and found values in the range  $10^{-3}$ - $200 \Omega^{-1} \text{cm}^{-1}$  depending on the nature of the anion present. The  $T^{\frac{1}{4}}$  temperature dependence of  $\log \sigma$  for fully oxidized polypyrrole has been observed between a temperature range of 10 to 220 K independent of the type of dopant anion as observed for

polyacetylene and other polyheterocycles (51-53). The dependency of electronic conductivity of polypyrrole on the nature of the anion present will be discussed in a later section.

The stability of polypyrrole is an important factor affecting its potential application. Among various aspects of the stability, the most important aspect is loss of conductivity as a function of time and exposure to various chemical environment. Erlandson *et al.* (54) and Cvetko *et al.* (55) studied the change in conductivity as a function of time and exposure to oxygen and water. These results show that the conductivity is fairly stable over time, but does depend on the polymerization conditions and the chemical environment. The presence of oxygen increases the degradation rate, while a mixture of oxygen and water vapor increases the rate even further. Diaz *et al.* (50) showed that polypyrrole was stable at elevated temperatures up to 200°C, depending on the nature of the anion. In addition, degradation due to electrolyte conditions, particularly the pH, is also important. Polypyrrole is also quite stable in the pH range 1 to 7 (39), but partially reversible loss of conductivity occurs above pH 7 because the nitrogen in the pyrrole rings tend to become deprotonated (17,56).

## E. Transport Properties

### 1. Electronic Transport

The origin of the electronic conductivity of polymers arises from a state of relative oxidation or reduction (57,58). In such states, the polymer loses (for oxidation) or gains (for reduction) electrons. The number of monomer units which gain or lose electrons is variable but a reasonable estimate is one electron per three monomer units (29).

Once the polymer is electronically charged, counterions from the solution enter the polymer fibril to produce electrostatic neutrality. It is these ions which are often referred to as dopants. However, this is not doping in the sense of semiconductor doping, where the dopant provides charge carriers. In conducting polymers, the charge carriers are generated within the polymer chain. On the other hand, it is convenient to refer to the counterions in the charged polymers as dopants.

Considering the polymer in terms of a semiconducting material and using the band structure model (59,60), oxidation and electron loss give rise to new energy states. Removal of one electron from a  $\pi$  bond leaves the remaining electron in a nonbonding orbital-different in energy from the valence and conduction states. These states are above the valence band and they give rise to the behavior of the polymer as though it were a heavily doped semiconductor.

The most commonly accepted conduction mechanism (57-60) is polaron and bipolaron formation upon oxidation. Oxidation of the polymer breaks one double bond, leaving a radical and a positive charge on the polymer chain which is commonly referred to as a polaron. Polarons converge into bipolaron when the polaron concentration gets high enough for the polarons to "feel" each other. The radical-cations are spread out through the adjacent  $\pi$  structure across approximately eight bond lengths, making contact with other radical cations. The combination of the two radicals (one from each polaron) forms a new  $\pi$  bond which is commonly referred to as a bipolaron. The bipolaron is more stable than the two radical-cation bonds at the same distance apart (i.e., the  $\Delta G$  of the bipolaron is greater than  $\Delta G$  of dissociations of the two polarons). The bipolarons are then free to hop along the polymer chain, which gives rise to the

electronic conductivity.

The electron hopping mechanisms proposed for the polyheterocyclics to date can be divided into three distinct categories: variants of Mott's variable range electron-hopping theory (61), polaron or bipolaron interchain hopping theory (62), and phonon-assisted hopping mechanisms (63). The essential features of these three mechanisms and several variants which have been recently proposed are discussed next.

i) Variable Range Hopping (VRH) Model – This model was proposed in 1969 to explain the electronic conductivity of crystalline semiconductors cooled to liquid helium temperatures so as to suppress band conduction (61). Currently, the VRH model is most often associated with the description of electron transport in amorphous semiconductor such as Ge, Si, III-V compound (53,64).

In conducting polyheterocycles, localized states (charge carriers) are introduced to the band-gap with the creation of polarons or bipolarons in addition to the electronic states present in the band-gap as a consequence of structural disorder in the polymer (53). In the application of the VRH model to the conducting polyheterocycles, carrier sites are assumed to be stationary, intersite distance are variable, and electron-hopping occurs in three dimensions. It should be noted that hopping is not assumed to be isoenergetic as it is in both of the other models discussed here. The rate of thermally-activated electron-hopping between localized sites is determined by the average difference in energy between them and by the extent of the wave function overlap.

The VRH theory predicts a  $T^{-\frac{1}{4}}$  temperature dependence of  $\log \sigma$ , as observed for polyacetylene and other polyheterocycles (53). However, several authors have noted that the density of electronic states at the Fermi level,

$N(E_F)$ , estimated from electron spin resonance (ESR) measurements are lower than that necessary to accommodate the  $\sigma$  values measured for both polypyrrole and polyacetylene (62,65). In addition, the thermoelectric power observed for polypyrrole or polyacetylene is not in agreement with model predictions.

On the basis of these data, Shen *et al.* (65) extended Mott's theory by considering localized states (bipolarons) which are mobile on a segment of conjugated polymer. Thus, electronic transport occurs as a composite process involving the "sliding" of a bipolaron on a conjugated polymer segment in conjunction with electron-hopping across defects and between chains. Better agreement for the thermoelectric power and values for  $N(E_F)$  were obtained with preliminary experimental data for polypyrrole samples prepared in aqueous electrolytes using this theory (65).

ii) Bipolaron Hopping Model - Polaron hopping mechanisms have previously competed with VRH theory to account for the mechanism of electronic transport in amorphous semiconductor (53,62). Chance *et al.* (62,66) have attempted to account qualitatively for electronic transport in the polyheterocycles at low doping levels with a model which considers interchain transport of charge via bipolaron hopping. They noted that interchain conduction pathways are likely to limit the macroscopically observed conductivity regardless of the mechanism proposed to account for intrachain charge transport (62,66). On this basis, it was assumed that ionization of an electronically conductive polymer yields localized charge carriers (solitons or bipolarons) which possess little intrachain mobility (62,66). A reduced potential energy barrier for the hopping process in *trans*-polyacetylene is achieved by coupling solitons to bipolarons (soliton pairs) which extend over just five lattice spaces (62). Consequently, bipolaron hopping is

assumed to account for interchain and intrachain charge transport in both *trans*-polyacetylene and in polymers like polypyrrole which do not possess a degenerate ground state and hence inherently possess bipolarons.

As compared to the Mott's mechanism, bipolaron hopping predicts truly spinless conductivity (62). However, the unique feature of this mechanism is the unusual conductivity versus % doping relation it predicts as a result of the fact that the bipolaron charge carriers cannot hop to other occupied sites in the polymer. Thus, the maximum contribution to the conductivity from bipolaron hopping occurs at intermediate doping levels, and reduced conductivity is predicted to result from doping in excess of this optimum level (62,66).

Unfortunately, comparison of this prediction is not possible in the case of polypyrrole since conductivity ( $\sigma$ ) versus concentration of bipolaron charge carriers data have not been reported for the polyheterocycles (62). However, satisfactory agreement with experimental data is obtained with the analogous bipolaron hopping expression for polyacetylene (62). The current expression of bipolaron hopping theory is relatively crude and entirely qualitative. Extensions are required before theoretically predicted thermoelectric power, Hall effect, and  $\log \sigma$  versus temperature relations can be done and compared with experimental measurements.

It should be noted that Chance *et al.* (66) proposed the bipolaron hopping mechanism to account for the electronic conductivity of a lightly doped system only. The argument is more advanced in that at moderate doping levels, the activation barrier for electron hopping is reduced by the overlap of charge carriers on the polymer chain and a delocalized conduction pathway develops.

iii) Soliton Hopping Model – Kivelson's three dimensional version (63), which

is an extension of the one-dimensional soliton hopping mechanism proposed by Su *et al.* (67), for transport in *trans*-polyacetylene also attempts to account for the mechanism of conduction at low doping levels. Since this model relies on the presence of both charged and uncharged carrier defects (solitons), its predictions are relevant to *trans*-polyacetylene only. In spite of this fundamental limitation, Pfluger *et al.* (53) have noted that this model may assist in the formulation of future models for phonon-assisted hopping between charged bipolaron sites in polyheterocycles because the transport data predicted with this model is in excellent agreement with experiment.

The Kivelson model assumes that the polymer is structurally disordered, and that localized electronic states are randomly distributed. The existence of significant numbers of both charged and neutral localized sites is also assumed in accordance with the observation of neutral solitons by ESR in lightly doped polyacetylene. It is likely that charged solitons are strongly pinned at low doping levels by electrostatically bound counterions whereas neutral solitons are highly mobile. Electronic transport is effected by the isoenergetic phonon-assisted hopping of electrons between charged and uncharged solitons.

Despite the success achieved by this model in predicting electronic transport data for *trans*-polyacetylene, the Kivelson model has generated considerable controversy. Ngai *et al.* (68) have questioned several of the assumptions inherent in the derivation of the Kivelson model. Chance *et al.* (66) have noted that a weakness of the Kivelson model is its dependence on an extrinsic factor, namely a substantial neutral soliton concentration, for the mechanism of conduction. In any case, elements of this model are likely to be employed in future electronic transport models appropriate for the polyheterocycles.

Despite numerous investigations in this area, the actual charge transport mechanisms by which these films conduct remain illusive.

## 2. Mass Transport

The unavailability of accurate values for the transport properties of electronically conducting polypyrroles has limited the characterization of these polymers. For example, the characterization of the ionic conductivity of polypyrrole membranes is limited by the absence of reliable permeability data. Diaz *et al.* (40,69) described polypyrrole as a densely packed, nonporous material principally on the basis of cyclic voltammetry of electroactive species. Noufi *et al.* (70), however, demonstrated both incorporation and mobility of  $\text{Fe}(\text{CN})_6^{-3}$  ions in polypyrrole. In addition, the photocorrosion of a polypyrrole coated semiconductor photoanode, although slowed by the polypyrrole film, seems to be associated with the permeability to solution species, since changes in solvent and electrolyte affect the rate of corrosion. Bull *et al.* (41) concluded from the AC impedance of oxidized polypyrrole films on solid electrodes that the polypyrrole films were quite permeable to solvent and electrolyte, and that the best description of the films behavior as an electronically conducting coating was as a porous electrode with electrochemical reactions occurring at both polypyrrole-solution interfaces and the solid electrode beneath the polypyrrole coating. This has been attributed to the large interfacial contact surface between the polymer and the electrolyte.

Additional evidence for the porosity of the polypyrrole film comes from the fact that electrochemical reactions occur at the substrate as in the oxidation of Si electrodes, although the reaction is considerably slower than with uncoated electrode (71,72). These observations suggest that polypyrrole cannot be considered simply as a nonporous metallic film. Burgmayer *et al.* (42) directly measured per-



meation rates for electrolytes through the polypyrrole membrane and concluded that the porosity characteristics lay somewhere between the limits suggested by Diaz *et al.* (40) and Bull *et al.* (41). They found the permeation rate of anion in the oxidized polypyrrole to be much faster than that in the neutral polypyrrole. This of course is the basis for the ion gate.

Based on these conclusions, attempts to estimate the apparent diffusion coefficients for counterions within the polypyrrole film have been conducted by several groups (73-76). Genies *et al.* (73) estimated the diffusion coefficient for  $\text{ClO}_4^-$  counterion in polypyrrole films as a function of the concentration of  $\text{LiClO}_4$  in the acetonitrile by using conventional chronocoulometry and chronoabsorptometry. The apparent diffusion coefficient was found between  $1.0 \times 10^{-10}$  and  $1.0 \times 10^{-9}$   $\text{cm}^2/\text{sec}$ , depending on the electrolyte concentration. However, the diffusion coefficient information derived from either of these experiments is unreliable because large capacitive current and uncompensated resistance effects in polypyrrole films were not considered.

Penner *et al.* (74) obtained apparent diffusion coefficients for  $\text{BF}_4^-$  within polypyrrole films in  $\text{Et}_4\text{NBF}_4/\text{acetonitrile}$  by use of a low amplitude current pulse technique. They found apparent diffusion coefficient values of  $4.0 \times 10^{-9}$  to  $8.0 \times 10^{-9}$   $\text{cm}^2/\text{sec}$ , depending on the polypyrrole film thickness. This analysis possesses several advantages for the determination of diffusion coefficients as compared to conventional chronocoulometry because the perturbation of the film redox state during the low amplitude current pulse experiment is extremely small.

Transient techniques have been also employed to estimate the apparent diffusion coefficient of  $\text{ClO}_4^-$  counterion in the polypyrrole films by Naoi *et al.* (75) and Panero *et al.* (76). The values found are in the range between  $2.0 \times 10^{-10}$

$\text{cm}^2/\text{sec}$  and  $3.0 \times 10^{-10} \text{ cm}^2/\text{sec}$ . The transient techniques, however, are not appropriate for the conducting polymers, unless proper account is taken of the influence of the polymer geometry.

The analysis shows that the values of the apparent diffusion coefficient of the counterions obtained with the doping process are larger than those obtained with the undoping process. It may be concluded that diffusion in polypyrrole film is a more complicated process than simply involving anions entering into the polymer as oxidation proceeds and leaving as reduction occurs. There is evidence from Kaufman *et al.* (77) and Chao *et al.* (78) that the diffusion process includes anions and cations. These results suggest that a realistic diffusion model should consider different mechanisms for the doping and undoping processes.

Another unsettled issue for transport properties of polypyrrole is the rate of electrochemical charge transport during redox reactions of the polymer itself and the effect of ion mobility on the rate. The shape sensitivity of the cyclic voltammogram suggests that the mobility of both the cation and the anion effect the kinetics of the polymer redox reaction but not the thermodynamics since the potentials corresponding to peak currents are essentially unshifted in various electrolytes (33,40). The rate at which polypyrrole can be charged and discharged between its oxidized and neutral states is very significant, especially in its application as an energy storage device. This rate is controlled primarily by the rate at which electrochemical charge can be propagated through the polymer. Unfortunately, because of its electronic conductivity, high surface area and associated large double layer charging currents, the usual method for investigating the rate of charge transport characterization (i.e., chronoamperometry) cannot be used for polypyrrole.

A few theoretical studies have been conducted on the characterization of the charge transport mechanisms within polypyrrole films. Feldberg (79) suggested a Butler-Volmer type reaction rate expression for the quasi-reversible switching behavior and a linear dependency of differential capacitance on doping level. However, this work failed to include the transport effect (diffusion and migration) of the counterion in the redox reaction rate. Pickup *et al.* (80) developed mathematical models, plane electrode and porous electrode models, for potential step chronoamperometry to study charging and discharging rate of polypyrrole film. They concluded that a porous electrode model has better prediction than a planar electrode model. However, their porous electrode model is not satisfactory because it is based on the assumption that faradaic reactions are negligible.

#### F. Dependency of Properties on Polymerization Conditions

It has been demonstrated that the microscopic structures and the properties of the polypyrrole films depend on polymerization conditions. Some of the variables which influence these properties and which can be controlled in the electrochemical environment are the substrate electrode material (71,81-85), solvent (1,16,17,42,51), electrolyte salt (1,33,36), driving force (31,86-90), pH (30), and temperature (55,87,88,91). Consequently, numbers of studies have been done to determine and optimize the polymerization conditions.

##### 1. Electrodes

The nature of the substrate electrode is critical in the preparation of polypyrrole films, particularly the adhesion of the film to the substrate. Since the films are produced by an oxidative process, it is important that the electrode does not oxidize concurrently with the aromatic monomer. For this reason,

most of the available films have been prepared using a platinum or a gold electrode. Metals such as silver, aluminum, indium, or iron, which oxidize more readily than the pyrrole monomer, would obviously not be good choices for the electrode (81). Polypyrrole films can also be prepared using a variety of semiconducting materials, including tin oxide, n-type polycrystalline silicon (71), gallium arsenide (82), cadmium sulfide and cadmium selenide (83), and graphite (84). Polymerizations on platinum and glassy carbon electrodes produce better adhering films than on tin oxide or single crystal n-type silicon (85).

## 2. Solvents

The polymerization reaction proceeds via radical cation intermediates. Therefore, the progress of this reaction will be sensitive to the nucleophilicity of the environment in the region near the electrode surface. This then places some limitations on the choice of solvent and electrolyte. For this reason, most of the reported studies have been performed in poor nucleophilic aprotic solvents. The effect of these solvents on the quality of polypyrrole films is shown in Table II (1). Among these, acetonitrile has been the most commonly used solvent, although a wide variety of other aprotic solvents can be used as long as the nucleophilic character of the solvent is poor. However, certain nucleophilic aprotic solvents (such as, dimethylformamide) and hydroxylic solvents can also be used to prepare good films if the nucleophilicity of the solution can be reduced using protic acids.

The ionic conductivity of polypyrrole film can be influenced by electrolytic conditions. Burgmayer *et al.* (42) investigated the effect on the ionic conductivity of polypyrrole, by varying type of solvent and electrolyte in the electropolymerization and assessing the results with measurement of in-phase impedance. The

Table II. Solvent effects on the quality of the polypyrrole films.

Solvent/Electrolyte	Film Quality	Electronic Conductivity ( $\Omega^{-1} \text{ cm}^{-1}$ )
Acetonitrile/0.1M TEAT <sup>†</sup>	Good	50.0
Acetonitrile/0.1M Toluenesulfonic Acid	Good	50.0
Acetonitrile/0.1M TEAT+1M Pyridine	No	-
Methylene Chloride/0.1M TBAT <sup>‡</sup>	Good	50.0
Butanone/0.1M TBAT	Good	40.0
Propylene Carbonate/0.1M TBAT	Good	50.0
Dimethylformamide/0.1M TEAT	No	-
Dimethylformamide/0.1M Toluenesulfonic Acid	Good	20.0
Dimethylsulfoxide/0.1M TEAT	No	-
Hexamethylphosphoramide/0.1M TEAT	No	-
Ethanol/0.1M TBAT	Bad	0.2
Ethanol/0.1M Toluenesulfonic Acid	Good	3.0
Ethanol/0.1M Sulfuric Acid	Good	3.0
Ethanol/0.1M Phosphoric Acid	No	-
Ethanol/0.1M Hydrochloric Acid	Bad	-

<sup>†</sup>TEAT(Tetraethylammonium Tetrafluoroborate)

<sup>‡</sup>TBAT(Tetrabutylammonium Tetrafluoroborate)

results showed that a solvent can alter the ionic conductivity of the resulting polymer. The change in ionic conductivity must reflect a microscopic structural change in the polymer that ensued during electropolymerization. Also, they observed that the electropolymerizing polymer film grows approximately two times faster in water than in acetonitrile. According to their results, the original choice of perchlorate in acetonitrile solvent gave a polypyrrole film with the lowest oxidized ionic resistance, which means the most desirable response. In contrast, ionic conductivity changes in counterions have much smaller effect.

Water content in the electrolyte also influences the performance of polypyrrole film. Diaz *et al.* (16,17,51) reported that films grown in anhydrous acetonitrile have a rough surface with dendrite-like structure as shown by scanning electron microscopy, while presence of as little as 1% H<sub>2</sub>O or other hydroxylic solvents led to much smoother and more adherent films.

### 3. Electrolytes

With regards to the electrolyte salt, the main considerations are the solubility, degree of dissociation, and the nucleophilicity (1). Most of the salts used are tetraalkylammonium salts, because they are soluble in aprotic solvents and dissociate quite easily. Although some lithium salts are soluble in aprotic solvents, these salts are highly aggregated. Most sodium and potassium salts show poor solubility in aprotic solvents.

The stability of the incipient cation of the electrolyte salt is an important factor to be taken into consideration for the formation of the polymer film. Film formation results from pyrrole cation intermediates with moderate stability favoring the radical coupling reaction. The more stable cations of the electrolyte salt diffuse away from the electrode surface and produce soluble products. The

very reactive cations of the electrolyte salt react indiscriminately with solvent and other nucleophiles in the region of the electrode surface thereby, minimizing the polymer forming reaction.

The electrochemically synthesized conducting polypyrrole films contain 10-35% anions (by weight) which are affiliated with the cationically charged polymer chains to produce electrostatic neutrality (33). The amount of anion found in each film is governed by the doping level of the polymer and it is characteristic of each film. The anions listed in Table III are poor nucleophiles commonly used in the preparation of good quality films. Common counterions to produce good polypyrrole film in nonaqueous solvents includes  $\text{BF}_4^-$ ,  $\text{ClO}_4^-$ , and  $\text{PF}_6^-$ . Sulfonates are commonly used anions in aqueous solvents. The doping level of polypyrrole is 0.25-0.32 per pyrrole unit, corresponding to one anion for every 3-4 pyrrole units. The doping level is an intrinsic characteristic of the polymer and is not sensitive to the nature of the anion. However, the anion does influence both the structural properties and the electroactivities of the films. The size and electronic structure of the anion affect both the conductivity and the structural properties of polypyrrole. In addition, good films are typically not produced when the anion is a halide, because halides are fairly nucleophilic and easily oxidized. Highly nucleophilic anions, such as hydroxide, alkoxide, cyanide, acetate, and benzoate do not produce good quality films either but instead lead to soluble products.

The anion influences the electrical properties of the films which are in the oxidized form (33). Because the counterion acts to separate polymer chains within the bulk, a larger counterion creates a larger chain separation, and therefore, a larger distance over which charge must hop to get from one chain to

Table III. Anion effects on the properties of the polypyrrole films.<sup>†</sup>

Doped Anion	Maximal Doping Level	Density (g/cm <sup>3</sup> )	Electronic Conductivity ( $\Omega^{-1}\text{cm}^{-1}$ )
Tetrafluoroborate ( $\text{BF}_4^-$ )	0.32	1.48	30-100
Hexafluoroarsenate ( $\text{PF}_6^-$ )	0.32	1.48	30-100
Hexafluorophosphate ( $\text{AsF}_6^-$ )	0.32	1.48	30-100
Perchlorate ( $\text{ClO}_4^-$ )	0.30	1.51	60-200
Hydrogensulfate ( $\text{HSO}_4^-$ )	0.30	1.58	0.3
Fluorosulfonate ( $\text{FSO}_3^-$ )	-	1.47	0.01
Trifluoromethylsulfonate ( $\text{CF}_3\text{SO}_3^-$ )	0.31	1.48	0.3-1
p-Bromobenzenesulfonate ( $\text{BrC}_6\text{H}_4\text{SO}_3^-$ )	0.33	1.58	50
p-Toluenesulfonate ( $\text{CH}_3\text{C}_6\text{H}_4\text{SO}_3^-$ )	0.32	1.37	20-100
Trifluoroacetate ( $\text{CF}_3\text{COO}^-$ )	0.25	1.45	12

<sup>†</sup>Tetraalkylammonium salts used



the next. The dependence of room temperature conductivity on the nature of the anion present in the electrolyte is shown in Table III (33). In general, the films with perfluoride or perchlorate anions are more conducting than the films with the sulfonate and carboxylate anions. Exceptions are films containing aromatic sulfonate anions.

The size and shape of the counterion also affect the structural and mechanical properties of polypyrrole films. As shown in Fig. 4, the topology of the surface is dramatically different for polypyrrole films containing various anions. The difference observed between the surfaces are not reflected in the packing structure of the bulk material. Therefore, all the films have similar flotation densities which fall in the range 1.45-1.51 g/cm<sup>3</sup>. In a similar manner, the mechanical properties of the films change with the type of anion in the electrolyte. Polypyrrole films containing toluenesulfonate, perchlorate, and fluoroborate anions are hard and strong films and stretch very little (4-5% elongation at break). However, the films containing toluenesulfonate anion are stronger and have a tensile strength 30-40% higher than for other films. The values of conductivity, elongation, and module are similar for these films.

The temperature sensitivity of the electrical properties of the films is also influenced by the nature of the anion. Film with fluoroborate, fluorophosphate, perchlorate, nitrate, and toluenesulfonate anions can be heated to approximately 160°C in air before they begin to decompose. Furthermore, the change in conductivity with temperature is very mild, 10-50% per 100°. Films with toluenesulfonate and trifluoroacetate anions can be heated to 280°C before they begin to decompose. The conductivity of the latter films increases by a factor of 3-5% per 100° increase in temperature, with the less conducting film showing

the biggest change.

Anions also show a strong influence on electroactivity. Several authors (33,36) have investigated the sensitivity of cyclic voltammetric behavior to the use of different counterions in electrochemical polymerization. Since the rate of switching is limited by the mobility of the anion in and out of the film, the switching rates are very sensitive to the anion. This rate dependency on the anion gives rise to very complicated cyclic voltammograms which represent the combined faradaic and capacitive currents. Anions influence only the kinetics of the reaction and not the switching potential.

#### 4. Driving Forces

It has been shown that polypyrrole can be electrochemically synthesized by controlled potential or controlled current (31,86-90). The conductivity, polymer structure, stability, and electroactivity are found to be a function of the choice of driving force (current or potential) and the magnitude of that on the polymerization.

The effects of the driving force on the electronic conductivity of polypyrrole films have been investigated by several groups (86-88). Hahn *et al.* (86) investigated a conductivity of polypyrrole films as a function of applied current density. Their analysis show a maximum conductivity of polypyrrole films prepared at constant current density of  $0.75 \text{ mA/cm}^2$ . Maddison *et al.* (87) also investigated a maximum conductivity for polypyrrole films as function of current density, but found at a current density of  $2.8 \text{ mA/cm}^2$ . In contrast to the acetonitrile used by Hahn *et al.*, they utilized an aqueous electrolyte. Satoh *et al.* (88) examined the effect of applied potential on the electronic conductivity. Their results show a maximum conductivity at potential of  $+0.6 \text{ V}$  versus SCE,

where a value of  $500 \Omega^{-1}\text{cm}^{-1}$  is obtained. The conductivities of films prepared at potentials above or below  $+0.6 \text{ V}$  versus SCE rapidly fell to below  $100 \Omega^{-1}\text{cm}^{-1}$ .

The applied potential or current on polymerization also affects the structural of polypyrrole films. Polypyrrole films formed at a relatively high anodic potential or current (89,90) were observed to have a porous morphology. Anions incorporated in the polypyrrole film lattice were found to accompany a smooth doping and undoping reaction because of their rough polymer structure. Although polypyrrole films so obtained may show a high charging-discharging efficiency, they have defects in mechanical strength and in the degree to which they adhere to the substrate.

Otero *et al.* (31) prepared polypyrrole films from acetonitrile solution containing lithium perchlorate under varying conditions of potential control: constant potential, square wave potential step, and potential sweep methods. The resulting films were analyzed by scanning electron microscopy. The square wave potential step method produced polypyrrole films having a smoother surface, that adhered more strongly to the platinum substrate. These characteristics increased with a decrease in the step duration, that is, a more rapid cycling of the potential resulted in smoother, more adherent films.

## 5. Others

Other factors which have been shown to affect the properties of polypyrrole films include the pH of the electrolyte used for synthesis, and the temperature under which the synthesis is carried out. In acid solution, the polypyrrole films become rougher and even take on a powdery appearance (6,30). In alkaline solution, only thin films may be grown and this may imply that a very compact film free of pores (essential at least for anion movement in the film) is formed

(30). Satoh *et al.* (88) investigated the effects of polymerization temperature of the electrolyte, and observed a maximum conductivity of polypyrrole films grown at a temperature of 10°C.

#### G. Modifications of Properties

Further encouraging features of the pyrrole polymer system were the degrees of freedom available to modify the electrical and physical properties by resorting to particular anions, derivatives, or copolymers in order to achieve any desired matrix of polymer properties. Several strategies directed at improving the properties of polypyrrole have been proposed recently (92-104).

There is now abundant experimental evidence to support the contention that the rate of polypyrrole redox reaction is limited by the mass transport of charge compensating ions in the polymer phase (36,40,41). The amorphous morphology of the polypyrrole, to compare polyacetylene, produces slower counterion transfer rates and results in slow electrochemical kinetics (i.e., low current density). Application of polypyrrole as a battery material requires that polypyrrole charge and discharge quickly (69). To synthesize conducting polymer films with a well-defined morphology generally involves the formation of a polypyrrole film within a somewhat porous host membrane, and a subsequent dissolution of the host membrane. Penner *et al.* (92) introduced a fibrillar-microporous morphology, in which polymer chains are organized into narrow fibers surrounded by micropores. Nuclepore polycarbonate membranes, which are soluble in dichloromethane, were used as the porous host membranes. An interesting and potentially useful attribute of this approach is that the conducting element can be grown to any desired diameter and thickness within the host material. Naoi *et al.* (75,93)

reported the superiority of the charging-discharging performance of lithium batteries employing modified polypyrrole with nitril rubber. The polypyrrole film formed with the aid of nitril rubber showed a highly enhanced anion doping-undoping process because it has a rough, porous structure in the direction perpendicular to the current collector substrate. Thus, it should be possible to improve the performance of polymer based devices by employing such transport optimized films.

The other class of techniques investigated is the formation of composites. De Paoli *et al.* (94,95) have prepared poly(vinyl chloride)-polypyrrole composite membranes by electropolymerizing pyrrole inside a poly(vinyl chloride) film on an electrode surface. Although these composites had the desirable mechanical properties of the poly(vinyl chloride) host and the high conductivity of the polypyrrole, poly(vinyl chloride) is not the ideal host material because it is neither porous nor conductive. Lindsey *et al.* (96) have demonstrated that polypyrrole can be deposited within the matrix of several swellable polymers to form a conducting composite. This composite membrane shows conductivities as high as  $10 \Omega^{-1}\text{cm}^{-1}$  and excellent mechanical properties which make the membrane easier to fold without cracking.

Fan *et al.* (97) prepared polypyrrole film in matrices of Nafion and clay (hectorite) by electropolymerization. These films display higher electronic conductivity and stability than films made of polypyrrole alone. Penner *et al.* (98) showed that electronically conducting composite membranes can be prepared by electropolymerizing pyrrole within Nafion-impregnated Gore-Tex (NiGT), which has an open-end porous structure. The electronic conductivity of the polypyrrole doped NiGT membrane is essentially identical to the conductivity of polypyrrole.

Novák *et al.* (99,100) prepared polypyrrole and polyethylene oxide composite polymer film. This composite polymer shows enhanced coulomb capacity and poor charge retention as compared to polypyrrole itself.

Copolymer formation is another technique for the production of conducting membranes. A variety of copolymers can be prepared by varying the nature, number, and ratios of polymers that are copolymerized with polypyrrole. Nazzari *et al.* (101) had prepared pyrrole and styrene copolymer films. The films vary in their properties, depending on the ratio of styrene to pyrrole. Films with a high concentration of styrene had electrical conductivities of about  $10 \Omega^{-1}\text{cm}^{-1}$  with mechanical properties similar to polystyrene. On the other hand, films with a low concentration of styrene had higher conductivities, about  $50 \Omega^{-1}\text{cm}^{-1}$ , with mechanical properties similar to polypyrrole tetrafluoroborate.

Also, attempts have been made to copolymerize different kinds of heterocyclic compounds, and electrochemical properties of the resulting copolymers have briefly been studied. So far copolymers of pyrrole and N-methyl pyrrole (19), pyrrole and phenol (102), pyrrole and terthienyl (103), and pyrrole and thiophene (104) have been prepared by electrolytic oxidation of mixtures of monomers.

Consequently, by appropriate choice of the polymerization condition or composite formation, satisfactory electrochemical and mechanical properties can be achieved for a particular application of polypyrrole.

## H. Applications

Commercially significant applications of electronically conducting polypyrrole films are most likely to stem from their unique properties and characteristics, the exact combination of which is not offered by any other material. These ap-

plications are on the area of energy storage (105-110), solar energy conversion (85,111-116), electrochromic display devices (40,43,50,117), etc.

### 1. Energy Storage Devices

The most common application of these polymer films has been in the area of energy storage and distribution. The main properties of polypyrrole films which make them attractive as electrode materials in the high-energy-density secondary battery technologies are ease of preparation, electrochemical redox behavior, high electrical conductivity, and ease of property modification. These polymers also offer flexible design characteristics.

Indeed, lithium/polypyrrole rechargeable batteries are under study in various laboratories with some encouraging preliminary results (105-110). They have demonstrated the charge/discharge behavior of lithium/polypyrrole cells and reported a open circuit voltage of 3.0-4.0 V, an energy density of 50-200 Wh/kg, and a power density of 200 W/kg. These results indicate that conducting polypyrrole films can be used as positive electrodes in rechargeable lithium organic electrolyte batteries, with good promise of long cycleability and high charge/discharge efficiency.

However, there are some major problems which appear to limit the applicability of these polymer electrode. The morphology of polypyrrole, which is relatively amorphous compare to polyacetylene, has been a major stumbling block in the development of the polypyrrole secondary battery system. The morphology of polypyrroles determines the facility of counterion transport and the rate of the electrochemical reaction of the dopants within polypyrrole film (105,106). Other problems are the lack of stability even in hermetically sealed environments, the poor stability of the organic solvent against a high open circuit voltage, the self

discharge of the polymer in the electrolytic medium, and their cost compared to alternative battery systems.

## 2. Solar Energy Devices

The conducting polymer can serve as an enhancer of properties for the basic components in solar energy cells and photoelectric devices. It is of significant importance to enhance the stability against the photodegradation of semiconductor photoanodes in electrochemical photovoltaic cells. The polypyrrole films can be grown on n-type semiconductor electrodes (such as, Si, GaAs, CdS, CdSe, and CdTe) in the photoelectrochemical cells by photo assisted electrochemical oxidation of the pyrrole monomer (71,82,85,111-115). Cooper *et al.* (116) showed that thin layer of polypyrrole deposited on n-type photoanodes can efficiently transfer charge over large distances and effectively inhibit the dissolution or oxidation of the n-type semiconductor, thus extending lifetime of photoelectrochemical cells.

A problem encountered with this application is that the film does not adhere to the electrode surface over a long period of time. Efforts are being made to solve this problem. For example, Fan *et al.* (112) and Skotheim *et al.* (113) reported an improvement in film adhesion by metallizing the Si surface prior to polymerization of the pyrrole. Other methods of improving the film adhesion include chemical binding of the film to the electrode (85,115).

## 3. Electrochromic Display Devices

Electrochromic effect is defined as a change of the visible absorption coefficient (a color change) induced in a material by the passage of a charge (an applied electric field or current). It has been demonstrated by many laboratories that polypyrrole films are brown-black in the doped state and light yellow in



the undoped state. A color change proceeds as a result of the insertion of ions from an electrolyte and electrons from an electrode. In the neutral state, yellow polypyrrole has a strong absorption band in the ultraviolet-blue range and the absorption in the visible range increases when the film is oxidized, giving the coating a brown color (40,50,117). This feature makes electronically conducting polypyrrole an attractive candidate for electrochromic display.

Response times are less than 100 msec and are acceptable, but lifetime is a problem ( $10^5$  cycles is the best) and does not compete with the lifetime obtained with inorganic electrochromic materials such as tungsten oxide ( $10^6$  cycles). Further improvements in contrast ratio, switching speed, and long-term stability are required before polypyrrole can gain general acceptance for use in display devices (43).

#### 4. Others

Recently, applications of organic conducting polymers, polypyrrole, polythiophene, etc., to electronic devices have been investigated by several workers; some devices are totally organic and the others are partially organic (118-121). Characteristics of these polymers, which are often very different from those of inorganic materials, enable us to fabricate new types of electronic devices which are superior to the conventional ones. By utilizing these polymers, memory devices (45,118,119), p-n junctions (120), and molecular based transistors (121) have been fabricated. Moreover, organic conducting polymers can be made with various kinds of functional molecules incorporated in their matrices, such as organic dyes, metal-organic compounds, biomolecules, etc.

Conducting pyrrole polymers have also found application in catalysis. Bull *et al.* (84) incorporated tetrasulfonated iron phthalocyanine anion in polypyrrole

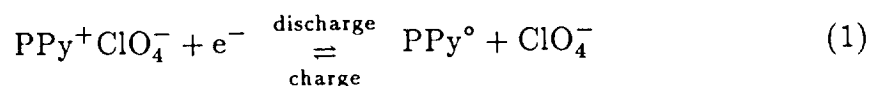
film and demonstrated that the films catalyzed the reaction of oxygen on glassy carbon electrodes, at potentials 250-800 mV less negative than at bare glassy carbon or glassy carbon electrodes coated with polypyrrole containing noncatalytic ions.

Polypyrrole membranes offer a lower resistance to ion transport when the polymer is in the neutral state and a higher resistance when in the oxidized state (44,45). For these reasons, they have been employed as electronically control ion-gates.

### III. MATHEMATICAL TREATMENT OF MATERIALS

#### A. Electrochemistry

The electrochemical reaction occurring at the polypyrrole electrode is known to be a doping-undoping process. That is, the polypyrrole itself loses electrons and gains dopants in its structure during the doping process, while it gains electrons and releases dopants during the undoping process



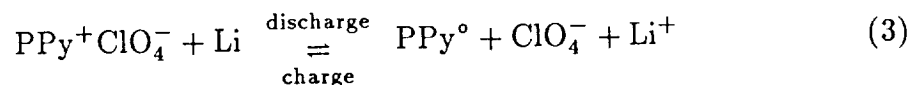
where  $\text{PPy}^\circ$  and  $\text{PPy}^+$  are the neutral and oxidized forms of polypyrrole. The counterion ( $\text{ClO}_4^-$ ) is incorporated into the solid structure of polypyrrole to produce electrostatic neutrality and is referred to as the dopant.

It is noted that the oxidized polypyrrole is generally believed to be comprised of localized defect states in the form of polarons (radical cations) at low doping levels and bipolarons (dications) at high doping levels. Of course, the doping process is inhomogeneous and must be considered as statistical. To avoid these complexities and inhomogeneities, a volume averaged doping level (i.e., the ratio of one doped anion to the number of pyrrole monomer units) is used to describe the doping (oxidation) state of polypyrrole without regards to the actual amount of polaron and bipolaron in the local polymer chain.

The electrochemical reaction at the lithium electrode is known to be the dissolution and deposition of the lithium cation as follows:



Therefore, the overall reaction within the lithium/polypyrrole secondary battery cell becomes



These equations can be written in Newman's general notation (122) as

$$\sum_i s_{j,i} M_i^{z_i} = n_j e^- \quad (4)$$

where  $s_{j,i}$  represents stoichiometric coefficient of species  $i$  for reaction  $j$ ,  $M_i$  represents the symbol for the chemical formula of species  $i$ ,  $z_i$  represents the charge number of species  $i$ , and  $n_j$  represents number of electrons transferred for reaction  $j$ . It should be noted that  $s_{j,i}$  has a positive or negative value depending on whether species  $i$  is an anodic or a cathodic reactant, respectively. That is, according to Eqs. [1] and [2]

$$\begin{aligned} s_{1,\text{Li}^+} &= 0 \\ s_{2,\text{Li}^+} &= -1 \\ s_{1,\text{ClO}_4^-} &= +1 \\ s_{2,\text{ClO}_4^-} &= 0 \end{aligned} \quad [5]$$

From the discussion above, it can be seen that the cation and anion of the electrolyte are responsible for the electrons produced or consumed at the electrode, such that

$$\sum_i s_{j,i} z_i = -n_j \quad (6)$$

#### B. Properties of 1M LiClO<sub>4</sub>-PC Electrolyte

The electrolyte in this study consists of 1M LiClO<sub>4</sub> in propylene carbonate and is referred to as a binary electrolyte because it is assumed that LiClO<sub>4</sub>

dissociates in propylene carbonate into charged  $\text{Li}^+$  and  $\text{ClO}_4^-$  species (123). Propylene carbonate is chosen as a solvent because it is a polar nonaqueous solvent which is stable, nontoxic, and can easily be purified. Because of its high dielectric constant, it can serve as a good solvent for different inorganic salts.

Various measurements of the physical and structural properties of 1M  $\text{LiClO}_4$ -PC were conducted by Keller *et al.* (123). Among those properties, the important ones are density ( $\rho_s$ ), viscosity ( $\mu$ ), equivalent molar conductance ( $\Lambda$ ), and transference number ( $t_i$ ). The density and viscosity were determined by a pycnometer and a viscometer with an accuracy of three decimal places. The equivalent molar conductance was calculated by a graphical extrapolation of the equivalent conductance plotted vs. the square root of the concentration and was reported as  $5.640 \text{ cm}^2/\Omega\text{-mol}$ . The transference number of a  $\text{Li}^+$  was reported as 0.19 by the Hittorf method.

The necessary parameter values, which are currently not available from literature or experimental work, can be obtained from experimental measurements and theoretical relationships. The kinematic viscosity ( $\nu$ ) can be obtained by (122)

$$\nu = \frac{\mu}{\rho_s} \quad (7)$$

The ionic equivalent conductance of species  $i$  ( $\lambda_i$ ) in a binary electrolyte can be obtained by (122)

$$\lambda_i = t_i \Lambda \quad (8)$$

and is related to the ionic mobility of species  $i$  ( $u_i$ ) as follows (122):

$$u_i = \frac{\lambda_i}{|z_i|F^2} \quad (9)$$

The ionic diffusion coefficient for species  $i$  ( $D_i$ ) can be then obtained by the

Nernst Einstein equation (122)

$$D_i = RTu_i \quad (10)$$

The physical and transport properties of 1M LiClO<sub>4</sub>-PC electrolyte discussed above are summarized in Table IV.

### C. Properties of Polypyrrole

Despite extensive work at a large number of laboratories (25-117), properties of the polypyrrole film are far from being understood. This is because of its complexity in the switching process and high reactivity toward air and moisture. Only a few measurements of the properties have been reported, and these are

Table IV. Properties of 1M LiClO<sub>4</sub>-PC electrolyte at 25°C.

#### A. Experimental Measurements.†

Density ( $\rho_s$ )	1.254 g/cm <sup>3</sup>
Viscosity ( $\mu$ )	70.80 mg/cm-sec
Equivalent Conductance ( $\Lambda$ )	5.640 cm <sup>2</sup> /Ω-mol
Transference Number of Li <sup>+</sup> ( $t_+$ )	0.190
Transference Number of ClO <sub>4</sub> <sup>-</sup> ( $t_-$ )	0.810

† Obtained from Ref. (123)

#### B. Theoretical Calculations.‡

Kinematic viscosity ( $\nu$ )	0.056 cm <sup>2</sup> /sec
Ionic Conductance of Li <sup>+</sup> ( $\lambda_+$ )	1.072 cm <sup>2</sup> /Ω-mol
Ionic Conductance of ClO <sub>4</sub> <sup>-</sup> ( $\lambda_-$ )	4.568 cm <sup>2</sup> /Ω-mol
Ionic Mobility of Li <sup>+</sup> ( $u_+$ )	1.151 × 10 <sup>-9</sup> cm <sup>2</sup> -mol/J-sec
Ionic Mobility of ClO <sub>4</sub> <sup>-</sup> ( $u_-$ )	4.907 × 10 <sup>-10</sup> cm <sup>2</sup> -mol/J-sec
Diffusion Coefficient of Li <sup>+</sup> ( $D_+$ )	2.853 × 10 <sup>-7</sup> cm <sup>2</sup> /sec
Diffusion Coefficient of ClO <sub>4</sub> <sup>-</sup> ( $D_-$ )	1.216 × 10 <sup>-6</sup> cm <sup>2</sup> /sec

‡ Calculated using relationship given by Ref. (122)

limited to the fully oxidized or neutral states as summarized in Table V (33). The necessary parameter values at the intermediate state, which are currently not available from the literature or experimental work, can be approximated as functions of the doping level,  $\lambda$  (i.e., the ratio of one doped anion to the number of pyrrole monomer units).

It is convenient to define the fractional doping level of polypyrrole film,  $\theta$ , as a function of the doping level as follows:

$$\theta = \frac{\lambda}{\lambda_{\max}} \quad (11)$$

where  $\lambda_{\max}$  represents the doping level of fully oxidized state. Since  $\theta$  varies linearly with the amount of oxidized polypyrrole,  $\theta$  can be expressed by the local faradaic charge of the polypyrrole film,  $Q_f$ , as follows:

$$\theta = \frac{Q_f - Q_{f,\text{red}}}{Q_{f,\text{oxd}} - Q_{f,\text{red}}} \quad (12)$$

where the subscripts, oxd and red, represent the fully oxidized and neutral states. It is noted that  $\theta = 0$  for a fully neutral state of polypyrrole with a minimal faradaic charge,  $Q_{f,\text{red}}$ , and  $\theta = 1$  for a fully oxidized state of polypyrrole with a maximal faradaic charge,  $Q_{f,\text{oxd}}$ .

The microscopic structures and the properties of the polypyrrole film at intermediate state can be considered as functions of  $\theta$  as summarized in Table

Table V. Properties of polypyrrole film doped with perchlorate.

Properties	Oxidized State	Neutral State
Doping Level ( $\lambda$ )	0.30	0.00
Density ( $\rho$ )	1.51 g/cm <sup>3</sup>	-
Conductivity ( $\sigma_p$ )	200.0 / $\Omega$ -cm	1.0 $\times$ 10 <sup>-5</sup> / $\Omega$ -cm

VI. The porosity of the polypyrrole film,  $\epsilon_p$ , is governed by a material balance on the solid phase because the density of the polypyrrole changes with doping level due to the amount of doped anion, and can be expressed in terms of  $\theta$  as follows:

$$\epsilon_p = \theta\epsilon_{\text{oxd}} + (1 - \theta)\epsilon_{\text{red}} \quad (13)$$

where  $\theta$  represents the amount of oxidized polypyrrole and  $(1 - \theta)$  represents the amount of neutral polypyrrole. The electronic conductivity of polypyrrole film ( $\sigma_p$ ) is also obtained in a same manner:

$$\sigma_p = \theta\sigma_{\text{oxd}} + (1 - \theta)\sigma_{\text{red}} \quad (14)$$

The faradaic charge ( $Q_f$ ) at the intermediate state can be expressed as a function of the electrochemical reaction rate which is discussed next in detail.

#### D. Electrochemical Reaction Rate of Polypyrrole

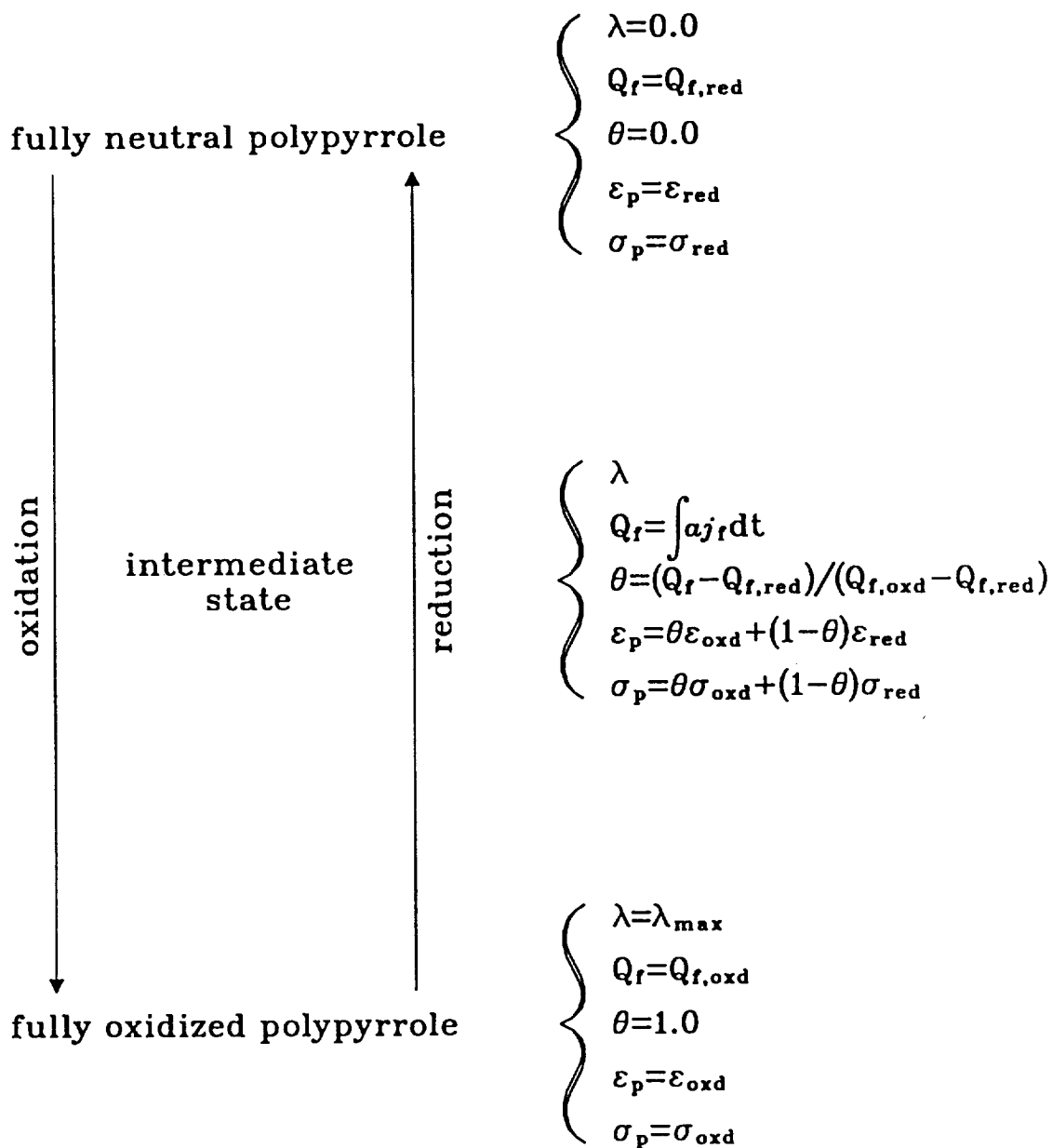
The reaction at the polypyrrole electrode described in Eq. [1] is assumed to be a pseudo-homogeneous reaction. The reaction rate during charge/discharge is controlled primarily by the available electroactive area and the transport (diffusion and migration) of the counterion to the electrode surface. This rate can be expressed by the local faradaic transfer current per unit volume (current transferred per unit volume of polypyrrole electrode by electrochemical reaction [1]), which is assumed to be represented by the Butler-Volmer equation as

$$aj_f = ai_{o1,\text{ref}} \left\{ \left( 1 - \theta \right) \left( \frac{c_-}{c_{-, \text{ref}}} \right) \exp \left( \frac{\alpha_{a1} F}{RT} \eta_1 \right) - \theta \exp \left( \frac{-\alpha_{c1} F}{RT} \eta_1 \right) \right\} \quad (15)$$

where  $a$  is the specific interfacial area per unit volume,  $i_{o1,\text{ref}}$  is the exchange current density for reaction [1] at a given reference concentration ( $c_{i,\text{ref}}$ ),  $\alpha_{a1}$



Table VI. Properties of polypyrrole film as a function of its oxidation state.



and  $\alpha_{c1}$  are anodic and cathodic transfer coefficients, and  $\eta_1$  is the overpotential for the reaction [1]. The term  $a(1 - \theta)$  represents the available electroactive area for oxidation (amount of neutral polypyrrole sites) and  $a\theta$  represents the available electroactive area for reduction (amount of oxidized polypyrrole sites). Anodic and cathodic current components are taken to be positive and negative, respectively. Note also that  $\alpha_{a1} + \alpha_{c1} = n_1$ .

The overpotential is defined as

$$\eta_1 = (\Phi_1 - \Phi_{\text{ref}}) - (\Phi_2 - \Phi_{\text{ref}}) - U_1 \quad (16)$$

where  $\Phi_1$  is the potential in the solid phase,  $\Phi_2$  is the potential in the solution phase,  $\Phi_{\text{ref}}$  is the reference potential, and  $U_1$  is the theoretical open circuit potential for reaction [1] at the given concentration ( $c_i$ ).  $U_1$  is given by

$$U_1 = U_{1,\text{ref}} - \frac{RT}{n_1 F} \ln \left( \frac{\theta}{1 - \theta} \right) \quad (17)$$

where  $U_{1,\text{ref}}$  is the open circuit potential for reaction [1] at a given reference concentration ( $c_{i,\text{ref}}$ ). It can be seen that the local transfer current predicted by the Butler-Volmer kinetic expression, Eq. [15], depends on the difference between the potential of the solid phase ( $\Phi_1$ ) and that of the adjacent solution within the porous electrode ( $\Phi_2$ ). The kinetic parameter values used to simulate the electrochemical reaction rate of the polypyrrole film are summarized in Table

Table VII. Kinetic parameter values used for polypyrrole.

Exchange Current Density ( $ai_{o1,\text{ref}}$ )	10.0 A/cm <sup>3†</sup>
Anodic Transfer Coefficient ( $\alpha_{a1}$ )	0.7 <sup>†</sup>
Cathodic Transfer Coefficient ( $\alpha_{c1}$ )	0.3 <sup>†</sup>
Open Circuit Potential ( $U_{1,\text{ref}}$ )	3.087 V (vs. Li)
Number of Electron ( $n_1$ )	1

<sup>†</sup> Estimated values

VII. The estimated value of each parameter was obtained by statistical comparison between the experimental results and model predictions and is discussed in a later section.

#### E. Electrochemical Reaction Rate of Lithium

Li/Li<sup>+</sup> electrode is quite stable in LiClO<sub>4</sub>-PC solutions in the absence of impurities in the electrolyte (124). Micropolarization tests on a lithium rod about the equilibrium potential indicate only ohmic losses. Lithium deposits at (nearly) 100% faradaic efficiency. The lithium electrode also exhibits a reversible Nernstian behavior (125).

The rate of electrochemical reaction at the lithium electrode in Eq. [2] during charge and discharge processes is controlled primarily by the transport (diffusion and migration) of lithium cations and can be approximated by the Butler-Volmer equation as follows:

$$j_2 = i_{o2,ref} \left\{ \exp\left(\frac{\alpha_{a2}F}{RT}\eta_2\right) - \exp\left(\frac{-\alpha_{c2}F}{RT}\eta_2\right) \right\} \quad (18)$$

where  $j_2$  is local faradaic transfer current density for reaction [2],  $i_{o2,ref}$  is the exchange current density for reaction [2] at a given reference concentration ( $c_{i,ref}$ ),  $\alpha_{a2}$  and  $\alpha_{c2}$  are the transfer coefficients for the anodic and the cathodic reactions, and  $\eta_2$  is the overpotential for reaction [2]. Again  $\alpha_{a2} + \alpha_{c2} = n_2$ .

The overpotential is defined as

$$\eta_2 = (\Phi_1 - \Phi_{ref}) - (\Phi_2 - \Phi_{ref}) - U_2 \quad (19)$$

where  $U_2$  is the theoretical open circuit potential for reaction [2] at the given concentration ( $c_i$ ) and is given by

$$U_2 = U_{2,ref} - \frac{RT}{n_2F} \ln\left(\frac{c_i}{c_{i,ref}}\right) \quad (20)$$

where  $U_{2,\text{ref}}$  is the open circuit potential for reaction [2] at a given reference concentration ( $c_{i,\text{ref}}$ ).

The kinetic parameter values used to simulate the electrochemical reaction rate of the lithium electrode are summarized in Table VIII. Li/Li<sup>+</sup> has a high exchange current density ( $i_{o2,\text{ref}}$ ) in 1M LiClO<sub>4</sub>-PC solution of the order of 2-5 mA/cm<sup>2</sup> for a smooth surface, and a value for the cathodic transfer coefficient ( $\alpha_{c2}$ ) in the range 0.66 to 0.72 (126).

Table VIII. Kinetic parameter values used for lithium.

Exchange Current Density ( $i_{o2,\text{ref}}$ )	0.002 A/cm <sup>2</sup> †
Anodic Transfer Coefficient ( $\alpha_{a2}$ )	0.3†
Cathodic Transfer Coefficient ( $\alpha_{c2}$ )	0.7†
Open Circuit Potential ( $U_{2,\text{ref}}$ )	0.0 V (vs. Li)
Number of Electron ( $n_2$ )	1

† Obtained from Ref. (126)

#### IV. CYCLIC VOLTAMMETRY

In recent years, considerable research effort has been expended on the characterizations of electronically conducting polypyrrole films (25-117). As the results of these studies, electronically conductive polypyrrole films have been approved as potential materials which have technological applications in the area of conductors, organic batteries, and display devices. However, many questions still remain about properties of polypyrrole. Among those unsettled problems, the electronic and ionic charge transport mechanisms within the polypyrrole films have been fundamentally important since the rate of the polymer redox reaction under most circumstances is controlled by these factors. Thus, an understanding of charge transport in these polymers is a prerequisite to further technological applications.

Among the available electroanalytical techniques, the cyclic voltammetry technique has been widely used to understand the electroactivity and the electrochemical properties of polypyrrole films because it can better describe the characteristics of the switching behavior between conducting and nonconducting states (40-43). General experimental cyclic voltammograms of polypyrrole film approximate the behavior of a quasi-reversible couple with the distinct characteristic of a large capacitive background current.

In this chapter, experimental and simulated cyclic voltammetry of 1  $\mu\text{m}$  polypyrrole doped with perchlorate are performed in 1M  $\text{LiClO}_4$ -PC solution. Both results are obtained from identical conditions and compared with each other to clarify the electrochemical reaction mechanisms and charge transport phenomena within the polypyrrole films.

In the mathematical modeling, the current density responses are analyzed in terms of the faradaic and capacitive current components associated with the electrochemical switching of a polypyrrole film between the insulating and conducting states (79). The model is used to characterize dynamic behavior (i.e., the relationship between polymer morphology, charge transport, and electrochemical characteristics) within the polypyrrole films by studying the effects of various parameters.

#### A. Experimental Descriptions

A single-compartment electrochemical cell used for the experiments is schematically presented in Fig. 5. The cell contains a platinum rotating disk electrode coated with polypyrrole film as a working electrode, a platinum counter electrode, a saturated calomel reference electrode (SCE), and a 1M LiClO<sub>4</sub>-PC electrolyte. A rotating disk electrode (RDE) is used here because of its well-defined hydrodynamics (127,128). A luggin capillary tip of the reference electrode is placed as close as possible to the center of the polypyrrole working electrode surface. This enables one to minimize ohmic loss and to use the reference electrode to detect the solution potential near the working electrode. The system is deoxygenated throughout experiments by nitrogen bubbling. The electrodeposition of thin polypyrrole film on the surface of platinum disk electrode is discussed in Appendix A.

Cyclic voltammetry is accomplished using an EG&G Princeton Applied Research (PAR) Model 173 potentiostat/galvanostat in conjunction with a PAR Model 175 programmer, and resulting current density responses are recorded on an IBM AT personal computer.

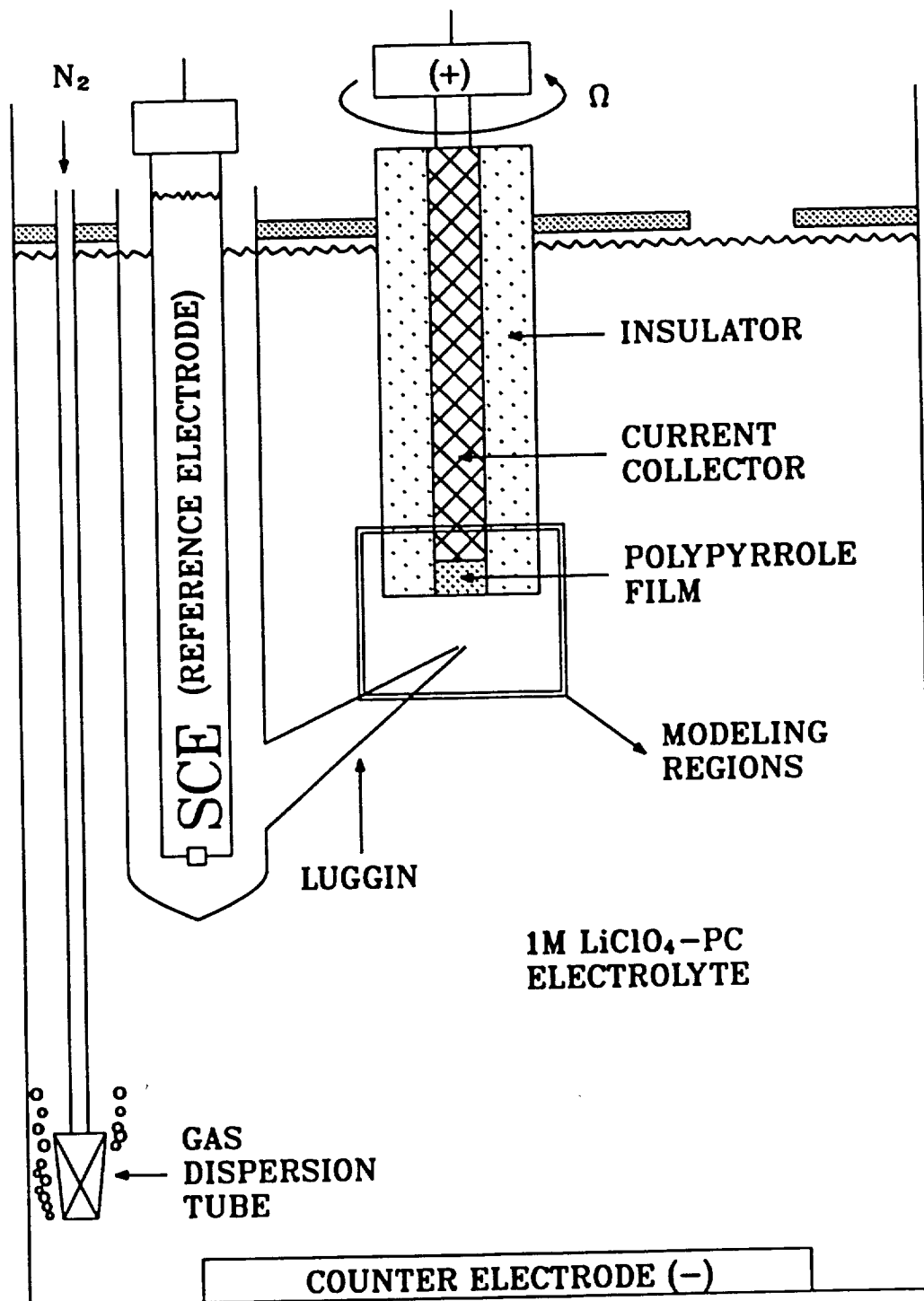


Fig. 5. A schematic diagram of a single-compartment electrochemical cell with a rotating disk electrode.

## B. Model Descriptions

The model presented here is for predicting the cyclic voltammetric behavior of the polypyrrole films doped with perchlorate. The modeling regions close to the rotating disk electrode, which are relevant to the development of the model equations, are schematically presented in Fig. 6.

The modeling regions consist of two main regions, two boundaries, and one inter-regional interface, and must be modeled simultaneously. These are the boundary interface between a platinum current collector and the polypyrrole electrode ( $y = 0$ ); the polypyrrole electrode region of width  $\delta_{pp}$ ; the inter-regional interface between the polypyrrole electrode and an electrolyte diffusion layer ( $y = y_{pp}$ ); the electrolyte diffusion layer of width  $\delta_{dl}$ ; and the boundary at a bulk electrolyte solution ( $y = y_{dl}$ ).

In all of the regions, the dependent variables are: the concentration of  $\text{Li}^+$  ( $c_+$ ), the concentration of  $\text{ClO}^-$  ( $c_-$ ), the local faradaic charge per unit volume ( $Q_f$ ), the potential of the solid phase ( $\Phi_1$ ), and the potential of the solution phase ( $\Phi_2$ ). Because the cyclic voltammetry controlled by sweeping potential at a constant scan rate, values for these unknowns depend on the perpendicular distance from the platinum current collector of the polypyrrole electrode ( $y$ ) and applied potential ( $E$ ), and they are obtained by solving the system of governing equations and assumptions for each region of the cell described next in detail.

### 1. Governing Equations – Polypyrrole Electrode Region

Polypyrrole electrode region has a porous structure and consists of a solid phase of polypyrrole and a solution phase of an organic electrolyte that penetrates the void spaces in the porous structure as shown in Fig. 6. It is assumed that the polypyrrole film and the void space are continuous to conduct electronically and



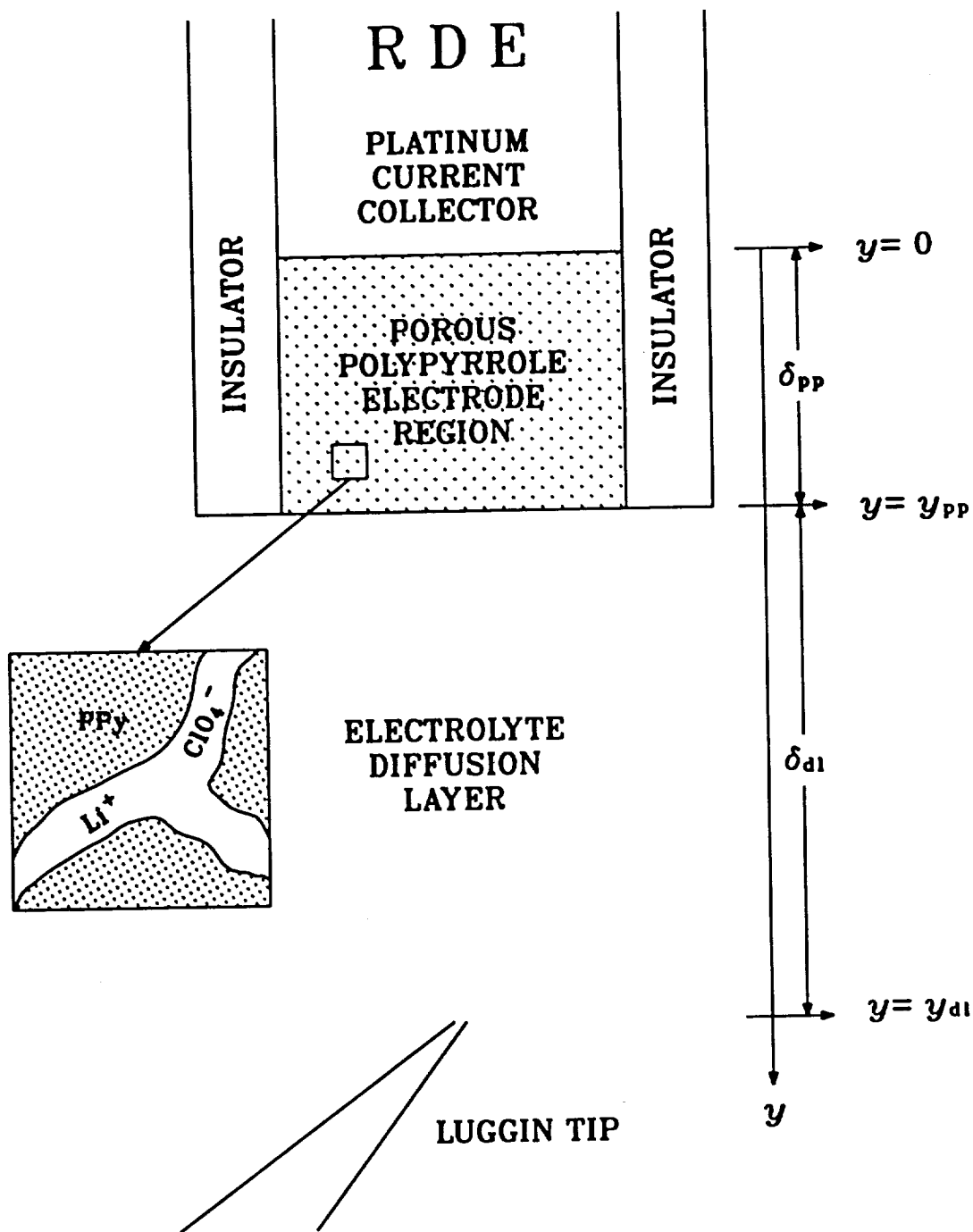


Fig. 6. A schematic diagram of modeling regions closed to the rotating disk electrode in the single-compartment electrochemical cell.

ionically (51). The solid polypyrrole has a non-homogeneous structure because of its impurities and structural defects (such as, crosslinking, reticulation, etc.). To account for the non-homogeneous nature of microscopic structure of polypyrrole, a porous electrode theory, where the details of the pore geometry are ignored and the entire porous structure is regarded as a single pseudo-homogeneous mixture, has been employed (129). That is, macroscopic properties and volume averaging technique are used to describe physically the porous material in terms of simple measurable parameters without regards to the actual geometrical details of the pore structure. An extensive discussion of volume averaging technique has been given by Dunning (130), Trainham (131), and Whitaker (132).

Two of macroscopic properties used here are a porosity ( $\epsilon_p$ ) and a tortuosity ( $\tau$ ). The porosity represents the void volume fraction occupied by the electrolyte within the volume element. The tortuosity represents structural defects of polymer chain. Here, the tortuosity is assumed to be related simply to the porosity as follows (133):

$$\tau = \epsilon_p^{-ex} \quad (21)$$

where  $ex$  is a proportional constant.

The properties of the electrolyte occupied the void spaces of the porous polypyrrole electrode (diffusivity, mobility, conductivity, etc.) must be modified to account for the porous nature of this region. The effective diffusivity ( $D_{i,p}$ ) and mobility ( $u_{i,p}$ ) of species  $i$  within the porous structure are related to the free stream diffusivity ( $D_i$ ) and mobility ( $u_i$ ) as follows (133):

$$D_{i,p} = D_i \epsilon_p^{1+ex} \quad (22)$$

$$u_{i,p} = u_i \epsilon_p^{1+ex} \quad (23)$$

The effective solution conductivity ( $\kappa_p$ ) within the porous structure is also related to the free stream solution conductivity ( $\kappa$ ) as follows:

$$\kappa_p = \kappa \epsilon_p^{1+ex} \quad (24)$$

and free stream solution conductivity ( $\kappa$ ) can be expressed as

$$\kappa = F^2 \sum_i z_i^2 u_i c_i \quad (25)$$

where  $c_i$  represents the concentration of species  $i$ .

#### Material Balance for Dissolved Species

The differential material balance equation in the solution phase is formulated for a dissolved species  $i$  in terms of average quantities as follows (129):

$$\frac{\partial(\epsilon_p c_i)}{\partial t} = -\nabla \cdot \mathbf{N}_{i,p} + R'_{1,i} \quad (26)$$

where  $c_i$  represents the concentration of species  $i$  per unit volume of electrolyte within the porous matrix,  $\epsilon_p c_i$  represents the average concentration per total unit volume including the solid polymer phase and the electrolyte that occupies the space within the matrix,  $\mathbf{N}_{i,p}$  represents the flux of species  $i$  within the porous region, and  $R'_{1,i}$  represents the consumption or production rate of species  $i$ .

The flux of species  $i$  within the porous polypyrrole electrode region ( $\mathbf{N}_{i,p}$ ) is due to migration in the electric field and diffusion in the concentration gradient, and is expressed as follows (129):

$$\mathbf{N}_{i,p} = -z_i u_{i,p} F c_i \nabla \Phi_2 - D_{i,p} \nabla c_i \quad (27)$$

where  $\Phi_2$  is the potential in the solution phase within the porous region. It is assumed that there is no convective flow within the porous region. That is, there

is no bulk flow through the pores and fresh feed must diffuse and migrate to the reactive sites within the porous region. This assumption seems reasonable as long as the thickness of the porous electrode ( $\delta_{pp}$ ) is much less than the electrolyte diffusion layer ( $\delta_{dl}$ ).

The consumption or production rate of species  $i$  within porous polypyrrole electrode region ( $R'_{1,i}$ ) is due to both the electrochemical reaction [1] and double layer charging. For oxidation, anions are doped to the polypyrrole structure by the electrochemical reaction [1]. Also, anions are attracted to the polypyrrole electrode surface for the double layer charging, while cations are repelled. For reduction, opposite effect hold. Anions are undoped from the polypyrrole structure by the electrochemical reaction [1] and are repelled because of double layer effects. Thus,  $R'_{1,i}$  becomes

$$R'_{1,i} = -\frac{s_{1,i}aj_1}{n_1F} \quad (28)$$

The term,  $aj_1$ , represents the local transfer current per unit volume (i.e., current passed per unit volume of electrode, A/cm<sup>3</sup>) and is discussed below in detail. No homogeneous and heterogeneous chemical reactions are considered here.

A one dimensional material balance equation for species  $i$  can be obtained by combining the normal component of Eqs. [26], [27], and [28] as follows:

$$\frac{\partial(\epsilon_p c_i)}{\partial t} = z_i F \frac{\partial}{\partial y} \left( u_{i,p} c_i \frac{\partial \Phi_2}{\partial y} \right) + \frac{\partial}{\partial y} \left( D_{i,p} \frac{\partial c_i}{\partial y} \right) - \frac{s_{1,i}aj_1}{n_1F} \quad (29)$$

### Charge Balance

The local charge accumulated within the porous polypyrrole electrode per unit volume,  $Q$ , is defined to be the sum of the local faradaic and capacitive charges per unit volume,  $Q_f$  and  $Q_c$ , as follows:

$$Q = Q_f + Q_c \quad (30)$$

The rate of accumulation of the local faradaic charge within the porous polypyrrole electrode per unit volume ( $Q_f$ ) is assumed to be related to the local faradaic transfer current per unit volume ( $aj_f$ ) as follows:

$$\frac{\partial Q_f}{\partial t} = aj_f \quad (31)$$

Combining Eqs. [15] and [31] shows that

$$\frac{\partial Q_f}{\partial t} = ai_{o1,ref} \left\{ \left( 1 - \theta \right) \left( \frac{c_-}{c_{-,ref}} \right) \exp \left( \frac{\alpha_{a1} F}{RT} \eta_1 \right) - \theta \exp \left( \frac{-\alpha_{c1} F}{RT} \eta_1 \right) \right\} \quad (32)$$

The flow of current through a porous polypyrrole electrode results in charging of the double layer within the pores of the polypyrrole electrode in a manner consistent with that proposed by Feldberg (79). That is, the amount of local capacitive charge that goes to charging the double layers within the pores of the polypyrrole electrode,  $Q_c$ , is related to the amount of the local faradaic charge added to the polymer electrode by the electrochemical reaction:

$$Q_c = a^* (\eta_1 - \eta_{1,pzc}) Q_f \quad (33)$$

where  $a^*$  is a double layer constant assumed to be independent of potential and  $\eta_{1,pzc}$  is the total overpotential across the double layer within polypyrrole electrode at the point of zero charge (PZC) which is given by

$$\eta_{1,pzc} = \left\{ (\Phi_1 - \Phi_{ref}) - (\Phi_2 - \Phi_{ref}) - U_{1,ref} \right\}_{pzc} \quad (34)$$

The local capacitive transfer current per unit volume,  $aj_c$ , associated with the charging of the double layer is defined as follows:

$$aj_c = \frac{\partial Q_c}{\partial t} \quad (35)$$

Differentiating Eq. [33] yields

$$aj_c = a^* \left( Q_f \frac{\partial \eta_1}{\partial t} + (\eta_1 - \eta_{1,pzc}) aj_f \right) \quad (36)$$

with the assumption that  $\Phi_{ref} = (\Phi_{ref})_{pzc}$ .

### Transfer Current Balance

The local transfer current per unit volume,  $aj_1$ , is consists of two terms (41,79,80):

$$aj_1 = aj_f + aj_c \quad (37)$$

and is defined by the current transferred from the solution phase to the solid phase as follows:

$$aj_1 = \nabla \cdot i_2 = -\nabla \cdot i_1 \quad (38)$$

It is assumed that the superficial current density in the solid phase ( $i_1$ ) is due to the movement of electrons and is governed by Ohm's law (122)

$$i_1 = -\sigma_p \frac{\partial \Phi_1}{\partial y} \quad (39)$$

and the superficial current density in the solution phase ( $i_2$ ) is due to the movement of charged species (122)

$$i_2 = F \sum_i z_i N_{i,p} \quad (40)$$

Substituting the  $y$  component of Eq. [27] into Eq. [40] yields

$$i_2 = -\kappa_p \frac{\partial \Phi_2}{\partial y} - F \sum_i z_i D_{i,p} \frac{\partial c_i}{\partial y} \quad (41)$$

The second term on the right in Eq. [41] represents the concentration potential; this term will disappear if the ionic diffusion coefficients are all the same, which is not the case here.

Combining Eqs. [38], [39], and [41] yields the one dimensional local transfer current balance within the porous polypyrrole electrode region:

$$\begin{aligned} aj_1 &= \frac{\partial}{\partial y} \left( \sigma_p \frac{\partial \Phi_1}{\partial y} \right) \\ &= -\frac{\partial}{\partial y} \left( \kappa_p \frac{\partial \Phi_2}{\partial y} \right) - F \sum_i z_i \frac{\partial}{\partial y} \left( D_{i,p} \frac{\partial c_i}{\partial y} \right) \end{aligned} \quad (42)$$

### Electroneutrality

Assuming that the double layer at the pore wall is extremely thin relative to the pore dimension, the electrolyte within the pores can be considered electronically neutral. Thus, the electroneutrality condition can be applied as follows:

$$\sum_i z_i c_i = 0 \quad (43)$$

### 2. Governing Equations – Solution Diffusion Layer

Mass transfer in the diffusion layer is governed by the following differential material balance equation for species  $i$ :

$$\frac{\partial c_i}{\partial t} = -\nabla \cdot \mathbf{N}_i \quad (44)$$

and  $\mathbf{N}_i$ , the flux of species  $i$ , is due to migration in the electric field, diffusion in the concentration gradient, and convection in the flow field

$$\mathbf{N}_i = -z_i u_i F c_i \nabla \Phi_2 - D_i \nabla c_i + c_i \mathbf{v} \quad (45)$$

where  $\mathbf{v}$  represents electrolyte velocity vector. Only the axial component of the flux is considered in the model and the velocity component in that direction depends only on the normal distance from the polypyrrole electrode surface ( $y = y_{pp}$ ) with the no-slip condition (134)

$$v_y = -a' \Omega \sqrt{\frac{\Omega}{\nu}} (y - \delta_{pp})^2 \quad (46)$$

where  $a'$  represents a rotating disk electrode constant,  $\Omega$  represents a disk rotation speed, and  $\nu$  represents a kinematic viscosity. Combining Eqs. [44], [45], and [46]

yields the one dimensional material balance for species  $i$  within the electrolyte diffusion layer (122):

$$\frac{\partial c_i}{\partial t} = \frac{z_i D_i F}{RT} \frac{\partial}{\partial y} \left( c_i \frac{\partial \Phi_2}{\partial y} \right) + D_i \frac{\partial^2 c_i}{\partial y^2} + a' \Omega \sqrt{\frac{\Omega}{\nu}} (y - \delta_{pp})^2 \frac{\partial c_i}{\partial y} \quad (47)$$

Since the solid electroactive material does not exist in the diffusion layer, the local faradaic charge ( $Q_f$ ) and the solid potential ( $\Phi_1$ ) are dummy variables treated as constants and are set arbitrarily equal to zero

$$Q_f = 0 \quad (48)$$

$$\Phi_1 = 0 \quad (49)$$

It is assumed that the electrolyte in the diffusion layer is electrically neutral, so that the solution potential profiles obey the condition of electroneutrality, Eq. [43].

### 3. Boundary and Interface Conditions

To complete the system of equations for the model, the boundary conditions at each end of the cell and inter-regional interface must be specified for the dependent variables:  $c_+$ ,  $c_-$ ,  $Q_f$ ,  $\Phi_1$ , and  $\Phi_2$ . Boundary and interface conditions for these dependent variables are specified in the order of the platinum current collector to the bulk solution.

The polypyrrole electrode is bounded by a platinum current collector on one face ( $y = 0$ ) and by the electrolyte diffusion layer on the other ( $y = y_{pp}$ ). At the current collector/polypyrrole electrode interface ( $y = 0$ ), the net normal component of the flux of each species  $i$  towards or away from the electrode is assumed to be equal to the rate of consumption or production by the



electrochemical reaction [1] and double layer charging ( $R'_{1,i}$ ). Thus

$$-z_i u_{i,p} F c_i \frac{\partial \Phi_2}{\partial y} - D_{i,p} \frac{\partial c_i}{\partial y} = -\frac{s_{1,i} a j_1}{n_1 F} \quad (50)$$

The rate of accumulation of the local faradaic charge within the polypyrrole electrode per unit volume ( $Q_f$ ) is obtained from the local faradaic transfer current per unit volume ( $a j_f$ ) as shown by Eq. [32]. The solid potential at this point expressed as a difference between the applied potential ( $E$ ) and reference electrode potential ( $\Phi_{ref}$ )

$$\Phi_1 = E + \Phi_{ref} \quad (51)$$

It is assumed that no potential drop exists between the lead of reference electrode and the solution in the luggin tip, which is a reasonable because no appreciable current flows through the reference electrode. The applied potential ( $E$ ) is varied between positive and negative potential limits under the constant scan rate ( $v_s$ ) by potentiostat as follows:

$$\begin{aligned} E &= E_{neg} + v_s t && \text{(For Anodic Scan)} \\ &= E_{pos} - v_s t && \text{(For Cathodic Scan)} \end{aligned} \quad (52)$$

At this point, because all of the current leaves the cell *via* the current collector, the superficial current density in the solution phase ( $i_2$ ) can be set equal to zero, so that

$$-\kappa_p \frac{\partial \Phi_2}{\partial y} - F \sum_i z_i D_{i,p} \frac{\partial c_i}{\partial y} = 0 \quad (53)$$

At the polypyrrole electrode/electrolyte diffusion layer interface ( $y = y_{pp}$ ), the flux of each species  $i$  across the two regions must be continuous, which can be written as follows:

$$-z_i u_{i,p} F c_i \frac{\partial \Phi_2}{\partial y} - D_{i,p} \frac{\partial c_i}{\partial y} = -z_i u_i F c_i \frac{\partial \Phi_2}{\partial y} - D_i \frac{\partial c_i}{\partial y} \quad (54)$$

Because the solid electrode phase ends at this point and all of the current is in the solution phase, the gradient of the local faradaic charge ( $Q_f$ ) and the solid potential ( $\Phi_1$ ) can be set equal to zero

$$\left. \frac{\partial Q_f}{\partial y} \right|_{y_{pp}} = 0 \quad (55)$$

$$\left. \frac{\partial \Phi_1}{\partial y} \right|_{y_{pp}} = 0 \quad (56)$$

The superficial current density in the solution phase ( $i_2$ ) must be also continuous across the two regions, so that

$$-\kappa_p \frac{\partial \Phi_2}{\partial y} - F \sum_i z_i D_{i,p} \frac{\partial c_i}{\partial y} = -\kappa \frac{\partial \Phi_2}{\partial y} - F \sum_i z_i D_i \frac{\partial c_i}{\partial y} \quad (57)$$

In the bulk solution ( $y = y_{dl}$ ), the concentration of each species  $i$  is set equal to the bulk concentration ( $c_{i,ref}$ ), which is maintained constant by excess electrolyte and rapid mixing

$$c_i = c_{i,ref} \quad (58)$$

and the solution potential is set equal to that of the reference electrode ( $\Phi_{ref}$ )

$$\Phi_2 = \Phi_{ref} \quad (59)$$

Note that this requires assuming that no potential drop exists between the reference electrode lead and the solution in the luggin tip, which is a reasonable assumption since no appreciable current flows through the reference electrode. Since no electroactive solid material exist at this point, the local faradaic charge ( $Q_f$ ) and the solid potential ( $\Phi_1$ ) are dummy variables treated as constants and are set arbitrarily equal to zero.

#### 4. Initial Conditions

Initial conditions are necessary for the variables which depend explicitly on time. For convenience, it is assumed that the polypyrrole electrode is in its fully neutral state and is ready to be oxidized. Consequently, the local faradaic charge per unit volume ( $Q_f$ ) is initially set equal to  $Q_{f,red}$ , a minimal charge state, throughout the porous polypyrrole electrode region. Therefore, porosity ( $\epsilon_p$ ) and conductivity ( $\sigma_p$ ) of the polypyrrole electrode are initially set equal to  $\epsilon_{red}$  and  $\sigma_{red}$ , values at this neutral state, throughout the porous polypyrrole electrode region. In the diffusion layer, these variables are treated as dummy variables and are arbitrarily set equal to zero.

The concentration of each species  $i$  throughout the cell is set equal to its bulk concentration:

$$c_i = c_{i,ref} \quad (60)$$

The conductivity of the electrolyte ( $\kappa$ ) can be obtained by combining Eqs. [25] and [60]. The other dependent variables ( $\Phi_1$  and  $\Phi_2$ ) do not require initial conditions and are arbitrarily set equal to zero at  $t = 0$  for all  $y$ .

#### 5. Solution Method

The governing equations and boundary conditions for the determination of the quantities  $c_+$ ,  $c_-$ ,  $Q_f$ ,  $\Phi_1$ , and  $\Phi_2$  in all of the regions of the cell have been summarized in Table IX. It is noted that the numbers in the tables refer to the equation numbers in the text. The system of equations are put into finite difference form and solved as function of time ( $t$ ) and position ( $y$ ) by using a numerical technique referred to as Newman's pentadiagonal block matrix equation solver (135) and implicit stepping (136).

Table IX. System of equations for cyclic voltammetry of polypyrrole.

## A. Governing equations.

Variables	Polypyrrole Electrode Region	Electrolyte Diffusion Layer
$c_+$	29	47
$c_-$	29	47
$Q_f$	32	48
$\Phi_1$	42	49
$\Phi_2$	43	43

## B. Boundary and interface conditions.

Variables	$y = 0$	$y = y_{pp}$	$y = y_{dl}$
$c_+$	50	54	58
$c_-$	50	54	58
$Q_f$	32	55	48
$\Phi_1$	51	56	49
$\Phi_2$	53	57	59

The whole cell is divided into  $NJ$  mesh points with  $J = 1$  designated to be the boundary of the platinum current collector and polypyrrole electrode,  $J = NJ1$  designated to be the inter-regional interface of the polypyrrole electrode and electrolyte diffusion layer, and  $J = NJ$  to be the bulk solution. Mesh point spacings are different in different regions because of the difference in the thickness of each region and the number of nodal points used.

Second order finite-difference approximations of the derivatives for an internal mesh point can be written as

$$\frac{\partial^2 C_k(J)}{\partial y^2} \simeq \frac{C_k(J-1) - 2C_k(J) + C_k(J+1)}{(\Delta y)^2} \quad (61)$$

$$\frac{\partial C_k(J)}{\partial y} \simeq \frac{-C_k(J-1) + C_k(J+1)}{2(\Delta y)} \quad (62)$$

and for a boundary node as

$$\frac{\partial C_k(J)}{\partial y} \simeq \frac{-3C_k(J) + 4C_k(J+1) - C_k(J+2)}{2(\Delta y)} \quad (63)$$

$$\frac{\partial C_k(J)}{\partial y} \simeq \frac{C_k(J-2) - 4C_k(J-1) + 3C_k(J)}{2(\Delta y)} \quad (64)$$

where  $\Delta y$  denotes the distance between node points, and  $C_k(J)$  represents the  $k^{\text{th}}$  unknown at node  $J$ .

The accuracy of the finite difference approximations of the above derivatives is  $(\Delta y)^2$ . Equation [63] (a forward difference form) is used at  $J = 1$ ; and Eq. [64] (a backward difference form) is used at  $J = NJ$ . For the inter-regional boundaries, Eq. [63] is used on the upper region (higher region number) side, and Eq. [64] is used on the lower region side. Note that to maintain  $(\Delta y)^2$  accuracy five node points, pentadiagonal block matrix equation solver are used at an inter-regional boundary node point (135).

For the time derivatives, implicit stepping is used (136):

$$\frac{\partial C_k(J)}{\partial t} \simeq \frac{C_k(J)|_{t+\Delta t} - C_k(J)|_t}{\Delta t} \quad (65)$$

where  $C_k(J)|_t$  refers to the known value obtained from the previous time step, and  $C_k(J)|_{t+\Delta t}$  represents the unknown value to be determined at  $t + \Delta t$ .

### C. Results and Discussion

The values used for the operating conditions in the cyclic voltammograms are given in Table X. The applied potential ( $E$ ) sweeps between  $-0.8$  V and  $+0.8$  V under the constant scan rates ( $v_s$ ) of 10 and 20 mV/sec at room temperature. The

scan rate and the potential interval are selected to obtain a complete oxidation and reduction of the polymer within the stability range of the electrolyte. The rotating speed of disk electrode ( $\Omega$ ) is arbitrarily chosen as 3600 rpm. A 1  $\mu\text{m}$  thick polypyrrole electrode is used in this study because a high doping level and a high efficiency have been observed for this thickness (107). All the potentials are referred to the SCE. The resulting anodic (oxidation) and cathodic (reduction) current densities are specified as being positive and negative because of the chosen coordinate system, respectively.

### 1. Experimental Results

Experimental cyclic voltammograms for a 1  $\mu\text{m}$  thick polypyrrole film in 1M  $\text{LiClO}_4$ -PC electrolyte at scan rates of 10 and 20 mV/sec are presented in Fig. 7. Two main considerations can be derived by the analysis of these cyclic voltammograms; well defined doping-undoping behaviors and large capacitance effects.

The current density is well defined as positive and negative for doping and

Table X. Operating conditions used for cyclic voltammograms of polypyrrole.

Operating Temperature ( $T$ )	298.15 K
Negative Potential Limit ( $E_{\text{neg}}$ )	-0.8 V (vs. SCE)
Positive Potential Limit ( $E_{\text{pos}}$ )	+0.8 V (vs. SCE)
Potential Scan Rate ( $v_s$ )	10 & 20 mV/sec
Disk Rotation Velocity ( $\Omega$ )	377 rad/sec
Reference Electrode Potential ( $\Phi_{\text{ref}}$ )	0.0 V (vs. SCE)
Geometric Electrode Surface Area ( $A$ )	1 $\text{cm}^2$
Thickness of Polypyrrole Film ( $\delta_{\text{pp}}$ )	1 $\mu\text{m}$
Thickness of Electrolyte Diffusion Layer ( $\delta_{\text{dl}}$ )	0.01 cm
Reference Concentration of $\text{Li}^+$ ( $c_{+, \text{ref}}$ )	0.001 mol/ $\text{cm}^3$
Reference Concentration of $\text{ClO}_4^-$ ( $c_{-, \text{ref}}$ )	0.001 mol/ $\text{cm}^3$

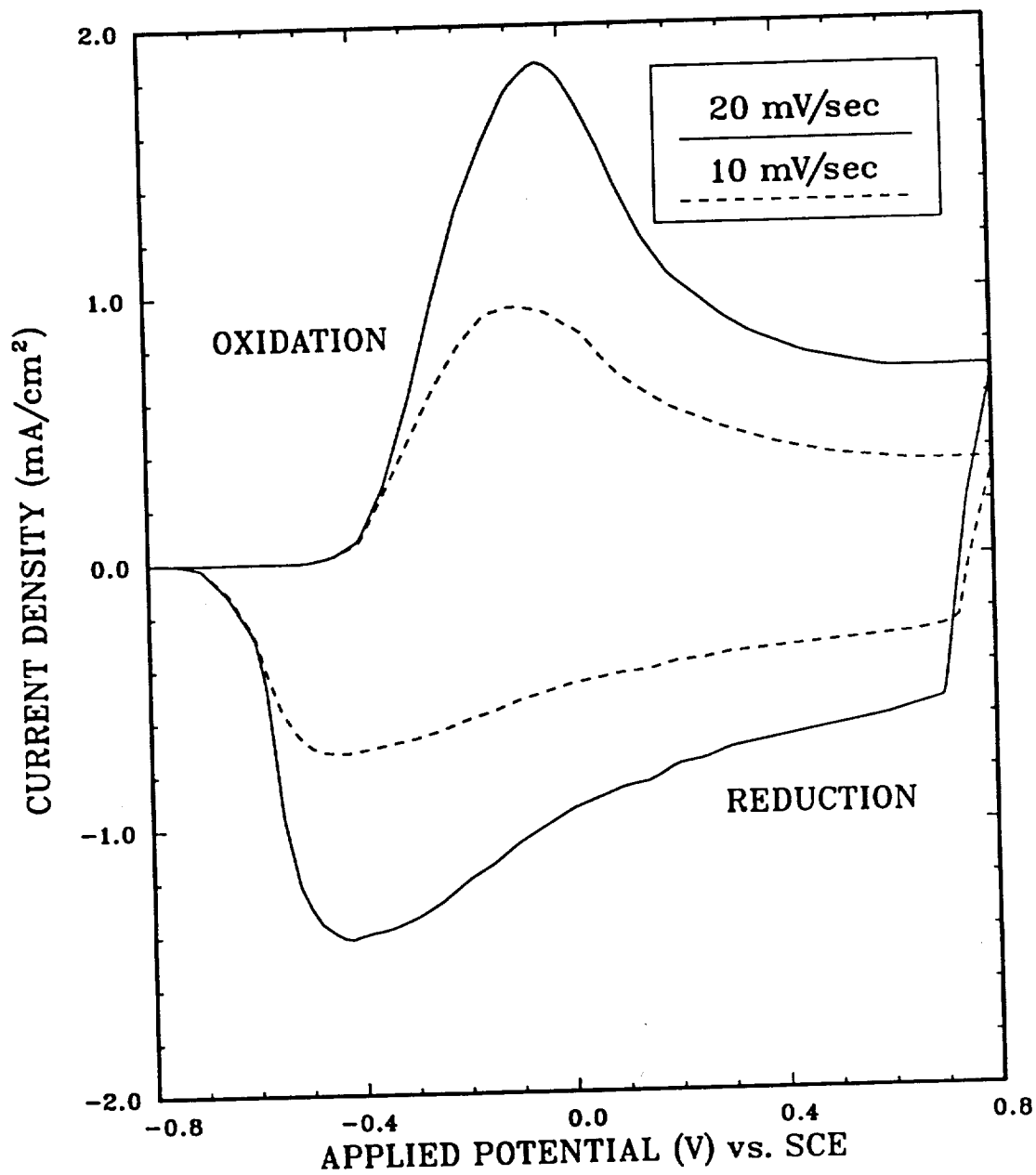


Fig. 7. Experimental cyclic voltammograms for a 1  $\mu\text{m}$  polypyrrole film in 1M  $\text{LiClO}_4\text{-PC}$  electrolyte at scan rates of 10 and 20 mV/sec.

undoping processes, and immediately changes sign when the scan is reversed. The electrochromic properties of polypyrrole are clearly demonstrated showing that polypyrrole is actually reduced and oxidized; brown-black at doped state and light yellow at undoped state. The cyclic voltammograms are not symmetrical but quasi-reversible. The oxidative and reductive charges in each cycle are the equivalent and are independent of scan rate. The cathodic peaks are significantly broader than the anodic peaks. The peak height is proportional to the scan rate as is expected for a reversible surface process (97). Accordingly, it can be suggested that the electrochemical behavior in cyclic voltammetry can be explained in relation to the diffusion of counterion. The electrochemical characteristics of the  $1\mu\text{m}$  polypyrrole film in the  $1\text{M LiClO}_4\text{-PC}$  electrolyte obtained from these experimental cyclic voltammograms are summarized in Table XI.

A large capacitive background current density ( $i_c$ ) in the potential region between  $+0.2$  and  $+0.8$  V vs. SCE (where the film is not oxidized or reduced) observed and is proportional to the scan rate. The related capacitance,  $C_1$ , may be obtained by simple calculation based on the expression (76,109)

$$C_1 = \frac{i_c}{v_s} \quad (66)$$

Table XI. Electrochemical characteristics of the  $1\mu\text{m}$  polypyrrole film in the  $1\text{M LiClO}_4\text{-PC}$  electrolyte.

Scan Rate ( $v_s$ )	10 mV/sec	20 mV/sec
Anodic Peak Potential ( $E_{pa}$ )	-0.1 V	-0.04 V
Cathodic Peak Potential ( $E_{pc}$ )	-0.43 V	-0.45 V
Anodic Peak Current Density ( $i_{pa}$ )	+0.95 mA	+1.86 mA
Cathodic Peak Current Density ( $i_{pc}$ )	-0.72 mA	-1.42 mA
Anodic Charge Density ( $Q_{ca}$ )	+56.3 mC/cm <sup>2</sup>	+56.3 mC/cm <sup>2</sup>
Cathodic Charge Density ( $Q_{cc}$ )	-53.8 mC/cm <sup>2</sup>	-53.8 mC/cm <sup>2</sup>



The related capacitance of fully oxidized polypyrrole from these experimental cyclic voltammogram has a value of about  $35 \text{ mF/cm}^2$  (compared to the usual  $\mu\text{F/cm}^2$  values for the bare electrodes), which is similar to values obtained by other laboratory (76,109). The origin of such large capacitance in polymer films has been discussed in detail by Tanguy *et al.* (46) and Mermilliod *et al.* (137). The behavior observed is similar to that of a capacitor with very high capacitance and is due to the highly porous structure of polypyrrole films (41).

The polypyrrole film is very stable between  $-0.8 \text{ V}$  and  $+0.8 \text{ V}$  vs. SCE. It is possible to obtain more than 200 cycles without significant loss of the coulombic capacity of the electrode. This indicates that the electroactivity is not destroyed and that counterion insertion and extraction is quite reversible. Extending negative limit had little effect on the cyclic voltammograms characteristics. However, when the upper limit is taken more positive, there is a progressive loss of capacity and film deterioration takes place after a few cycles.

## 2. Simulated Results

The simulated cyclic voltammograms for the polypyrrole film can be obtained by using the model developed above and fixed parameter values given in Tables IV, V, VII, X, and XII as shown in Fig. 8. The estimated values of parameters in Table XII are obtained by comparison between experimental and simulated cyclic voltammograms and are discussed in the later section.

The current density relative to the projected electrode area,  $i$ , are obtained by integrating the local transfer current per unit volume ( $aj_1$ ) over the porous polypyrrole electrode region:

$$i = \int_{y=0}^{y=y_{pp}} aj_1 dy \quad (67)$$

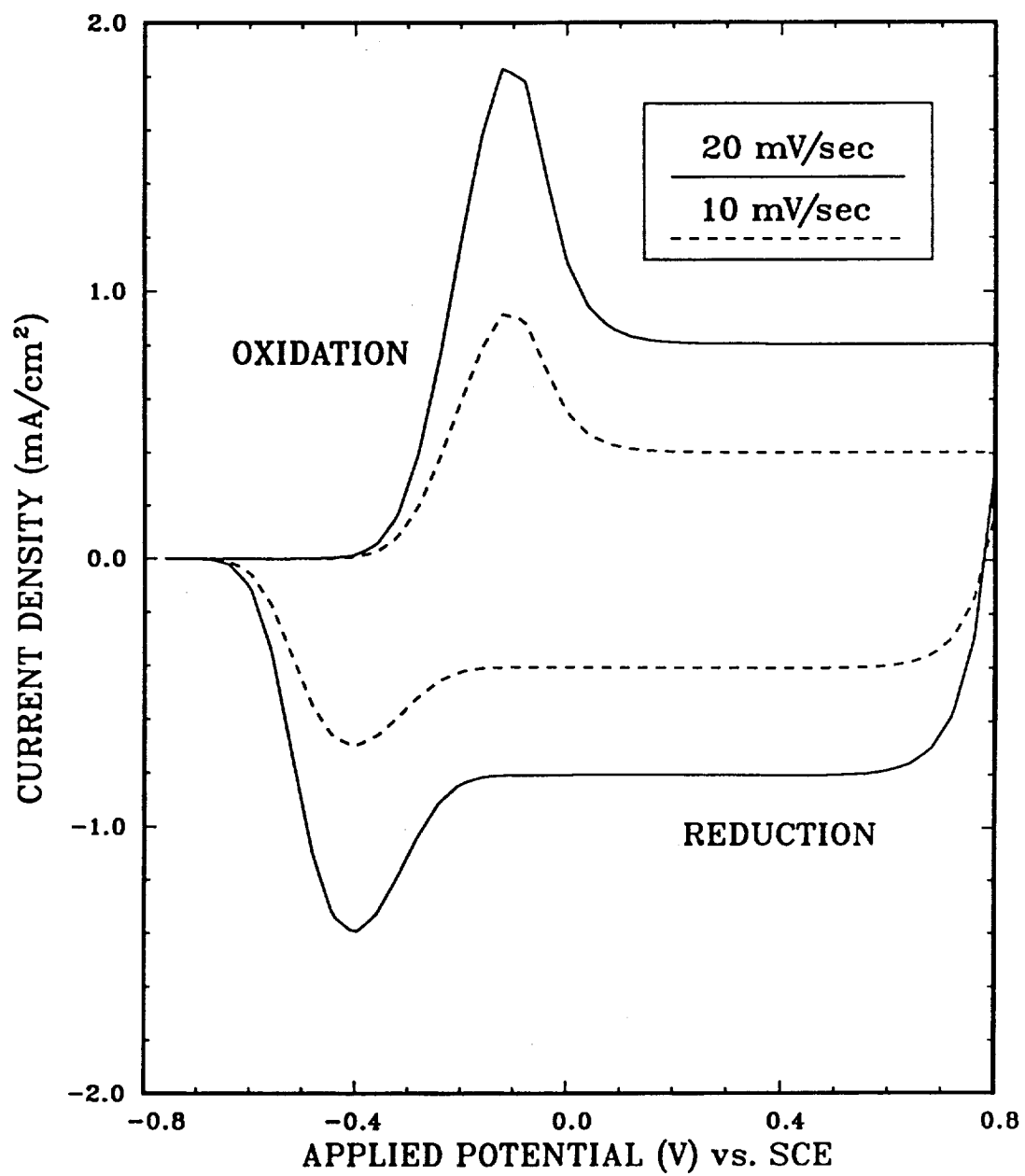


Fig. 8. Simulated cyclic voltammograms for a 1  $\mu\text{m}$  polypyrrole film in 1M  $\text{LiClO}_4\text{-PC}$  electrolyte at scan rates of 10 and 20 mV/sec.

It is noted that the value of the current density should be equal to the superficial current density in the solid phase ( $i_1$ ) at the current collector/polypyrrole electrode interface ( $y = 0$ )

$$i = i_1 \Big|_{y=0} \quad (68)$$

This is because all of the current leaves the cell *via* the current collector.

As discussed earlier, the current density in the cyclic voltammogram of the polypyrrole film consists of two distinctive components, faradaic current density caused by the electrochemical reaction [1] and capacitive current density caused by the double layer within the porous polypyrrole film,  $i_f$  and  $i_c$ . These are obtained by integrating the local faradaic and capacitive transfer currents per unit volume ( $aj_f$  and  $aj_c$ ) over the porous polypyrrole electrode region as shown in Eq. [67]. Typical cyclic voltammogram and its components of 1  $\mu\text{m}$  polypyrrole film at a scan rate of 20 mV/sec are shown in Fig. 9 as a function of the applied potential.

At potentials negative of  $-0.4$  V, polypyrrole electrode is in its fully neutral state. For anodic sweep of potential (increasing potential), neutral polypyrrole starts to converge to oxidized state at potentials positive of  $-0.4$  V. The electrochemical oxidation yields the consumption of both faradaic and capacitive

Table XII. Fixed parameter values used for polypyrrole.

Faradaic Charge of Neutral Polypyrrole ( $Q_{f,\text{red}}$ )	$1.0 \times 10^{-5} \text{ C/cm}^3$
Faradaic Charge of Oxidized Polypyrrole ( $Q_{f,\text{oxd}}$ )	$120.0 \text{ C/cm}^3$ †
Porosity of Neutral Polypyrrole ( $\epsilon_{\text{red}}$ )	$1.0 \times 10^{-2}$
Porosity of Oxidized Polypyrrole ( $\epsilon_{\text{oxd}}$ )	$1.0 \times 10^{-3}$
Double Layer Constant ( $a^*$ )	$2.8 / \text{V}^\dagger$
Zero Charge Potential ( $\eta_{1,\text{pzc}}$ )	$-0.3 \text{ V (vs. SCE)}^\dagger$
Exponent on Porosity Term ( $ex$ )	$0.5^\dagger$

† Estimated values

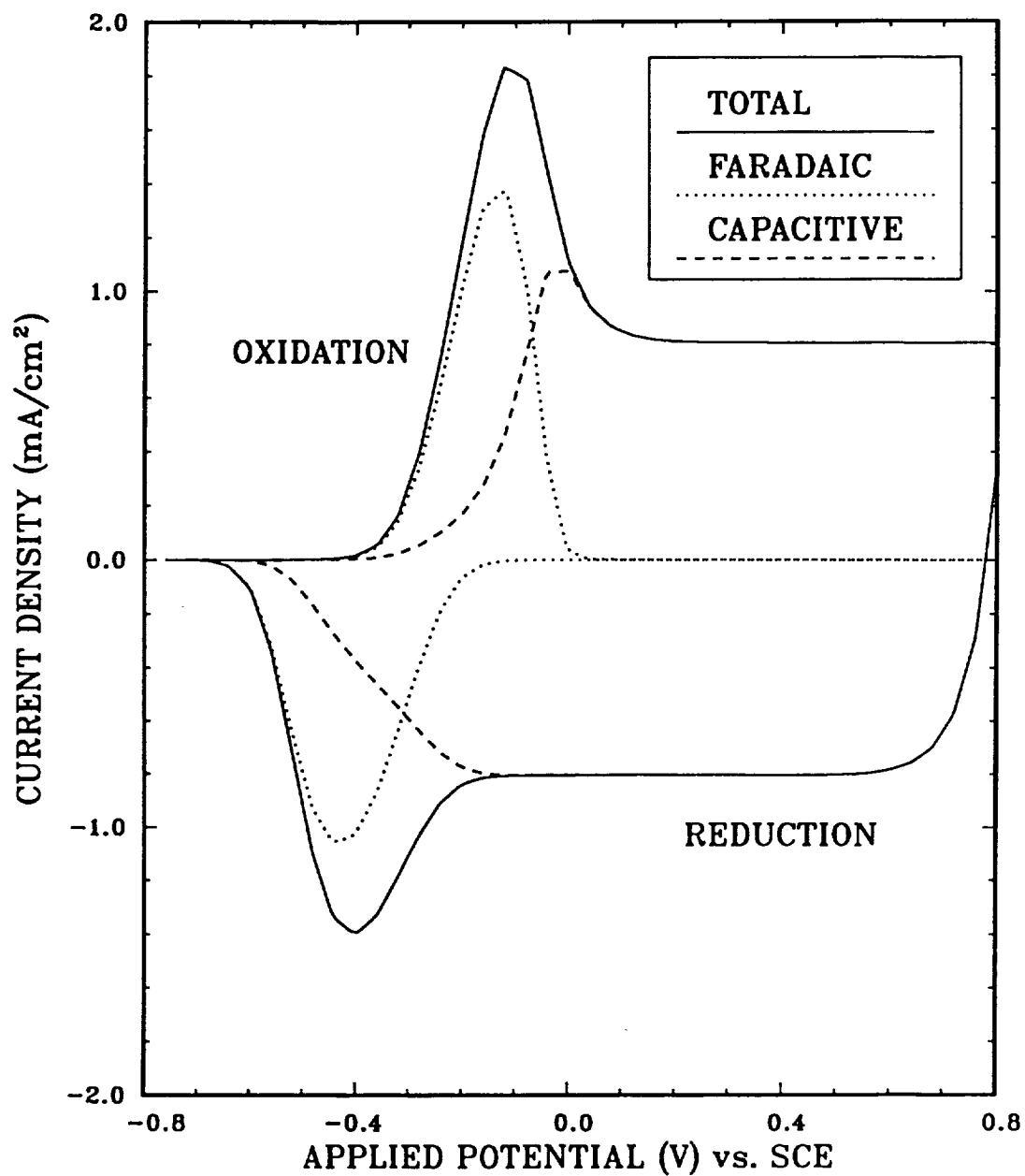


Fig. 9. Decomposition of a cyclic voltammogram into its two components, the faradaic and capacitive current densities, at a scan rate of 20 mV/sec.

charges within polypyrrole film. The faradaic current density ( $i_f$ ) initially increases with time because of the increasing driving force (applied potential), then decreases because of the limited electroactive area (neutral polypyrrole sites) and the concentration of counterion within the polymer film as the polypyrrole electrode is significantly oxidized. However, the capacitive current density ( $i_c$ ) increases continuously with time until the polypyrrole electrode is fully oxidized. At potentials positive of +0.2 V, the oxidation reaction is complete and entire polypyrrole electrode is in its fully oxidized state. That is, the current density is entirely dominated by the double layer effects because no more oxidation of the polypyrrole can occur. The related capacitance ( $C_1$ ) of fully oxidized polypyrrole from these simulated cyclic voltammogram has a value of about 38 mF/cm<sup>2</sup> and is well matched with that obtained from experiment.

When the scan is reversed to cathodic direction (decreasing potential), the pure capacitive current density immediately changed sign. Oxidized polypyrrole start to converge to neutral state at potentials negative of +0.2 V, and yield decreasing faradaic and capacitive charges. At a potential -0.6 V, entire polypyrrole electrode is again in its fully neutral state.

#### Dependent Variables Profiles

The dynamic profiles of the dependent variables in the porous polypyrrole electrode region at a scan rate of 20 mV/sec are shown in Figs. 10 through 12 as function of applied potential ( $E$ ) and position ( $y$ ). In the position coordinate,  $y = 0$  represents the platinum current collector side and  $y = 1$  represents the electrolyte diffusion layer side as shown in Fig. 6.

The dynamic concentration profiles of the anion ( $\text{ClO}_4^-$ ) within the porous polypyrrole electrode region at a scan rate of 20 mV/sec are shown in Fig. 10.

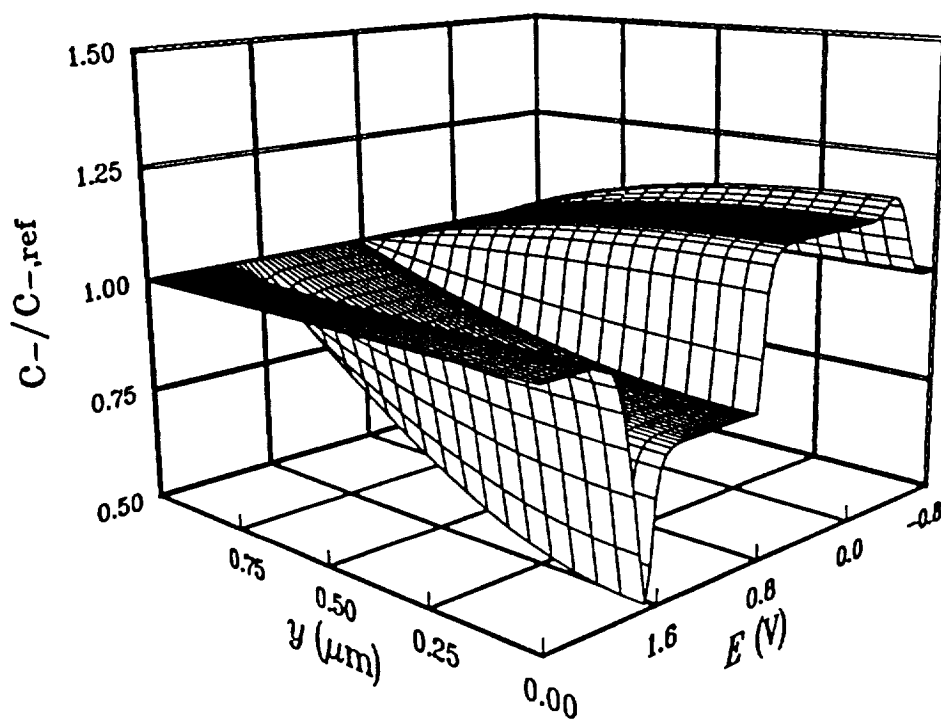


Fig. 10. Dimensionless concentration profiles of the anion ( $\text{ClO}_4^-$ ) within the polypyrrole electrode region at a scan rate of 20 mV/sec.

The concentration is made dimensionless relative to its reference concentrations ( $c_{-,ref}$ ). It is noted that the concentration profiles of the cation ( $Li^+$ ) have similar distributions because of the electroneutrality.

Initially, the concentration of the anion ( $ClO_4^-$ ) is uniform throughout the cell at reference concentration ( $c_{-,ref}$ ). For anodic scan, anions are consumed at the porous polypyrrole electrode region because of oxidation of polypyrrole and increase of double layer charge. The reacting species ( $ClO_4^-$ ) is transported from the bulk to the porous electrode layer where it diffuses and migrates to reactive sites within the porous layer. After polypyrrole has been fully oxidized, the concentration distribution within the porous polypyrrole electrode region bounced back to certain equilibrium state. This is because no more oxidation of polypyrrole occurs and counterions are consumed by double layer charge only.

For cathodic scan, the oxidized polypyrrole sites are reduced and the opposite phenomena are occurred. Anions ( $ClO_4^-$ ) are produced within the porous polypyrrole electrode region because of reduction of polypyrrole and decrease of double layer charge. The reacting species ( $ClO_4^-$ ) is transported from the porous electrode region to the bulk. Since the effective diffusivities of  $Li^+$  and  $ClO_4^-$  within the porous layer are much smaller than the free stream diffusivity of these species, the concentration gradients within the porous region must be larger to make up for the slower movement of the ions.

Figure 11 shows the profiles of the faradaic charge per unit volume consumed within polypyrrole electrode due to the electrochemical reaction [1] at a sweep rate of 20 mV/sec. The faradaic charge per unit volume is made dimensionless by using the maximum faradaic charge value ( $Q_{f,oxd}$ ) as the reference point.

Initially, polypyrrole electrode is in its fully neutral state ( $Q_f = Q_{f,red}$ ) and

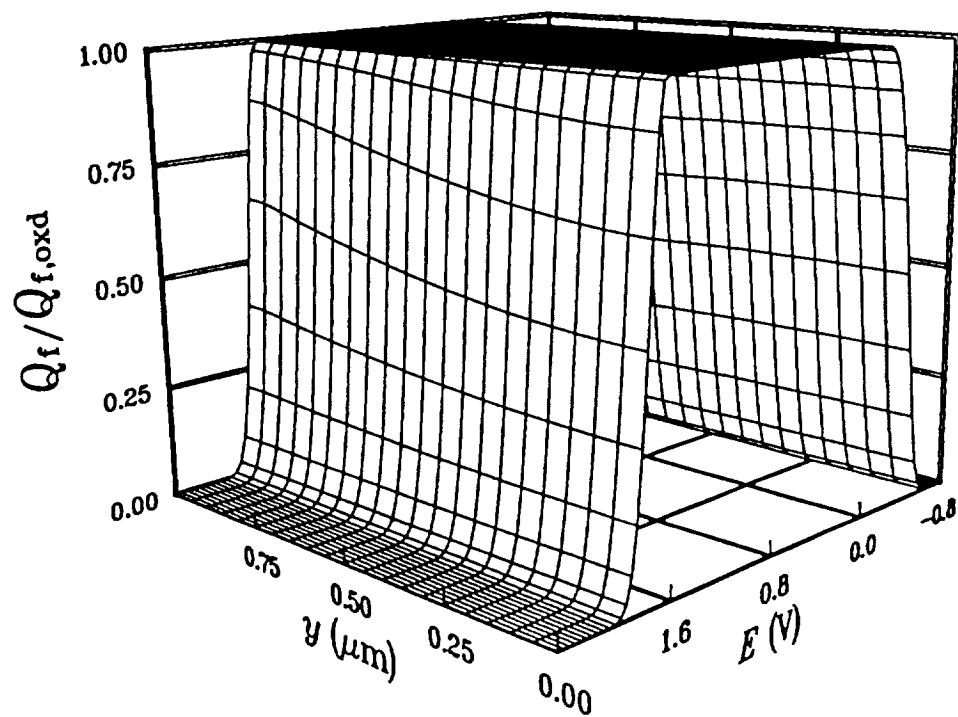


Fig. 11. Dimensionless faradaic charge profiles within the polypyrrole electrode region at a scan rate of 20 mV/sec.



is ready to be oxidized. For anodic scan, the faradaic charge is accumulated throughout the polypyrrole electrode region by the electrochemical reaction [1]. The faradaic charge accumulation in the outer layer of the polypyrrole electrode (electrolyte diffusion layer side) is faster because of the concentration gradient effect within polypyrrole electrode as shown in Fig. 11. After polypyrrole has been fully oxidized, the faradaic charge distribution becomes uniform at  $Q_f = Q_{f,oxd}$ . During reduction, the faradaic charge is withdrawn slower in the inner layer of the polypyrrole electrode (current collector side) because of the diffusion limitation. Note that charge accumulates rapidly throughout the entire electrode.

The electrochemical properties (such as, porosity, conductivity, diffusivity, mobility, etc.) have the similar distribution throughout the polypyrrole electrode region because of the assumption that these properties are proportional to the faradaic charge per unit volume consumed within polypyrrole electrode (See Eqs. [13], [14], [22], [23], and [24]).

Figure 12 shows the distribution of <sup>the</sup> potential difference between solid and solution phases, driving force for the electrochemical reaction [1] and the double layer charge, within the porous polypyrrole electrode region at a sweep rate of 20 mV/sec. For convenience, the potential difference is represented by  $\Phi_1 - \Phi_2 - E$ .

The potential difference increases with time indicating that the electrochemical reaction must proceed at a faster rate to compensate for decreasing available active surface area and reactive species in solution phase. It shows that the potential difference at the inner layer (current collector side) is higher because of diffusion limitation of counterion. The positive and negative values lead cathodic (reduction) and anodic (oxidation) reactions, respectively.

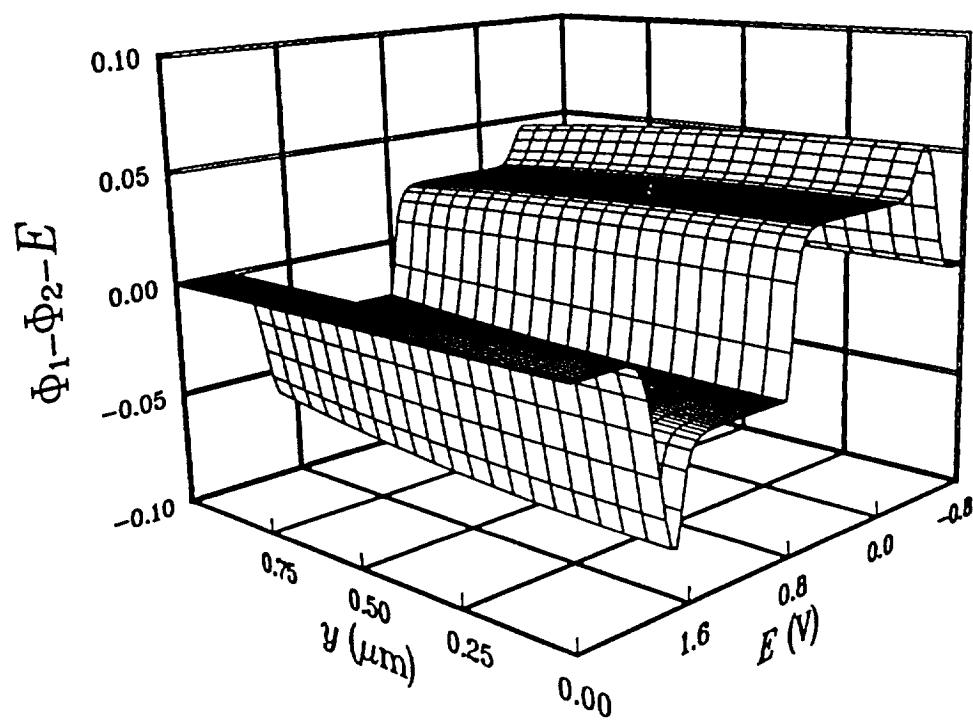


Fig. 12. Potential difference between solid and solution phases within the polypyrrole electrode region at a scan rate of 20 mV/sec.

### 3. Sensitivity Analysis

Since the results predicted by the model depend on the independent parameters describing the physical and electrochemical characteristics of system, it is necessary to examine the sensitivity of the model predictions on these parameters and identify parameters which can be discarded from the further parametric analysis. If the model predictions are relatively insensitive to a parameter, then a fairly wide range of values for that parameter could be used without significantly affecting the predictions of the model. It often the case that the more parameters that are estimated, the more uncertain are the estimates due to interaction between the parameters, poor scaling, and round-off error (138).

The sensitivity coefficient of each parameter of interest,  $S_k$ , can be determined as follows:

$$S_k = \sum_{E=-0.8}^{E=0.8} \frac{\Delta i_a(E)}{m \Delta P_k} \quad (69)$$

where

$$\Delta i_a(E) = |i_a(E) - i_a^*(E)|$$

$$\Delta P_k = |(P_k - P_k^*)/P_k^*|$$

$$i_a = \text{predicted anodic current density with } P_k$$

$$i_a^* = \text{predicted anodic current densities with } P_k^*$$

$$P_k = \text{perturbed value of parameter } k$$

$$P_k^* = \text{reference value of parameter } k$$

$$m = \text{number of data points}$$

For convenience, only anodic (oxidation) current density responses are used to analyze the sensitivity of the model predictions in here. Anodic current density responses shown in Fig. 8 and their conditions are used as the reference case. When an interesting parameter is perturbed slightly (i.e., multiplying by 1.05

to the reference value) while holding the values of all other parameters equal to that of the reference case, a new set of data of predicted anodic current density responses ( $i_a$ ) vs. applied potential ( $E$ ) is obtained. Then, the difference in the anodic current density responses between the reference and perturbed cases ( $\Delta i_a$ ) is calculated at each potential interval and summed over the entire potential region used. The results of the sensitivity analysis are shown in Tables XIII and XIV.

Table XIII shows the sensitivity of the anodic current density to the physical parameters, such as the porosity of polypyrrole electrode ( $\epsilon_p$ ), the thickness of polypyrrole electrode ( $\delta_{pp}$ ), and the thickness of diffusion layer ( $\delta_{dl}$ ). The predicted anodic current density responses are found to be more sensitive to the electrode thickness ( $\delta_{pp}$ ) and porosity ( $\epsilon_p$ ) than the thickness of the diffusion layer ( $\delta_{dl}$ ). This is expected because the switching process of polypyrrole electrode is limited by ion transfer rate within porous structure. The effective diffusivities of  $\text{Li}^+$  and  $\text{ClO}_4^-$  within the porous layer are much smaller than the free stream diffusivity of these species. The fact that the current density responses are relatively insensitive to the thickness of the diffusion layer is comforting because it is usually much easier to measure the electrode thickness and porosity with high degree of accuracy than that is possible for the diffusion layer. Note also that the porosity of the electrode has to be measured experimentally. A porosity

Table XIII. Sensitivity analysis on various physical parameters.

Physical Parameters	Sensitivity Coefficient ( $S_k$ )
Thickness of Polypyrrole Film ( $\delta_{pp}$ )	0.68867
Porosity of Polypyrrole Film ( $\epsilon_p$ )	0.20020
Thickness of Diffusion Layer ( $\delta_{dl}$ )	0.06169

value calculated theoretically from the material balance on the solid phase is not applicable because it ignores the existence of closed pores.

Table XIV shows the sensitivity of the anodic current density to the electrochemical parameters describing the electrochemical reaction [1] and the double layer effects on switching process. The most influential parameter is the maximal faradaic charge of polypyrrole ( $Q_{f,oxd}$ ). This is expected because the amount of electroactive material is proportional to this quantity. The double layer constant ( $a^*$ ) and the zero charge potential ( $\eta_{1,pzc}$ ) are next followed by the anodic transfer coefficient ( $\alpha_{a1}$ ) and the exchange current per unit volume ( $ai_{o1,ref}$ ). The electrokinetic parameters describing the doping/undoping of polypyrrole have less influence than those describing the double layer effects. This could be due to the fact that polypyrrole has the large capacitive background current density as shown in Fig. 7.

In a similar manner, a sensitivity analysis could be used to determine the operating conditions where the sensitivity of a parameter is maximal as shown in Table XV. The effects of scan rate ( $v_s$ ) on the performance of cyclic voltammogram are very significant. The oxidation and reduction peak height is proportional to the scan rate as is expected for a reversible surface process. However, the oxidation and reduction charge densities in each cycle are the same

Table XIV. Sensitivity analysis on various electrochemical parameters.

Electrochemical Parameters	Sensitivity Coefficient ( $S_k$ )
Maximal Faradaic Charge ( $Q_{f,oxd}$ )	0.66469
Double Layer Constant ( $a^*$ )	0.52289
Zero Charge Potential ( $\eta_{1,pzc}$ )	0.49472
Anodic Transfer Coefficient ( $\alpha_{a1}$ )	0.12216
Exchange Current Density ( $ai_{o1,ref}$ )	0.08758

and do not depend on the scan rate. The effects of rotating speed ( $\Omega$ ) on the performance of cyclic voltammogram are not significant. Increasing rotating speed cause more convective effects in the electrolyte diffusion layer. However, convective effect by rotating disk electrode is negligible within the porous polypyrrole electrode region.

#### 4. Effects of Parameters

Many factors come into play when calculating the sensitivity coefficients. For example, the exchange current density and transfer coefficient strongly influence the initial slope in the cell current density. On the other hand, the maximum faradaic charge and double layer constant have more influence later when polypyrrole films are significantly oxidized. Thus, it is necessary to understand the detailed effects of each independent parameter, which is identified as relatively sensitive on model prediction. The effects of the maximal faradaic charge ( $Q_{f,oxd}$ ), the double layer constant ( $a^*$ ), the anodic transfer coefficient ( $\alpha_{a1}$ ), and the exchange current density ( $ai_{o1,ref}$ ), on the cyclic voltammograms are examined and estimated next in detail.

Figure 13 shows the effects of the maximum faradaic charge ( $Q_{f,oxd}$ ) in the cyclic voltammograms. This parameter affected both faradaic and capacitive current densities. The value does not influence the initial slope of the current density. However, the larger value of maximal faradaic charge yields higher and

Table XV. Sensitivity analysis on various operating conditions.

Operating Conditions	Sensitivity Coefficient ( $S_k$ )
Potential Scan Rate ( $v_s$ )	0.66468
Disk Rotation Velocity ( $\Omega$ )	0.00002

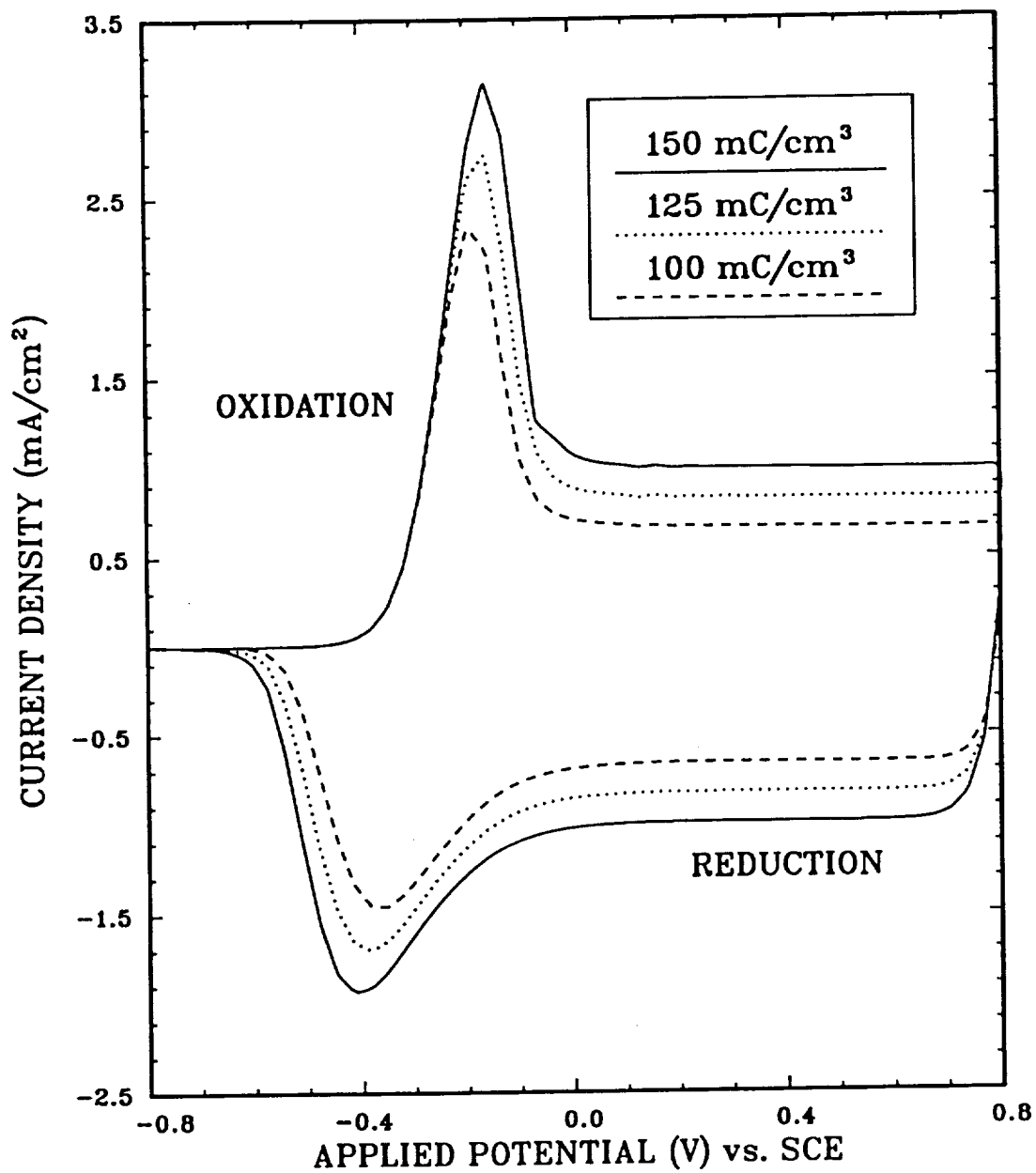


Fig. 13. The effects of maximal faradaic charge ( $Q_{f,oxd}$ ) on the cyclic voltammograms at a scan rate of 20 mV/sec.

broader peak current densities, and higher background capacitive current density. This is because the amount of electroactive material is proportional to this value.

Figure 14 shows the effects of double layer constant ( $a^*$ ) in the cyclic voltammograms. The region, where polypyrrole is significantly reduced, is not affected because this parameter does influence only the double layer charging. Because the local capacitive transfer current per unit volume ( $aj_c$ ) is proportional to this parameter by Eq. [36], larger value of proportional constant ( $a^*$ ) yields higher capacitive current density.

Figures 15 and 16 show the effects of the electrokinetic parameters describing the electrochemical reaction of polypyrrole. These parameters show significant effects in the region where polypyrrole is oxidizing or reducing. No effects are observed in the background capacitive current density. Figure 15 shows the effects of anodic transfer coefficient ( $\alpha_{a1}$ ) in the cyclic voltammograms. This value strongly influences the shape of the peak current density. Increasing anodic transfer coefficient ( $\alpha_{a1}$ ) yields higher and narrower anodic peak current density. The opposite is true for cathodic direction because the sum of anodic and cathodic transfer coefficients ( $\alpha_{a1}$  and  $\alpha_{c1}$ ) is set equal to 1.

Figure 16 shows the effects of exchange current per unit volume ( $ai_{o1,ref}$ ) in the cyclic voltammograms. This parameter shows the most significant influence in the peak current density. Increasing exchange current per unit volume yields increasing both anodic and cathodic peak current densities, and reducing potential difference between anodic and cathodic peak. This is because the electrochemical reaction rate is proportional to this value.

The value of each independent parameter discussed above has been estimated by comparing the peak and background current densities predicted by the model



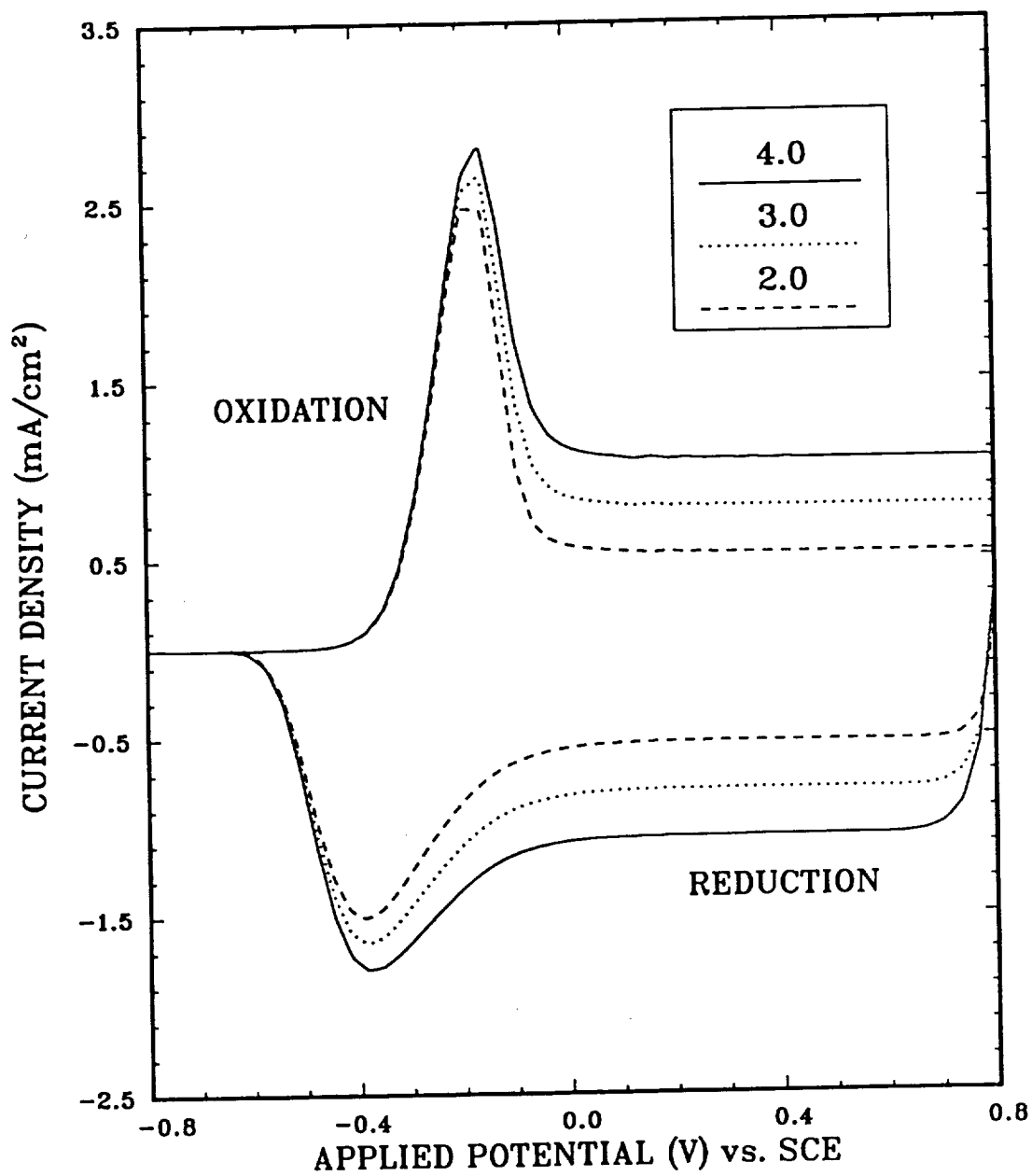


Fig. 14. The effects of double layer constant ( $a^*$ ) on the cyclic voltammograms at a scan rate of 20 mV/sec.

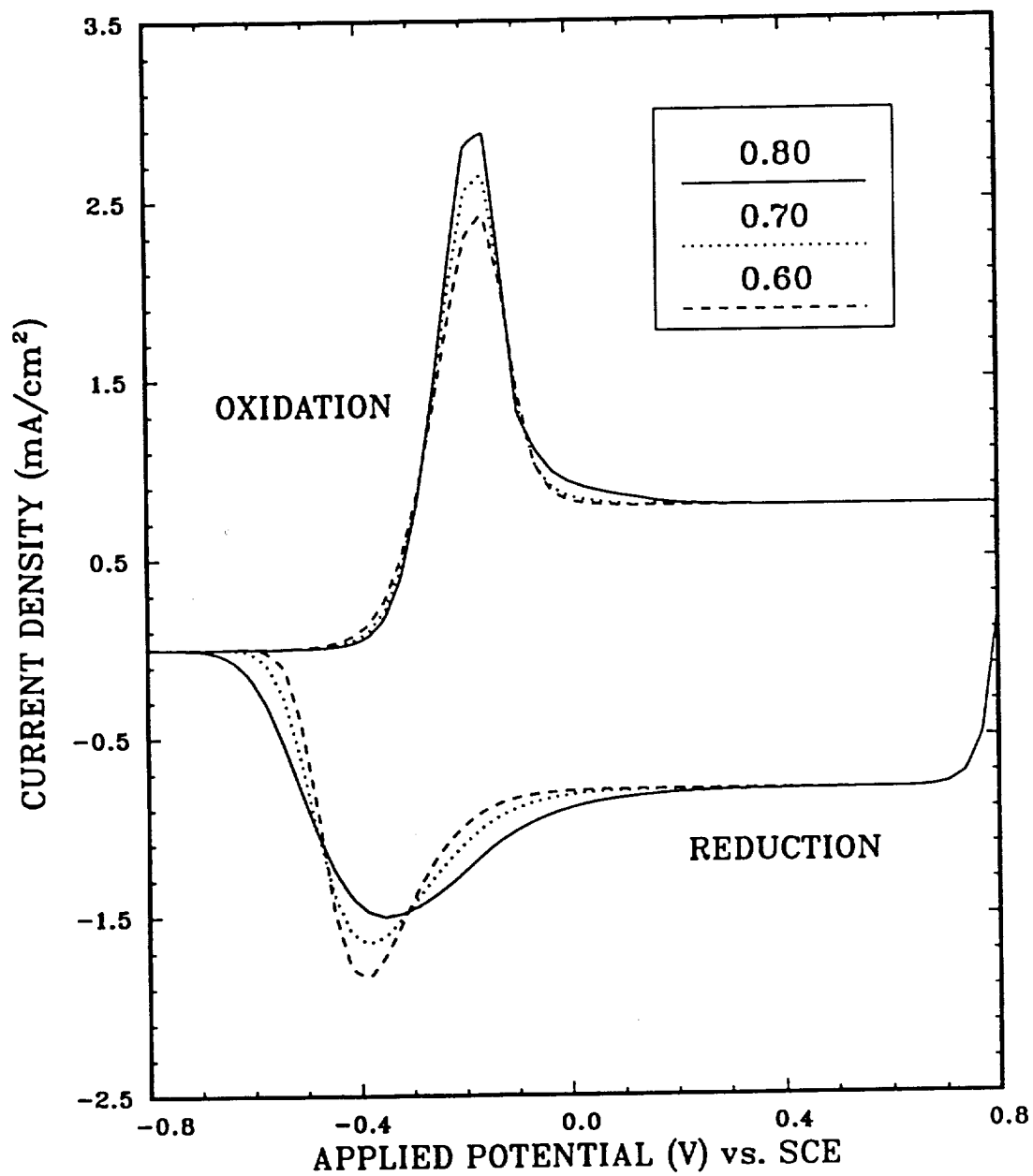


Fig. 15. The effects of anodic transfer coefficient ( $\alpha_{a1}$ ) on the cyclic voltammograms at a scan rate of 20 mV/sec.

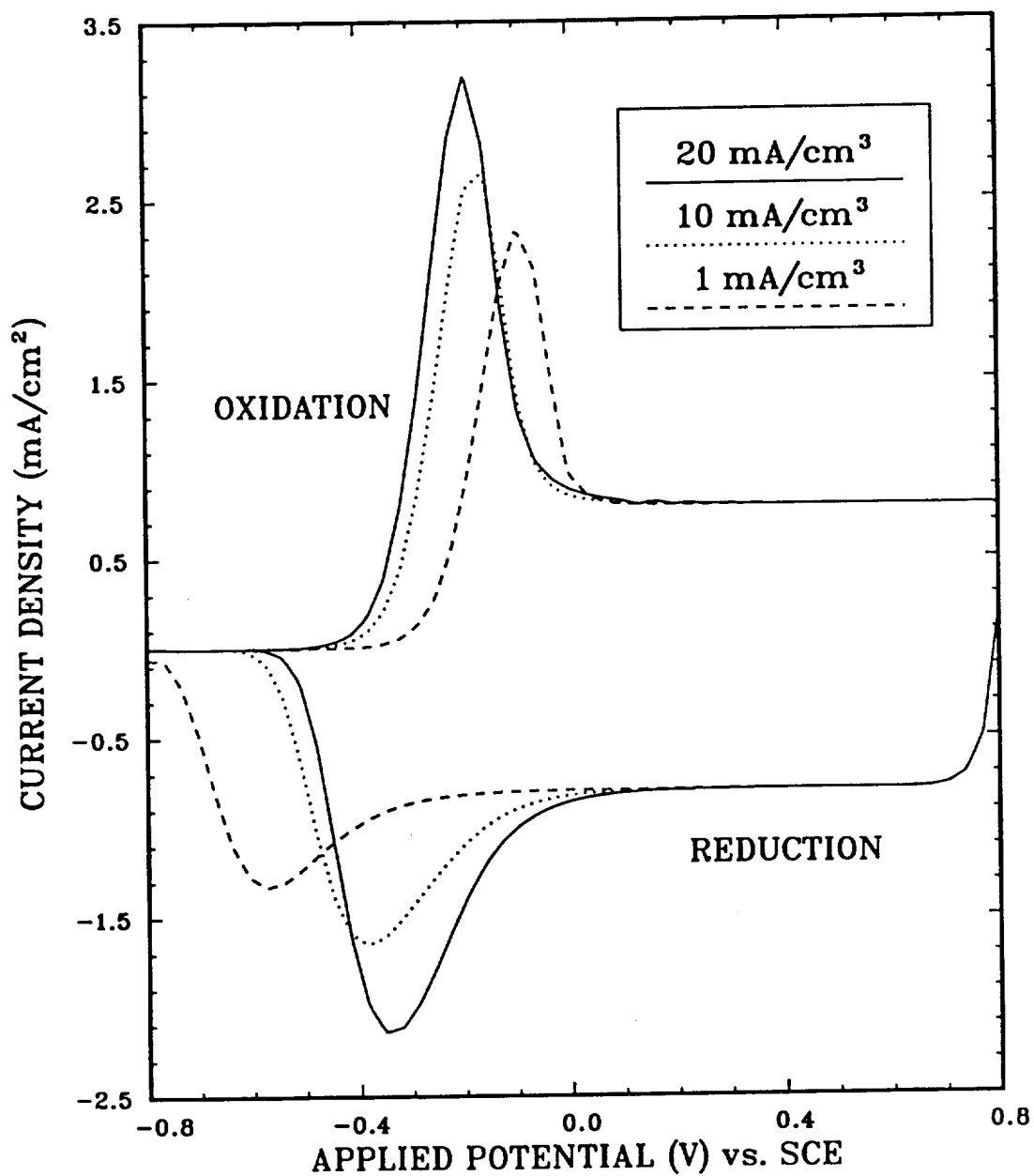


Fig. 16. The effects of exchange current per unit volume ( $ai_{o1,ref}$ ) on the cyclic voltammograms at a scan rate of 20 mV/sec.

with the experimental results. Tables VII and XII summarize these values. The dependent parameters (diffusion coefficients, mobilities, conductivities, etc.) can be calculated from the relationships given in the model development using the values of the independent parameters estimated here. For example, the effective diffusion coefficients of the counterion ( $\text{ClO}_4^-$ ) within the doped and undoped states of the polypyrrole film are  $4.0 \times 10^{-11} \text{ cm}^2/\text{sec}$  and  $1.0 \times 10^{-9} \text{ cm}^2/\text{sec}$ , respectively. These values are smaller than those obtained from experimental measurements. This may be due to the large capacitive and uncompensated resistance effects in polypyrrole films which are not addressed properly in experiments.

#### D. Conclusions and Recommendations

The electronically conducting polypyrrole film has been synthesized electrochemically and used in cyclic voltammetry to study the electrochemical characteristics. The experimental results show that:

- a. The simple one-step electrochemical oxidation of pyrrole monomer yields a flexible, metallic, and organic polymer film.
- b. The polypyrrole film has a quasi-reversible switching behavior with large capacitive background effects.
- c. The switching process of the polypyrrole film is accompanied by distinctive color changes, brown-black at doped state and light yellow at undoped state.
- d. The polypyrrole film can be cycled more than 200 times without significant loss of the coulombic capacity of the electrode.

These observations make polypyrrole a prospective candidate in the area of energy

storage devices.

The mathematical model based on the porous electrode, dilute solution, and double layer theories, coupled to the Butler-Volmer type rate expression has been developed to predict the cyclic voltammograms of a polypyrrole film under identical conditions of the experiments. The simulated results show that:

- a. Despite the fact that the present model involves a number of simplifications such as the presumption that the electronic conductivity varies linearly with the doping level, a comparison of the simulated and experimental cyclic voltammograms shows quantitative agreement.
- b. The modified Butler-Volmer type rate expression can be applied for the quasi-reversible switching behavior of polypyrrole. This assumes that the appearance of the quasi-reversible peak in the cyclic voltammograms for conducting polymers is not necessary evidence for the presence of an additional redox process.
- c. The profiles of the dependent variables show that the switching process is governed by the availability of the counterion to the polypyrrole electrode and the amount of electroactive sites. Thus, the performance of the polypyrrole based devices could be improved by physical modifications that increase electroactive surface area and optimize the rate of ionic charge transport.
- d. Sensitivity analysis shows that the parameters describing the double layer effects have more influence than those describing the electrokinetic process. This observation suggests that more emphasis should be placed on evaluating the capacitive effects affiliated with the doping state of polypyrrole.

Better agreement between the simulated and experimental data will be obtained if different charge transport mechanisms are considered for the doping and undoping processes. In addition, the factors which determine the electrochemical characteristics of polypyrrole are the doping level and its functional relationship to the microscopic structure, conductivity, and capacitance. In the absence of any experimental or theoretical data, the preassumptions used are adequate for these preliminary analysis. With pertinent experimental or theoretical data to quantify these factors, the model can be used, together with parameter estimation techniques, to determine the electrochemical characteristics of polypyrrole.

The model developed here can be modified to study cyclic voltammetric behavior of other conducting polymers, such as polythiophene, polyaniline, polycarbajole, etc., by simply adjusting the input parameters and their relationships. Also, the model can be extended to predict other electroanalytical techniques, such as AC impedance, chronocoulometry, and chronoabsorptometry. AC impedance can be useful to obtain more detail of double layer effects.

## V. SECONDARY BATTERY

The electronically conductive polypyrrole has received tremendous interest as energy storage materials in recent years. Among the potential applications, the most promising is the lithium/polypyrrole secondary battery system (105-110). Combining polypyrrole with lithium in a secondary battery provides an inexpensive and noncorrodible battery with a high cell potential and unusual design flexibility.

Conducting polymers in general possess several technologically important features in the battery technology. The polymeric electrodes differ from conventional electrodes in that the polymer does not dissolve and is not redeposited during charge-discharge cycles, although some swelling of the polymer does occur during oxidation or reduction. This absence of dissolution and redeposition is expected to promote longer life for polymer electrodes owing to the absence of mechanical changes in electrode dimensions and so on, such as those observed with many conventional electrodes. Also, in most batteries complete deep discharge leads to rapid deterioration. Hence only partial utilization of the energy density of a battery can be achieved if it is only partly discharged in order to prolong its effective operating life. The energy density of a polymer electrode can, however, be completely utilized in repeated deep discharges at good discharge rates without adverse effects. The flexibility of polymeric films may be significant in their use in certain types of thin batteries. It would appear that the use of organic substances as electrode-active materials in batteries for certain specific types of uses is still in its infancy.

A disadvantage of all polymer electrode is that they will be expected to

exhibit smaller volumetric energy densities than conventional electrodes, since organic materials are usually less dense than metals and inorganic substances. To what extent this is a serious disadvantage will depend on the use to which the cell in which they are incorporated might be put.

Although the conductive polymers have already attracted considerable attention in battery technology, a secondary battery system based on these polymers is still in the experimental stage and its charge/discharge behavior is not fully understood. To gain a better understanding of the dynamic behavior and to provide guidance toward designs of new secondary batteries utilizing electrochemically conductive polymers, a one-dimensional mathematical model is presented here for the charge/discharge behavior of the lithium/polypyrrole system.

The model is used to predict the dynamic behavior of the cell during charge and discharge at constant applied current density. The spatial and time dependence of concentration, electrochemical potential, and electrode capacity profiles within the cell are presented. Also, the effects of various design parameters, such as the thickness of the polypyrrole electrode, the reservoir, and the separator, are discussed.

#### A. System Descriptions

A typical monopolar Li/LiClO<sub>4</sub>-PC/PPy secondary battery cell is presented schematically in Fig. 17. One unit cell is considered here, consisting of a polypyrrole positive electrode which has been electrochemically coated on a platinum current collector, a electrolyte reservoir containing 1M LiClO<sub>4</sub> in propylene carbonate, a separator consisting of a porous inert material, and a lithium metal negative electrode. The lithium electrode is treated as own current



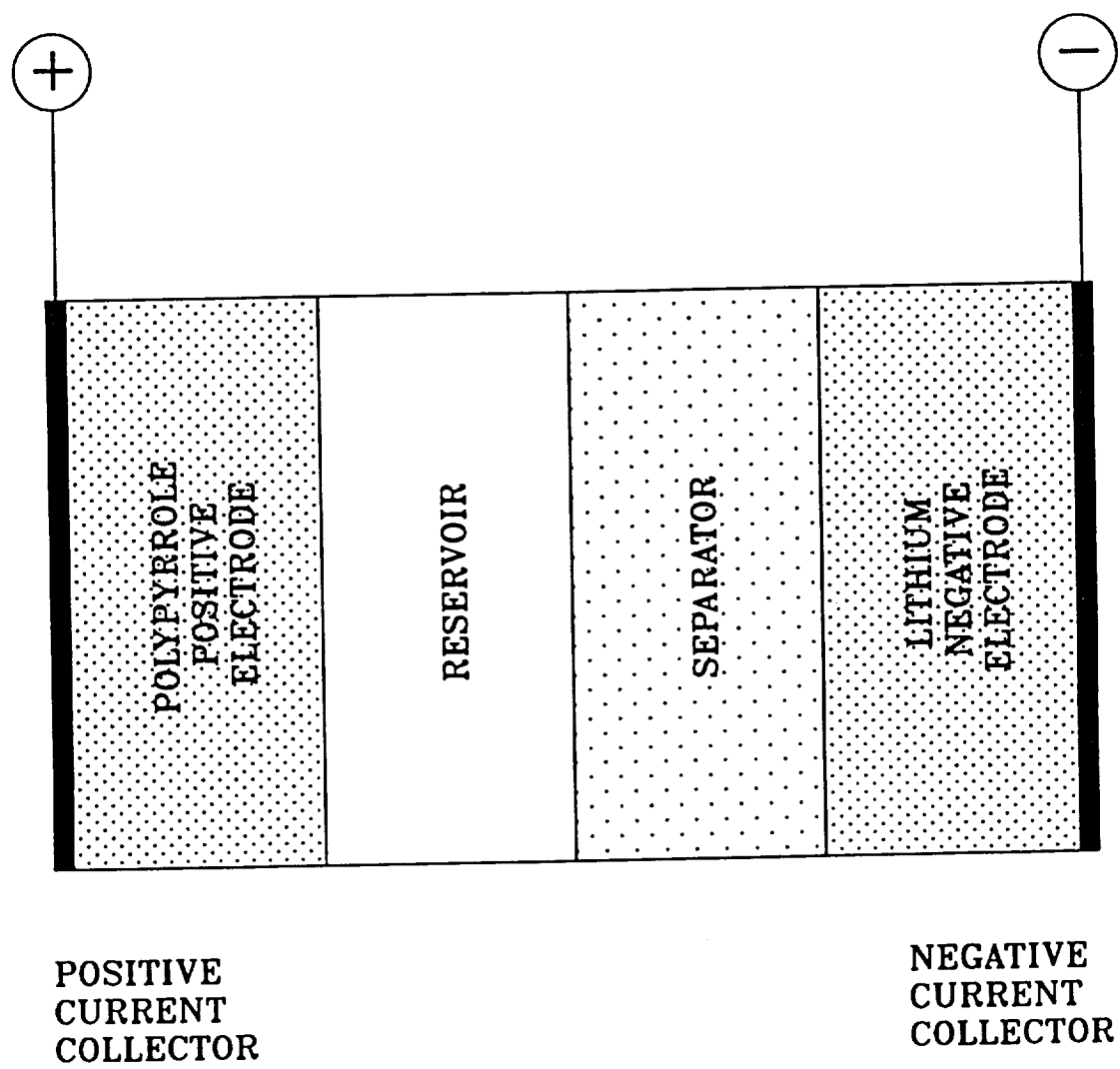


Fig. 17. A schematic diagram of a typical monopolar  $\text{Li/LiClO}_4\text{-PC/PPy}$  secondary battery cell.

collector. These four elements of the cell are repeated alternately to form a monopolar stack of cells called a battery (139).

## B. Model Descriptions

The model presented here is for predicting the charge/discharge behavior of the lithium/polypyrrole secondary battery cell at a constant current density. The modeling regions of the cell, which are relevant to the development of the model equations, are schematically presented in Fig. 18. The regions include three main regions, two boundaries, and two inter-regional interfaces, and must be modeled simultaneously. These are the boundary interface between the platinum current collector and the polypyrrole positive electrode ( $y = 0$ ); the porous polypyrrole positive electrode region of width  $\delta_{ppe}$  (region 1); the inter-regional interface between the polypyrrole positive electrode and the electrolyte reservoir ( $y = y_{ppe}$ ); the electrolyte reservoir region of width  $\delta_{res}$  (region 2); the inter-regional interface between the reservoir and the separator ( $y = y_{res}$ ); the separator region of width  $\delta_{sep}$  (region 3); the boundary interface between the separator and the lithium negative electrode ( $y = y_{sep}$ ).

The cell is operated at the constant applied current density of  $i_{cell}$  by a galvanostat. For discharge, the current flows from the lithium negative electrode to the polypyrrole positive electrode through the separator and reservoir. For charge, the opposite is true. The reaction mechanisms at the polypyrrole positive electrode, the lithium negative electrode, and the overall system are discussed in Chapter III (See Eqs. [1], [2], and [3]).

In all of the regions, the unknowns are the concentration of  $\text{Li}^+$  ( $c_+$ ), the concentration of  $\text{ClO}^-$  ( $c_-$ ), the local faradaic charge per unit volume ( $Q_f$ ),

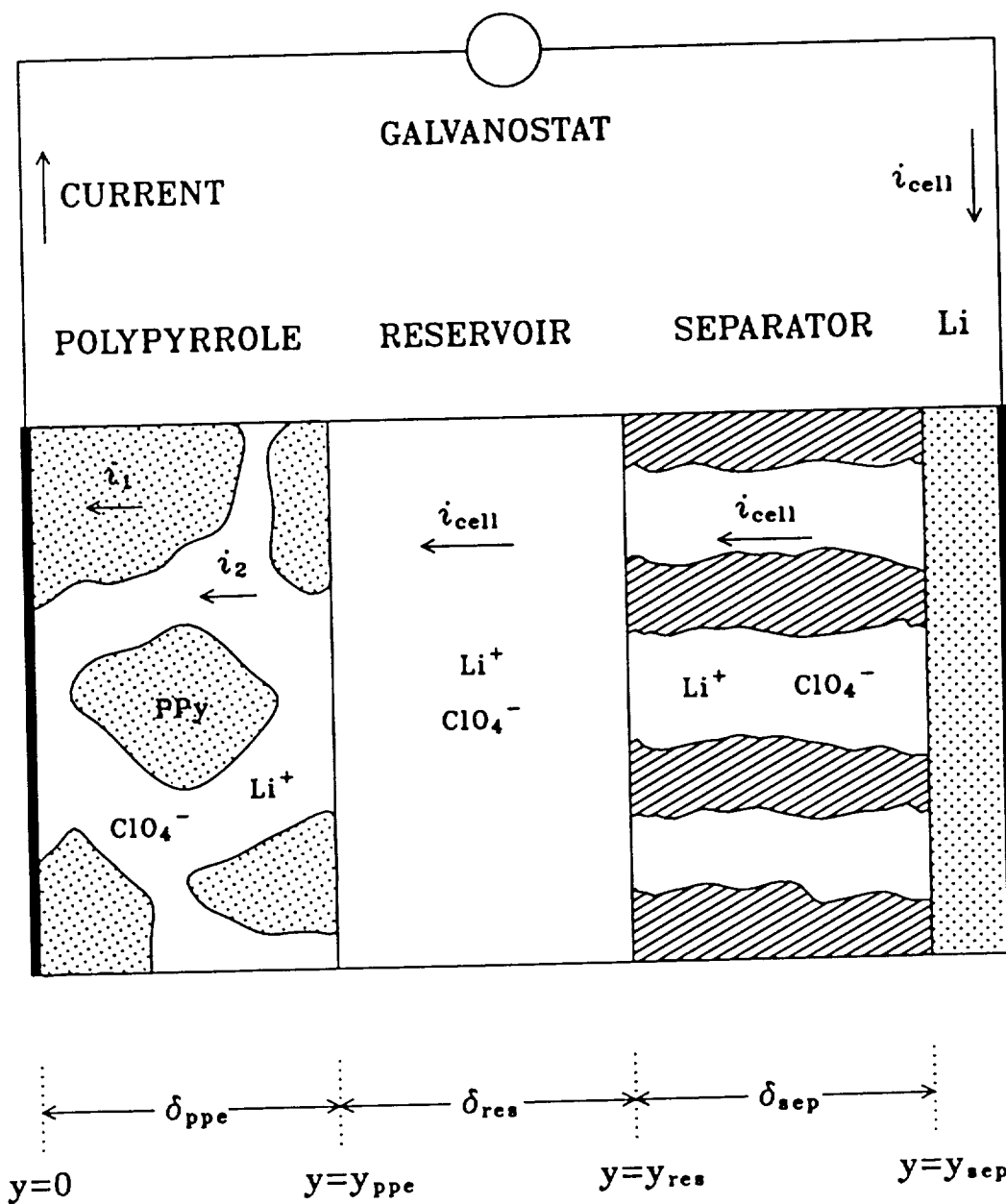


Fig. 18. A schematic diagram of modeling regions in Li/LiClO<sub>4</sub>-PC/PPy secondary battery cell.

the potential of the solid phase ( $\Phi_1$ ), and the potential of the solution phase ( $\Phi_2$ ). Because the cell is charged and discharged at a constant current density, values for the unknowns depend on the perpendicular distance from the platinum current collector of the polypyrrole positive electrode ( $y$ ) and time ( $t$ ), and they are obtained by solving the system of governing equations and assumptions for each region of the cell described next.

### 1. Governing Equations – Polypyrrole Positive Electrode

Polypyrrole positive electrode region consists of a solid phase of polypyrrole and a solution phase of an organic electrolyte that penetrates the void spaces in the porous structure as shown in Fig. 18. Since the system operated at a constant current density by galvanostat in charge and discharge processes (instead of operating at a potential scan by potentiostat in the cyclic voltammetry), the governing equations in this region are similar to that in the porous polypyrrole electrode region in chapter IV except Current Balance used instead of Transfer Current Balance.

#### Material Balance for Dissolved Species

A one dimensional material balance equation for species  $i$  in the porous polypyrrole positive electrode is given by (See Eq. [29])

$$\frac{\partial(\epsilon_p c_i)}{\partial t} = z_i F \frac{\partial}{\partial y} \left( u_{i,p} c_i \frac{\partial \Phi_2}{\partial y} \right) + \frac{\partial}{\partial y} \left( D_{i,p} \frac{\partial c_i}{\partial y} \right) - \frac{s_{1,i} a j_1}{n_1 F} \quad (70)$$

#### Charge Balance

The state of the local faradaic charge within the polypyrrole film per unit volume ( $Q_f$ ) can be obtained by integrating the local faradaic transfer current

per unit volume ( $aj_f$ ) as follows (See Eq. [32]):

$$\frac{\partial Q_f}{\partial t} = ai_{o1,ref} \left\{ \left( 1 - \theta \right) \left( \frac{c_-}{c_{-,ref}} \right) \exp \left( \frac{\alpha_{a1} F}{RT} \eta_1 \right) - \theta \exp \left( \frac{-\alpha_{c1} F}{RT} \eta_1 \right) \right\} \quad (71)$$

### Current Balance

The current density flowing through the porous polypyrrole positive electrode ( $i_{cell}$ ) consists of the superficial current densities in the solid and solution phases ( $i_1$  and  $i_2$ ) as shown in Fig. 18

$$i_{cell} = i_1 + i_2 \quad (72)$$

Since the superficial current densities in the solid and solution phases ( $i_1$  and  $i_2$ ) are given by (See Eqs. [39] and [41])

$$i_1 = -\sigma_p \frac{\partial \Phi_1}{\partial y} \quad (73)$$

$$i_2 = -\kappa_p \frac{\partial \Phi_2}{\partial y} - F \sum_i z_i D_{i,p} \frac{\partial c_i}{\partial y} \quad (74)$$

the current balance in this region can be expressed as

$$-\sigma_p \frac{\partial \Phi_1}{\partial y} - \kappa_p \frac{\partial \Phi_2}{\partial y} - F \sum_i z_i D_{i,p} \frac{\partial c_i}{\partial y} = i_{cell} \quad (75)$$

### Electroneutrality

It is assumed here that the thickness of double layer within the pore is very thin to compare with pore size, and the solution inside the pores obeys the electroneutrality relationship, which describes as follows:

$$\sum_i z_i c_i = 0 \quad (76)$$

## 2. Governing Equations – Reservoir

The reservoir is the region between the polypyrrole positive electrode and the separator, and is initially filled with the electrolyte of 1M LiClO<sub>4</sub>-PC as shown in Fig. 18. The reservoir serves to supply electrolyte to the positive and negative electrodes as it is consumed via electrochemical reactions and double layer charging.

Mass transfer in the reservoir is governed by the following material balance equation for species *i* (129):

$$\frac{\partial c_i}{\partial t} = -\nabla \cdot \mathbf{N}_i \quad (77)$$

The flux of species *i* in the reservoir,  $\mathbf{N}_i$ , is due to migration in the electric field and diffusion in the concentration gradient

$$\mathbf{N}_i = -z_i u_i F c_i \nabla \Phi_2 - D_i \nabla c_i \quad (78)$$

Only the axial component of the flux is considered here. Substituting the normal component of Eq. [78] into Eq. [77] gives the one dimensional material balance for a dissolved species *i* within the reservoir:

$$\frac{\partial c_i}{\partial t} = \frac{z_i D_i F}{RT} \frac{\partial}{\partial y} \left( c_i \frac{\partial \Phi_2}{\partial y} \right) + \frac{\partial^2 c_i}{\partial y^2} \quad (79)$$

The solid electroactive material does not exist in this region, therefore the local faradaic charge ( $Q_f$ ) and the solid potential ( $\Phi_1$ ) are treated as dummy variables and their values are set arbitrarily equal to zero

$$Q_f = 0 \quad (80)$$

$$\Phi_1 = 0 \quad (81)$$

Since all the current flowing through the reservoir is carried by the electrolyte, the superficial current density in the solution phase ( $i_2$ ) can be set equal to the applied current density ( $i_{\text{cell}}$ ), and can be expressed similar to that used in the positive electrode region except that the free stream conductivity ( $\kappa$ ) and diffusivity ( $D_i$ ) applies (See Eq. [74])

$$i_2 = -\kappa \frac{\partial \Phi_2}{\partial y} - F \sum_i z_i D_i \frac{\partial c_i}{\partial y} = i_{\text{cell}} \quad (82)$$

### 3. Governing Equations - Separator

The separator consists of a porous inert material which is mainly used to prevent physical contact between the polypyrrole positive electrode and the lithium negative electrode, and a solution phase which fills the void spaces of the porous structure. Since the solid material is inert, the porosity of separator ( $\epsilon_s$ ) does not change with time and is set arbitrarily equal to a constant. An effective diffusivity ( $D_{i,s}$ ) and mobility ( $u_{i,s}$ ) of species  $i$ , and ionic conductivity of electrolyte ( $\kappa_s$ ) within the separator are obtained in the similar manner as those for the porous polypyrrole electrode region in Chapter IV (See Eqs. [22], [23], and [24]):

$$D_{i,s} = D_i \epsilon_s^{1+\text{ex}} \quad (83)$$

$$u_{i,s} = u_i \epsilon_s^{1+\text{ex}} \quad (84)$$

$$\kappa_s = \kappa \epsilon_s^{1+\text{ex}} \quad (85)$$

The differential material balance equation in the solution phase is formulated for a dissolved species  $i$  in terms of average quantities as follows (129):

$$\frac{\partial(\epsilon_s c_i)}{\partial t} = -\nabla \cdot \mathbf{N}_{i,s} \quad (86)$$

where  $\epsilon_s c_i$  represents the average concentration per total unit volume in separator including the solid inert phase and the electrolyte that occupies the void space within the matrix, and  $N_{i,s}$  represents the flux of species  $i$  within the porous separator region.

The flux of species  $i$  within the separator ( $N_{i,s}$ ) is given by an equation that is similar to that for the reservoir except that the effective diffusivity ( $D_{i,s}$ ) and mobility ( $u_{i,s}$ ) applies (See Eq. [78]):

$$N_{i,s} = -z_i u_{i,s} F c_i \nabla \Phi_2 - D_{i,s} \nabla c_i \quad (87)$$

A one dimensional differential material balance equation for species  $i$  in this region can be obtained by substituting the normal component of Eq. [87] into Eq. [86] as follows:

$$\epsilon_s \frac{\partial c_i}{\partial t} = z_i u_{i,s} F \frac{\partial}{\partial y} \left( c_i \frac{\partial \Phi_2}{\partial y} \right) + D_{i,s} \left( \frac{\partial^2 c_i}{\partial y^2} \right) \quad (88)$$

Since the solid material is inert, the local faradaic charge ( $Q_f$ ) and the solid potential ( $\Phi_1$ ) are treated as dummy variables and their values are set arbitrarily equal to zero as shown in Eqs. [80] and [81].

All of the current flowing through the separator is carried by the electrolyte, the superficial current density in the solution phase ( $i_2$ ) can be set equal to the applied current density ( $i_{\text{cell}}$ ), and can be expressed as

$$i_2 = -\kappa_s \frac{\partial \Phi_2}{\partial y} - F \sum_i z_i D_{i,s} \frac{\partial c_i}{\partial y} = i_{\text{cell}} \quad (89)$$

#### 4. Boundary and Interface Conditions

To complete the system of equations for the model, the boundary conditions at each end of the cell and inter-regional interfaces must be specified for the



dependent variables:  $c_+$ ,  $c_-$ ,  $Q_f$ ,  $\Phi_1$ , and  $\Phi_2$ . Boundary and interface conditions for these dependent variables are specified in the order of the polypyrrole positive electrode to the lithium negative electrode.

The porous polypyrrole positive electrode is bounded by a platinum current collector on one face ( $y = 0$ ) and by the reservoir on the other ( $y = y_{ppe}$ ). At the current collector/polypyrrole positive electrode interface ( $y = 0$ ), the rate of consumption (charge) or production (discharge) of each species  $i$  by the electrochemical reaction [1] and the double layer charge ( $R'_{1,i}$ ) is equal to the net normal component of the flux of  $\text{ClO}_4^-$  towards or away from the electrode. Thus

$$-z_i u_{i,p} F c_i \frac{\partial \Phi_2}{\partial y} - D_{i,p} \frac{\partial c_i}{\partial y} = -\frac{s_{1,i} a j_1}{n_1 F} \quad (90)$$

The rate of accumulation of the local faradaic charge per unit volume within the polypyrrole positive electrode ( $Q_f$ ) is obtained from the local faradaic transfer current per unit volume ( $a j_f$ ) as shown in Eq. [71]. At this point, all of the current leaves the cell via the current collector which can be represented with constant  $i_{\text{cell}}$ . Thus, the superficial current density in the solid and solution phases ( $i_1$  and  $i_2$ ) can be set to  $i_{\text{cell}}$  and zero, so that

$$i_1 = -\sigma_p \frac{\partial \Phi_1}{\partial y} = i_{\text{cell}} \quad (91)$$

$$i_2 = -\kappa_p \frac{\partial \Phi_2}{\partial y} - F \sum_i z_i D_{i,p} \frac{\partial c_i}{\partial y} = 0 \quad (92)$$

At the polypyrrole positive electrode/reservoir interface ( $y = y_{ppe}$ ), the flux of each species  $i$  across the two regions must be continuous, which can be written as follows:

$$-z_i u_{i,p} F c_i \frac{\partial \Phi_2}{\partial y} - D_{i,p} \frac{\partial c_i}{\partial y} = -z_i u_i F c_i \frac{\partial \Phi_2}{\partial y} - D_i \frac{\partial c_i}{\partial y} \quad (93)$$

Because the solid electrode phase ends at this point and all of the current is in the solution phase, the gradient of the local faradaic charge ( $Q_f$ ) and the solid potential ( $\Phi_1$ ) are set equal to zero

$$\left. \frac{\partial Q_f}{\partial y} \right|_{y_{ppe}} = 0 \quad (94)$$

$$\left. \frac{\partial \Phi_1}{\partial y} \right|_{y_{ppe}} = 0 \quad (95)$$

Also, the superficial current density in the solution phase ( $i_2$ ) is set equal to the applied current density,  $i_{cell}$ , as follows:

$$i_2 = -\kappa_p \frac{\partial \Phi_2}{\partial y} - F \sum_i z_i D_{i,p} \frac{\partial c_i}{\partial y} = i_{cell} \quad (96)$$

At the reservoir/separator interface ( $y = y_{res}$ ), the boundary conditions are derived in the same manner as those for the positive electrode/reservoir interface. The flux of each species  $i$  across the two regions must be continuous

$$-z_i u_i F c_i \frac{\partial \Phi_2}{\partial y} - D_i \frac{\partial c_i}{\partial y} = -z_i u_{i,s} F c_i \frac{\partial \Phi_2}{\partial y} - D_{i,s} \frac{\partial c_i}{\partial y} \quad (97)$$

and the superficial current density ( $i_2$ ) in the solution phase is set equal to constant  $i_{cell}$

$$i_2 = -\kappa \frac{\partial \Phi_2}{\partial y} - F \sum_i z_i D_i \frac{\partial c_i}{\partial y} = i_{cell} \quad (98)$$

The local faradaic charge ( $Q_f$ ) and the solid potential ( $\Phi_1$ ) are treated as dummy variables and are arbitrarily set equal to zero as shown in Eqs. [80] and [81].

At the separator/lithium negative electrode interface ( $y = y_{sep}$ ), the rate of consumption (charge) or production (discharge) of a  $\text{Li}^+$  by the electrochemical reaction [2] is equal to the net normal component of the flux of  $\text{Li}^+$  towards or away from the electrode

$$-z_+ u_{+,s} F c_+ \frac{\partial \Phi_2}{\partial y} - D_{+,s} \frac{\partial c_+}{\partial y} = \frac{s_{2,+} j_2}{n_2 F} \quad (99)$$

where  $j_2$  represents local transfer current density for the electrochemical reaction [2] and is discussed in Chapter III. Combining Eqs. [18] and [99] yields

$$-z_+ u_{+,s} F c_+ \frac{\partial \Phi_2}{\partial y} - D_{+,s} \frac{\partial c_+}{\partial y} = \frac{s_{2,+}}{n_2 F} i_{o2,ref} \left\{ \exp\left(\frac{\alpha_{a2} F}{RT} \eta_2\right) - \exp\left(\frac{-\alpha_{c2} F}{RT} \eta_2\right) \right\} \quad (100)$$

The normal component of the flux of  $\text{ClO}_4^-$  is assumed to be equal to zero

$$-z_- u_{-,s} F c_- \frac{\partial \Phi_2}{\partial y} - D_{-,s} \frac{\partial c_-}{\partial y} = 0 \quad (101)$$

The local faradaic charge ( $Q_f$ ) is treated as a dummy variable and is arbitrarily set equal to zero (See Eq. [80]). The potential in the solid lithium ( $\Phi_1$ ) at this point is set arbitrarily equal to zero volt:

$$\Phi_1 = 0 \quad (102)$$

This is done to provide a reference point and consequently a particular solution for the model. Of course, the solid potential ( $\Phi_1$ ) could be alternatively set to zero at the other end of the cell (i.e., at the current collector/polypyrrole positive electrode interface). At this point ( $y = y_{sep}$ ), all the current in the cell leaves the electrolyte and enters the lithium negative electrode by the electrochemical reaction [2]

$$i_{cell} = -j_2 \quad (103)$$

It is noted that the electroactive area is same as the projected electrode area at this point. Substituting Eq. [18] into Eq. [103] yields

$$-i_{o2,ref} \left\{ \exp\left(\frac{\alpha_{a2} F}{RT} \eta_2\right) - \exp\left(\frac{-\alpha_{c2} F}{RT} \eta_2\right) \right\} = i_{cell} \quad (104)$$

As mentioned earlier, the lithium electrode is treated in here as own current collector.

## 5. Initial Conditions

Initial conditions are necessary for the variables which depend explicitly on time. For convenience, it is assumed that the cell is in its fully discharged state and ready to be charged. Consequently, the local faradaic charge per unit volume is initially set equal to  $Q_{f,\text{red}}$ , a minimal charge state, throughout the porous polypyrrole positive electrode. Therefore, porosity ( $\epsilon_p$ ) and conductivity ( $\sigma_p$ ) of the polypyrrole positive electrode are initially set equal to  $\epsilon_{\text{red}}$  and  $\sigma_{\text{red}}$ , values at this reduced state, throughout the porous polypyrrole positive electrode. In the other regions, these variables are treated as a dummy variable and are arbitrarily set equal to zero.

The concentration of each species  $i$  throughout the cell is set equal to its reference concentration:

$$c_i = c_{i,\text{ref}} \quad (105)$$

The conductivity of the electrolyte ( $\kappa$ ) can be obtained by combining Eqs. [24] and [105]. Other dependent variables ( $\Phi_1$ , and  $\Phi_2$ ) do not require initial conditions and are arbitrarily set equal to zero at  $t = 0$  for all  $y$ .

## 6. Solution Method

The governing equations, boundary conditions, and interface conditions for the determination of the quantities  $c_+$ ,  $c_-$ ,  $Q_f$ ,  $\Phi_1$ , and  $\Phi_2$ , have been summarized in Table XVI. The system of equations is solved in the similar manner as discussed in chapter IV.

The whole cell is divided into  $NJ$  mesh points with  $J = 1$  designated to be the interface of the platinum current collector and polypyrrole positive electrode,  $J = NJ1$  designated to be the inter-regional interface of the polypyrrole positive

electrode and electrolyte reservoir,  $J = NJ2$  designated to be the inter-regional interface of the electrolyte reservoir and separator, and  $J = NJ$  to be the interface of the separator and negative lithium electrode. Mesh point spacing may vary in each region because of the difference in the thickness of each region and the number of nodal points used.

Once the values of unknowns ( $c_+$ ,  $c_-$ ,  $Q_f$ ,  $\Phi_1$ , and  $\Phi_2$ ) are obtained, values of  $i_1$  and  $i_2$  for each region, and  $Q_c$  can be obtained from those dependent variables using Eqs. [39], [41], and [33]. The applied current density ( $i_{\text{cell}}$ ) flowing through the cell is constant and is equal to the sum of the current density flowing in the solid phase ( $i_1$ ) and the solution phase ( $i_2$ ).

Table XVI. System of equations for charge/discharge behavior of lithium/polypyrrole secondary battery cell.

A. Governing equations.

Variables	Region 1	Region 2	Region 3
$c_+$	70	79	88
$c_-$	70	79	88
$Q_f$	71	80	80
$\Phi_1$	75	81	81
$\Phi_2$	76	82	89

B. Boundary and interface conditions.

Variables	$y = 0$	$y = y_{\text{ppe}}$	$y = y_{\text{res}}$	$y = y_{\text{sep}}$
$c_+$	90	93	97	100
$c_-$	90	93	97	101
$Q_f$	32	94	80	80
$\Phi_1$	91	95	81	102
$\Phi_2$	92	96	98	104

### C. Results and Discussion

The model is used to simulate the dynamic charge/discharge behavior of a typical Li/LiClO<sub>4</sub>-PC/PPy secondary battery cell under various operating conditions. The effects of various design parameters, such as the thickness of the electrode, the reservoir, and separator, etc., on the cell discharge performance are also examined.

The values used for the operating conditions in charging and discharging processes are given in Table XVII. It is assumed that charge/discharge process occurs under the constant current density of 0.2 mA/cm<sup>2</sup> at room temperature. The charge and discharge current densities are specified as being positive and negative because of the chosen coordinate system, respectively. A 1 μm thick polypyrrole film is used in this study because a high doping level and a high efficiency have been observed for this thickness (107). To minimize ohmic loss in a cell, the separator is chosen to have an overall porosity of 0.5 to permit better diffusion of electrolyte and migration of ions between electrodes. The thickness of the reservoir and the separator are chosen arbitrarily to contain 30% of electrolyte for a fully charged cell. All the potentials are referred to the Li/Li<sup>+</sup> electrode.

Table XVII. Operating conditions used for charge/discharge behavior of lithium/polypyrrole secondary battery cell.

Operating Temperature ( $T$ )	298.15 K
Applied Cell Current Density ( $i_{\text{cell}}$ )	0.2 mA/cm <sup>2</sup>
Geometric Electrode Surface Area ( $A$ )	1.0 cm <sup>2</sup>
Thickness of Polypyrrole Positive Electrode ( $\delta_{\text{ppe}}$ )	1.0 μm
Thickness of Reservoir ( $\delta_{\text{res}}$ )	3.0 μm
Thickness of Separator ( $\delta_{\text{sep}}$ )	2.0 μm
Porosity of Separator ( $\epsilon_s$ )	0.5
Reference Potential ( $\Phi_{\text{ref}}$ )	0.0 (vs. Li)

### 1. Charge and Discharge Behavior

The simulated charge/discharge curve of the lithium/polypyrrole secondary battery cell at the applied current density of  $0.2 \text{ mA/cm}^2$  are obtained by using the model developed above and fixed parameter values given in Tables IV, V, VII, VIII, XII, and XVII as shown in Fig. 19. The cell potential,  $\Phi_{\text{cell}}$ , represents the difference between the potential of the solid phase at the current collector of the polypyrrole positive electrode at  $y = 0$  and that of the lithium negative electrode at  $y = y_{\text{sep}}$ . For convenience, the charge and discharge processes are terminated when the faradaic charge state of the cell ( $Q_f/Q_{f,\text{oxd}}$ ) reaches 99.9% and 0.1%, respectively.

The values of predicted cell potential are 3.444 V for 99.9% charged state and 2.853 V for 0.01% charged state, respectively. At the end of the discharge, the sharp potential drop indicates that the polymer becomes insulator. The average discharge potential ( $\Phi_{\text{ave}}$ ) of the typical cell is estimated as 3.160 V from the discharge curve in Fig. 19.

Important properties of a battery are the energy and power densities. The energy density of the cell is defined here as the amount of energy extracted per unit mass of polypyrrole in the cell and is calculated by using the following equation (105):

$$\text{Energy Density} = \frac{I_{\text{cell}} \Phi_{\text{ave}} t_d}{M} \quad (106)$$

where,  $I_{\text{cell}}$  represents the total cell current,  $t_d$  represents the discharge time of the cell, and  $M$  represents the mass of the polypyrrole electrode. The total cell current ( $I_{\text{cell}}$ ) can be obtained by multiplying by the cell current density ( $i_{\text{cell}}$ ) by the cross-sectional area of the electrode ( $A$ ). The theoretical energy density obtained from the discharge curve in Fig. 19 is about 191.9 Wh/kg of polypyrrole

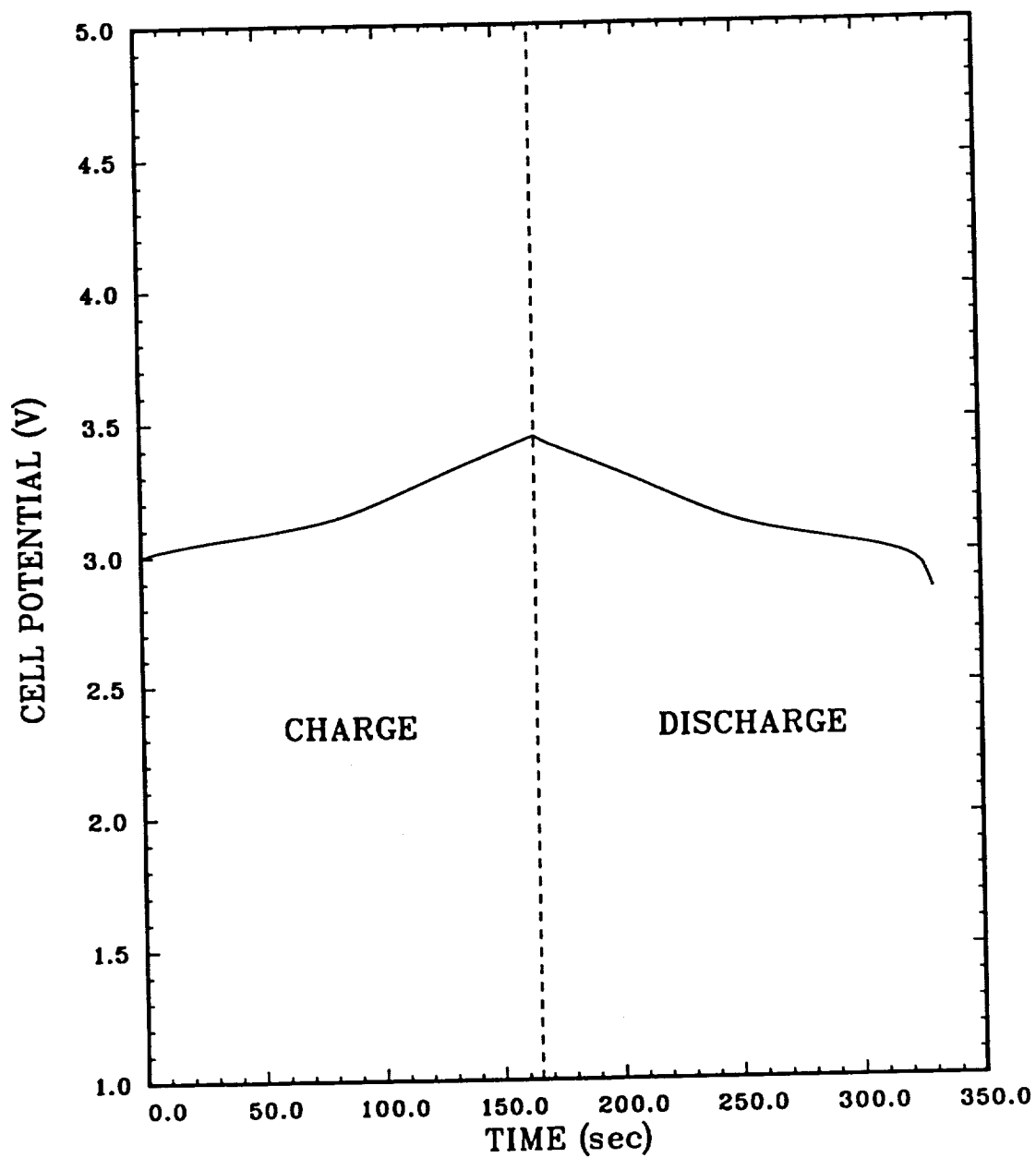


Fig. 19. Simulated charge and discharge behaviors of a typical Li/LiClO<sub>4</sub>-PC/PPy secondary battery cell at  $i_{\text{cell}} = 0.2 \text{ mA/cm}^2$ .



positive electrode.

The power density of the cell is defined as the rate of delivering energy per unit mass of polypyrrole in the cell and is calculated as follows (105):

$$\text{Power Density} = \frac{I_{\text{cell}} \Phi_{\text{ave}}}{M} \quad (107)$$

The theoretical power density obtained from the discharge curve in Fig. 19 is about 4185 W/kg of polypyrrole positive electrode. The characteristics of the cell estimated from this study are summarized in Table XVIII. Direct comparison of the theoretical prediction to those of the experimental data available in the literature is not attempted, although the predictions of charge/discharge behavior seems reasonable.

The cell potential versus time curve shown in Fig. 19 increases with a certain initial slope which changes to a different slope midway through both charge and discharge. This is because the charging and discharging processes are affected by two distinctive factors, faradaic and capacitive current densities ( $i_f$  and  $i_c$ ) as shown in Fig. 20 as a function of time. They are obtained by integrating the local faradaic and capacitive transfer current ( $aj_f$  and  $aj_c$ ) over the porous polypyrrole positive electrode region as discussed in Eq. [66].

Table XVIII. Electrochemical characteristic of one square centimeter lithium/polypyrrole secondary battery cell during discharge.

Mass of Polypyrrole Positive Electrode ( $M$ )	$1.51 \times 10^{-4} \text{g}$
Applied Cell Current ( $I_{\text{cell}}$ )	0.2 mA
Average Cell Potential ( $\Phi_{\text{ave}}$ )	3.160 V
Discharge Time ( $t_d$ )	165.0 sec
Energy Density	191.9 Wh/Kg <sup>†</sup>
Power Density	4185 W/Kg <sup>†</sup>

<sup>†</sup> Based on the mass of the polypyrrole positive electrode.

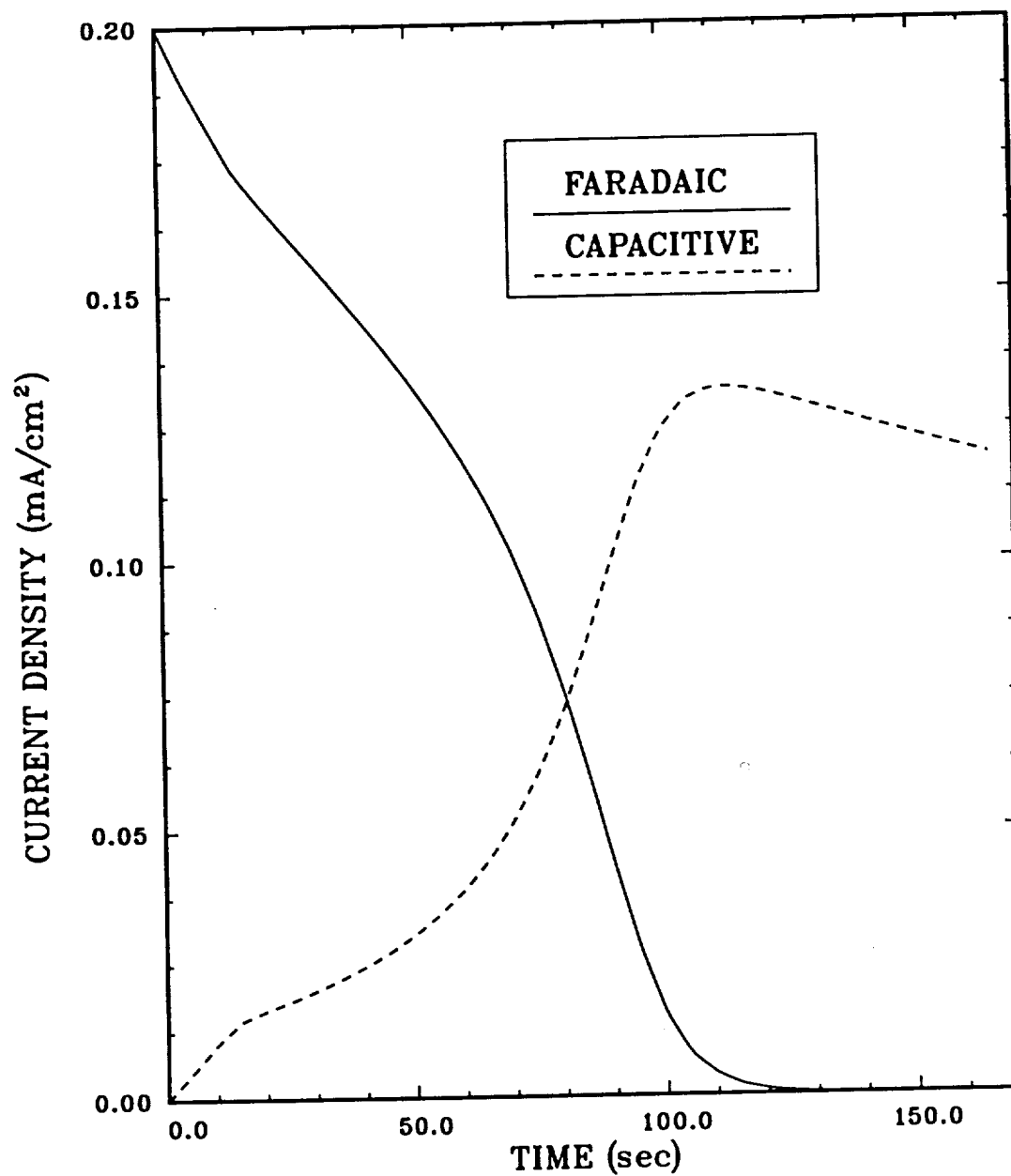


Fig. 20. Faradaic and capacitive current components within the polypyrrole positive electrode during charge at  $i_{\text{cell}} = 0.2 \text{ mA/cm}^2$ .

During charge, the first slope in Fig. 20 is dominated by the faradaic effect, while the second slope is dominated by the capacitive effect. The faradaic current density ( $i_f$ ) decreases with time because the electroactive area (reduced polypyrrole sites) and the concentration of the counterion decrease as the cell is charging. However, the capacitive current density ( $i_c$ ) increases with time because oxidized polypyrrole sites increase continuously with time until the polypyrrole electrode is fully oxidized at about 100 seconds. When the polypyrrole positive electrode is fully oxidized, faradaic current density becomes flat (no further oxidation of polypyrrole occurs), while capacitive current density still exists because of the double layer on the polypyrrole which is fully oxidized and the total current density is dominated by capacitive effect only. For discharge, the opposite phenomena are true.

## 2. Dependent Variables Profiles

The dynamic profiles of the dependent variables across a typical cell during charge and discharge at a constant current density of  $0.2 \text{ mA/cm}^2$  are shown in Figs. 21 through 23 as functions of time ( $t$ ) and position ( $y$ ). In the position coordinate,  $y = 0$  represents the interface between platinum current collector/polypyrrole positive electrode and  $y = 6$  represents the interface between the separator/lithium negative electrode as shown in Fig. 18. In the time coordinate, the cell is in its fully discharged state and ready to be charged at  $t = 0$ .

The dynamic concentration profiles of the anion ( $\text{ClO}_4^-$ ) are shown in Fig. 21. The concentration is made dimensionless relative to its reference concentrations ( $c_{-,ref}$ ). It is noted that the concentration profiles of the cation ( $\text{Li}^+$ ) have similar distributions because of the electroneutrality.

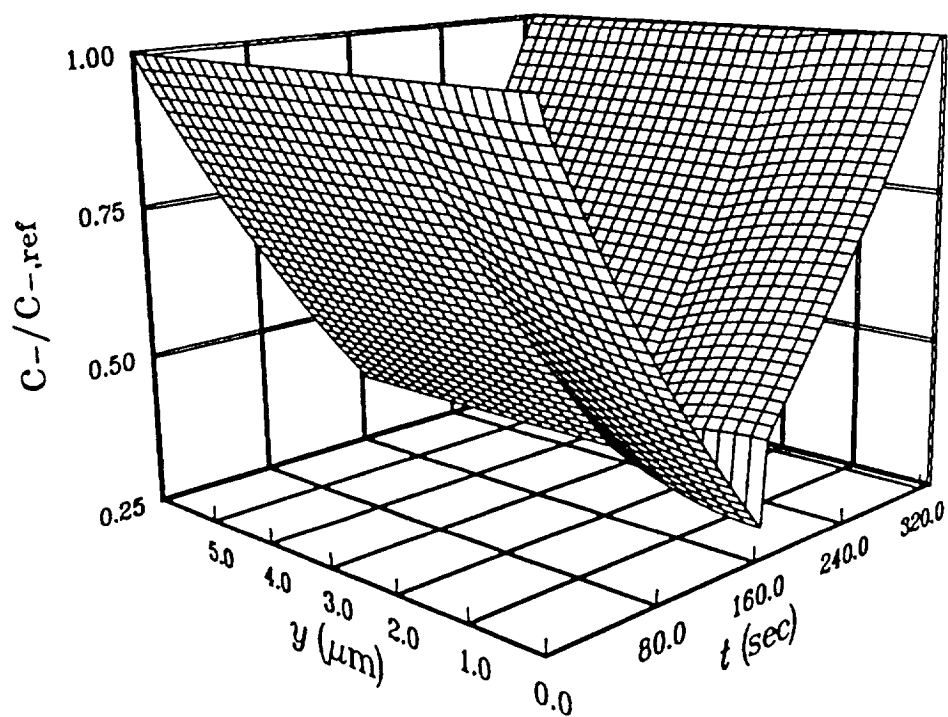


Fig. 21. Dimensionless concentration profiles of the anion ( $\text{ClO}_4^-$ ) across a typical cell during charge and discharge at  $i_{\text{cell}} = 0.2 \text{ mA/cm}^2$ .

Initially, the concentration of the anion is uniform throughout the cell at reference concentration ( $c_{-,ref}$ ). Applying a constant current density of 0.2 mA/cm<sup>2</sup> causes the anions to be consumed at the polypyrrole positive electrode by the oxidation of polypyrrole (electrochemical reaction [1]) and double layer charging. Also, cations are consumed at the lithium negative electrode by the reduction of lithium (electrochemical reaction [2]). The reacting species ( $\text{ClO}_4^-$  for the polypyrrole electrode and  $\text{Li}^+$  for the lithium electrode) are transported from the reservoir to the electrodes.

For discharge, the opposite phenomena are true. Anions are produced at the polypyrrole positive electrode by the reduction of polypyrrole and decrease of double layer charge. Also, cations are produced at the lithium negative electrode by the oxidation of lithium (electrochemical reaction [2]). The reacting species ( $\text{ClO}_4^-$  for the polypyrrole electrode and  $\text{Li}^+$  for the lithium electrode) are transported from the electrodes to the reservoir. Since the effective diffusivity of  $\text{Li}^+$  and  $\text{ClO}_4^-$  within the porous regions (polypyrrole positive electrode and separator) are smaller than the free stream diffusivity of those species, the concentration gradients within the porous regions must be larger to make up for the slower movement of the ions.

Figure 22 shows the faradaic charge profiles. The faradaic charge per unit volume is made dimensionless by using the maximum faradaic charge value ( $Q_{f,oxd}$ ) as the reference point. It is noted that the faradaic charges in the reservoir and separator regions are treated as dummy variables and their value are set arbitrarily equal to zero.

Initially, the polypyrrole positive electrode is in its fully neutral state at  $Q_f = Q_{f,red}$  and is ready to be oxidized. By applying a constant current density

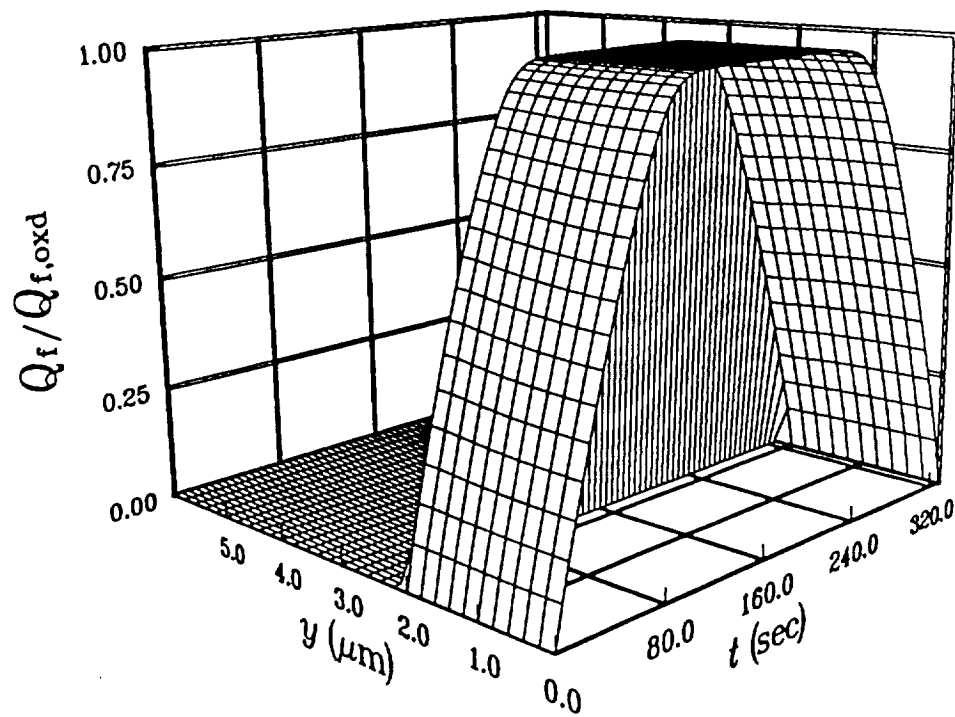


Fig. 22. Dimensionless faradaic charge profiles across a typical cell during charge and discharge at  $i_{cell} = 0.2 \text{ mA/cm}^2$ .

of  $0.2 \text{ mA/cm}^2$ , the faradaic charge is accumulated throughout the polypyrrole electrode by the electrochemical reaction [1]. The faradaic charge accumulation in the outer layer of the polypyrrole electrode (reservoir side) is faster because of the concentration gradient effect within polypyrrole electrode as shown in Fig. 21. After the polypyrrole electrode has been fully oxidized, the charge distribution becomes uniform again at  $Q_f = Q_{f,\text{oxd}}$ . During discharge, the opposite phenomena are true. The faradaic charge is withdrawn slower in the inner layer of the polypyrrole electrode (current collector side) because of the diffusion limitation.

The electrochemical properties of polypyrrole positive electrode (such as, porosity, conductivity, diffusivity, mobility, etc.) have the similar distributions throughout the polypyrrole positive electrode because of the assumption that these properties are proportional to the faradaic charge consumed within the polypyrrole electrode.

Figure 23 shows the potential profiles of the solution phase. The solution potential decreases during charge and increases during discharge. These are due to the compensation for changing available electroactive area in the solid phase and reactive species in the solution phase. During charge, the solution potential decreases with two different slope because of two distinctive factors, faradaic and capacitive effects, as discussed in Fig. 20. For discharge, opposite phenomena are true. At the end of discharge, the sharp potential increase indicates that the cell is fully discharged.

### 3. Effects of Operating Conditions

The effects of various operating conditions on the charge/discharge cell performance can be examined by the model developed here. For example, the

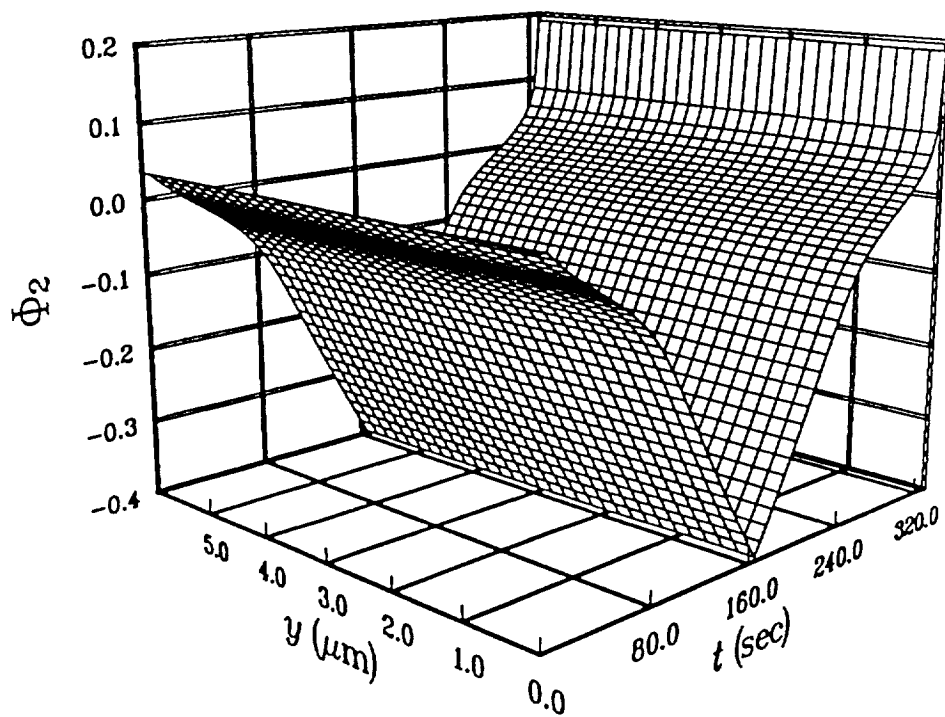


Fig. 23. Solution potential profiles across a typical cell during charge and discharge at  $i_{\text{cell}} = 0.2 \text{ mA/cm}^2$ .



effects of discharge rate on the predicted behavior of the cell discharge are examined in Fig. 24. By increasing discharge rates 0.2, 0.3, and 0.4 mV/sec, the energy densities of the cell decrease 191.9, 191.0, and 172.4 Wh/kg of polypyrrole positive electrode. This clearly illustrates that the cell is better utilized at lower discharge rate. At discharge rate higher than 0.5 mV/sec, the cell is dead before the cell is completely utilized because of the effect of pore-plugging, which prevents the counterion in the reservoir from diffusing into the pores and supporting the electrode reaction [1] and the double layer charging.

#### 4. Effects of Design Parameters

The effects of various cell physical parameters on the predicted behavior of the cell and their implications can be examined by the model developed here. Since the capacity of the cell is determined by the amount of electrode active material and the amount of electrolyte available in the system, the effects of the thickness of the polypyrrole positive electrode, reservoir, and separator on the discharge cell performance at a constant current density of 0.2 mA/cm<sup>2</sup> are examined in Figs. 25 through 27.

Figure 25 shows the effect of the thickness of the polypyrrole positive electrode (equivalent to changing the amount of polypyrrole electroactive material). Increasing the thickness of the polypyrrole electrode yields more electroactive sites so that a slightly larger cell discharge potential and a longer discharge time are obtained.

Figure 26 shows the effect of the thickness of the reservoir (equivalent to changing the amount of electroactive counterion). Increasing the thickness of the reservoir yields a slightly smaller cell discharge potential and a shorter discharge time. This is because the thicker reservoir tends to increase ohmic drop, although

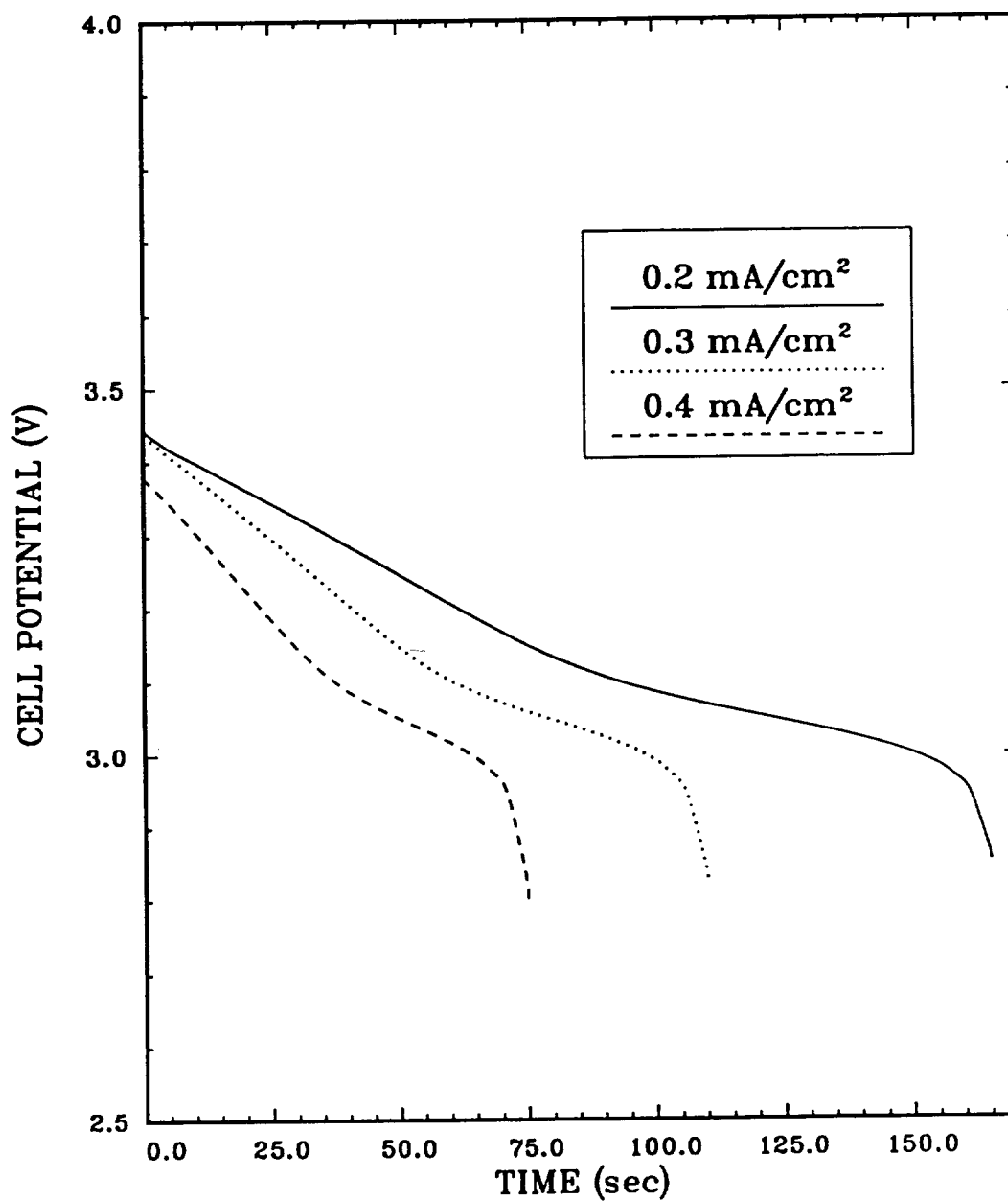


Fig. 24. The effect of the discharge rate on the cell discharge performance.

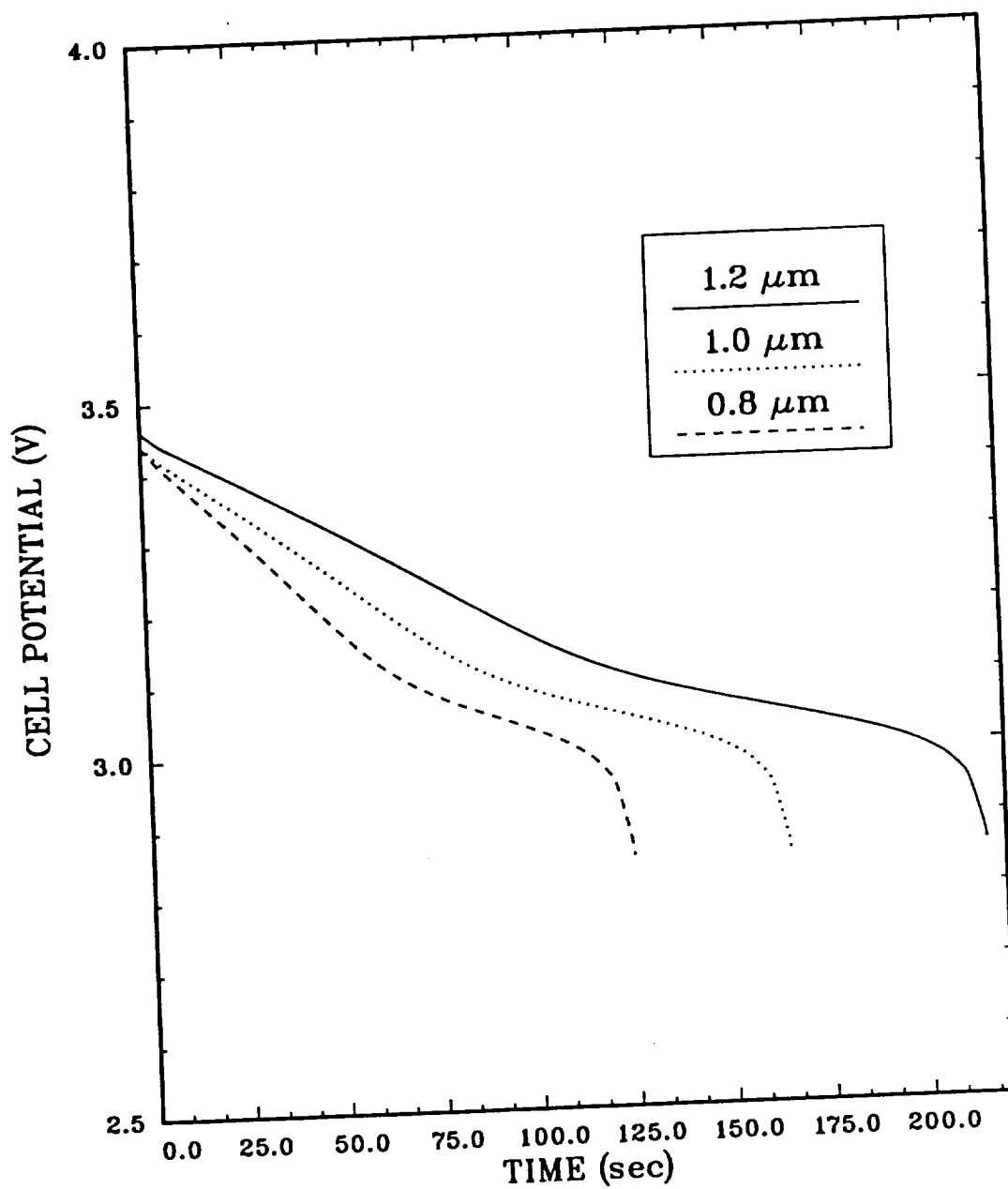


Fig. 25. The effect of the thickness of the polypyrrole positive electrode on the cell discharge performance at  $i_{\text{cell}} = 0.2 \text{ mA/cm}^2$ .

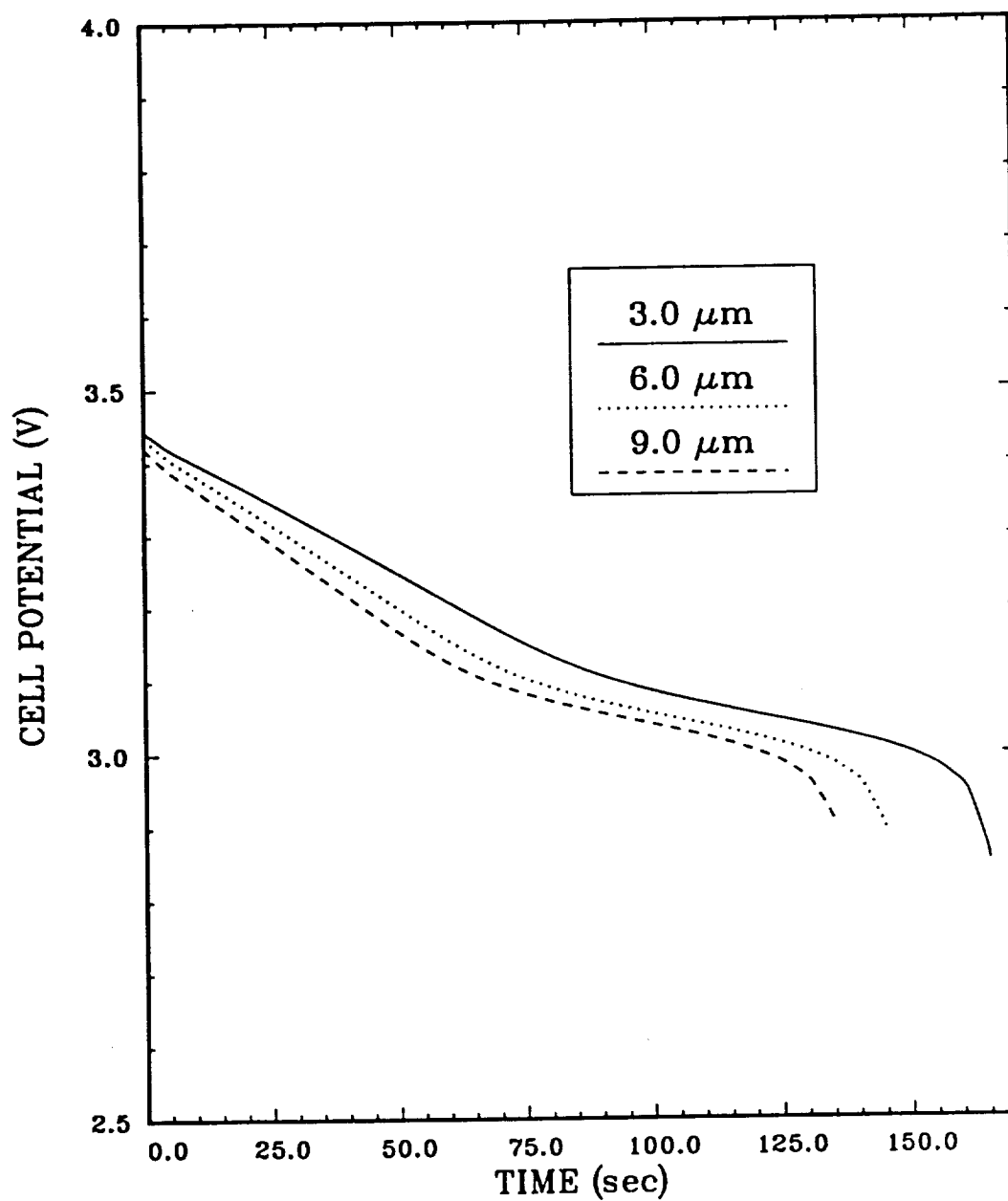


Fig. 26. The effect of the thickness of the reservoir on the cell discharge performance at  $i_{\text{cell}} = 0.2 \text{ mA/cm}^2$ .

more reactive species.

Figure 27 shows the effect of the thickness of the separator. Also, increasing the thickness of the separator yields a slightly smaller cell discharge potential and a shorter discharge time. This is because the thicker separator tends to increase ohmic drop.

Consequently, the optimal values of design parameters discussed above have to be determined in conjunction with other design parameters and operating conditions.

#### D. Conclusions and Recommendations

A one dimensional mathematical model for a lithium/polypyrrole secondary battery system is developed and used to predict dynamic behaviors of charging and discharging processes. A set of independent design criteria is specified and the model is used to show the effects of changes in these criteria on the cell performance. The results of this work show that:

- a. A comparison of the predicted results from this model to those of the experimental data available in the literature shows a qualitative agreement. Based on the theoretical calculations, lithium/polypyrrole secondary battery system can offer higher energy density, power density, and cell potential than any existing battery system.
- b. Discharging process at room temperature is governed by the amount of the electroactive sites within polypyrrole positive electrode and the availability of the counterion to those sites. Thus, the cell performance could be improved by modifying the microscopic structure of polypyrrole positive electrode which yields more electroactive sites and easier

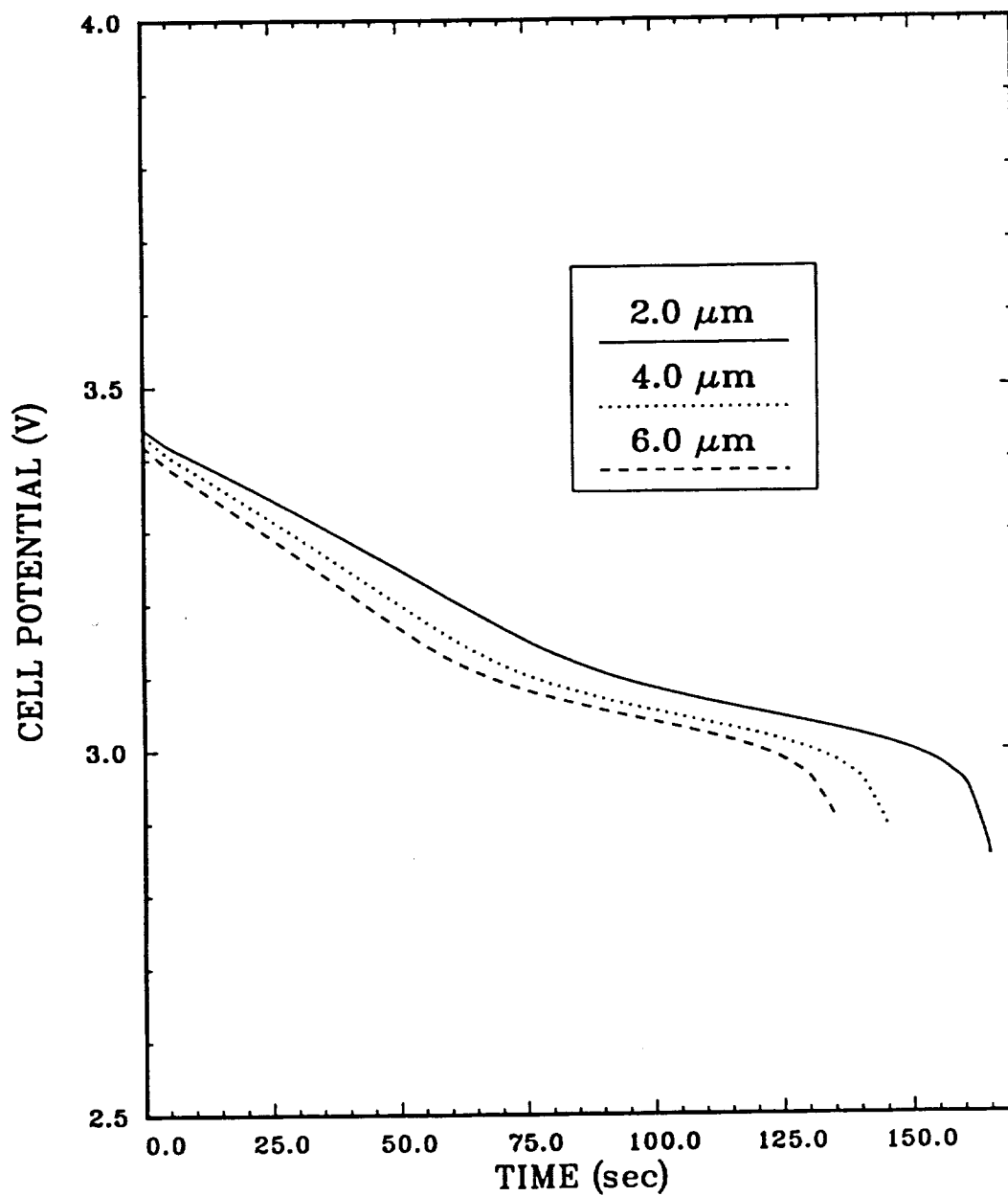


Fig. 27. The effect of the thickness of the separator on the cell discharge performance at  $i_{\text{cell}} = 0.2 \text{ mA/cm}^2$ .

counterion diffusion.

A large number of cases could be studied using the model to help better understand the physical phenomena occurring at charge/discharge process and thus determine optimal and safe designs for various cell specifications and discharge rates. It may be possible to use this model together with experimental data and parameter estimation techniques to determine the characteristic of charge/discharge behavior of the lithium/polypyrrole secondary battery cell. The lithium/polypyrrole model developed here could be modified to study other polymeric battery systems. Improvements of the model could be yield by accounting the capacity loss in the cycling and the self discharge reaction mechanisms.

## LIST OF SYMBOLS

<u>Symbol</u>	<u>Definition</u>
$A$	Geometric electrode surface area, $\text{cm}^2$
$a$	Specific surface area of polypyrrole film, $/\text{cm}$
$a'$	Rotating disk electrode constant, 0.51023
$a^*$	Double layer constant, $/V$
$C_k(J)$	$k^{\text{th}}$ unknown at node $J$
$C_l$	Related capacitance of polypyrrole film
$c_i$	Concentration of species $i$ , $\text{mol}/\text{cm}^3$
$c_{i,\text{ref}}$	Reference concentration of species $i$ , $\text{mol}/\text{cm}^3$
$D_i$	Diffusion coefficient of species $i$ , $\text{cm}^2/\text{sec}$
$D_{i,p}$	Effective diffusion coefficient of species $i$ within the polypyrrole film, $\text{cm}^2/\text{sec}$
$D_{i,s}$	Effective diffusion coefficient of species $i$ within the separator, $\text{cm}^2/\text{sec}$
$E$	Applied potential (potential difference between the current collector and reference electrode), $V$
$E_{\text{neg}}$	Negative potential limit, $V$
$E_{\text{pa}}$	Anodic peak potential, $V$
$E_{\text{pc}}$	Cathodic peak potential, $V$
$E_{\text{pos}}$	Positive potential limit, $V$
$e$	Quantity of charge on the electron, $1.60219 \times 10^{-19} \text{ C}$
$\text{ex}$	Exponent on the porosity term, 0.5
$F$	Faraday's constant, $96487 \text{ C}/\text{mol}$
$\Delta G$	Gibbs free energy change in a chemical process, $\text{kJ}$
$I_{\text{cell}}$	Total cell current, $A$
$i$	Current density based on projected electrode area, $A/\text{cm}^2$
$i_a$	Anodic current density with perturbed value of parameter $k$ , $A/\text{cm}^2$
$i_a^*$	Anodic current density with reference value of parameter $k$ , $A/\text{cm}^2$
$i_c$	Capacitive current density based on projected electrode area, $A/\text{cm}^2$
$i_{\text{cell}}$	Applied cell current density based on projected electrode area, $A/\text{cm}^2$
$i_f$	Faradaic current density based on projected electrode area, $A/\text{cm}^2$
$i_{o,j,\text{ref}}$	Exchange current density based on projected electrode area at reference concentrations for reaction $j$ , $A/\text{cm}^2$
$i_{\text{pa}}$	Anodic peak current density based on projected electrode area, $A/\text{cm}^2$
$i_{\text{pc}}$	Cathodic peak current density based on projected electrode area, $A/\text{cm}^2$
$i_1$	Superficial current density in the solid phase based on projected



	electrode area, $A/cm^2$
$i_2$	Superficial current density in the solution phase based on projected electrode area, $A/cm^2$
$\Delta i_a$	Difference of anodic current densities between reference and perturbed values of parameter $k$ , $A/cm^2$
$j_c$	Local capacitive transfer current density within the polypyrrole positive electrode based on electroactive area, $A/cm^2$
$j_f$	Local faradaic transfer current density within the polypyrrole positive electrode based on electroactive area, $A/cm^2$
$j_1$	Local transfer current density within the polypyrrole positive electrode based on electroactive area, $A/cm^2$
$j_2$	Local transfer current density at the lithium negative electrode based on electroactive area, $A/cm^2$
$M_i$	Chemical formula of species $i$
$m$	Number of data points for sensitivity analysis
$N(E_f)$	Density of electronic states at the Fermi level
$N_i$	Flux vector of species $i$ , $mol/cm^2\text{-sec}$
$N_{i,p}$	Flux vector of species $i$ within the polypyrrole film, $mol/cm^2\text{-sec}$
$N_{i,s}$	Flux vector of species $i$ within the separator, $mol/cm^2\text{-sec}$
$n_j$	Number of electrons transferred for reaction $j$
$P_k$	Perturbed value of parameter $k$
$P_k^*$	Reference value of parameter $k$
$\Delta P_k$	Dimensionless difference between perturbed and reference values of parameter $k$
$Q$	Local charge of the polypyrrole film per unit volume, $C/cm^3$
$Q_c$	Local capacitive charge of the polypyrrole film per unit volume, $C/cm^3$
$Q_{ca}$	Anodic charge density of the polypyrrole film based on projected electrode area $C/cm^2$
$Q_{cc}$	Cathodic charge density of the polypyrrole film based on projected electrode area, $C/cm^2$
$Q_f$	Local faradaic charge of the polypyrrole film per unit volume, $C/cm^3$
$Q_{f,oxd}$	Faradaic charge of the fully oxidized polypyrrole film per unit volume, $C/cm^3$
$Q_{f,red}$	Faradaic charge of the fully neutral polypyrrole film per unit volume, $C/cm^3$
$R$	Universal gas constant, $8.3143 J/mol\text{-K}$
$R'_{j,i}$	Pseudohomogenous reaction rate of species $i$ for reaction $j$ , $mol/cm^3\text{-sec}$
$S_k$	Sensitivity coefficient of parameter $k$
$s_{j,i}$	Stoichiometric coefficient of species $i$ for reaction $j$

$T$	Absolute temperature, K
$t$	Time, sec
$t_d$	Discharge time of the lithium/polypyrrole secondary battery cell, sec
$t_i$	Transference number of species $i$
$\Delta t$	Time step, sec
$U_j$	Theoretical open circuit potential at the surface concentration for reaction $j$ , V
$U_{j,ref}$	Theoretical open circuit potential at reference concentration for reaction $j$ , V
$u_i$	Mobility of species $i$ , mol-cm <sup>2</sup> /J-sec
$u_{i,p}$	Effective mobility of species $i$ within polypyrrole electrode, mol-cm <sup>2</sup> /J-sec
$u_{i,s}$	Effective mobility of species $i$ within separator, mol-cm <sup>2</sup> /J-sec
$V$	Volume of polypyrrole film, cm <sup>3</sup>
$\mathbf{v}$	Electrolyte velocity vector, cm/sec
$v_s$	Scan rate, V/sec
$v_y$	Electrolyte velocity in the normal direction, cm/sec
$y$	Perpendicular distance from the current collector/polypyrrole electrode interface, cm
$y_{dl}$	Position of the bulk solution in $y$ coordinate, cm
$y_{pp}$	Position of the polypyrrole electrode/diffusion layer interface in $y$ coordinate, cm
$y_{ppe}$	Position of the positive electrode/reservoir interface in $y$ coordinate, cm
$y_{res}$	Position of the reservoir/separator interface in $y$ coordinate, cm
$y_{sep}$	Position of the separator/negative electrode interface in $y$ coordinate, cm
$\Delta y$	Distance between node points, cm
$z_i$	Charge number of species $i$

### Greek

$\alpha_{aj}$	Anodic transfer coefficient for reaction $j$
$\alpha_{cj}$	Cathodic transfer coefficient for reaction $j$
$\delta_{dl}$	Thickness of the electrolyte diffusion layer, cm
$\delta_{pp}$	Thickness of the polypyrrole film, cm
$\delta_{ppe}$	Thickness of the polypyrrole positive electrode, cm
$\delta_{res}$	Thickness of the reservoir, cm
$\delta_{sep}$	Thickness of the separator, cm
$\epsilon_p$	Porosity of the polypyrrole film
$\epsilon_{oxd}$	Porosity of the fully oxidized polypyrrole film
$\epsilon_{red}$	Porosity of the fully neutral polypyrrole film

$\epsilon_s$	Porosity of the separator
$\eta_j$	Overpotential for reaction j, V
$\eta_{j,pzc}$	Overpotential at the point of zero charge for reaction j, V
$\kappa$	Free-stream solution conductivity, / $\Omega$ -cm
$\kappa_p$	Effective solution conductivity within the polypyrrole film, / $\Omega$ -cm
$\kappa_s$	Effective solution conductivity within the separator, / $\Omega$ -cm
$\Lambda$	Equivalent conductance of binary electrolyte, $\text{cm}^2/\Omega\text{-cm}$
$\lambda$	Doping level of polypyrrole film
$\lambda_i$	Ionic conductance, $\text{cm}^2/\Omega\text{-cm}$
$\lambda_{\max}$	Maximum doping level of polypyrrole film, 0.30
$\theta$	Fractional doping level of polypyrrole film,
$\mu$	Viscosity, g/cm-sec
$\nu$	Kinematic viscosity, $\text{cm}^2/\text{sec}$
$\rho$	Density of polypyrrole film, $\text{g}/\text{cm}^3$
$\rho_s$	Density of 1M LiClO <sub>4</sub> -PC solution, $\text{g}/\text{cm}^3$
$\sigma_{\text{oxd}}$	Electronic conductivity of the fully oxidized polypyrrole film, / $\Omega$ -cm
$\sigma_p$	Electronic conductivity of the polypyrrole film, / $\Omega$ -cm
$\sigma_{\text{red}}$	Electronic conductivity of the fully neutral polypyrrole film, / $\Omega$ -cm
$\tau$	Tortuosity of the polypyrrole film
$\Phi_{\text{cell}}$	Cell potential, V
$\Phi_{\text{ave}}$	Average cell potential during discharge, V
$\Phi_{\text{ref}}$	Reference electrode potential, V
$\Phi_1$	Potential at the solid phase, V
$\Phi_2$	Potential at the solution phase, V
$\Omega$	Disk rotation velocity, rad/sec

### Subscript

+	Cation, Li <sup>+</sup>
-	Anion, ClO <sub>4</sub> <sup>-</sup>

## REFERENCES

1. A. F. Diaz and J. Bargon, "Handbook of Conducting Polymers, Volume 1," T. A. Skotheim, Ed., p. 81, Marcel Dekker, Inc., New York, NY (1986).
2. G. B. Street, "Handbook of Conducting Polymers, Volume 1," T. A. Skotheim, Ed., p. 265, Marcel Dekker, Inc., New York, NY (1986).
3. J. Bargon, S. Mohmand, and R. J. Waltman, *IBM J. Res. Dev.*, **27**, 330 (1983).
4. A. Angeli, *Gazz. Chim. Ital.*, **46**, II, 279 (1916).
5. A. Angeli and L. Alessandri, *Gazz. Chim. Ital.*, **46**, II, 283 (1916).
6. A. Dall'Olio, G. Dascola, V. Varacca, and V. Bocchi, *Compt. Rend. Sci. Scr., C*, **267**, 433 (1968).
7. V. V. Walatka, Jr., M. M. Labes, and J. H. Perlstein, *Phys. Rev. Lett.*, **31**, 1139 (1973).
8. R. L. Greene, G. B. Street, and L. J. Suter, *Phys. Rev. Lett.*, **34**, 577 (1975).
9. H. Shirakawa, E. J. Louis, A. G. MacDiarmid, C. K. Chiang, and A. J. Heeger, *J. Chem. Soc., Chem. Commun.*, 578 (1977).
10. C. K. Chiang, C. R. Fincher, Jr., Y. W. Park, A. J. Heeger, H. Shirakawa, E. J. Louis, S. C. Gau, and A. G. MacDiarmid, *Phys. Rev. Lett.*, **39**, 1098 (1977).
11. C. K. Chiang, M. A. Druy, S. C. Gau, A. J. Heeger, E. J. Louis, A. G. MacDiarmid, Y. W. Park, and H. Shirakawa, *J. Am. Chem. Soc.*, **100**, 1013 (1978).
12. P. J. Nigrey, A. G. MacDiarmid, and A. J. Heeger, *J. Chem. Soc., Chem. Commun.*, 594 (1979).

13. P. J. Nigrey, D. MacInnes, Jr., D. P. Nairns, A. G. MacDiarmid, and A. J. Heeger, *J. Electrochem. Soc.*, **128**, 1651 (1981).
14. P. J. Nigrey, A. G. MacDiarmid, and A. J. Heeger, *Mol. Cryst. Liq. Cryst.*, **83**, 309 (1982).
15. J. R. Ellis, "Handbook of Conducting Polymers, Volume 1," T. A. Skotheim, Ed., p. 489, Marcel Dekker, Inc., New York, NY (1986).
16. A. F. Diaz, K. K. Kanazawa, and G. P. Gardini, *J. Chem. Soc., Chem. Commun.*, 635 (1979).
17. K. K. Kanazawa, A. F. Diaz, R. H. Geiss, W. D. Gill, J. F. Kwak, J. A. Logan, J. F. Rabolt, and G. B. Street, *J. Chem. Soc., Chem. Commun.*, 854 (1979).
18. L. W. Shacklette, R. R. Chance, D. M. Ivory, G. G. Miller, and R. H. Baughman, *Synth. Met.*, **1**, 307 (1979/1980).
19. K. K. Kanazawa, A. F. Diaz, M. T. Krounbi, and G. B. Street, *Synth. Met.*, **4**, 119 (1981).
20. T. Yamamoto, K. Saneckika, and A. Yamamoto, *J. Polym. Sci. Polym. Lett. Ed.*, **18**, 9 (1980).
21. G. Tourillon and F. Garnier, *J. Electroanal. Chem.*, **135**, 173 (1982).
22. R. J. Waltman, J. Bargon, and A. F. Diaz, *J. Electrochem. Soc.*, **131**, 1452 (1984).
23. R. J. Waltman, J. Bargon, and A. F. Diaz, *J. Phys. Chem.*, **87**, 1459 (1983).
24. G. Tourillon and F. Garnier, *J. Electroanal. Chem.*, **161**, 51 (1984).
25. R. McNeill, R. Siudak, J. H. Wardlaw, and D. E. Weiss, *Austr. J. Chem.*, **16**, 1056 (1963).
26. G. P. Gardini, *Adv. Heterocycl. Chem.*, **15**, 67 (1973).

27. M. Salmon, K. K. Kanazawa, A. F. Diaz, and M. Krounbi, *J. Polym. Sci., Polym. Lett. Ed.*, **20**, 187 (1982).
28. G. F. Smith, *Adv. Heterocycl. Chem.*, **2**, 287 (1963).
29. G. B. Street, T. C. Clarke, M. Krounbi, K. K. Kanazawa, V. Lee, P. Pfluger, J. C. Scott, and G. Weiser, *Mol. Cryst. Liq. Cryst.*, **83**, 253 (1982).
30. S. Asavapiriyant, G. K. Chandler, G. A. Gunawardena, and D. Pletcher, *J. Electroanal. Chem.*, **177**, 229 (1984).
31. T. F. Otero and E. De Larreta, *Synth. Met.*, **26**, 79 (1988).
32. G. Zotti, C. Callarin, and N. Comisso, *J. Electroanal. Chem.*, **235**, 259 (1987).
33. M. Salmon, A. F. Diaz, A. J. Logan, M. Krounbi, and J. Bargon, *Mol. Cryst. Liq. Cryst.*, **83**, 265 (1982).
34. G. B. Street, *J. Phys. Paris, C3*, **44**, 599 (1983).
35. R. J. Waltman and J. Bargon, *Can. J. Chem.*, **64**, 76 (1986).
36. E. M. Genies, G. Bidan, and A. F. Diaz, *J. Electroanal. Chem.*, **149**, 101 (1983).
37. G. B. Street, T. C. Clarke, R. H. Geiss, V. Y. Lee, A. Nazzal, P. Pfluger, J. C. Scott, *J. Phys. Paris Colloq.*, **599**, C3 (1983).
38. J. Roncali, F. Garnier, M. Lemaire, and R. Garreau, *Synth. Met.*, **15**, 323 (1986).
39. G. B. Street, R. H. Geiss, S. E. Lindsey, A. Nazzal, and P. Pfluger, "Proceedings of the conference on electronic Excitation and Interaction Process in Organic Molecular Aggregates," P. Reineker, H. Hakn, and H. C. Wolf, Ed., p. 265, Springer, New York, NY (1983).
40. A. F. Diaz, J. I. Castillo, J. A. Logan, and W. Lee, *J. Electroanal. Chem.*,

- 129, 115 (1981).
41. R. A. Bull, F. F. Fan, and A. J. Bard, *J. Electrochem. Soc.*, **129**, 1009 (1982).
  42. P. Burgmayer and R. W. Murray, "Handbook of Conducting Polymers, Volume 1," T. J. Skotheim, Ed., p. 507, Marcel Dekker, Inc., New York, NY (1986).
  43. M. Gazard, "Handbook of Conducting Polymers, Volume 1," T. J. Skotheim, Ed., p. 673, Marcel Dekker, Inc., New York, NY (1986).
  44. P. Burgmayer and R. W. Murray, *J. Am. Chem. Soc.*, **104**, 6139 (1982).
  45. P. Burgmayer and R. W. Murray, *J. Phys. Chem.*, **88**, 2515 (1984).
  46. J. Tanguy, N. Mermilliod, and M. Hoclet, *J. Electrochem. Soc.*, **134**, 795 (1987).
  47. J. Tanguy, N. Mermilliod, and M. Hoclet, *Synth. Met.*, **18**, 7 (1987).
  48. R. M. Penner and C. R. Martin, *J. Phys. Chem.*, **93**, 984 (1989).
  49. A. K. Hauser and J. Newman, *J. Electrochem. Soc.*, **136**, 2820 (1989).
  50. A. F. Diaz and K. K. Kanazawa, *Chem. Scr.*, **17**, 145 (1981).
  51. K. K. Kanazawa, A. F. Diaz, W. D. Gill, P. M. Grant, G. B. Street, G. P. Gardini, and J. F. Kwak, *Synth. Met.*, **1**, 329 (1979/80).
  52. K. J. Wynne and G. B. Street, *Macromolecules*, **18**, 2361 (1985).
  53. P. Pfluger, G. Weiser, J. C. Scott, and G. B. Street, "Handbook of Conducting Polymers, Volume 2," T. J. Skotheim, Ed., p. 1373, Marcel Dekker, Inc., New York, NY (1986).
  54. R. Erlandsson, O. Inganäs, I. Lundström, and W. R. Salaneck, *Synth. Met.*, **10**, 303 (1985).
  55. B. F. Cvetko, M. P. Brungs, R. P. Burford, and M. Skyllas-Kazacos, *J. Appl.*

- Electrochem.*, **17**, 1198 (1987).
56. O. Inganäs, R. Erlandsson, C. Nylander, and I. Lundström, *J. Phys. Chem. Solids*, **45**, 427 (1984).
  57. J. L. Bredas, R. R. Chance, and R. Silberg, *Mol. Cryst. Liq. Cryst.*, **77**, 319 (1981).
  58. J. L. Bredas, B. Themans, J. M. Andre, R. R. Chance, D. S. Boudreaux, and R. Silberg, *J. Phys. Coll*, **44**, C3-373 (1983).
  59. P. M. Grant and I. P. Batra, *Syn. Met.*, **1**, 193 (1979/1980).
  60. W. P. See, J. R. Schrieffer, and A. J. Heeger, *Phys. Rev. Lett.*, **42**, 1698 (1979).
  61. N. F. Mott and E. A. Davis, "Electronic Processes in Non-crystalline Materials," Clarendon Press, Oxford (1969).
  62. R. R. Chance, J. L. Bredas, and R. Silbey, *Phys. Rev. B.*, **29**, 4491 (1984).
  63. S. Kivelson, *Phys. Rev. B.*, **25**, 3798 (1982).
  64. N. F. Mott, *J. Phys. C., Solid State Phys.*, **13**, 5433 (1980).
  65. Y. Shen, K. Carneiro, C. Jacobsen, R. Qian, and J. Qiu, *Synth. Met.*, **18**, 77 (1987).
  66. R. R. Chance, D. S. Boudreaux, J. L. Bredas, and R. Silbey, "Handbook of Conducting Polymers, Volume 2," T. J. Skotheim, Ed., p. 915, Marcel Dekker, Inc., New York, NY (1986).
  67. W. P. Su, Jr., Schrieffer, and A. J. Heeger, *Phys. Rev. B*, **22**, 2099 (1980).
  68. K. L. Ngai and R. W. Rendell, "Handbook of Conducting Polymers, Volume 2," T. J. Skotheim, Ed., p. 967, Marcel Dekker, Inc., New York, NY (1986).
  69. A. F. Diaz, V. Vasquez, and A. M. Duran, *IBM J. Res. Dev.*, **25**, 42 (1981).
  70. R. Noufi, A. J. Frank, and A. J. Nozik, *J. Electrochem. Soc.*, **128**, 2596



- (1981).
71. R. Noufi, A. J. Frank, and A. J. Nozik, *J. Am. Chem. Soc.*, **103**, 1849 (1981).
  72. T. Skotheim, L. G. Petterson, O. Inganäs, and I. Lundström, *J. Electrochem. Soc.*, **129**, 1737 (1982).
  73. E. M. Genies and J. M. Pernaut, *Synth. Met.*, **10**, 117 (1984/85).
  74. R. M. Penner, L. S. Van Dyke, and C. R. Martin, *J. Phys. Chem.*, **92**, 5274 (1988).
  75. K. Naoi and T. Osaka, *J. Electrochem. Soc.*, **134**, 2479 (1987).
  76. S. Panero, P. Prospero, S. Passerini, B. Scrosati, and D. D. Perlmutter, *J. Electrochem. Soc.*, **136**, 3729 (1989).
  77. J. H. Kaufman, K. K. Kanazawa, and G. B. Street, *Phys. Rev. Lett.*, **53**, N. 26, 2461 (1984).
  78. F. Chao, J. L. Baudoin, M. Costa, and P. Lang, *Makromol. Chem. Makromol. Symp.*, **8**, 173 (1987).
  79. S. W. Feldberg, *J. Am. Chem. Soc.*, **106**, 4671 (1984).
  80. P. G. Pickup and R. A. Osteryoung, *J. Electroanal. Chem.*, **195**, 271 (1985).
  81. J. Prejza, I. Lundström, and T. Skotheim, *J. Electrochem. Soc.*, **129**, 1685 (1982).
  82. R. Noufi, D. Tench, and L. F. Warren, *J. Electrochem. Soc.*, **127**, 2310 (1980).
  83. A. J. Frank and K. Honda, paper presented at the 182nd American Chemical Society Meeting, Las Vegas, NV, April 1981
  84. R. A. Bull, F. R. Fan, and A. J. Bard, *J. Electrochem. Soc.*, **130**, 1636 (1983).

85. A. J. Frank, *Mol. Cryst. Liq. Cryst.*, **83**, 341 (1982).
86. S. J. Hahn, W. J. Gajda, P. O. Vogelhut, and M. V. Zeller, *Synth. Met.*, **14**, 89 (1986).
87. D. S. Maddison and J. Unsworth, *Synth. Met.*, **30**, 47 (1989).
88. M. Satoh, K. Kaneto, and K. Yoshino, *Synth. Met.*, **14**, 289 (1986).
89. Y. Yatsuda, H. Sakai, and T. Osaka, *J. Chem. Soc., Jpn.*, **7**, 1331 (1985).
90. K. Okabayashi, F. Goto, K. Abe, T. Yoshida, and M. Morimoto, in "Proceedings of 25th Battery Symposium," In Japan, p. 260 (1984).
91. M. Ogasawara, K. Funahashi, and K. Iwata, *Mol. Cryst. Liq. Cryst.*, **118**, 159 (1985).
92. R. M. Penner and C. R. Martin, *J. Electrochem. Soc.*, **113**, 2206 (1986).
93. K. Naoi, A. Ishijima, and T. Osaka, *J. Electroanal. Chem.*, **217**, 203 (1987).
94. M. A. De Paoli, R. J. Waltman, A. F. Diaz, and J. Bargon, *J. Chem. Soc., Chem. Commun.*, 1016 (1984).
95. M. A. De Paoli, R. J. Waltman, A. F. Diaz, and J. Bargon, *J. Poly. Sci., Poly. Chem. Ed.*, **23**, 1687 (1985).
96. S. E. Lindsey and G. B. Street, *Synth. Met.*, **10**, 67 (1985).
97. F. Fan and A. J. Bard, *J. Electrochem. Soc.*, **133**, 301 (1986).
98. R. M. Penner and C. R. Martin, *J. Electrochem. Soc.*, **133**, 310 (1986).
99. P. Novák, O. Inganäs, and R. Bjorklund, *J. Electrochem. Soc.*, **134**, 1341 (1987).
100. P. Novák and O. Inganäs, *J. Electrochem. Soc.*, **135**, 2485 (1988).
101. A. Nazzal and G. B. Street, *J. Chem. Soc., Chem. Commun.*, 375 (1985).
102. N. Kumar, B. D. Malhotra, and S. Chandra, *J. Polym. Sci. Polym. Lett. Ed.*, **23**, 57 (1985).

103. O. Inganäs, B. Liedberg, and W. Chang-Ru, *Synth. Met.*, **11**, 239 (1985).
104. S. Kuwabata, S. Ito, and H. Yoneyama, *J. Electrochem. Soc.*, **135**, 1691 (1988).
105. T. Osaka, K. Naoi, H. Sakai, and S. Ogano, *J. Electrochem. Soc.*, **134**, 285 (1987).
106. T. Osaka, K. Naoi, S. Ogano, and S. Nakamura, *J. Electrochem. Soc.*, **134**, 2096 (1987).
107. S. Panero, P. Prospero, and B. Scrosati, *Electrochim. Acta*, **32**, 1465 (1987).
108. A. Mohammadi, O. Inganäs, and I. Lundström, *J. Electrochem. Soc.*, **133**, 947 (1986).
109. F. Trinidad, J. Alonso-Lopez, and M. Nebot, *J. App. Electrochem.*, **17**, 215 (1987).
110. H. Münstedt, G. Köhler, H. Möhwald, D. Naegele, R. Bitthin, G. Ely, and E. Meissner, *Synth. Met.*, **18**, 259 (1987).
111. R. Noufi, D. Tench, and L. F. Warren, *J. Electrochem. Soc.*, **127**, 1625 (1980).
112. F. F. Fan, B. Wheeler, A. J. Bard, and R. Noufi, *J. Electrochem. Soc.*, **128**, 2042 (1981).
113. T. Skotheim, O. Inganäs, J. Prejza, and I. Lundström, *Mol. Cryst. Liq. Cryst.*, **83**, 329 (1982).
114. T. Skotheim, I. Lundström, and J. Prejza, *J. Electrochem. Soc.*, **128**, 1625 (1981).
115. A. J. Frank and R. J. Honda, *J. Phys. Chem.*, **86**, 1933 (1982).
116. G. Cooper, R. Noufi, A. J. Frank, and A. J. Nozik, *Nature*, **295**, 578 (1982).
117. A. F. Diaz, M. Salmon, and J. Addy, *Proceedings of the First European*

- Display Research Conference*, Munich, p. 111, VDE-Verlag GmbH, Berlin (1981)
118. O. Inganäs and I. Lundström, *J. Electrochem. Soc.*, **131**, 1129 (1984).
  119. K. Murao and K. Suzuki, *J. Chem. Soc., Chem. Commun.*, 238 (1984).
  120. K. Kaneto, S. Takeda, and K. Yoshino, *Jpn. J. Appl. Phys.*, **24**, L553 (1985).
  121. H. S. White, G. P. Kittlesen, and M. S. Wrighton, *J. Am. Chem. Soc.*, **106**, 5375 (1984).
  122. J. S. Newman, "Electrochemical Systems," Prentice-Hall, Englewood Cliffs, NJ (1973).
  123. R. Keller, J. N. Foster, D. C. Hanson, J. F. Hon, and J. S. Muirhead, "Properties of nonaqueous Electrolyte," NAS 3-8521, NASA CR-1425 (1969).
  124. F. Breivogel and M. Eisenberg, *Electrochem. Acta.*, **14**, 459 (1969).
  125. M. Salmon, *J. Phys. Chem.*, **73**, 3299 (1969).
  126. R. Jasinski, in "Advanced in Electrochemistry and Electrochemical Engineering, vol. 8" C. W. Tobias, Ed., pp 253-335, John Wilry & Sons, Inc., New York, NY (1971).
  127. W. G. Cochran, *Proc. Cambridge Phil. Soc.*, **30**, 365 (1934).
  128. M. H. Rogers and G. N. Lance, *J. Fluid Mechan.*, **7**, 617 (1960).
  129. J. Newman and W. Tiedemann, *AIChE*, **21**, 25 (1975).
  130. J. S. Dunning, Ph. D. Dissertation, University of California, Los Angeles, CA (1971).
  131. J. A. Trainham, Jr., Ph. D. Dissertation, University of California, Los Angeles, CA (1979).
  132. S. Whitaker, "A Simple Geometrical Derivation of the Spatial Averaging

- Theorem," *Chemical Engineering Education*, 18 (Winter 1985).
133. T. V. Nguyen, Ph. D. Dissertation, Texas A&M University, College Station, TX (1988).
  134. W. E. Ryan, R. E. White, and S. L. Kelly, *J. Electrochem. Soc.*, **134**, 2154 (1987).
  135. J. Van Zee, G. Kleine, R. E. White, and J. Newman, in "Electrochemical Cell Design," R. E. White, Ed., pp 377-389, Plenum Press, New York, NY (1984).
  136. B. Carnahan, H. A. Luther, and J. O. Wilkes, "Applied Numerical Methods," John Wiley & Sons, New York, NY (1969).
  137. N. Mermilliod, J. Tanguy, and F. Petiot, *J. Electrochem. Soc.*, **133**, 1073 (1986).
  138. P. E. Gill, W. Murray, and M. H. Wright, "Practical Optimization," Academic Press, New York, NY (1984).
  139. M. Barak, Editor, "Electrochemical Power Sources: Primary and Secondary Batteries," The Institution of Electrical Engineers, New York (1980).

## APPENDIX A

## ELECTROCHEMICAL POLYMERIZATION OF POLYPYRROLE FILMS

Electronically conducting polypyrrole film is deposited electrochemically on the polished surface of platinum rotating disk electrode in the system shown in Fig. 5. Supporting electrolyte is propylene carbonate solution containing 0.1M LiClO<sub>4</sub> and 0.1M pyrrole monomer.

Electrochemical synthesis is carried out using an EG&G Princeton Applied Research (PAR) Model 173 potentiostat/galvanostat equipped with a PAR Model 179 digital coulometer. Applying a constant current density of 1 mA/cm<sup>2</sup> for 240 seconds yields 1 μm thick polypyrrole film with little difficulty. The film thickness is controlled by monitoring the amount of total charge consumed during polymerization. That is, the film thickness is proportional to the total passed charge, and 0.24 C/cm<sup>2</sup> of passed charge yields 1 μm thick polypyrrole film (29,30). The surface of platinum disk electrode is cleaned and polished to a mirror finish with 1 μm, 0.3 μm, then 0.05 μm alumina powder (Banner Scientific) on a Metron polishing cloth before polymerization. After the electrochemical synthesis, the cell is thoroughly rinsed with propylene carbonate and then filled with 1M LiClO<sub>4</sub>-PC electrolyte solution to perform the cyclic voltammetry.

All chemicals used are reagent grade (Aldrich Chemicals). Pyrrole is distilled twice in a vacuum and then stored under nitrogen. LiClO<sub>4</sub> is used without further purification. The propylene carbonate used as a solvent is further purified by fractional distillation and percolation through activated alumina. The water in the propylene carbonate is removed by adding molecular sieves for a few days.

## VITA

Taewhan Yeu was born on [REDACTED] to Dalyoung Yeu and Hwoaja Koak in [REDACTED] which is second largest city in South Korea. He finished basic education, in Pusan. In 1975, he moved to Seoul and attended Chung-Ang University. He majored in Chemical Engineering at this University until August 1976 when he went to army for 3 years duty. He began graduate studies in Chemical Engineering at University of Detroit in August 1982. In August 1985, he transferred to Texas A&M University to continue Ph.D. in Chemical Engineering. He married Kyung Mi on June 25, 1988. They are the proud parents of one son, Christopher Edward, born on [REDACTED].

The Author's permanent mailing address is:

Taewhan Yeu  
293-5 Manduck-Dong, Buck-Gu  
Pusan, Korea 601-81

*End Date Aug 7, 1991*

